

2014

Synthetic Routes to Therapeutic Agents Via Masked Functionalities: From Orthogonal Peptide Crosslink to Photothermal Cancer Prodrug

Chyree Shantel Batton

Louisiana State University and Agricultural and Mechanical College, chyree.batton@gmail.com

Follow this and additional works at: https://digitalcommons.lsu.edu/gradschool_dissertations

 Part of the [Chemistry Commons](#)

Recommended Citation

Batton, Chyree Shantel, "Synthetic Routes to Therapeutic Agents Via Masked Functionalities: From Orthogonal Peptide Crosslink to Photothermal Cancer Prodrug" (2014). *LSU Doctoral Dissertations*. 1176.
https://digitalcommons.lsu.edu/gradschool_dissertations/1176

This Dissertation is brought to you for free and open access by the Graduate School at LSU Digital Commons. It has been accepted for inclusion in LSU Doctoral Dissertations by an authorized graduate school editor of LSU Digital Commons. For more information, please contact gradetd@lsu.edu.

SYNTHETIC ROUTES TO THERAPEUTIC AGENTS VIA MASKED FUNCTIONALITIES: FROM
ORTHOGONAL PEPTIDE CROSSLINK TO PHOTOTHERMAL CANCER PRODRUG

A Dissertation

Submitted to the Graduate Faculty of the
Louisiana State University and
Agricultural and Mechanical College
in partial fulfillment of the
requirements for the degree of
Doctor of Philosophy

in

The Department of Chemistry

by

Chyree Shantel Batton
B.S., Spelman College, 2009
December 2014

To My Family...

My mother for being a cornerstone in my life, and always challenging me to excel in all aspects
of life

My brother for teaching me how to find the humor in everything

My younger sister, whose laugh and smiles are extremely infectious

My baby sister, the high achiever, who is a constant reminder that I should never take anything
for granted

...This Dissertation Is For You

ACKNOWLEDGMENTS

I wouldn't be the chemist I am today without the support and guidance of my advisor, Dr. Carol Taylor. Her hard work and dedication to her field has been invaluable to me, as it has positively influenced my mental capacity to solve problems, and fine-tuned my synthetic skills. Outside of academics, she has shown me by example how to be patient and persevere. One aspect that will always stand true is her commitment to always being there if and when you need her, and for that, I am forever grateful.

I would like to thank Dr. Isiah Warner, my co-advisor. Thank you for always believing in me. I am very appreciative of you adopting the role of my mentor inside and outside of academia. Your constant encouragement helped me to stay focused and to never give up.

To my former labmates: Ning, Chamini, Doug, Benson, and Saroj, you guys were helpful from day one, whether it was a quick question, or bringing me home-cooked food. Our group dynamic was one of constant encouragement and teamwork, and that was thanks to you guys. Molly, who although I shared a fume hood with for five years, I don't regret, because I gained a lifetime friendship with one of the most honest, upbeat, joy-filled person I know. Thanks for the many laughs, dance sessions, and listening ear for my grievances. My little sisters, Jessica and Kristina, who came late to the party, but nevertheless, made my last years in the program happy ones. You guys are some of the sweetest people I have ever met, your unwavering loyalty in our friendship is something I don't take lightly. Keep the laughs and good times going after I leave.

Special thanks to Dr. Thomas Weldeghiorghis and the late Dr. Dale Treleven, for always lending a helpful hand with my NMR studies. Dr. Daniel Hayes and Mohammad Abu-Laban for

their invaluable help with my laser irradiation studies. I would like to give a very big thank you to the Department of Chemistry at LSU for supporting me on fellowship throughout the entirety of my tenure. Finally, I would like to give thanks to my lord and heavenly father Jesus Christ, for through him all things are possible.

TABLE OF CONTENTS

ACKNOWLEDGMENTS.....	iii
LIST OF TABLES.....	viii
LIST OF FIGURES.....	ix
LIST OF SCHEMES.....	xi
LIST OF ABBREVIATIONS AND SYMBOLS.....	xvi
ABSTRACT.....	xx
CHAPTER 1: τ -HISTIDINOALANINE AND CHALLENGES ASSOCIATED WITH ITS SYNTHESIS IN A TETRAORTHOAGONALLY PROTECTED FORMAT	1
1.1 Introduction: Occurrence and Origin	1
1.2 HAL in Theonellamides.....	2
1.3 Retrosynthetic Analysis: Need for Flexible Protecting Group Strategy	5
1.4 The Concept of Orthogonality vis-à-vis Protecting Groups	6
1.4.1 Two Dimensional Orthogonal Protection: Solid Phase Peptide Synthesis	8
1.5 Examples of the Use of Orthogonal Protecting Group Strategies	9
1.5.1 Tunable Protecting Groups	9
1.5.2 Protecting Group Free Synthesis	11
1.5.3 Higher Dimensional Orthogonal System: Utilizing Resins as a Temporary Masking Group	12
1.6 <i>bis</i> -Amino Acid Protecting Group Strategies.....	13
1.7 Toward an Orthogonally Protected τ -HAL	18
1.8 References.....	19
CHAPTER 2: SYNTHESIS OF ORTHOGONALLY PROTECTED τ -HISTIDINOALANINE	23
2.1 Early Syntheses of τ -HAL	23
2.2 Synthetic Routes to τ -HAL.....	25
2.2.1 Protected β -Iodoalanine Electrophile and Bicyclic Urea	25
2.2.2 β -Iodoalanine Electrophile and (N_{im}), π -Blocked Histidine Nucleophiles.....	30
2.2.3 Cyclic Sulfamidates	31
2.3 Synthesis of Orthogonally Protected τ -HAL via a Cyclic Sulfamidate	34
2.4 Orthogonal Deprotection.....	39
2.5 Experimental Section	41
2.5.1 Procedures	41
2.5.2 ^1H and ^{13}C NMR Spectra.....	62
2.6 References.....	106

CHAPTER 3: NEAR-INFRARED NANOGUMBOS PRODRUG DELIVERY SYSTEM	109
3.1 Cancer: An Overview	109
3.1.1 Chemotherapy	110
3.2 Paclitaxel	110
3.2.1 Paclitaxel Mode of Action	111
3.2.2 Taxol Solubility in Aqueous Media.....	111
3.2.3 Multidrug Resistance	112
3.3 Prodrugs	114
3.3.1 Trimethyl Lock – Kinetics and Application	116
3.4 Nanomaterials	119
3.4.1 Targeted Drug Delivery	120
3.4.2 NanoGUMBOS: NIR-based Targeted Drug Delivery Application	122
3.5 Drug Delivery System Overview	125
3.6 References.....	126
CHAPTER 4: SYNTHESIS OF ALLYL AND PRENYL ETHERS AND INVESTIGATION OF THE TANDEM CLAISEN REARRANGEMENT-LACTONIZATION REACTIONS.....	130
4.1 Drug Delivery System: Mechanism of Action.....	130
4.2 Claisen Rearrangement: A [3,3']-Sigmatropic Rearrangement.....	130
4.2.1 Aromatic Claisen Rearrangement: Solvent Effects	132
4.2.2 Water Promoted Claisen Rearrangement: Mechanistic Studies	132
4.3 Synthesis of Prodrug Conjugate Model System	134
4.3.1 Retrosynthetic Analysis.....	135
4.3.2 Previous Synthesis of Taxol Sidechain Amino Alcohol.....	135
4.4 Rearrangement Studies.....	138
4.5 “On-Water” Claisen Rearrangement.....	139
4.6 Prenyl Moiety and its Derivatives	140
4.6.1 Claisen Rearrangement: Is There An Enzyme In Nature?	141
4.6.2 Computational Studies of Water-Accelerated <i>gem</i> -Dimethyl Allyl Ether Rearrangement	142
4.6.3 Experimental Evidence of <i>gem</i> -Dimethyl Allyl Ether Rearrangement.....	143
4.7 Synthesis of <i>O</i> -Prenylated Derivatives	144
4.8 Synthesis of Second Generation Prodrug Model System: Preliminary Results	147
4.9 Experimental Section	150
4.9.1 Procedures	150
4.9.2 ¹ H and ¹³ C-NMR Spectra	161
4.10 References.....	191
CHAPTER 5: INCORPORATION OF AN ANIONIC SUBSTRATE FOR A CLAISEN REARRANGEMENT INTO NANOGUMBOS	194
5.1 1,1-Dimethylallyl Aryl Ether Building Block: A Model System for Photothermal Rearrangement	194
5.2 Synthesis of an Anionic Substrate for a Claisen Rearrangement.....	194
5.3 Kinetic Studies of Claisen Rearrangement of Aryl Prenyl Ethers	195
5.4 Assembly of NIR-GUMBOS Model System	198

5.4.1 IR-780: An Antitumorigenic Cationic Dye.....	200
5.4.2 Single Solvent Ion Exchange	202
5.4.3 Ion Exchange Resin Chromatography.....	203
5.5 Preparation of nanoGUMBOS	206
5.6 Future Work	207
5.7 Experimental Section	209
5.7.1 Procedures.....	209
5.7.2 ¹ H and ¹³ C- NMR Spectra	213
5.8 References.....	220
APPENDIX	221
VITA.....	229

LIST OF TABLES

Table 2.1: Optimization of cyclization/oxidation sequence in conversion of 80→109→110	38
Table 3.1: Ten leading cancer types for estimated new cancer cases in 2014 by sex in the United States, adapted with permission.	109
Table 4.1: Various solvents, temperatures, and reaction times for thermal Claisen rearrangement trials of model system 141. Yields are given.	139
Table 4.2: Comparison of solvents for aromatic Claisen rearrangement of 1-(4-chloronaphthyl)-1,1-dimethylallyl ether and associated yields.	140
Table 4.3: Relative rates of cyclization and chemical yields of propargyl aryl ether derivatives in <i>o</i> -dichlorobenzene	144
Table 4.4: Comparison of solvents and reaction times for the aromatic claisen rearrangement of aryl prenyl ether 168 and associated yields.	147
Table 5.1: Rate constants and relative rates for rearrangement of aryl prenyl ethers (185, 173c, 173b, 168) at 60 °C in 1:1 CD ₃ OD:H ₂ O compared with the rate constant of 1-(allyloxy)-4-methoxybenzene in carbitol at 181 °C prepared by White <i>et al.</i>	198

LIST OF FIGURES

Figure 1.1: τ -Histidinoalanine and π -Histidinoalanine.....	1
Figure 1.2: Theonellamides A-F	3
Figure 1.3: Structures of 3 β -hydroxysterols cholesterol and ergosterol, and 3 α -hydroxysterol epicholesterol	3
Figure 1.4: Lanthione stereoisomers 38a, 38b, 38c.....	14
Figure 1.5: "Orthogonal" lanthionine Fragments	16
Figure 2.1: Protecting group strategy for tetra-orthogonal τ -HAL.....	26
Figure 2.2: Minimum energy TS for some of the proposed pathways starting from sulfamidate 94 and mono- and disubstituted imidazoles. Distances are given in Å and activation energies (ΔG^\ddagger) in kcal/mol.	33
Figure 3.1: Structure of Paclitaxel.....	111
Figure 3.2: Drug-resistant cell expelling chemotherapeutic agents via P-gp efflux pump. Adapted with permission.....	113
Figure 3.3: S16020-2	114
Figure 3.4: Biotransformation of prodrug into parent molecule	116
Figure 3.5: Structures of Taxol TM (115), phosphorylated Taxol TM derivatives (119-120), and trimethyl lock-based Taxol TM prodrugs (121-122).....	118
Figure 3.6: Selected examples of organic and inorganic nanoparticles. Reprinted with permission.....	119
Figure 3.7: Tumor uptake of nanoscale drug carriers via the EPR effect. Reprinted with permission.....	120
Figure 3.8: NIR Therapeutic Optical Window.	121
Figure 3.9: Common cations and anions used in ionic liquids.....	123
Figure 3.10: Photothermal profile of 4 mg bulk GUMBOS and nanoGUMBOS samples under continuous NIR irradiation for five minutes at a 1000 mW. Reprinted with permission.....	124
Figure 3.11: Trimethyl lock-based Taxol TM prodrug incorporated into NIR-absorbing nanoGUMBOS	126
Figure 4.1: Solvent hydrogen bonding in vinyl ether transition state	133
Figure 4.2: Amino acid residues of active site in EcCM and BsCM complexed with dianionic competitive inhibitor 137	134

Figure 4.3: Prenyl group and its derivatives	140
Figure 4.4: 1 st and 2 nd generation prodrug model systems	148
Figure 5.1: Crystal structures of 4-(1,1-dimethylallyloxy)benzoic acid (185) and 4-(allyloxy)benzoic acid (186) reported by Zugenmaier	195
Figure 5.2: Time profile of ¹ H-NMR spectra of reaction mixture	196
Figure 5.3: Plot of percentage of product formed versus reaction time of prenyl phenyl ethers.	197
Figure 5.4: Phthalocyanine-based dyes that absorb at 655 and 780 nm	200
Figure 5.5: Cancer cell lines incubated with IR-780 A) Treated with endocytosis inhibitors: control (blue), with Cyto-D (maroon), PAO (yellow) B) Treated with OATP inhibitors: control (blue), Bromsulphthalein (BSP) (maroon), Pravastatin (yellow), Doxorubicin (light blue), Hoechst 33342 (purple). Reprinted with permission.....	201
Figure 5.6: A) The uptake of IR-780 and the influence on the mitochondrial activities of A549/DR cells. A549/DR cells exhibit increased staining of IR-780 B) The tumor volume and weight of mice received cyclophosphamide (CTX), doxorubicin hydrochloride (ADM) and IR-780 treatment at dosage of 20, 2.0 and 5.0 mg/kg respectively. Reprinted with permission.	202
Figure 5.7: ¹ H-NMR of aryl prenyl ether 186, IR-780, and IR-780 based GUMBOS.....	203
Figure 5.8: FT-IR spectrum of NIR GUMBOS 197 (A) and IR-780 iodide 196 (B)	205
Figure 5.9: Ion diffusion method for making nanoparticles	206
Figure 5.10: nanoGUMBOS prepared using sonication probe with 24 hour crystal growth.....	206
Figure 5.11: NanoGUMBOS prepared using sonication bath with 24 hour crystal growth	207

LIST OF SCHEMES

Scheme 1.1: Formation of HAL by serine phosphorylation followed by β -elimination; then conjugate addition	2
Scheme 1.2: Degradation studies of histidinoalanine	4
Scheme 1.3: Retrosynthetic analysis of τ -histidinoalanine	6
Scheme 1.4: Example of a modulated Lability Transformation – a ribonuclease A (RNase A) fragment with a Boc N-terminus, and benzyl-based resin C-terminus	7
Scheme 1.5: Sequential Orthogonal Transformation	7
Scheme 1.6: A general representation of an Fmoc <i>tert</i> -butyl strategy (orthogonality based) for peptide synthesis	9
Scheme 1.7: Protocol for Pd-catalyzed amination and subsequent acid-catalyzed cascade deprotection	10
Scheme 1.8: PCB: <i>p</i> -chlorobenzyl, PBB: <i>p</i> -bromobenzyl, PIB: <i>p</i> -iodobenzyl, L ₁ : 1-(<i>N,N</i> -dimethylamino)-1' (dicyclohexylphosphino)biphenyl, L ₂ : (<i>o</i> -biphenyl)P(^t Bu) ₂ as defined in Scheme 1.7.....	10
Scheme 1.9: LiHMDS-mediated coupling of carvone and indole	11
Scheme 1.10: Deprotection scheme for precursor to Somatostatin analog 37 with protecting groups	12
Scheme 1.11: Disulfide bridge mimetic with protecting groups and deprotection conditions ...	15
Scheme 1.12: Deprotection scheme of disulfide bridge mimetic	16
Scheme 1.13: Precursor to orthogonally protected linear peptide 50.....	17
Scheme 1.14: Quadruply 'orthogonally' protected peptide fragment 51.....	17
Scheme 1.15: Retrosynthetic analysis of the synthesis of orthogonally protected τ -HAL.....	19
Scheme 2.1: Synthesis of HAL isomers via conjugate addition of Ac- <i>L</i> -His-OH (56) to 2-acetylaminoacrylate (57)	23
Scheme 2.2: Shioiri's synthesis of HAL regioisomers employing a β -lactone.....	24
Scheme 2.3: Intramolecular base-catalyzed proton abstraction and enolization mechanism proposed by Jones <i>et al.</i> ⁵	25
Scheme 2.4: Synthesis of τ -HAL 68 via nucleophilic ring opening of fused bicyclic urea derivative	26

Scheme 2.5: Synthesis of <i>N</i> -fluorenylmethoxycarbonyl- β -iodoalanine	27
Scheme 2.6: Synthesis of τ -HAL via bicyclic urea opening with <i>tert</i> -butanol.....	27
Scheme 2.7: Based mediated β -elimination of Fmoc moiety (Path 1) and iodine (Path 2)	28
Scheme 2.8: Attempted synthesis of <i>N</i> -Fmoc- β -iodoalanine SEM ester	29
Scheme 2.9: Attempted synthesis of <i>N</i> -Fmoc- β -iodoalanine SEM ester	29
Scheme 2.10: Formation of Boc-His(π -Pac)-OMe	30
Scheme 2.11: Synthesis of τ -HAL via Boc-His(π -Pac)-OMe.....	31
Scheme 2.12: Synthesis of HAL regioisomers via coupling of Boc- <i>L</i> -His-OMe (59) and Cbz-protected β -lactone (60).....	31
Scheme 2.13: Conditions for synthesis of sulfamidate, and imidazole nucleophilic ring opening	32
Scheme 2.14: Taylor and Thabrew De Silva HAL synthesis via coupling of Boc-His-OMe and sulfamidate 92	32
Scheme 2.15: Nucleophilic attack of sterically hindered sulfamidate by imidazole tautomers yields a mixture of regioisomers.....	32
Scheme 2.16: Mechanism of sulfamidate ring opening by mono-substituted imidazole nucleophile.....	34
Scheme 2.17: Retrosynthetic analysis of orthogonally protected τ -HAL	34
Scheme 2.18: Transesterification of Boc- <i>L</i> -His(Boc)-OTCE (96) and intramolecular ring formation mechanisms	35
Scheme 2.19: Direct synthesis of Boc- <i>L</i> -His-OTCE (97).....	36
Scheme 2.20: Synthesis of cyclic sulfamidate 98 derived from Fmoc- <i>D</i> -Ser-OBn.....	36
Scheme 2.21: Synthesis of τ -HAL 72 via coupling of sulfamidate 98 and Boc- <i>L</i> -His-OMe (59)....	37
Scheme 2.22: Synthesis of Fmoc- <i>D</i> -Ser-O ^t Bu (80)	37
Scheme 2.23: Synthesis of sulfamidate 110 derived from Fmoc- <i>D</i> -Ser-O ^t Bu	38
Scheme 2.24: Synthesis of tetra-orthogonally protected τ -HAL via coupling of Boc- <i>L</i> -His-OTCE and Fmoc- <i>D</i> -Ser-OBn derived sulfamidate	39
Scheme 2.25: Orthogonal deprotection conditions for τ -HAL 15	39
Scheme 2.26: Synthesis of compound 69	41
Scheme 2.27: Synthesis of compound 70.....	42

Scheme 2.28: Synthesis of compound 76.....	43
Scheme 2.29: Synthesis of compound 80.....	44
Scheme 2.30: Synthesis of compound 81.....	45
Scheme 2.31: Synthesis of compound 78.....	46
Scheme 2.32: Synthesis of compound 82.....	46
Scheme 2.33: Synthesis of compound 83.....	47
Scheme 2.34: Synthesis of compound 84.....	48
Scheme 3.35: Synthesis of compound 100.....	48
Scheme 2.36: Synthesis of compound 97.....	49
Scheme 2.37: Synthesis of compound 98.....	50
Scheme 2.38: Synthesis of compound 72.....	51
Scheme 2.39: Synthesis of compound 106.....	52
Scheme 2.40: Synthesis of compound 107.....	53
Scheme 2.41: Synthesis of compound 108.....	54
Scheme 2.42: Synthesis of compound 80.....	55
Scheme 2.43: Synthesis of compound 110.....	55
Scheme 2.44: Synthesis of compound 15.....	56
Scheme 2.45: Synthesis of compound 111.....	58
Scheme 2.46: Synthesis of compound 112.....	59
Scheme 2.47: Synthesis of compound 113.....	59
Scheme 2.48: Synthesis of compound 114.....	60
Scheme 3.1: Rapid lactonization to hydrocoumarin facilitated by the trimethyl lock phenomenon.....	116
Scheme 3.2: Reduction of benzquinone-based trimethyl lock prodrug by sodium dithionate to release Taxol TM , and dihydrocoumarin-derivative and a water soluble polymer chain as byproduct.....	118
Scheme 3.3: Ion exchange of NIR laser dye IR-1048 and deoxycholate or ascorbate.	124
Scheme 4.1: Ionic liquid-based prodrug drug delivery system. NIR ⁺ = cationic near-infrared laser dye.....	130
Scheme 4.2: [3,3]-Sigmatropic rearrangement of allyl vinyl ether	130

Scheme 4.3: Aromatic Claisen rearrangement mechanism with alternative transition state ...	131
Scheme 4.4: Chorismate rearrangement to prephenate ion catalyzed by chorismate mutase	133
Scheme 4.5: Retrosynthetic analysis of prodrug model system 140	135
Scheme 4.6: Asymmetric aminohydroxylation of isopropyl <i>trans</i> -cinnamate	136
Scheme 4.7: Synthesis of Taxol amido alcohol sidechain.....	137
Scheme 4.8: Synthesis of allyl ether trimethylock linker 143.....	137
Scheme 4.9: Coupling of amido alcohol 142 and acid 143 to give prodrug model system 141	138
Scheme 4.10: Thermal rearrangement of prodrug model system 141	138
Scheme 4.11: Aromatic Claisen rearrangement of 1-(4-chloronaphthyl)-1,1-dimethylallyl ether at room temperature	140
Scheme 4.12: 1) Mechanism of action for LynF demonstrated on tyrosine (Pathway I) 2) LynF enzyme sequence 159 3) Traditional prenyl transferase mechanism of installation of prenyl group <i>ortho</i> to the phenol	141
Scheme 4.13: Relative rates of cyclization and chemical yields of propargyl aryl ether derivatives in <i>o</i> -dichlorobenzene	144
Scheme 4.14: Sharpless and coworkers synthesis of 4-chloro-1,1-dimethylallyl naphthyl ether	145
Scheme 4.15: Attempted synthesis of aryl prenyl ether 168	145
Scheme 4.16: Synthesis of 1,1-dimethylallyl ether derivatives	146
Scheme 4.17: Thermal rearrangement of aryl prenyl ether 168.....	147
Scheme 4.18: Attempted aromatic alkylation of aryl prenyl ether 173b.....	148
Scheme 4.19: Attempted synthesis of compound 178.....	149
Scheme 4.20: Proposed synthesis of second generation prodrug model system 175.....	149
Scheme 4.21: Synthesis of compound 144.....	150
Scheme 4.22: Synthesis of compound 145.....	151
Scheme 4.23: Synthesis of compound 142, 149, and 146.....	152
Scheme 4.24: Synthesis of compound 151.....	154
Scheme 4.25: Synthesis of compound 143	154
Scheme 4.26: Synthesis of compound 141	155
Scheme 4.27: Synthesis of compound 171	156
Scheme 4.28: Synthesis of aryl prenyl ether derivatives.....	157

Scheme 4.29: Synthesis of compound 179	159
Scheme 4.30: Synthesis of compound 180	160
Scheme 5.1: Synthesis of 4-(1,1-dimethylallyloxy)benzoic acid 185	194
Scheme 5.2: Aryl Claisen rearrangement of prenyl ether 185	196
Scheme 5.3: Ion exchange of aryl prenyl ether 186 and IR-1061 and IR-1048 laser dye	199
Scheme 5.4: Single solvent ion exchange of aryl prenyl ether 186 and IR-780 laser dye	203
Scheme 5.5: Halide exchange of IR-780 from iodide to chloride anion via ion exchange resin	204
Scheme 5.6: Single solvent ion exchange of chlorinated IR-780 and DMA aryl ether	205
Scheme 5.7: Synthesis of the 2 nd generation NIR GUMBO 203	208
Scheme 5.8: Synthesis of compound 184	209
Scheme 5.9: Synthesis of compound 186	210
Scheme 5.10: Preparation of IR-780 ⁺ Cl ⁻ through ion exchange chromatography	211

LIST OF ABBREVIATIONS AND SYMBOLS

ABC	ATP-binding cassette
Aboa	(3 <i>S</i> ,4 <i>S</i> ,5 <i>E</i> ,7 <i>E</i>)-3-amino-8-(4-bromophenyl)-4-hydroxy-6-methyl-5,7-octadienoic acid
Ac	acetyl
AcOH/HOAc	acetic acid
ADMET	absorption, distribution, metabolism, excretion, toxicity
Ahad	(2 <i>S</i> ,4 <i>R</i>)- α -amino- γ -hydroxy adipic acid
Alloc	allyloxycarbonyl
ANSI	American national standards institute
ATP	adenosine triphosphate
Bn	benzyl
Boc	<i>tert</i> -butoxycarbonyl
BsCM	<i>B. subtilis</i> chorismate mutase
Bz	benzoyl
<i>t</i> -Bu	<i>tert</i> -butyl
Cbz	benzyloxycarbonyl
CDI	carbonyldiimidazole
ClAc	chloroacetyl
DMA	1,1-dimethylallyl
DMAP	4-dimethylaminopyridine

DME	dimethoxyethane
DMF	dimethylformamide
DMSO	dimethylsulfoxide
DNA	deoxyribonucleic acid
Dpa	2,3-diaminopropionic acid
EcCM	<i>E. Coli</i> chorismate mutase
ee	enantiomeric excess
EDC	1-ethyl-3-(3-dimethylaminopropyl)carbodiimide hydrochloride
eHyAsn	<i>erythro</i> - β -hydroxyasparagine
EPR	enhance permeation and retention
Et	ethyl
Et ₂ O	diethylether
Fmoc	9-fluorenylmethyloxycarbonyl
GUMBOS	groups of uniform materials based on organic salts
τ -HAL	tau-histidinoalanine
π -HAL	pi-histidinoalanine
HAL	histidinoalanine
HPLC	high-performance liquid chromatography
IC ₅₀	half maximal inhibitory concentration
Im	imidazole

<i>i</i> -Pr	isopropyl
LiHMDS	lithium hexamethyldisilazide
MDR	multidrug resistance
Me	methyl
MeCN	acetonitrile
NIR	near-infrared
NIS	<i>N</i> -iodosuccinamide
NMR	nuclear magnetic resonance
Pac	phenacyl
PBB	<i>p</i> -bromobenzyl
PCB	<i>p</i> -chlorobenzyl
PDGF	platelet-derived growth factor
PEG	polyethylene glycol
PG	protecting group
P-gp	<i>p</i> -glycoprotein
Ph	phenyl
PhFl	9-phenylfluorenyl
PIB	<i>p</i> -iodobenzyl
PMB	paramethoxybenzyl
POPC	palmitoyloleoylphosphatidylcholine

PSMA	prostate-specific membrane antigen
RTIL	room temperature ionic liquids
SEM	2-(trimethylsilyl)ethoxymethyl
SOCl ₂	thionyl chloride
SPION	superparamagnetic iron oxide nanoparticles
SPPS	solid phase peptide synthesis
SPR	surface plasmon resonance
TBDMS	tert-butyldimethylsilyl
TBDPS	tert-butyldiphenylsilyl
TCE	trichloroethyl
TFA	trifluoroacetic acid
THF	tetrahydrofuran
TLC	thin layer chromatography
TML	trimethyl lock
TMSCHN ₂	trimethylsilyldiazomethane
Trt	triphenylmethyl
ts/TS	transition state

Standard 3 letter codes are utilized throughout the document for amino acids

ABSTRACT

The theonellamides are a family of compounds distinguished by their crosslinking τ -histidinoalanine (τ -HAL) residue. Part one of this dissertation details the synthesis of an orthogonally protected τ -HAL building block that will be incorporated into a total synthesis of theonellamide C. Selective deprotection of each amine and acid of this orthogonally protected building block is also demonstrated.

Various reaction partners for the assembly of τ -histidinoalanine were explored. One approach involved the coupling of *N*-Fmoc- β -iodoalanine benzyl ester and (*N* _{π} *im*)-blocked histidine nucleophiles including a fused bicyclic urea and a Boc-His(*N* _{π} -Pac)-OMe. While the imidazolium salts were identified by mass spectrometry, elimination of the iodide group was a major side reaction.

Successful nucleophilic opening of a five-membered ring sulfamidate (derived from Fmoc-*D*-Ser-OH) by Boc-*L*-His-OTCE led to preparation of a regiochemically and stereochemically pure τ -HAL derivative. Thus, a new set of orthogonal protecting groups have been identified: Fluorenylmethyloxycarbonyl (Fmoc), 2,2,2-trichloroethyl ester (TCE), *tert*-butyl carbamate (Boc), and benzyl (Bn) ester.

Part two of this dissertation outlines the synthesis of a trimethyl lock-based prodrug model system, wherein photothermal activation of a salt containing a cationic near-IR dye and an anionic prodrug, releases a paclitaxel side-chain fragment via a tandem aryl Claisen rearrangement and lactonization.

The prodrug model system was prepared via coupling of the paclitaxel sidechain alcohol to an acid with a pendant substrate for the rearrangement-lactonization. Claisen

rearrangement studies in various solvent systems on the release of the paclitaxel fragment demonstrated that aqueous alcoholic solutions of allyl aryl ethers accelerated the rearrangement relative to hydrocarbon solvents, temperatures achieved were still too high to be feasible in biological systems. The 1,1-dimethylallyl group was identified for its rate-accelerating properties. Studies of the Claisen rearrangement in aqueous methanol demonstrated that the aryl dimethylallyl ether derivatives rearranged significantly faster than the unsubstituted allyl ethers. Moreover, electron donating groups facilitated the reaction.

A salt was formed from a cationic near-IR laser dye (IR-780) and 1-(1,1-dimethylallyl ether)-4-benzoic acid, then suspended as nanoparticles in water. Photothermal studies of these aggregated species are underway.

CHAPTER 1: τ -HISTIDINOALANINE AND CHALLENGES ASSOCIATED WITH ITS SYNTHESIS IN A TETRAORTHOAGONALLY PROTECTED FORMAT

1.1 Introduction: Occurrence and Origin

Fujimoto and co-workers first isolated histidinoalanine (HAL) in 1982 from the hydrolyzate of human dentin.¹ This *bis*-amino acid cross-link can exist as two regioisomers, τ -HAL and π -HAL (Figure 1.1). HAL is derived from the covalent linkage formed between a dehydroalanine residue coupling to the τ - or π -nitrogen on the imidazole of the histidine side chain.

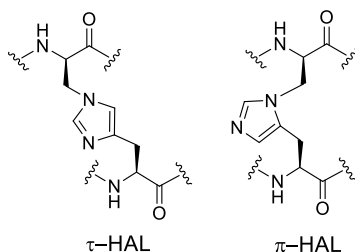
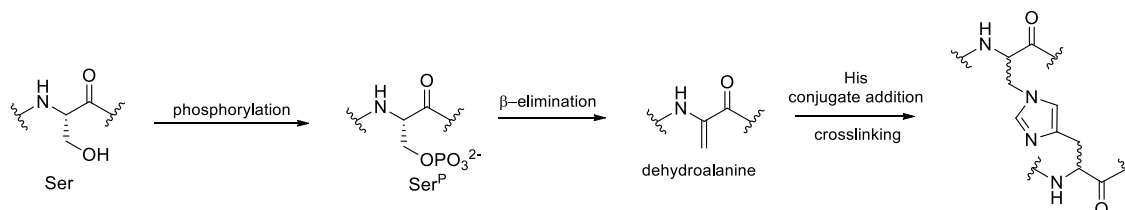


Figure 1.1: τ -Histidinoalanine and π -Histidinoalanine

Since its initial isolation, HAL has been identified from numerous sources.² Histidinoalanine is produced in milk products that have been heated and/or treated with alkali, and although the nutritional consequences are unknown, their stability to enzymes and subsequent increase in protein crosslinks suggests some nutritional consequences.³ τ -Histidinoalanine also occurs naturally in human tissues including dentin,⁴ eye cataracts,⁵ and connective tissue. The connective tissue that is responsible for the elasticity in the aorta, which is important for blood pressure, loses its elasticity over time. This has been attributed to production of *bis*-amino acids like τ -HAL.¹ Furthermore, HALs have been identified in phosphoproteins of bivalve mollusks where they are integral to the process of mineralization.⁶

Although the biosynthetic mechanism of the formation of HAL is not known, it is structurally similar to lanthionine and lysinoalanine crosslinks whose biosynthesis has been studied extensively.⁷ Presumably, serine is phosphorylated to give phosphoserine that readily undergoes β -elimination to yield dehydroalanine. By analogy to the formation of lanthionine and lysinoalanine, in which thiol and ϵ -amino nucleophiles add to dehydroalanine, a histidine residue is conjugated to dehydroalanine, giving histidinoalanine (Scheme 1.1).



Scheme 1.1: Formation of HAL by serine phosphorylation followed by β -elimination; then conjugate addition

1.2 HAL in Theonellamides

Theonellamide C is bicyclic peptide from the genus *Theonella*, and is part of a family of cyclic peptides, theonellamides A-F (Figure 1.2). These *bis*-macrocyclic peptides are characterized by structurally interesting amino acid residues, such as (2*S*,4*R*)- α -amino- γ -hydroxy adipic acid (Ahad), (3*S*,4*S*,5*E*,7*E*)-3-amino-8-(4-bromophenyl)-4-hydroxy-6-methyl-5,7-octadienoic acid (Aboa), and *erythro*- β -hydroxyasparagine (eHyAsn). To-date, there has been no reported total synthesis of a theonellamide, and there has been only one partial synthesis of theonellamide F.⁸ Therefore, most bioactivity studies have been conducted using theonellamide F obtained from isolation which has demonstrated moderate cytotoxic activity towards P388 leukemia cells with IC₅₀ values ranging from 0.9-5.0 μ g/mL.⁹

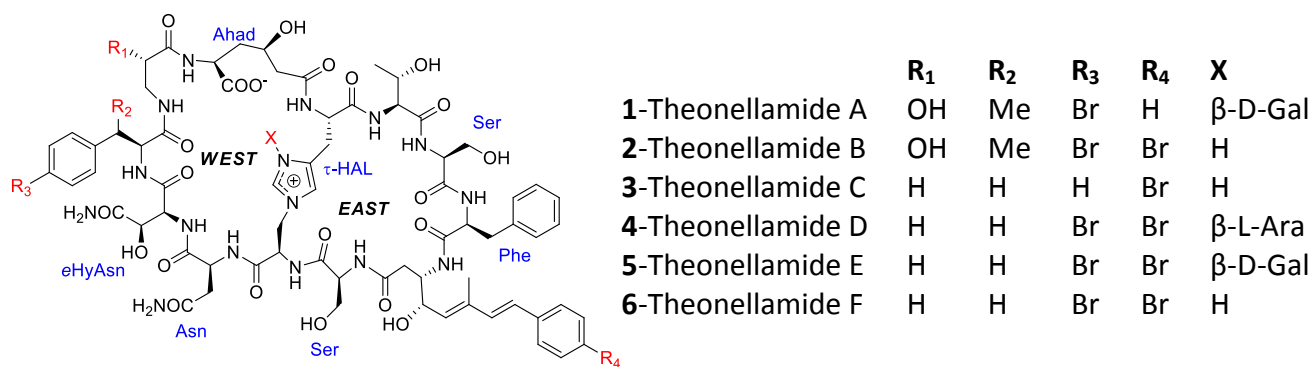


Figure 1.2: Theonellamides A-F

Other natural products originating from the genus *Theonella* have shown promising therapeutic potential.¹⁰ These marine natural products include theopalauamide,¹¹ and theonegramide.¹² Biological and mechanistic studies of the structurally-related theopalauamide have helped shed light on the mode of action of the theonellamides. Theonellamides have been shown to recognize lipid bilayers containing cholesterol and other 3β-hydroxysterols and induce 1,3-β-D-glucan biosynthesis¹³ – both of which likely play a role in the compound's antifungal and cytotoxic effects. To understand how theonellamides recognize and bind to lipid bilayers containing 3β-hydroxysterols, the Yoshida group conducted surface plasmon resonance (SPR) and solid-state ²H-NMR experiments on theonellamide A and its interactions with sterols and palmitoylcholine (POPC) liposomes containing cholesterol, ergosterol, or epicholesterol (Figure 1.3).¹⁴

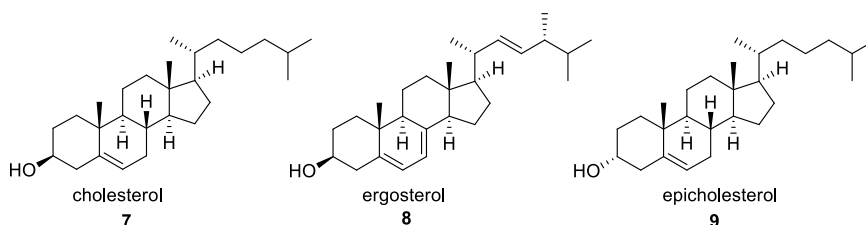
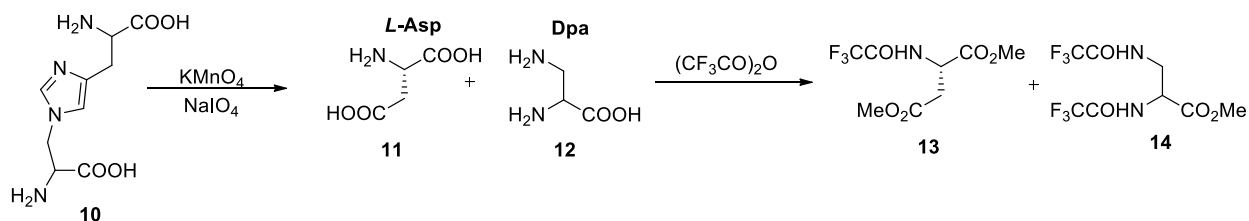


Figure 1.3: Structures of 3β-hydroxysterols cholesterol and ergosterol, and 3α-hydroxysterol epicholesterol

Though they were not able to identify the exact chemistry behind these interactions, they were able to demonstrate that theonellamide A undergoes a two-step binding process with lipid bilayers, which involves interaction with cholesterol and other 3β -hydroxysterols present. Because the theonellamides' proposed mode of action is different from polyene antibiotics which also interact with sterols, the Yoshida group postulated that theonellamides "could be a new tool for exploring the function and localization of sterols in cells".¹⁴

Theonellamides A-F all share a τ -HAL bridging residue. In theonellamides A, D, and E a sugar moiety is attached to the π -nitrogen of the imidazole of the bridge (Figure 1.2) yet seems to play no significant role in the biological activity studied to-date. The τ -regioisomer of HAL was found to be the only regioisomer in degradation studies of the theonellamides performed by Matsunaga *et al* (Scheme 1.2).^{9a}



Scheme 1.2: Degradation studies of histidinoalanine

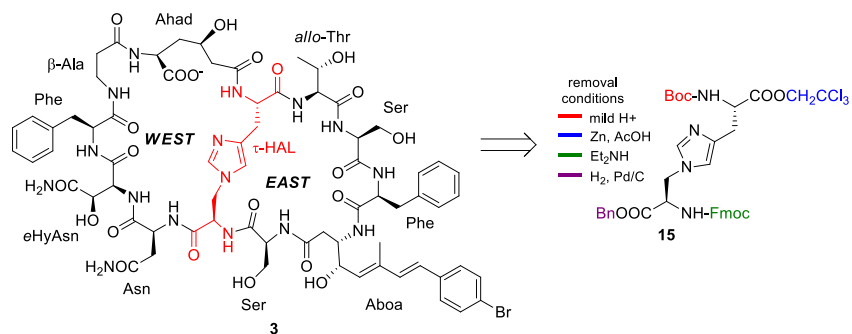
Histidinoalanine was treated with $\text{KMnO}_4/\text{NaIO}_4$, resulting in the cleavage of the imidazole ring to yield a 1:1 mixture of 2,3-diaminopropionic acid (Dpa) (11) and L-aspartic acid (Asp) (12). Subsequent esterification of the amino acid residues, and treatment with trifluoroacetic anhydride gave derivatives 13 and 14. The isolation of L-Asp designated L-His as the naturally occurring stereoisomer, while an isolated 1:1 (D:L) mixture of Dpa, and later a 3:1 mixture strongly suggests D as the major isomer. These stereochemical assignments were

further confirmed by derivatization of compounds **11** and **12** using both enantiomers of Marfey's reagent.^{8b}

1.3 Retrosynthetic Analysis: Need for Flexible Protecting Group Strategy

Our goal is to synthesize theonellamide C via conjugation of the eastern hemisphere and western hemisphere to the τ -HAL bridging residue. Synthetically, theonellamide C is the easiest congener to make, requiring the synthesis of the least number of amino acids, prior to fragment condensations and cyclizations. The theonellamides are the only example of a HAL residue in a well-defined molecule. The three fragments include τ -HAL, and two pentapeptides, one which includes Aha and eHyAsn and makes up the western hemisphere and the other which includes Aboa and encompasses the eastern hemisphere (Scheme 1.3). τ -Histidinoalanine has four reactive sites, two carboxylic acids, and two amino groups. To direct coupling at the desired sites, the reactivity of each site needs to be selectively activated and deactivated using protecting groups. Therefore, it's crucial to develop an orthogonally protected building block that will be flexible enough to facilitate assembly of the eastern and western hemispheres without competition of free functional groups present.

We chose four different protecting groups, each with different deprotection mechanisms: trichloroethyl (TCE) and benzyl (Bn) esters along with fluorenylmethyloxycarbonyl (Fmoc), and *tert*-butoxycarbonyl (Boc) carbamates (Scheme 1.3). In principle, each could be selectively removed in the presence of one another.



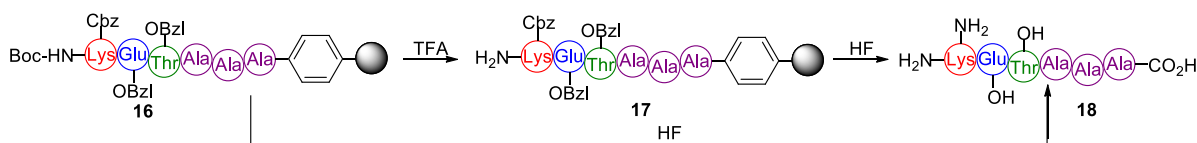
Scheme 1.3: Retrosynthetic analysis of τ -histidinoalanine

1.4 The Concept of Orthogonality vis-à-vis Protecting Groups

In 1977, Merrifield introduced the term 'orthogonal' to designate "[orthogonal protecting groups are] classes of protecting groups which are removed by differing chemical mechanisms. Therefore they can be removed in any order and in the presence of the other classes".¹⁵ This distinction was made from the Boc and benzyl peptide protecting group chemistry¹⁶ that utilized what is now called the modulated lability approach, which is the process of chemoselectively removing two structurally similar functionalities under one mechanism with graduated reactivity. Since then, with the discovery of more robust, tunable protecting groups the application of the term 'orthogonality' has expanded in organic chemistry to include orthogonal coupling reactions, chromatic orthogonality (a differentiation based on the wavelength of light) and orthogonal chemical ligation of peptides (which we will not review) just to name a few.

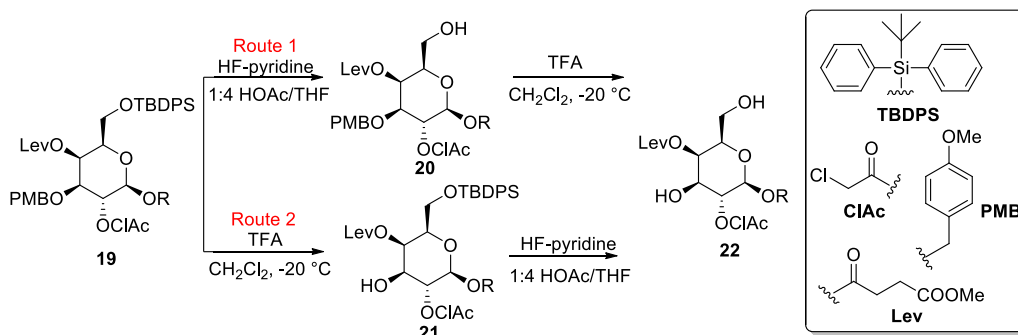
In a recent communication,¹⁷ Wong and Zimmerman outlined three main categories of chemoselective transformations involving two orthogonal protecting groups. The three categories: modulated lability, sequential orthogonal, and simultaneous transformations. As mentioned earlier, Merrifield made use of the modulated lability approach during his original

solid phase peptide synthesis. He was able to exploit the reactivity difference between Boc carbamates and benzyl esters towards TFA which is 1000:1. By increasing the acidity, Merrifield was able to remove the Boc group followed by the benzyl ester, while using a stronger acid (*i.e.*, HF) removed both groups simultaneously and cleaved the peptide from the resin (Scheme 1.4).¹⁵



Scheme 1.4: Example of a modulated Lability Transformation – a ribonuclease A (RNase A) fragment with a Boc N-terminus, and benzyl-based resin C-terminus

Sequential orthogonal transformation is the ability to arrive at the same substrate regardless of the order of reagents used to effect deprotections. The Zhang group demonstrated sequential orthogonal transformations during their deprotection of a tetra-orthogonally protected galactose building block (Scheme 1.5).¹⁸ Building block **19** was treated with HF-pyridine to remove the TBDPS group, leaving the chloroacetyl (ClAc) ester intact. Subsequent treatment with TFA gave the diol **22** (Scheme 1.5, Route 1). If Route 2 was carried out first, the PMB ether would be cleaved first. Subsequent TBDPS cleavage by HF-pyridine would also give diol **22**.

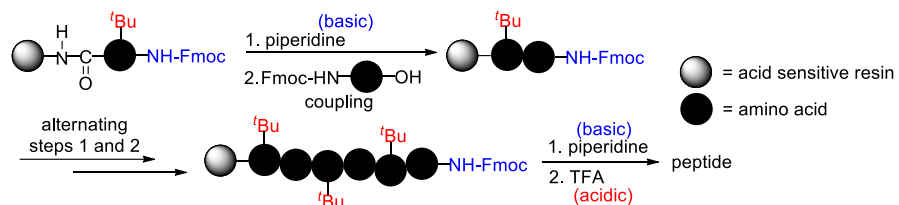


Scheme 1.5: Sequential Orthogonal Transformation

1.4.1 Two Dimensional Orthogonal Protection: Solid Phase Peptide Synthesis

The most widely-utilized orthogonal protecting group pair in modern solid phase peptide synthesis is the Fmoc carbamate and *tert*-butyl ester, ether, and carbamate. Development of the Fmoc group by Carpino¹⁹ has made the Fmoc-*tert*-butyl strategy a mainstay in modern solid phase peptide synthesis,²⁰ due to the differing chemical mechanisms of deprotection. Fmoc is cleaved with mild base via β -elimination, and *tert*-butyl based functional groups by acid hydrolysis. This qualifies as a sequential orthogonal transformation. Sequential orthogonal transformation fits within the traditional definition that Merrifield put forth, in that using different reagents one can selectively deprotect a protecting group without affecting the other.

The importance of orthogonal protecting group chemistry is readily illustrated in solid phase peptide synthesis (SPPS). SPPS follows a series of steps, outlined generically in Scheme 1.6. In the Fmoc/*tert*-butyl strategy representation below, the α -nitrogen of the amino acid is protected with the Fmoc group and the side chain functional groups can be protected as *tert*-butyl ethers, esters, or carbamates. This is an orthogonal protection system, since the side chain protecting groups can be removed without displacing the *N*-terminal protection and vice versa. For the sake of brevity we have highlighted the Fmoc/*tert*-butyl strategy, but understand that there are a myriad of protecting groups used in solid phase peptide synthesis. This strategy has allowed large libraries of very large peptides to be synthesized using automation, with large pharmaceutical companies relying on this classical protection method to synthesize important compounds in a short amount of time.²⁰



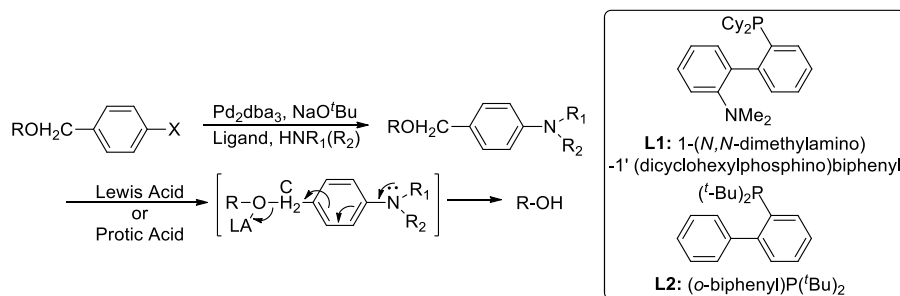
Scheme 1.6: A general representation of an Fmoc *tert*-butyl strategy (orthogonality based) for peptide synthesis

1.5 Examples of the Use of Orthogonal Protecting Group Strategies

So far we have only discussed two dimensional orthogonal protection systems. There are inherent challenges in developing higher dimensional systems, mainly mechanistic compatibility and reagent sensitivity. There are a few examples in the literature where different groups have attempted to tackle this challenge with varying degrees of success.

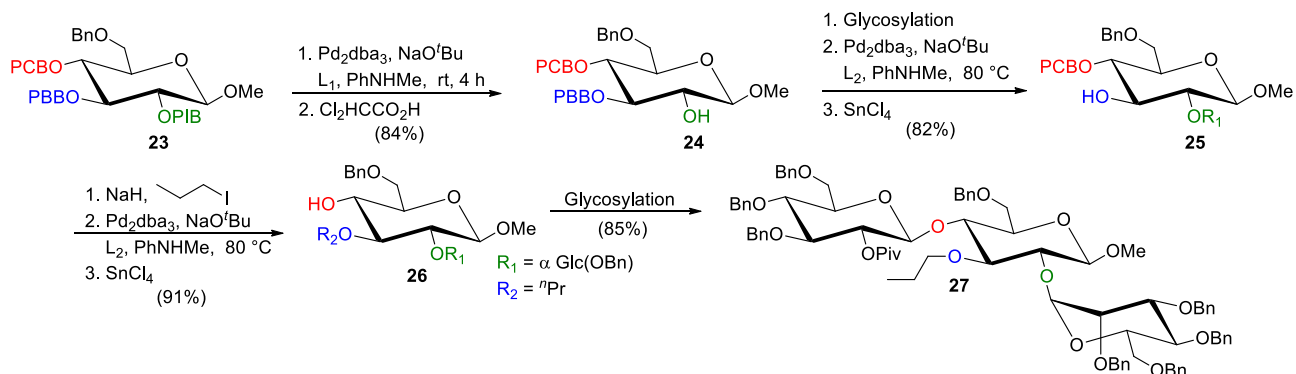
1.5.1 Tunable Protecting Groups

One technique is to create custom protecting groups which has the advantage of tunability and tailoring the group with specific properties. This strategy is particularly useful for oligosaccharides and monosaccharides which bear multiple hydroxyl groups with similar reactivity. The Seeberger group adopted this strategy when developing halogenated benzyl ether protecting groups for the synthesis of differentiated monosaccharides.²¹ These specialized protecting groups allowed the assembly of a branched trisaccharide through facile conversion of the blocking groups into labile arylamines by Pd-catalyzed amination (Scheme 1.7).²² They started with a penta-orthogonally protected monosaccharide **23**, with three of the hydroxyl groups bearing the *para*-halogenated benzyl protecting groups. They found that different combinations of arylamines, acids, and phosphine ligands could selectively deprotect each *para*-halogenated benzyl ether protecting group in the presence of each other.



Scheme 1.7: Protocol for Pd-catalyzed amination and subsequent acid-catalyzed cascade deprotection

They attributed the differences in reactivity to the relative reactivities of the halogens. To convert the PIB group into its aryl group, they used *N*-methyl aniline, L₁, and a protic acid to give free alcohol **24**, which was then glycosylated. These steps were repeated twice more, using L₂, *N*-methylaniline, and SnCl₄ to remove the PBB group (Scheme 1.8, **25**), and morpholine, L₂, and SnCl₄ to remove the PCB group (Scheme 1.8, **26**). Glycosylation gave compound **27** in 85% yield.

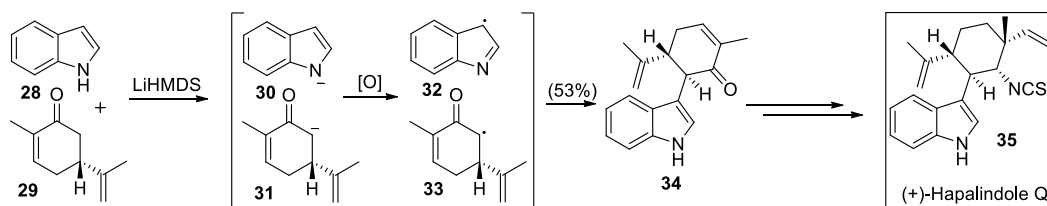


Scheme 1.8: PCB: *p*-chlorobenzyl, PBB: *p*-bromobenzyl, PIB: *p*-iodobenzyl, L₁: 1-(*N,N*-dimethylamino)-1'-(dicyclohexylphosphino)biphenyl, L₂: (*o*-biphenyl)P(^{*t*}Bu)₂ as defined in Scheme 1.7

Even though these specialized protecting groups are highly applicable for the synthesis of saccharides, they are limited to one type of functional group (hydroxyl) and would have limited utility on a more diverse molecule, bearing more diverse functional groups.

1.5.2 Protecting Group Free Synthesis

Another popular strategy is to avoid protecting groups and instead rely on the inherent chemoselectivity of different functional groups. It is generally understood that each protecting group adds two overall steps to a synthetic route for introduction and removal. Eliminating protecting/leaving group manipulations could streamline the assembly of many complex natural products and biomolecules. Through the use of carefully screened reagents and reaction conditions Baran and coworkers were able to demonstrate the protecting-group free synthesis of hapalindole Q (Scheme 1.9).²³ To achieve this they had to develop new reaction chemistry. It was found that treating a solution of indole (**28**) and carvone (**29**) with lithium hexamethyldisilazide (LiHMDS) gave anions **30** and **31**. Subsequent oxidation in the same pot with copper (II) 2-ethylhexanoate led to a direct coupling of the indole C3 position and the α -position of carvone to produce compound **34**. Previous synthesis of this molecule employed a tosyl protecting group on the nitrogen in the indole ring. However, this led to more steps in the synthesis.²⁴

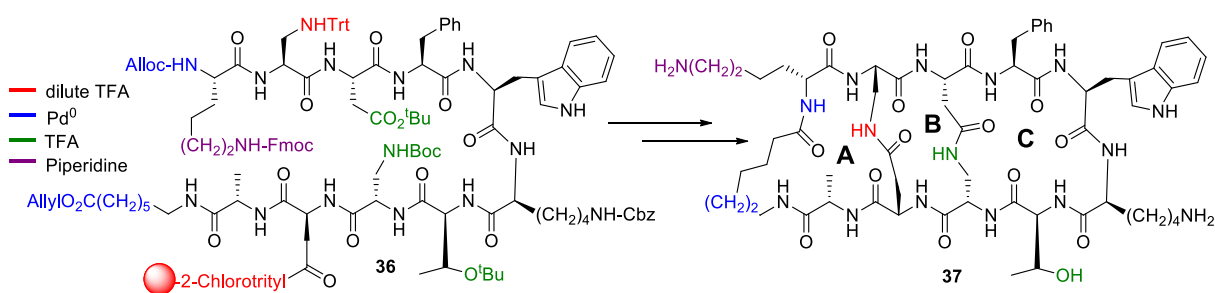


Scheme 1.9: LiHMDS-mediated coupling of carvone and indole

Adhering to this strategy has allowed Baran to synthesize many natural products without the use of protecting groups. However, Baran admitted that the use of protecting groups has led to the successful synthesis of many targeted compounds of varying complexity. He states that the masking of competitive reaction sites offers an increased level of security and predictability, which are important factors in total synthesis. With the large library of protecting groups that have been developed, numerous creative retrosynthetic disconnections can be proposed for a molecule that would most likely be impossible without the assistance of protecting groups.²⁵

1.5.3 Higher Dimensional Orthogonal System: Utilizing Resins as a Temporary Masking Group

In 1996, Hirschmann and Smith published the synthesis of a tricyclic homodetic peptide, an analog of somatostatin.²⁶ They employed a 5-dimensional orthogonal amino protection strategy,^{26,27} a sequential selective deprotection of carboxyl groups alongside their amino partner. They chose three different amine/carboxyl protecting group partners; Boc/*tert*-Butyl, Alloc/Allyl, and trityl/2-chlorotrityl solid support (Scheme 1.10).



Scheme 1.10: Deprotection scheme for precursor to Somatostatin analog **37** with protecting groups

They treated peptide **36** with dilute TFA (0.75%) which resulted in the cleavage of the trityl amine/2-chlorotrityl resin pair. This generated the unprotected Asp side chain and the β -

amino group of 2,3-diaminopropionic acid (Dpr). Following macrolactamization, the Alloc/Allyl pair of protecting groups was cleaved using palladium, followed by ring formation to generate ring A. Next, a stronger solution of TFA was used to remove the Boc/*tert*-butyl protecting groups, and subsequent coupling led to formation of the final two rings B and C. Lastly, mild base, followed by hydrogenolysis gave the analog of somatostatin.

The complexity of this peptide required a multi-stage protecting group strategy that combined modulated lability and solid phase support. This method of using resins in tandem with traditional solution phase protecting groups allows for the development of higher dimensional orthogonal systems that wouldn't be accessible by traditional protecting groups alone. It should be noted that each group was taken off in a pre-determined sequence. The order could not be rearranged without affecting multiple protecting groups, which in practice prevents this method from being a true orthogonal protection scheme.

1.6 *bis*-Amino Acid Protecting Group Strategies

Lanthionines are closely related to histidinoalanine in biological assembly and role as a bridging crosslink. Because the literature for syntheses of τ -HAL is very scarce, we looked to syntheses of lanthionines as our most relevant building blocks for four-dimensional protecting group strategies for *bis*-amino acids.

Lanthionines consist of two alanine residues that are linked at their β -carbons by a thioether bridge (Figure 1.4). In lantibiotics,^{28,29} these lanthionines are embedded within cyclic peptides. In addition, lantibiotics typically (but not always) contain the unsaturated amino acids 2,3-dehydroalanine (Dha) and (*Z*)-2,3-dehydrobutyrine (Dhb).

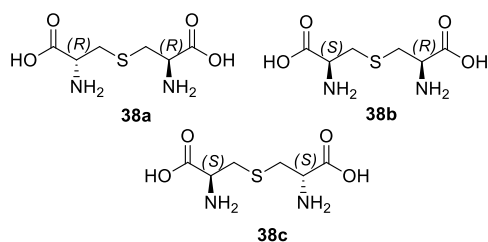


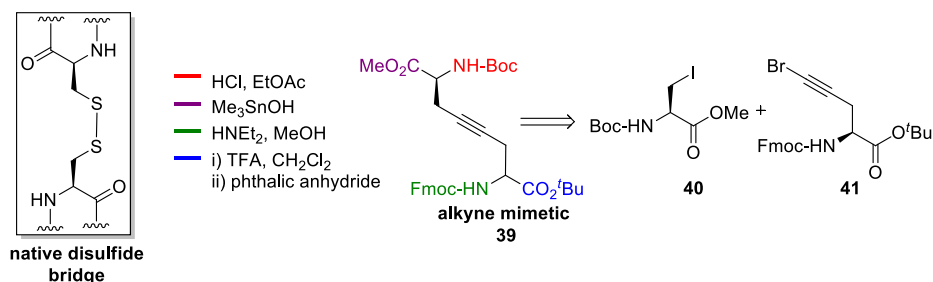
Figure 1.4: Lanthione stereoisomers **38a**, **38b**, **38c**

Lantibiotics are a class of post-translationally modified peptides that belong to the family of *bacteriocins*. They possess high antimicrobial activity against a broad spectrum of Gram-positive bacteria, including food pathogens (*e.g. Listeria monocytogenes*) and organisms that exhibit resistance to conventional antibiotics (i.e. methicillin-resistant *Staphylococcus aureus* or *MRSA* and vancomycin-resistant *Enterococcus* or *VRE*). They have been used in a variety of applications including food preservation.

Lanthionines are a great test case for orthogonal protection methods because they contain two carboxyl and two amino groups. There have been numerous publications on the synthesis of orthogonally protected lanthionines,³⁰ with the most commonly used protecting group schemes including Boc/Fmoc/Alloc carbamates and trityl (Trt) amine for *N*-protection in combination with *tert*-Bu/allyl esters. Each approach has used one or more strategies discussed previously. While two-dimensional systems using traditional orthogonal protecting groups are common (*i.e.*, Boc/Fmoc carbamates), achieving quadruple orthogonal protection has proven to be more challenging.

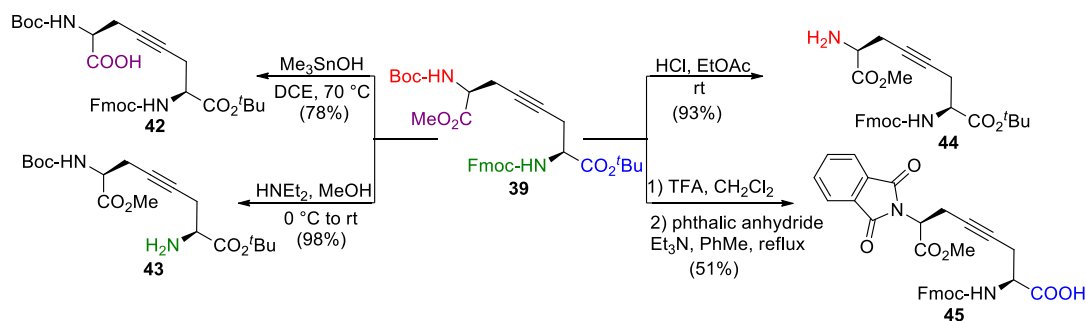
In 2011, Tadd and co-workers reported the synthesis of an “orthogonally” protected disulfide bridge mimetic (Scheme 1.11), to be used in the synthesis of bicyclic peptides with non-terminal disulfide bridges.³¹ To assemble the mimetic with the alkyne bridge, the Tadd

group coupled a β -iodoalanine **40** with bromoacetylene **41** using copper-mediated organozinc/haloalkyne chemistry.



Scheme 1.11: Disulfide bridge mimetic with protecting groups and deprotection conditions

To demonstrate the orthogonality of this building block, deprotections were conducted (Scheme 1.12). They cleaved the Fmoc carbamate using standard diethylamine conditions, giving the free amine **43** in high yield. They cleaved the methyl ester under hydrolysis conditions in good yield using trimethyltin hydroxide, conditions pioneered by the Nicolaou group with impressive selectivity for methyl esters.³² Because the Boc and *tert*-butyl groups are removed via the same chemical mechanism, they had to use a modulated lability approach to ensure chemoselectivity. They were able to cleave the Boc carbamate selectively using a 1 M HCl solution. Due to Boc carbamates being more acid-sensitive than *tert*-butyl esters, selectivity cannot be achieved, resulting in cleavage of both acid-labile groups when alkyne **39** was treated with TFA. To mediate this, they reprotected the free amine as a phthalimide group to leave only the free acid. This work-around does provide them with four substrates with different points of attachment, but due to the double cleavage, adds another two steps and does not classify this collection of protecting groups as completely orthogonal.



Scheme 1.12: Deprotection scheme of disulfide bridge mimetic

The Tabor group claimed a “quadruply”-orthogonal protecting group strategy for the on-resin synthesis of overlapping lanthionine rings.³³ They synthesized two lanthionine fragments, one with Pd(0) labile protecting groups: Alloc carbamate and allyl ester. The other bore fluoride labile groups: 2-trimethylsilylethoxycarbonyloxy (Teoc) carbamate, and trimethylsilylethyl (TMSE) ester (Figure 1.5). Both substrates had orthogonal transient Fmoc groups.

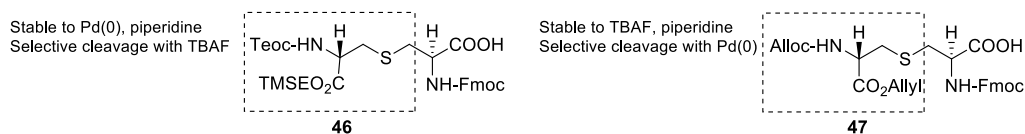
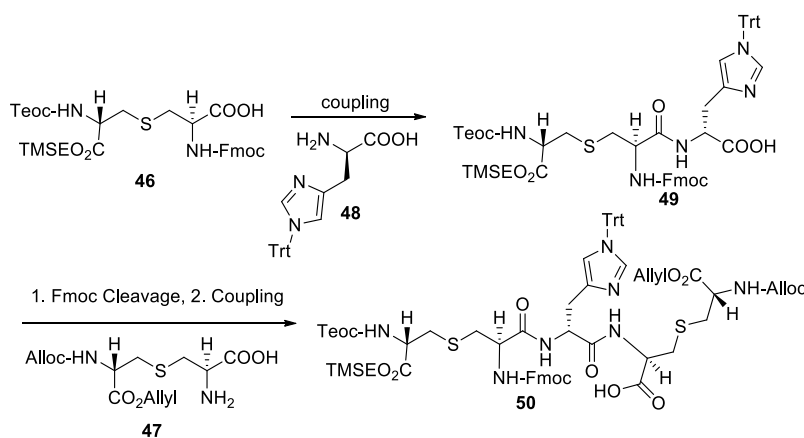


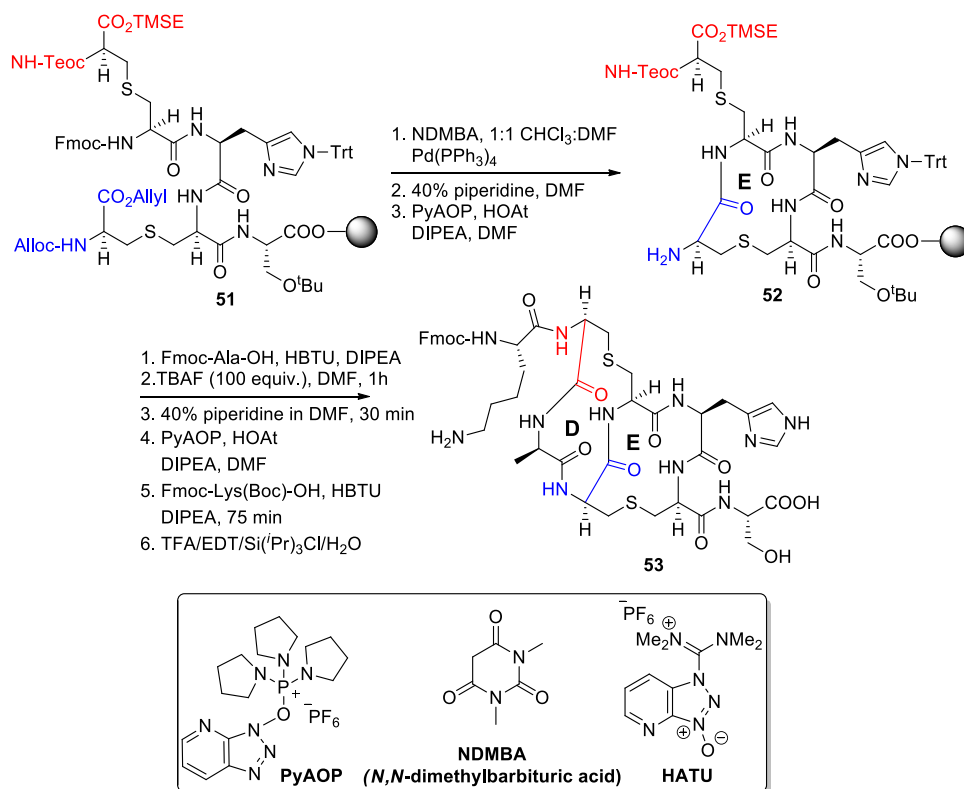
Figure 1.5: "Orthogonal" lanthionine Fragments

The carboxylic acid functional group in compound **46** was coupled to a *N*-im-trityl protected histidine residue to give tripeptide **49**. After the cleavage of the Fmoc group, lanthionine **47** was introduced to afford **50**, which contains two orthogonally protected LAN residues (Scheme 1.13).



Scheme 1.13: Precursor to orthogonally protected linear peptide **50**

Compound **50** was used to acylate a resin-bound serine, affording compound **51** (Scheme 1.14). In this approach, the Tabor group used an acid-labile Wang resin as one of their protecting groups, as well as the modulated lability concept.



Scheme 1.14: Quadruply 'orthogonally' protected peptide fragment **51**

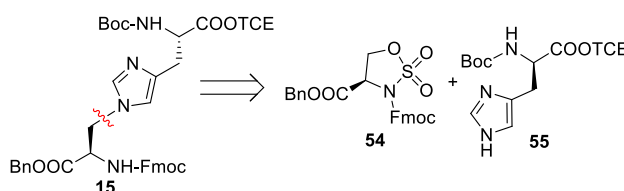
The allyl ester and Alloc carbamate were cleaved simultaneously using Pd(0), followed by cleavage of the Fmoc moiety with a piperidine solution. (7-Azabenzotriazol-1-yloxy)tripyrrolidinophosphonium hexafluorophosphate (PyAOP) facilitated ring closure to form ring E of the Nisin fragment, viz. compound **52**. An alanine residue was added at the *N*-terminus and then one hundred equivalents of TBAF was employed to cleave the Teoc and TMSE groups. This allowed for the second ring closure facilitated by PyAOP to form ring D. The remaining free amine was coupled to Fmoc-Lys(Boc)-OH, followed by global deprotection of the remaining acid-labile protecting groups to give ring fragments D and E of nisin.

If these protecting groups are removed in a pre-determined order they could be considered orthogonal to each other, however that does not fit the stringent definition put forth by Merrifield. Notably, the TMSE group is susceptible to acidic reagents, and would not remain intact under the global deprotection conditions.

1.7 Toward an Orthogonally Protected τ -HAL

To our knowledge, there is no synthesis of a tetra-orthogonally protected τ -histidinoalanine in the literature. While routes to differentially protected *bis*-amino acids have been explored, these routes either require a lengthy synthesis, solid-phase methods in conjugation with solution-phase protecting groups, or do not possess the appropriate protecting groups for our study. In Chapter 2, we will discuss the concise synthesis of an orthogonally protected τ -HAL. Nucleophilic opening of a 5-membered ring sulfamidate by an orthogonally protected histidine nucleophile allows for facile preparation of a regiochemically and stereochemically pure τ -HAL derivative (Scheme 1.15).

A new set of orthogonal protecting groups have been proposed: fluorenylmethyloxycarbonyl (Fmoc), 2,2,2-trichloroethyl ester (TCE), *tert*-butyl carbamate (Boc), and benzyl (Bn) ester. These protecting groups are ideally suited for the preparation of diamino dicarboxylic acids. Selective deprotection of each amine and acid of this orthogonally protected building block is also demonstrated in Chapter 2.



Scheme 1.15: Retrosynthetic analysis of the synthesis of orthogonally protected τ -HAL

1.8 References

1. Fujimoto, D., Hiramata, M., Iwashita, T. "Histidinoalanine, a new crosslinking amino acid, in calcified tissue collagen" *Biochem. Biophys. Res. Commun.* **1982**, *104*, 1102-1106.
2. Taylor, C. M., Wang, W. "Histidinoalanine: a crosslinking amino acid" *Tetrahedron* **2007**, *63*, 9033-9047.
3. Henle, T., Walter, A. W., Klostermeyer, H. Z. "Detection and identification of the cross-linking amino acids $N\tau$ and $N\pi$ -(2'-amino-2'-carboxy-ethyl)-L-histidine ("histidinoalanine", HAL) in heated milk products" *Lebensm.-Unters. Forsch.* **1993**, *197*, 114-117.
4. Cloos, P. A. C., Jensen, A. L. "Age-related de-phosphorylation of proteins in dentin: a biological tool for assessment of protein age," *Biogerontology* **2000**, *1*, 341-356.
5. Kanayama, T., Miyayama, Y., Horiuchi, K., Fujimoto, D. "Detection of the crosslinking amino acid, histidinoalanine, in human brown cataractous lens protein," *Exp. Eye. Res.* **1987**, *44*, 165-169.
6. Sass, R. L., Marsh, M. E. "Histidinoalanine: a naturally occurring crosslinking amino acid," *Methods Enzymol.* **1984**, *106*, 351-355.
7. a) Zhu, Y., Gieselmann, M. D., Zhou, H., Averin, O., van der Donk, W. A. "Biomimetic studies on the mechanism of stereoselective lanthionine formation" *Org. Biomol. Chem.* **2003**, *1*, 3304-3315 b) Goto, Y., Li, B., Claesen, J., Shi, Y., Bibb, M. J., van der Donk, W. A. "Discovery of unique lanthionine synthetases reveals new mechanistic and evolutionary insights" *PLoS* **2010**, *8*, e1000339

8. a) Tohdo, K., Hamada, Y., Shioiri, T. "Synthesis of the northern hemisphere of theonellamide F: A bicyclic dodecapeptide of marine origin" *Synlett* **1994**, *4*, 250 b) Tohdo, K., Hamada, Y., Shioiri, T. "Synthesis of the southern hemisphere of theonellamide F, a bicyclic dodecapeptide of marine origin" *Synlett* **1994**, *4*, 247-249.
9. a) Matsunaga, S., Fusetani, N., Hashimoto, K., Walchli, M. "Theonellamide F. A novel antifungal bicyclic peptide from a marine sponge *Theonella* sp" *J. Am. Chem. Soc.* **1989**, *111*, 2582-2588. b) Matsunaga, S., Fusetani, N. "Theonellamides A-E, cytotoxic bicyclic peptides, from a marine sponge *Theonella* sp." *J. Org. Chem.* **1995**, *60*, 1177-1181.
10. Wright, A. E. "The Lithistida: Important sources of compounds useful in biomedical research" *Curr. Opin. Biotechnol.* **2010**, *21*, 801-807.
11. Schmidt, E. W., Bewley, C. A., Faulkner, D. J. "Theopalauamide, a bicyclic glycopeptide from filamentous bacterial symbionts of the lithistid sponge *Theonella swinhoei* from Palau and Mozambique" *J. Org. Chem.* **1998**, *63*, 1254-1258.
12. Bewley, C. A., Faulkner, D. J. "Theonegramide, an antifungal glycopeptide from the Philippine lithistid sponge *Theonella swinhoei*" *J. Org. Chem.* **1994**, *59*, 4849-4852.
13. Nishimura, S., Arita, Y., Honda, M., Iwamoto, K., Matsuyama, A., Shirai, A., Kawasaki, H., Kakeya, H., Kobayashi, T., Matsunaga, S., Yoshida, M. "Marine antifungal theonellamides target β -hydroxysterol to activate Rho1 signaling" *Nat. Chem. Biol.* **2010**, *6*, 519-526.
14. Espiritu, R. A., Matsumori, N., Murata, M., Nishimura, S., Kakeya, H., Matsunaga, S., Yoshida, M. "Interaction between the marine sponge cyclic peptide theonellamide A and sterols in lipid bilayers as viewed by surface plasmon resonance and solid-state ^2H nuclear magnetic resonance" *Biochemistry*, **2013**, *52*, 2410-2418.
15. Barany, G., Merrifield, R.B. "A new amino protecting group removable by reduction. Chemistry of the dithiasuccinoyl (Dts) function," *J. Am. Chem. Soc.* **1977**, *99*, 7363-7365.
16. Merrifield, R. B. "Solid phase synthesis" *Angew. Chem. Int. Ed. Engl.* **1985**, *24*, 799-810.
17. Wong, C-H., Zimmerman, S. C. "Orthogonality in organic, polymer, and supramolecular chemistry: from Merrifield to click chemistry" *Chem. Commun.* **2013**, *49*, 1679-1695.
18. Wong, C.-H., Ye, X.-S., Zhang, Z. "Assembly of oligosaccharide libraries with a designed building block and an efficient orthogonal protection-deprotection strategy" *J. Am. Chem. Soc.* **1998**, *120*, 7137-7138.
19. Carpino, L. A., Han, G. Y. "The 9-fluorenylmethoxycarbonyl amino-protecting group" *J. Org. Chem.* **1972**, *37*, 3404-3409.
20. Amblard, M. Fehrentz, J. A., Martinez, J., Subra, G. "Methods and protocols of modern solid phase peptide synthesis" *Mol. Biotechnol.* **2006**, *33*, 239-254.

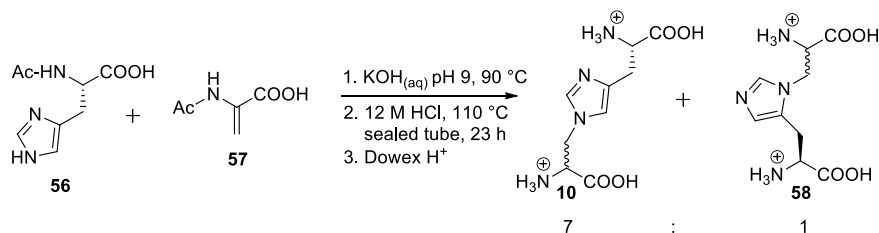
21. Plante, O. J., Buchwald, S. L., Seeberger, P. H. "Halobenzyl ethers as protecting groups for organic synthesis" *J. Am. Chem. Soc.* **2000**, *122*, 7148-7149.
22. Aranyos, A., Old, D. W., Kiyomori, A., Wolfe, J. P., Sadighi, J. P., Buchwald, S. L. "Novel electron-rich bulky phosphine ligands facilitate the palladium-catalyzed preparation of diaryl ethers" *J. Am. Chem. Soc.* **1999**, *121*, 4369-4378.
23. Baran, P. S., Richter, J. M. "Direct coupling of indoles with carbonyl compounds: Short, enantioselective, gram-scale synthetic entry into the hapalindole and Fischer indole alkaloid families" *J. Am. Chem. Soc.* **2004**, *126*, 7450-7451.
24. Kinsman, A. C., Kerr, M. A. "Total synthesis of (\pm)-hapalindole Q" *Org. Lett.* **2001**, *3*, 3189-3191.
25. Young, I. S., Baran, P. S. "Protecting-group free synthesis as an opportunity for invention" *Nature Chem.* **2009**, *1*, 193-205.
26. Hirschmann, R., Yao, W., Arison, B., Maechler, L., Rosegay, A., Sprengeler, P. A., Smith III, A. B. "The first synthesis of a tricyclic homodetic peptide employing coordinated orthogonal protection" *Tetrahedron Lett.* **1996**, *37*, 5637-5640.
27. Hirschmann, R., Yao, W., Arison, B., Maechler, L., Rosegay, A., Sprengeler, P. A., Smith, A. B. III "Synthesis of the first tricyclic homodetic peptide. Use of coordinated orthogonal deprotection to achieve directed ring closure" *Tetrahedron* **1998**, *54*, 7179-7202.
28. a) Guder, A., Wiedemann, I., Sahl, H-G. "Posttranslationally modified bacteriocins--the lantibiotics" *Biopolymers* **2000**, *55*, 62-73 b) Harpp, D. N., Gleason, J. G. "Preparation and mass spectral properties of cystine and lanthionine derivatives. Novel synthesis of *L*-lanthionine by selective desulfurization" *J. Org. Chem.* **1971**, *36*, 73-80 c) Dugave, C., Menez, A. "Synthesis of natural and non-natural orthogonally protected lanthionines from *N*-tritylserine and allo-threonine derivatives" *Tetrahedron: Asymm.* **1997**, *8*, 1453-1465.
29. Willey, J. M., van Der Donk, W. A. "Lantibiotics: Peptides of diverse structure and function" *Annu. Rev. Microbiol.* **2007**, *61*, 477-501.
30. a) Bregant, S., Tabor, A. B. "Orthogonally protected lanthionines: synthesis and use for the solid-phase synthesis of an analogue of nisin ring C" *J. Org. Chem.* **2005**, *70*, 2430-2438. b) Cobb, S. L., Vederas, J. C. "A concise stereoselective synthesis of orthogonally protected lanthionines and β -methyllanthionine" *Org. Biomol. Chem.* **2007**, *5*, 1031-1038. c) Martin, N. I. "Concise preparation of tetra-orthogonally protected (2S-6R)-lanthionines" *J. Org. Chem.* **2009**, *74*, 946-949.
31. Tadd, A. C., Meinander, K., Luthman, K., Wallén, E. A. A. "Synthesis of orthogonally protected disulfide bridge mimetics" *J. Org. Chem.* **2011**, *76*, 673-675.

32. Nicolaou, K. C., Estrada, A. A., Zak, M., Lee, S. H., Safina, B. S. "A mild and selective method for the hydrolysis of esters with trimethyltin hydroxide" *Angew. Chem. Int. Ed.* **2005**, *44*, 1378-1382.
33. Mothia, B., Appleyard, A. N., Wadman, S., Tabor, A. B. "Synthesis of peptides containing overlapping lanthionine bridges on the solid phase: An analogue of rings D and E of the lantibiotic nisin" *Org. Lett.* **2011**, *13*, 4216-4219.

CHAPTER 2: SYNTHESIS OF ORTHOGONALLY PROTECTED τ -HISTIDINOALANINE

2.1 Early Syntheses of τ -HAL

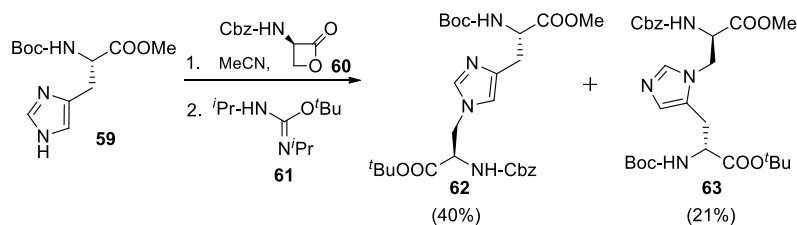
In 1977, Finley and Friedman prepared what was presumed to be histidinoalanine via conjugate addition of histidine to a dehydroalanine electrophile, however they did not report any characterization data.¹ It wasn't until 1993 that characterization data and experimental details were reported for HAL by Henle *et al.*² They assembled HAL in a manner similar to their predecessors through conjugate addition of the imidazole of Ac-L-His-OH (**56**) to 2-acetylaminoacrylate (**57**) (Scheme 2.1), with the major isomer, τ -HAL, being formed preferentially in a 7:1 ratio with π -HAL.



Scheme 2.1: Synthesis of HAL isomers via conjugate addition of Ac-L-His-OH (**56**) to 2-acetylaminoacrylate (**57**)

Between the years 1992-1994, the Shioiri group published a series of papers documenting their progress towards the total synthesis of theonellamide F.³ They acknowledged the τ -HAL regioisomer as the naturally occurring bridging residue for theonellamide F, and thus outlined a stereoselective synthesis. They moved away from previous syntheses that utilized dehydroalanine derivatives, as that approach leads to mixtures of regioisomers due to lack of selectivity of the τ -nitrogen of the histidine nucleophile and stereoisomers at C α of the alanine residue. Instead, they employed an enantiopure serine β -

lactone as their electrophile, and Boc-*L*-His-OMe, which has an established stereocenter, as their nucleophile alleviating the stereoisomers issue (Scheme 2.2).



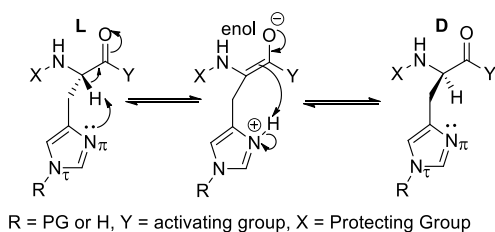
Scheme 2.2: Shioiri's synthesis of HAL regioisomers employing a β -lactone

Even though the Shiori group's β -lactone yielded a single stereoisomer of each regioisomer, it did not achieve regioselectivity in terms of the imidazole, giving a 2:1 mixture of regioisomers in favor of τ -HAL. Their efforts highlight two main challenges one faces when synthesizing τ -histidinoalanine, mainly histidine's unprotected imidazole side-chain; with its innate nucleophilicity that leads to regioisomers and controlling stereoselectivity at the α -carbon of the alanine residue.

As discussed previously, histidine contains an imidazole side-chain with two nucleophilic nitrogens, the τ -nitrogen and π -nitrogen. Although the τ -nitrogen is less hindered and will be the preferred nucleophilic nitrogen atom on the imidazole ring, the π -nitrogen is more basic and will compete for alkylation which results in a mixture of regioisomers.⁴ To combat this lack of differential reactivity, the π -nitrogen can be blocked with a protecting group to force alkylation at the τ -nitrogen. The π -nitrogen reactivity can also be blocked by intramolecular ring formation between $N\alpha$ and the imidazole side-chain. These two methods will be explored later in the chapter.

Moreover, another benefit of blocking the π -nitrogen is preventing epimerization at the α -carbon. Histidine derivatives with an unprotected π -nitrogen are prone to epimerization

during peptide coupling or during protection of the histidine carboxyl group (Scheme 2.3).⁵ Substitution at the τ -nitrogen, as in τ -HAL, alters the basicity of the π -nitrogen and may diminish its ability to abstract the α -proton. Blocking the reactivity completely would be the best case scenario.⁶



Scheme 2.3: Intramolecular base-catalyzed proton abstraction and enolization mechanism proposed by Jones *et al.*⁵

Retention of the $C\alpha$ -stereocenter of the alanine residue during the formation of τ -HAL can be ensured via an enantiopure electrophile. One example of enantiopure electrophiles are β -cation synthons with an enantiopure $C\alpha$ installed, which includes β -iodoalanine electrophiles and cyclic sulfamidates.

2.2 Synthetic Routes to τ -HAL

In pursuit of a tetra-orthogonally protected τ -histidinoalanine (Figure 2.1), different routes were explored to reach a functional building block in a practical and efficient manner. Each route has pros and cons and will be discussed in more detail.

2.2.1 Protected β -Iodoalanine Electrophile and Bicyclic Urea

We investigated a π -nitrogen blocking strategy (Scheme 2.4) that was explored previously by former group members, Julia Strautmann and Weihua Wang. In 2004, Strautmann prepared cyclic urea **65**⁷ and β -lactone **66**.⁸

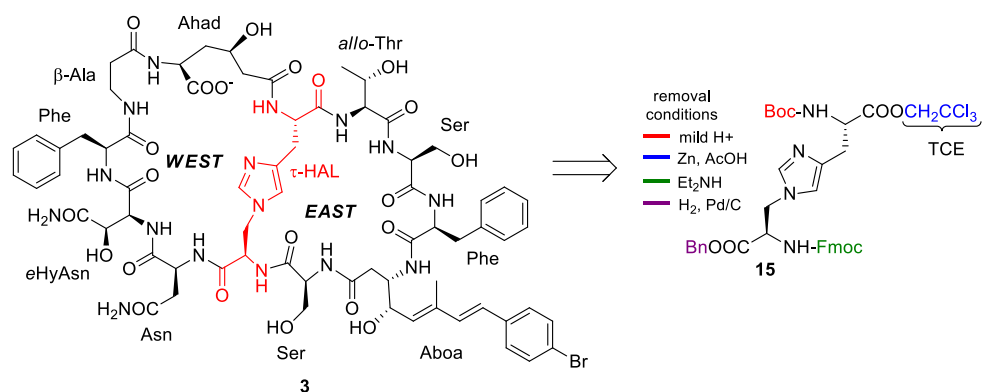
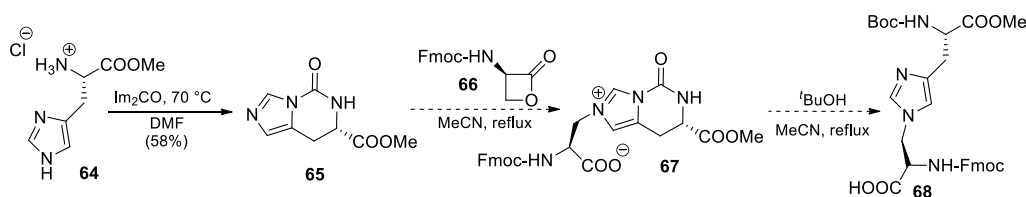


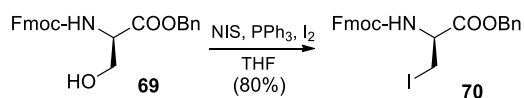
Figure 2.1: Protecting group strategy for tetra-orthogonal τ -HAL

In 2006, Wang repeated these preparations and investigated their coupling to give τ -HAL. Unfortunately, while salt **67** and ring-opened product **68** were identified by mass spectrometry, neither compound was ever isolated pure or in more than trace amounts.



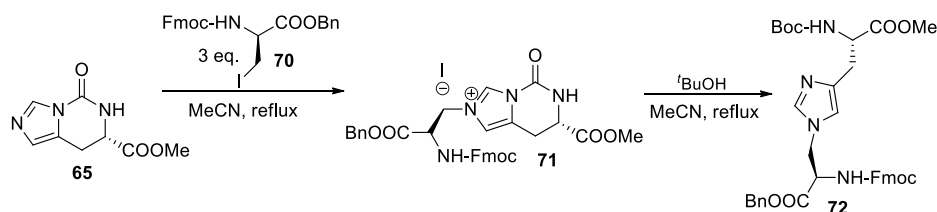
Scheme 2.4: Synthesis of τ -HAL **68** via nucleophilic ring opening of fused bicyclic urea derivative

We decided to revisit this route, substituting a β -iodoalanine for the β -lactone. A halide salt was hypothesized to be more stable than an intramolecular salt. Additionally, this approach would eliminate the step to install a carboxylate protecting group after opening of the β -lactone. Since iodide is considered the best leaving group amongst the halides, we sought procedures that would convert the Fmoc-*D*-Ser-OBn into its β -iodoalanine derivative. This reaction was achieved using a modified Appel reaction (Scheme 2.5) according to Kawai *et al.*⁹



Scheme 2.5: Synthesis of *N*-fluorenylmethoxycarbonyl- β -iodoalanine

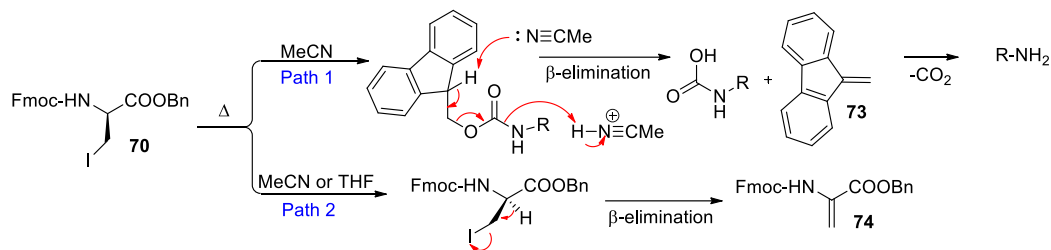
Urea **65**, previously prepared by Strautmman, was coupled with iodide **70** to give the imidazolium salt **71** (Scheme 2.6). Imidazolium salts can be stable, and are quite frequently used as ionic liquids.¹⁰ However, some of these salts are hygroscopic, and not stable at room temperature. Fortunately, no degradation of compound **71** was observed at room temperature over several days. The identity of **71** was confirmed by NMR spectroscopy and mass spectrometry. The urea ring was then opened with *tert*-butanol to yield the τ -HAL derivative **72**.



Scheme 2.6: Synthesis of τ -HAL via bicyclic urea opening with *tert*-butanol

During the initial coupling between urea **65** and iodide **70**, it was observed that upon concentration of **71** from the reaction solvent, dibenzofulvene (**73**) (Scheme 2.7, Path 1) would precipitate out, which was confirmed by NMR. It was postulated that the Fmoc-protecting group was being cleaved at elevated temperatures during the course of the reaction. A report by Höck *et al.* supports this observation and states that “in DMF, DMSO, and MeCN, Fmoc groups can be cleaved at temperatures of 120 °C or higher”.¹¹ The reaction solvent was changed to THF because of solubility, lower boiling point, and lack of basic functionality. Switching to THF reduced Fmoc cleavage, but did not prevent β -elimination of hydrogen iodide

(Scheme 2.7, Path 2). Heating of *N*-fluorenylmethoxycarbonyl- β -iodoalanine benzyl ester (**70**) increases the rate of spontaneous β -elimination and presumably competes with salt formation.



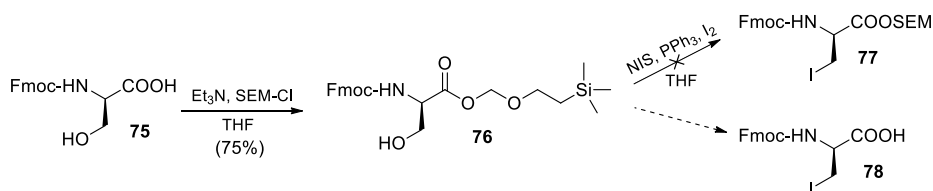
Scheme 2.7: Based mediated β -elimination of Fmoc moiety (Path 1) and iodine (Path 2)

Because of this, the temperature of the reaction was eventually decreased from 90 °C to room temperature. It should be noted that whenever thermal conditions were used the urea was never completely consumed, thus requiring three equivalents of iodide to compensate for losses due to competing side-reactions. When the reaction was run at room temperature, the number of equivalents could be reduced because side-reactions were less competitive with the desired coupling.

With a clearer understanding of the reaction chemistry of β -iodoalanine electrophiles and cyclic ureas, another protecting group was sought for the serine carboxylic acid. *N*-Fmoc- β -iodoalanine benzyl ester **70** provided a suitable building block for the synthesis of τ -HAL derivative **72**, however by Merrifield's definition of orthogonality, τ -HAL **72**, with its methyl group, is not considered to be orthogonally protected.

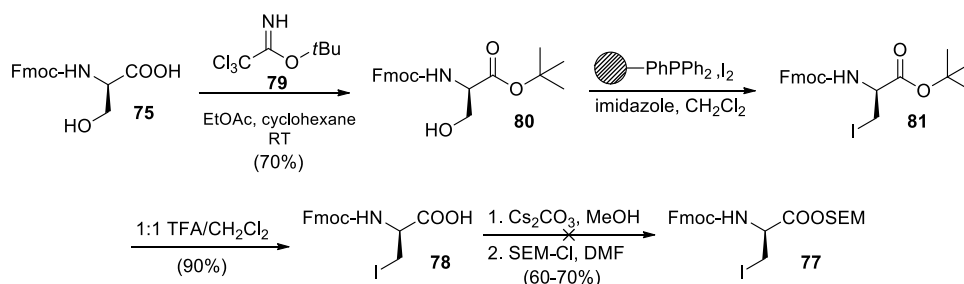
We employed an alternative protecting group for the serine carboxylic acid - β -(trimethylsilyl)ethoxymethyl (SEM) - which should give us more flexibility in the order of deprotection events in the assembly of theonellamide C. While SEM is most often removed by fluoride, Joullié and co-workers have reported that this protecting group can be removed from

complex peptide substrates under mild conditions using MgBr_2 .¹² We attempted to prepare the SEM ester derivative of Fmoc-*D*-Ser-OH in an analogous manner to *N*-Fmoc β -iodoalanine benzyl ester. Standard iodination of **76** resulted in cleavage of the SEM ester to give **78** (Scheme 2.8). Analysis by NMR showed that compound **78** was identical to *N*-Fmoc- β -iodoalanine prepared by Benito and Meldal.¹³



Scheme 2.8: Attempted synthesis of *N*-Fmoc- β -iodoalanine SEM ester

It is thought that the iodine is behaving as a mild Lewis acid. To circumvent this, we proposed changing the order of events, via synthesis of the *N*-Fmoc β -iodoalanine free acid and then protection as a SEM ester (Scheme 2.9).



Scheme 2.9: Attempted synthesis of *N*-Fmoc- β -iodoalanine SEM ester

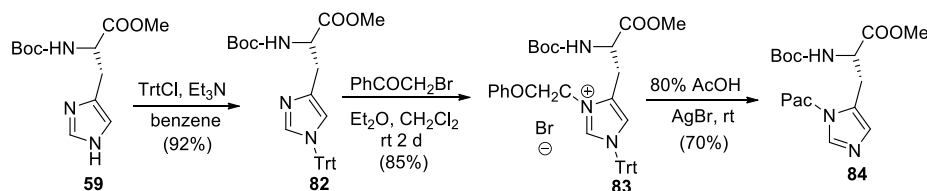
Unfortunately, the SEM ester protection resulted in β -elimination with stronger bases (*i.e.* triethylamine), and standard coupling procedures (*viz.* EDC, DMAP, SEM-OH).

Since our attempts to prepare compound **77** were unsuccessful, and coupling with the bicyclic urea required high temperatures which eliminated the iodide group, we decided to

investigate another π -blocked nucleophile that would hopefully require far less harsh conditions for coupling.

2.2.2 β -Iodoalanine Electrophile and (N_{im}), π -Blocked Histidine Nucleophiles

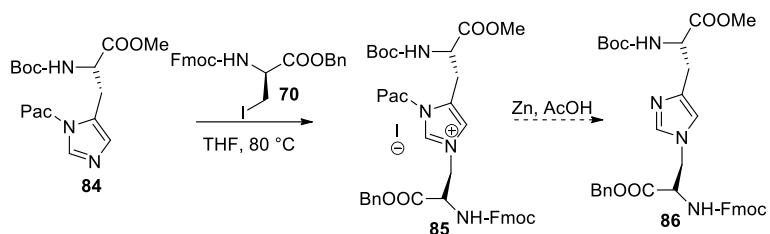
We explored the phenacyl (Pac) group¹⁴ in another π -nitrogen blocking strategy (Scheme 2.10). Due to the lack of protecting groups available that selectively protect the π -nitrogen of the imidazole ring, this necessitated protection of the τ -nitrogen first (**82**), then the π -nitrogen (**83**), and finally deprotection of the τ -nitrogen to give **84**. Although the route to **84** is circuitous, this approach ought to assure regioselectivity for reaction of the τ -nitrogen during HAL formation. We chose the Pac group because of its orthogonality to our desired protecting groups already installed on histidine **59**. It is removed via reduction by zinc in the presence of acetic acid. Compound **84** is a known compound and was made following the procedures of Fletcher *et al.*¹⁴



Scheme 2.10: Formation of Boc-His(π -Pac)-OMe

The next step was to couple compound **84** with β -iodoalanine **70** to yield an imidazolium halide salt and then subsequent removal of the Pac group (Scheme 2.11). Because β -iodoalanine is the electrophile in this reaction sequence, β -elimination under thermal conditions has posed a problem. However, when applying the optimized conditions developed for the bicyclic urea to this reaction sequence the desired salt was formed in trace amounts, as confirmed by mass spectrometry, but was never characterized by NMR. The salt, when

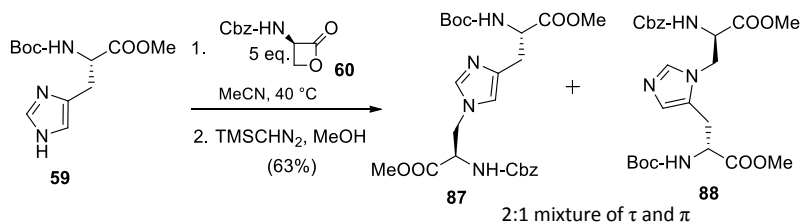
subjected directly to Zn, AcOH conditions gave a mixture of products from which the desired compound **86** could not be identified or isolated.



Scheme 2.11: Synthesis of τ -HAL via Boc-His(π -Pac)-OMe

2.2.3 Cyclic Sulfamidates

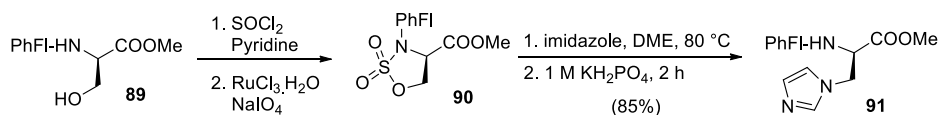
Samanthi T. De Silva, a previous group member, was tasked with reinvestigating Tohdo and Shioiri's approach (Scheme 2.12). The lack of details in the short communication required De Silva to interpret and develop related procedures; fortunately she was able to obtain yields that were comparable to previously reported results.



Scheme 2.12: Synthesis of HAL regioisomers via coupling of Boc-*L*-His-OMe (**59**) and Cbz-protected β -lactone (**60**)

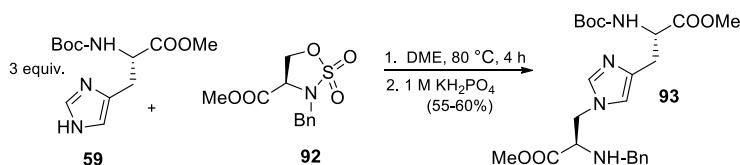
Poor τ -selectivity and the difficulty of separating the HAL regioisomers encouraged us to look for a less reactive electrophile that would give better τ -regioselectivity. We surveyed other alanine β -cation synthons and it seemed that sulfamidates, as introduced by Baldwin and co-workers,¹⁵ might provide a viable solution. These cyclic sulfamidates are similar to β -lactones in that the β -carbon in the ring is activated toward nucleophilic attack by the two electron-withdrawing groups at the α and β -carbons. Sulfamidates, such as **90** (Scheme 2.13), retain the

α -stereocenter that is derived from *D*-serine. Later, Lubell *et al.* demonstrated that an imidazole nucleophile can be used to open cyclic sulfamidates in good yield (Scheme 2.13).¹⁶



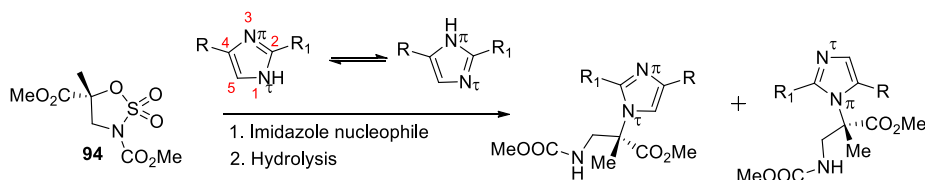
Scheme 2.13: Conditions for synthesis of sulfamidate, and imidazole nucleophilic ring opening

Taylor and De Silva reported the regioselective synthesis of τ -HAL (**93**) via the coupling of Boc-His-OMe (**59**) and sulfamidate **92** (Scheme 2.14).¹⁷ Boc-His-OMe was employed as a nucleophile in order to make a meaningful comparison with the β -lactone route. Analysis by NMR and HPLC confirmed the existence of only the τ -HAL isomer.



Scheme 2.14: Taylor and Thabrew De Silva HAL synthesis via coupling of Boc-His-OMe and sulfamidate **92**

In 2011, Avenzoa and co-workers reported theoretical studies on the reactivity and selectivity of substituted imidazoles with sulfamidates (Scheme 2.15).¹⁸ First they calculated the minimum energy of S_N2 transition states (TS) for three types of substituted imidazoles and sulfamidate **94** using the B3LYP/6-31G+ basis set. They found the nucleophilic ring opening process to be concerted and with full inversion of configuration at the quaternary carbon.



Scheme 2.15: Nucleophilic attack of sterically hindered sulfamidate by imidazole tautomers yields a mixture of regioisomers

They next investigated computationally the high site selectivity demonstrated by non-symmetrically substituted imidazoles. Complete selectivity for nucleophilic attack by the less hindered N_τ atom is a reflection of the great difference between the lowest energies of activation calculated for both reaction pathways labeled as ts1 and ts2 (Figure 2.2). They concluded that the steric interactions between the alkyl group at the C-4 position on the imidazole and the substituents at the quaternary center at the most crowded TS are most likely the reason for high selectivity.

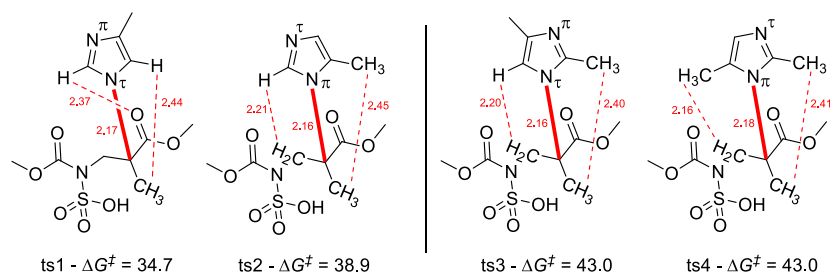
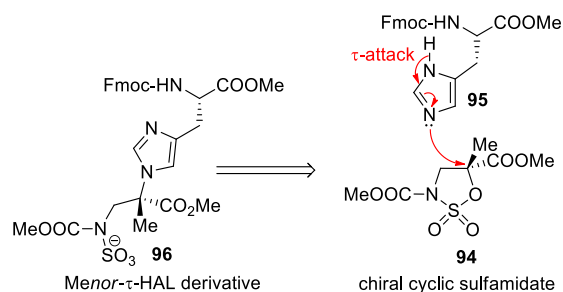


Figure 2.2: Minimum energy TS for some of the proposed pathways starting from sulfamidate **94** and mono- and disubstituted imidazoles. Distances are given in Å and activation energies (ΔG^\ddagger) in kcal/mol.

With these results in hand, they turned to the synthesis of *bis*-amino acid *Menor*- τ -HAL (Scheme 2.16), as this substrate could potentially be obtained by ring opening of cyclic sulfamidates with nitrogen or sulfur nucleophiles. They outlined the synthesis of *Menor*- τ -HAL (**96**), a *bis*-amino acid that bears a quaternary center (Scheme 2.16). This protected analog of τ -HAL involves the covalent linkage of the τ -nitrogen of the imidazole of histidine with the α -carbon of the β -alanine.

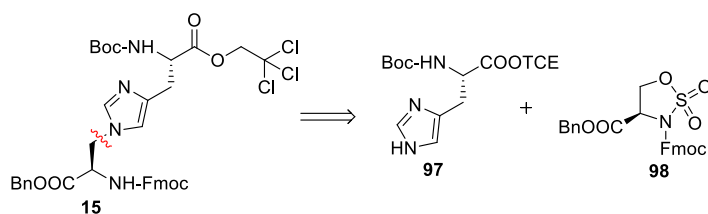


Scheme 2.16: Mechanism of sulfamidate ring opening by mono-substituted imidazole nucleophile

Subsequent synthesis of a τ -HAL analog and these computational studies served to further solidify our decision to continue pursuing cyclic sulfamidates as our preferred β -cation synthon.

2.3 Synthesis of Orthogonally Protected τ -HAL via a Cyclic Sulfamidate

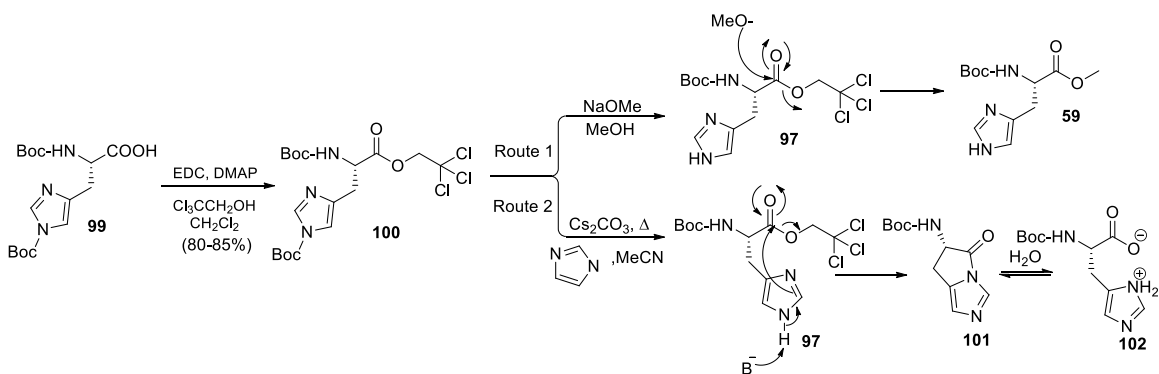
Ultimately, cyclic sulfamidates proved to be the superior electrophile, giving regioselectivity at the τ -nitrogen which permitted a successful synthesis of an orthogonally protected τ -HAL. Our approach featured the coupling of reaction partners Boc-*L*-His-OTCE (**97**) with a sulfamidate **98** derived from *N*-Fmoc-*D*-Ser-OBn (Scheme 2.17).



Scheme 2.17: Retrosynthetic analysis of orthogonally protected τ -HAL

Initial synthesis of Boc-*L*-His-OTCE involved a two-step process, which was modeled after earlier group efforts on a similar substrate. First, we installed the TCE protecting group, and then attempted to remove the imidazole Boc group (Scheme 2.18). The first step proceeded smoothly via EDC coupling in great yield to give Boc-*L*-His-(Boc)-OTCE (**100**). Unfortunately, attempted removal of the Boc group under NaOMe/MeOH conditions resulted

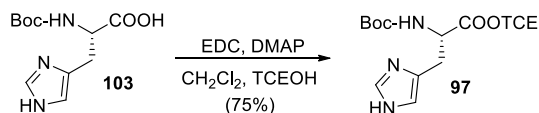
in transesterification of the TCE group by the methoxy group to give Boc-*L*-His-OMe (**59**) (Scheme 2.18, Route 1). This suggests that the trichloroethyl ester behaves as a good leaving group and is susceptible to nucleophilic attack. To prevent the transesterification side-reaction we switched to a milder, less nucleophilic base (Cs_2CO_3). However, using these conditions yielded trace amounts of the desired product **97**, but mostly an insoluble salt (Scheme 2.18, Route 2). Preliminary NMR analysis of the crude product suggests the formation of the reversible fused lactam byproduct **101** and intramolecular salt **102**. Tentative peak assignments agreed with previously reported data for the same compound by the Ogrel group,¹⁹ however no further purification or characterization was carried out.



Scheme 2.18: Transesterification of Boc-*L*-His(Boc)-OTCE (**96**) and intramolecular ring formation mechanisms

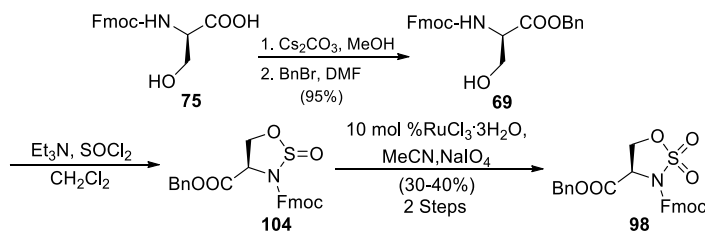
To avoid the use of bases and subsequent transesterification, we decided to employ a one-step synthesis that installs the TCE group using traditional EDC/DMAP conditions (Scheme 2.19). We were able to isolate the desired product in great yield. We postulated the high yield and absence of byproducts to the lack of strong base present to initiate the intramolecular ring formation. The imidazole side chain of histidine has a pKa of 6.0. The imidazole is inherently basic, but a weak base due to delocalization of the electron lone pair across the imidazole

nitrogens. Therefore, it is not strong enough on its own to initiate intramolecular ring formation (viz. **101**).



Scheme 2.19: Direct synthesis of Boc-*L*-His-OTCE (**97**)

With the histidine reaction partner in hand, we now turned our efforts to making the cyclic sulfamidate. We first started with commercially available Fmoc-*D*-Ser-OH (**75**) which reacted smoothly with benzyl bromide to give Fmoc-*D*-Ser-OBn (**69**) in high yield. This was converted to the 5-membered ring using SOCl_2 , and subsequent oxidation of the sulfamidite to give cyclic sulfamidate **98** as a colorless oil in 30-40% yield (Scheme 2.20).

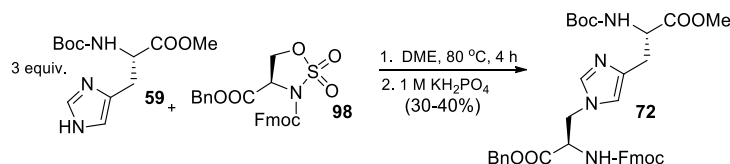


Scheme 2.20: Synthesis of cyclic sulfamidate **98** derived from Fmoc-*D*-Ser-OBn

It was found that sulfamidate **98** undergoes degradation at room temperature after 24 hours. When stored neat at 0 °C, degradation was observed after one week, which is in agreement with the Lubell group who reported similar observations for a homologous substrate.²⁰ We found that the sulfamidate was most stable when stored at 0 °C in a minimal amount of CHCl_3 or CH_2Cl_2 .

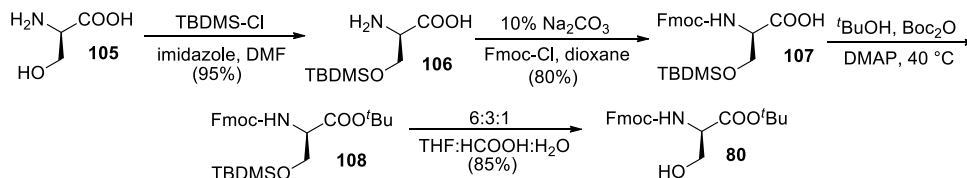
Initial attempts to recrystallize the cyclic sulfamidate failed. In previous work in our group¹⁷ it was observed that when the methyl ester sulfamidate **92** was recrystallized, the yields for the coupling reaction with Boc-*L*-His-OMe (**59**) increased to 55-60% (Scheme 2.14). In

contrast, when non-crystalline Fmoc-*D*-Ser-OBn derived cyclic sulfamidate was coupled with commercially available Boc-*L*-His-OMe, only 30-40% of τ -HAL derivative **72** was recovered (Scheme 2.21).



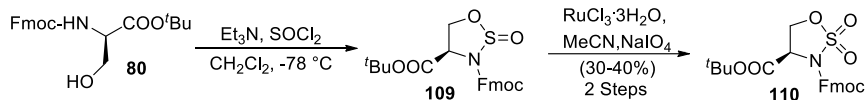
Scheme 2.21: Synthesis of τ -HAL **72** via coupling of sulfamidate **98** and Boc-*L*-His-OMe (**59**)

For this coupling reaction to be viable for scale up, steps were taken to optimize the formation of the sulfamidate reaction partner. We chose to do the optimization on a cyclic sulfamidate derived from Fmoc-*D*-Ser-O^{*t*}Bu due to initial reproducibility issues with sulfamidate **98**. Our rationale was that the *tert*-butyl group will lend stability to the sulfamidate because it is bulky and will shield the α -carbon from deprotonation and the β -carbon from nucleophilic attack. Fmoc-*D*-Ser-O^{*t*}Bu **80** was initially prepared according to Scheme 2.22.



Scheme 2.22: Synthesis of Fmoc-*D*-Ser-O^{*t*}Bu (**80**)

The alcohol was smoothly converted to a TBDMS ether in excellent yield, followed by Fmoc protection of the amino group in good yield. However protection of the carboxylic acid as the *tert*-butyl ester, a reaction that was not reproducible, and tedious purification of **107**, led to a modified synthesis^{21,22} (Scheme 2.23) giving Fmoc-*D*-Ser-O^{*t*}Bu in good yield.



Scheme 2.23: Synthesis of sulfamidate **110** derived from Fmoc-*D*-Ser-O^tBu

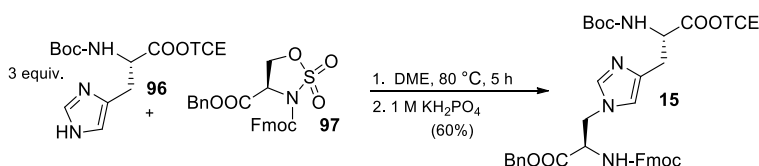
Initial sulfamidate preparation from Fmoc-*D*-Ser-O^tBu also gave poor yields of 30-40% (Scheme 2.23), however the product was crystalline as predicted. Encouraged by these results, efforts were made to optimize the cyclization/oxidation step.

In a related synthesis of cyclic sulfates, Kim and Sharpless²³ found that the presence of triethylamine or pyridine inactivated the ruthenium catalyst, greatly reducing the efficiency of the oxidation reaction. They reported that purification of the sulfite intermediate before oxidation increased reaction yields to greater than 90%. Table 2.1 outlines the steps taken to increase the yields for the cyclization/oxidation sequence depicted in Scheme 2.23. Entry 2 shows an increased yield to 60% and reduced oxidation time when chromatography was applied to the intermediate. A citric acid wash to neutralize the excess triethylamine before chromatography slightly decreased the overall yield, perhaps due to loss of product in work-up however it decreased the oxidation time to 1 h. A 5% citric acid wash alone proved to be the best conditions, giving cyclic sulfamidate in 74% yield.

Table 2.1: Optimization of cyclization/oxidation sequence in conversion of 80→109→110

Entry	Citric Acid Wash Sulfamidite 109	Chromatography Sulfamidite 109	Oxidation Sulfamidite 109	Yield Sulfamidate 110
1	No	No	16 h	30-40%
2	No	Yes	3 h	60%
3	Yes	Yes	1 h	50%
4	Yes (10%)	No	1 h	55%
5	Yes (5%)	No	1 h	74%

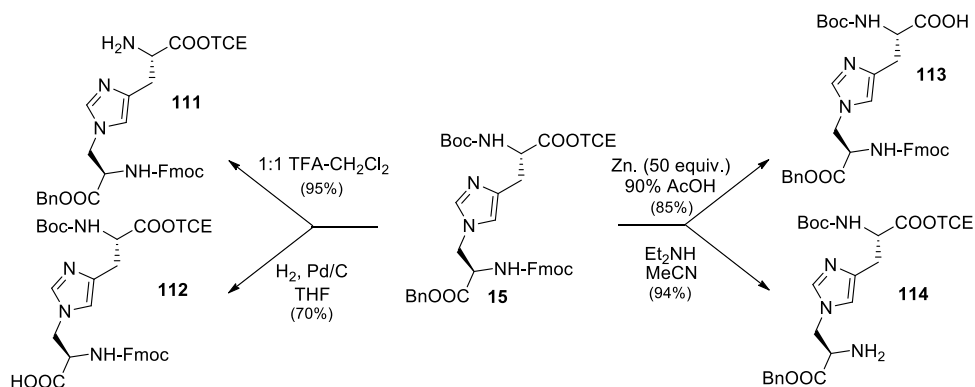
These optimized conditions were applied to the cyclization of Fmoc-*D*-Ser-OBn, and improved the yields to over 70%. With reproducible yields of Fmoc-*D*-Ser-OBn derived cyclic sulfamidate **97**, coupling of Boc-*L*-His-OTCE (**96**) and cyclic sulfamidate **97** was carried out to give orthogonally protected τ -HAL **15** in moderate yield (Scheme 2.24).



Scheme 2.24: Synthesis of tetra-orthogonally protected τ -HAL via coupling of Boc-*L*-His-OTCE and Fmoc-*D*-Ser-OBn derived sulfamidate

2.4 Orthogonal Deprotection

When reasonable quantities of τ -HAL **15** had been synthesized, deprotection studies were undertaken to demonstrate the orthogonality of the four protecting groups (Scheme 2.25). Each deprotection product was characterized by ^1H NMR and ^{13}C NMR, and mass spectrometry.



Scheme 2.25: Orthogonal deprotection conditions for τ -HAL **15**

All four derivatives were readily accessed using traditional deprotection conditions. Cleavage of the two amine protecting groups proceeded smoothly in high yield using 1:1 TFA-

CH₂Cl₂ to remove the Boc carbamate and diethylamine in acetonitrile to remove the Fmoc residue. Amines **111** and **114** were isolated in 95% and 94% yields respectively.

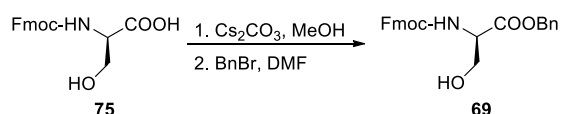
To remove the benzyl ester we followed standard protocol, initially using H₂ and Pd/C in MeOH. However we found that when MeOH was utilized as a solvent, reduction of the carbon-chlorine bonds in the TCE group occurred, giving undesired side products. Changing the reaction solvent to THF suppressed the formation of this byproduct and gave us the desired compound in good yield. Ethyl acetate was also explored, and although it produced the desired product, it didn't suppress the TCE reduction as effectively as THF and gave lower yields. Finally, the TCE ester was cleaved using zinc dust and acetic acid to give the free acid also in good yield.

Initially, purification of the free acids proved to be difficult, as derivative **113** in particular proved to be very polar and adhered to the silica gel, lowering yields. Recovery of derivative **112** from column chromatography also proved difficult. Passing the compounds through a short plug of silica with 15% ethanol in dichloromethane increased the yields to 80% and 65% respectively.

2.5 Experimental Section

General Methods: All reactions were performed under a dry nitrogen atmosphere unless otherwise noted. All chemicals and reagents were purchased from Sigma-Aldrich, Fisher, Acros, and NovaBiochem and used without further purification. Triethylamine and diethylamine were dried and distilled from CaH₂ and stored over KOH pellets. Dry methanol was distilled from Mg turnings and stored over 3Å molecular sieves. Flash chromatography was performed using 230-400 mesh silica gel (40-63 mm) from Sigma-Aldrich. Reactions were followed by thin layer chromatography (TLC) on pre-coated aluminum-backed 60 F254 silica plates from EMD Chemicals, Inc. Compounds were visualized under UV fluorescence or by staining with KMnO₄, or an acidic, ethanolic solution of ninhydrin. ¹H and ¹³C NMR spectra were recorded at room temperature on a Bruker AV-400 and are reported in parts per million (ppm) on the δ scale relative to residual CHCl₃ or (CH₃)₂SO in deuterated solvents or tetramethylsilane as an internal standard. Coupling constants (*J*) are reported in Hertz (Hz). High resolution mass spectrometry (HRMS) was carried out using an Agilent 6210 electrospray ionization-time-of-flight (ESI-TOF) mass spectrometer. Optical rotations were recorded under the specified conditions.

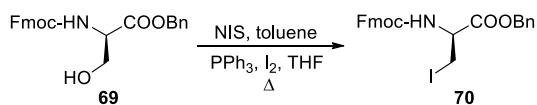
2.5.1 Procedures



Scheme 2.26: Synthesis of compound **69**

Fmoc-*D*-Ser-OBn (**69**).²⁴ Cesium carbonate (199 mg, 0.61 mmol, 0.50 equiv.) was added to a solution of Fmoc-*D*-Ser-OH (**75**) (400 mg, 1.22 mmol, 1.00 equiv.) in dry MeOH (5.3 mL). The mixture was stirred at rt for 2 h, concentrated, and the residue dissolved in dry DMF (2.7 mL)

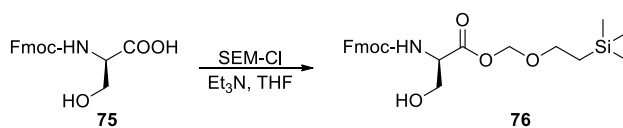
under N₂. Benzyl bromide (175 μ L, 125 mg, 1.47 mmol, 1.20 equiv.) was added dropwise and the mixture stirred overnight. The mixture was then partitioned between EtOAc (10 mL) and H₂O (10 mL). The aqueous layer was extracted with EtOAc (10 mL), and the combined organic extracts were washed with sat'd aq. NaHCO₃ (3 x 8 mL) to remove Fmoc-*D*-Ser-OH completely. The organic layer was then washed with brine (8 mL), dried over MgSO₄ and concentrated. The pale yellow oil was purified by flash chromatography on silica gel, eluting with 2:1 Hexanes-EtOAc, to give Fmoc-*D*-Ser-OBn (**69**) as a clear oil that gave a colorless solid upon overnight refrigeration (332 mg, 83%). *R*_f 0.68 (95:5 CH₂Cl₂-MeOH). [α]_D²⁵ -3.4 (*c* 1.0, MeOH); ¹H NMR (400 MHz, CDCl₃) δ 2.22 (br s, 1H, OH), 3.91 (d, *J* = 9.8 Hz, 1H), 4.01 (d, *J* = 9.8 Hz, 1H), 4.20 (t, *J* = 6.5, 1H), 4.36-4.48 (m, 3H), 5.21 (s, 2H), 5.77 (d, *J* = 7.5 Hz, 1H), 7.28-7.33 (m, 7H), 7.39 (t, *J* = 7.4 Hz, 2H), 7.58 (d, *J* = 7.1 Hz, 2H), 7.75 (d, *J* = 7.5 Hz, 2H); ¹³C NMR (100 MHz, CDCl₃) δ 47.1, 56.2, 63.2, 67.3, 67.6, 120.0, 125.1, 127.1, 127.1, 127.8, 128.2, 128.6, 128.7, 135.1, 141.3, 141.4, 143.7, 143.8, 156.4, 170.5.



Scheme 2.27: Synthesis of compound 70

Fmoc-*D*-Ser(I)-OBn (**70**).⁹ A solution of triphenylphosphine (942 mg, 3.59 mmol, 3.0 equiv.) in toluene (7.0 mL) was added dropwise over 5 min to a suspension of *N*-iodosuccinimide (808 mg, 3.59 mmol, 3.0 equiv.) in toluene (3.6 mL) at rt under N₂. The mixture was stirred for 5 min, followed by the dropwise addition of a solution of Fmoc-*D*-Ser-OBn (**69**) (500 mg, 1.20 mmol, 1 equiv.) in THF (7.0 mL). Finally, iodine (912 mg, 3.59 mmol, 3 equiv.) was added as a solid. The mixture was stirred for 1 h under reflux. The reaction mixture was concentrated (35 °C), then

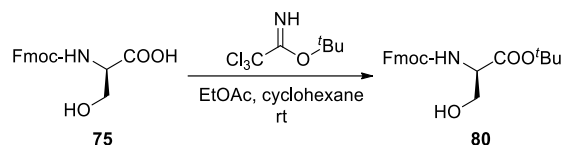
diluted with EtOAc (20 mL). The organic layer was washed with H₂O (2 x 10 mL). The aqueous layers were combined and back-extracted with EtOAc (20 mL). The organic layers were combined, and washed with sat'd aq. Na₂S₂O₃ (12 mL). The black precipitate was removed by filtration through a plug of Celite™. The filtrate was washed with sat'd aq. Na₂S₂O₃ (12 mL), sat'd aq. NaHCO₃ (8 mL), H₂O (20 mL) and brine (12 mL), dried over MgSO₄, filtered and concentrated. The deep brown oil was purified by flash chromatography on silica gel, eluting with 10:1 hexanes-EtOAc. Appropriate fractions were concentrated to give Fmoc-*D*-Ser(1)-OBn (**70**) as a colorless powder (505 mg, 80%). *R*_f 0.35 (2:1 Hexanes-EtOAc). [α]²⁶_D +6.7 (c 0.6, CHCl₃), Lit.⁹ [α]²⁶_D +6.7 (c 0.6, CHCl₃). ¹H NMR (400 MHz, CDCl₃) δ 3.62 (br s, 2H, Hβ), 4.25 (t, *J* = 7.0 Hz, 1H, Fmoc-CH), 4.36-4.46 (m, 2H, Fmoc-CH₂), 4.61-4.65 (m, 1H, Hα), 5.24 (dd, *J* = 13.5, 4.0 Hz, 2H, CH₂OBn), 5.72 (d, *J* = 7.2 Hz, 1H, NH), 7.31-7.43 (m, 9H, Ar), 7.62 (d, *J* = 7.3 Hz, 2H, Fmoc-Ar), 7.78 (d, *J* = 7.4 Hz, 2H, Fmoc-Ar); ¹³C NMR (100 MHz, CDCl₃) δ 7.4, 47.1, 54.1, 67.4, 68.2, 120.1, 125.0, 125.2, 127.2, 127.8, 128.3, 128.6, 128.7, 128.8, 134.7, 141.3, 143.6, 143.8, 155.4, 169.2.



Scheme 2.28: Synthesis of compound **76**

Fmoc-*D*-Ser-OSEM (**76**). Fmoc-*D*-Ser-OH (**75**) (250 mg, 0.76 mmol, 1.0 equiv.) was dissolved in THF (5 mL) and cooled to 0 °C. Triethylamine (213 μL, 77.3 mg, 1.53 mmol, 2.0 equiv.) was added to the cooled solution and allowed to stir for 5 min. 2-(Trimethylsilyl)ethoxymethyl chloride (135 μL, 127 mg, 0.76 mmol, 1.0 equiv.) was added all at once. The mixture was stirred at 0 °C for 3 h and then diluted with sat'd aq. NH₄Cl (17 mL). The aqueous layer was extracted with CH₂Cl₂ (3 x 8.5 mL). The organic layers were combined, dried over MgSO₄, filtered and

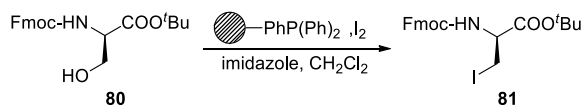
concentrated. The pale yellow oil was purified by flash chromatography on silica gel, eluting with 3:1 hexanes-EtOAc, to give Fmoc-*D*-Ser-OSEM (**76**) as a colorless oil (505 mg, 75%). R_f 0.50 (95:5 CH₂Cl₂-MeOH). ¹H NMR (400 MHz, CDCl₃) δ 0.02 (s, 9H, SiMe₃), 0.97 (t, J = 16.5 Hz, 2H, CH₂), 3.73 (t, J = 16.5 Hz, 2H, CH₂), 3.93 (br d, J = 8.9 Hz, 1H, H β), 4.04 (br d, J = 11.0 Hz, 2H, H β'), 4.22 (t, J = 6.9 Hz, 1H, Fmoc-CH), 4.41 (quin., J = 7.5 Hz, 2H, Fmoc-CH₂), 4.48-4.50 (m, 1H, H α), 5.38 (dd, J = 11.5, 5.7 Hz, 2H, OCH₂O), 5.96 (d, J = 7.6 Hz, 1H, NH), 7.31 (t, J = 7.4 Hz, 2H, Fmoc-Ar), 7.40 (t, J = 7.4 Hz, 2H, Fmoc-Ar), 7.61 (t, J = 5.4 Hz, 2H, Fmoc-Ar), 7.76 (d, J = 7.5 Hz, 2H, Fmoc-Ar); ¹³C NMR (100 MHz, CDCl₃) δ -1.4, 14.2, 17.9, 47.1, 56.2, 60.5, 63.1, 67.3, 68.3, 90.1, 120.0, 125.1, 127.1, 127.8, 141.3, 141.3, 143.7, 143.9, 156.3, 170.4.



Scheme 2.29: Synthesis of compound **80**

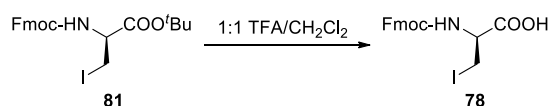
Fmoc-*D*-Ser-O^tBu (**80**).²¹ To a solution of Fmoc-*D*-Ser-OH (**75**) (200 mg, 0.61 mmol, 1.0 equiv.) in EtOAc (5.5 mL) was added *tert*-butyl 2,2,2-trichloroacetimidate (534 mg, 437 μ L, 2.4 mmol, 4.0 equiv.) in cyclohexane (2.6 mL). The mixture was stirred at rt for 24 h under N₂, and then concentrated and purified by flash chromatography on silica gel, eluting with 5:1 hexanes-EtOAc to yield Fmoc-*D*-Ser-O^tBu (**80**) as a colorless solid upon concentration (181 mg, 70%). R_f 0.41 (95:5 CH₂Cl₂-MeOH). $[\alpha]_D^{20}$ +2.4 (c 1.0, CH₂Cl₂), Lit.²¹ $[\alpha]_D^{20}$ +2.0 (c 1.0, CH₂Cl₂); ¹H NMR (400 MHz, MeOD) δ 1.44 (s, 9H, ^tBu), 3.80 (dd, J = 11.2, 4.2 Hz, 1H, H β), 3.84 (dd, J = 11.2, 4.2 Hz, 1H, H β) 4.13-4.20 (m, 2H, Fmoc-CH, H α), 4.26 (dd, J = 10.4, 7.1 Hz, 1H, Fmoc-CH₂), 4.34 (dd, J = 10.4, 7.1 Hz, 1H, Fmoc-CH₂), 7.23 (t, J = 7.4 Hz, 2H, Fmoc-Ar), 7.32 (t, J = 7.4 Hz, 2H, Fmoc-Ar), 7.61 (t, J = 6.6 Hz, 2H, Fmoc-Ar), 7.71 (d, J = 7.5 Hz, 2H, Fmoc-Ar); ¹³C NMR (100 MHz, MeOD) δ

28.7, 48.6, 58.8, 63.5, 68.5, 83.5, 121.3, 126.6, 126.6, 128.5, 129.2, 142.9, 145.5, 145.6, 158.9, 171.7.



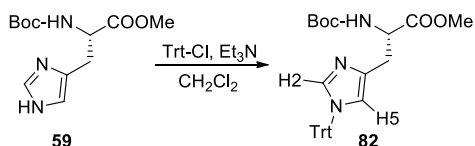
Scheme 2.30: Synthesis of compound **81**

Fmoc-*D*-Ser(I)-O^tBu (**81**).²⁵ Iodine (642 mg, 2.53 mmol, 2.2 equiv.) was added to a suspension of triphenylphosphine polymer (664 mg, 2.53 mmol, 2.2 equiv.) in anhydrous CH₂Cl₂ (19 mL) under N₂. The reaction was stirred at rt. After 15 min, imidazole (196 mg, 2.88 mmol, 2.5 equiv.) was added at rt and the stirring was continued for an additional 15 min. A solution of Fmoc-*D*-Ser-O^tBu (**80**) (445 mg, 1.16 mmol, 1.0 equiv.) in anhydrous CH₂Cl₂ (4.6 mL) was then added to the suspension. The reaction was heated at reflux for 1 h. After filtration through a pad of Celite™ and washing with CH₂Cl₂ (3 x 5 mL), the filtrate was washed with sat'd aq. Na₂S₂O₃ (8 mL), H₂O (2 x 8 mL), dried over MgSO₄, filtered and concentrated. The residue was purified by flash chromatography on silica gel eluting with 5:1 hexanes:EtOAc to give Fmoc-*D*-Ser(I)-O^tBu (**81**) as a colorless oil (449 mg, 78%). *R*_f 0.31 (2:1 hexanes-EtOAc). Lit.²⁶ ^{ent-81}[α]²³_D 16.3 (*c* 1.05, CHCl₃); ¹H NMR (400 MHz, CDCl₃) δ 1.53 (s, 9H, ^tBu), 3.58-3.65 (m, 2H, Hβ), 4.25 (t, *J* = 7.2 Hz, 1H, Fmoc-CH), 4.35 (dd, *J* = 10.4, 7.2 Hz, 1H, Fmoc-CH₂), 4.41-4.45 (m, 3H, Fmoc-CH₂, Hα), 5.71 (d, *J* = 6.8 Hz, 1H, NH), 7.33 (t, *J* = 7.4 Hz, 2H, Fmoc-Ar), 7.41 (t, *J* = 7.4 Hz, 2H, Fmoc-Ar), 7.60 (d, *J* = 7.1 Hz, 2H, Fmoc-Ar), 7.77 (d, *J* = 7.5 Hz, 2H, Fmoc-Ar); ¹³C NMR (100 MHz, CDCl₃) δ 8.4, 28.0, 47.1, 54.1, 67.3, 83.7, 120.0, 125.2, 125.2, 127.1, 127.8, 141.3, 143.7, 143.7, 155.4, 168.2.



Scheme 2.31: Synthesis of compound **78**

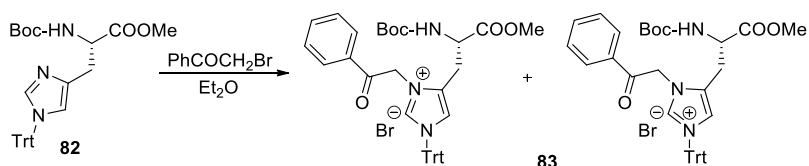
Fmoc-*D*-Ser(1)-OH (**78**).¹³ Fmoc-*D*-Ser(1)-O^tBu (**81**) (148 mg, 0.30 mmol, 1.0 equiv.) was treated with 50% TFA in CH₂Cl₂ (4.2 mL) for 1 h under N₂. Evaporation of the solvents and coevaporation with toluene (4.2 mL) furnished Fmoc-*D*-Ser(1)-OH (**78**) (118 mg, 90%). *R_f* 0.15 (9:1 C H₂Cl₂-MeOH). [α]_D²⁵ -4.2(c 1.0, CH₃OH); ¹H NMR (400 MHz, CD₃OD) δ 3.51 (dd, *J* = 10.3, 7.5 Hz, 1H, Hβ) 3.64 (dd, *J* = 10.3, 4.1 Hz, 1H, H'β), 4.24 (t, *J* = 7.0 Hz, 1H, Fmoc-CH), 4.30-4.42 (m, 3H, Fmoc-CH₂, Hα), 6.01 (d, *J* = 8.0 Hz, 1H, NH), 7.31 (t, *J* = 7.4 Hz, 2H, Fmoc-Ar), 7.38 (t, *J* = 7.4 Hz, 2H, Fmoc-Ar), 7.68 (d, *J* = 7.2 Hz, 2H, Fmoc-Ar), 7.79 (d, *J* = 7.4 Hz, 2H, Fmoc-Ar); ¹³C NMR (100 MHz, CD₃OD) δ 3.7, 47.0, 55.4, 66.8, 119.5, 124.9, 126.8, 127.4, 141.2, 143.7, 143.8, 156.7, 170.7.



Scheme 2.32: Synthesis of compound **82**

Boc-*L*-His(Trt)-OMe (**82**). Boc-*L*-His-OMe (**59**) (1.00 g, 3.71 mmol, 1.0 equiv.) was added to a solution of triphenylmethyl chloride (1.14 g, 4.08 mmol, 1.1 equiv.) and triethylamine (543 μL, 395 mg, 3.90 mmol, 1.05 equiv.) in dry benzene (7.5 mL) under N₂. The mixture was heated at reflux for 1 h, and the resultant triethylammonium chloride precipitate was removed by filtration and washed with benzene. The combined filtrate and washings were washed with H₂O (20 mL), dried over MgSO₄, filtered and concentrated. The pale yellow oil was purified by flash chromatography on silica gel, eluting with 3:1 hexanes-EtOAc, to give Boc-*L*-His(Trt)-OMe (**82**) as a colorless oil, that was redissolved in CH₂Cl₂ (5 mL) and concentrated to give a colorless

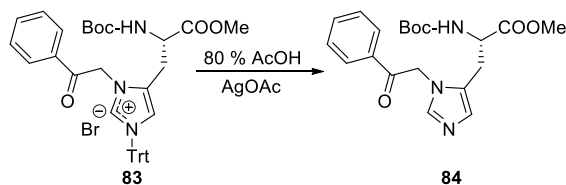
solid (1.78 g, 94%). R_f 0.68 (95:5 CH₂Cl₂-MeOH). $[\alpha]_D^{20} +3.1$ (c 1.0, MeOH), Lit.27 $[\alpha]_D^{20} +3.8$ (c 1.0, MeOH). ¹H NMR (400 MHz, CDCl₃) δ 1.43 (s, 9H, ^tBu), 2.96 (dd, $J = 14.5, 4.7$ Hz, 1H, H β), 3.03 (dd, $J = 14.5, 5.1$ Hz, 1H, H' β), 3.57 (s, 3H, OMe), 4.54 (dt, $J = 9.0, 8.3$ Hz, 1H, H α), 6.09 (d, $J = 8.4$ Hz, 1H, NH), 6.52 (s, 1H, H5), 7.07-7.12 (m, 5H, Trt-Ar), 7.28-7.31 (m, 10 H, Trt-Ar), 7.34 (s, 1H, H2); ¹³C NMR (100 MHz, CDCl₃) δ 28.4, 30.3, 52.0, 53.8, 75.2, 79.5, 119.6, 128.1, 129.8, 136.5, 138.8, 142.3, 155.6, 172.4; HRMS (ESI) calcd for C₃₁H₃₄N₃O₄ (M+H)⁺ 512.2544, obsd 512.2567.



Scheme 2.33: Synthesis of compound **83**

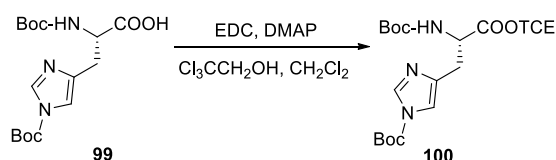
Boc-*L*-His(N_π -Pac, N_τ -Trt)-OMe imidazolium bromide salt (**83**).¹⁴ Boc-*L*-His(Trt)-OMe (**82**) (500 mg, 0.98 mmol, 1.0 equiv.) and phenacyl bromide (195 mg, 0.98 mmol, 1.0 equiv.) were dissolved in diethyl ether (0.83 mL), and stirred at rt for 2 d. The precipitate was filtered and washed with ether to yield the Boc-*L*-His(π -Pac, τ -Trt)-OMe imidazolium bromide salt (**83**) (591 mg, 85%). R_f 0.20-0.50 (95:5 CH₂Cl₂-MeOH). $[\alpha]_D^{20} -8.2$ (c 1.0, MeOH), Lit.14 $[\alpha]_D^{20} -9.2$ (c 1.0, MeOH). ¹H NMR (400 MHz, CDCl₃) δ 1.36[1.28]* (s, 9H, ^tBu), 3.06-3.20 (m, 2H, H β), 3.73[3.63] (s, 3H, OMe), 4.45-4.51 (m, 1H, H α), 5.50[5.88] (br s, 1H, NH), 6.16[6.50] (d, $J = 18.3$ Hz, 1H, CH₂), 6.36[6.69] (d, $J = 18.3$ Hz, 1H, CH₂), 6.91 (s, 1H, H5), 7.20-7.31 (m, 10 H, Trt-Ar), 7.47-7.54 (m, 2H, Pac-Ar), 7.62 (p, $J = 5.8$ Hz, 1H, Pac-Ar), 8.07[8.12] (d, $J = 7.3$ Hz, 2H, Pac-Ar), 9.47[9.21] (s, 1H, H2); ¹³C NMR (100 MHz, CDCl₃) δ 26.5, 28.1, 52.4, 52.9, 55.0, 79.7, 80.5, 121.8, 128.8, 129.0, 129.1, 129.3, 129.7, 132.0, 133.4, 134.7, 139.1, 139.4, 155.4, 170.7, 191.2; HRMS (ESI) calcd for C₃₉H₄₀N₃O₅ (M+H)⁺ 630.2962, obsd 630.2974

* [] denotes minor tautomer peak



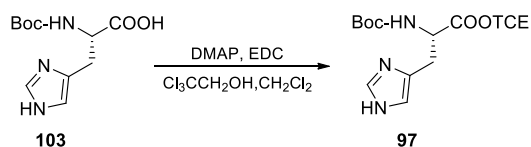
Scheme 2.34: Synthesis of compound **84**

Boc-*L*-His(*N*_π-Pac)-OMe (**84**).¹⁴ Silver acetate (195 mg, 0.98 mmol, 1.0 equiv.) was added to a stirred solution of Boc-*L*-His(*π*-Pac, *τ*-Trt)-OMe imidazolium bromide salt (**83**) (500 mg, 0.98 mmol, 1.0 equiv.) in 80% acetic acid (1.32 mL). The precipitated silver bromide was then filtered off, and the solution was left to stir at rt for 24 h. The triphenylmethanol precipitate was removed by filtration, and the filtrate was concentrated. Sat'd aq. NaHCO₃ was added to the residue, and the mixture was extracted with ether (5 x 5 mL). The organic extracts were left to stand at rt while the methyl ester crystallized from the solution (217 mg, 85%). *R*_f 0.65 (95:5 CH₂Cl₂-MeOH). [α]_D²⁰ -8.3 (c 1.0, MeOH), Lit.¹⁴ [α]_D²⁰ -9.3 (c 1.0, MeOH). ¹H NMR (400 MHz, CDCl₃) δ 1.37 (s, 9H, ^tBu), 3.00 (br d, *J* = 4.8 Hz, 1H, Hβ), 3.70 (s, 3H, OMe), 4.47 (br d, *J* = 5.6 Hz, 1H, Hα), 5.33 (d, *J* = 6.3 Hz, 1H, NH), 5.39 (d, *J* = 18.3 Hz, 1H, CH₂Ph), 5.48 (d, *J* = 18.3 Hz, 1H, CH₂Ph), 6.88 (s, 1H, H5), 7.42 (s, 1H, H2), 7.54 (t, *J* = 7.5 Hz, 2H, Pac-Ar), 7.67 (t, *J* = 7.4 Hz, 1H, Pac-Ar), 8.01 (d, *J* = 7.6 Hz, 2H, Pac-Ar); ¹³C NMR (100 MHz, THF-d₈) δ 26.5, 27.6, 50.4, 51.1, 53.3, 78.3, 127.3, 127.7, 127.9, 128.6, 133.4, 135.1, 138.2, 155.3, 171.7, 192.4; HRMS (ESI) calcd for C₂₀H₂₆N₃O₅ (M)⁺ 388.1867, obsd 388.1873.



Scheme 3.35: Synthesis of compound **100**

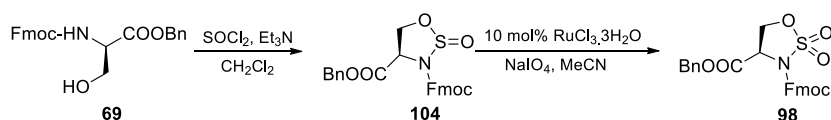
Boc-*L*-His-Boc-OTCE (**100**). *N,N*-Dimethylaminopyridine (289 mg, 2.31 mmol, 0.5 equiv.) and trichloroethanol (530 μ L, 103 mg, 5.54 mmol, 1.2 equiv.) were added sequentially to a solution of commercially available Boc-*L*-His(τ -Boc)-OH (**99**) (2.00 g, 4.61 mmol, 1.0 equiv.) in CH₂Cl₂ (16 mL) at rt under N₂. The mixture was cooled to 0 °C, and EDC (1.06 g, 5.54 mmol, 1.2 equiv.) was added. The solution was stirred for 21 h at 0 °C. The mixture was diluted with EtOAc (200 mL), washed with sat'd aq. NaHCO₃ (2 x 40 mL), water (2 x 100 mL) and brine (40 mL), dried over MgSO₄, filtered and concentrated. The clear yellow oil was subjected to flash chromatography on silica gel, eluting with 2:1 hexanes-EtOAc, to give Boc-*L*-His-(Boc)-OTCE (**100**) as a colorless oil that was crystallized from methanol to yield a colorless solid (2.03 g, 90%). *R*_f 0.68 (95:5 CH₂Cl₂-MeOH). ¹H NMR (CDCl₃, 400 MHz) δ 1.44 (s, 9H, ^tBu), 1.61 (s, 9H, ^tBu), 3.10 (dd, *J* = 14.9, 5.0 Hz, 1H, H β), 3.16 (dd, *J* = 14.9, 5.8 Hz, 1H, H' β), 4.67 (d, *J* = 11.9 Hz, 1H, CH₂CCl₃), 4.69-4.74 (m, 1H, H α), 4.82 (d, *J* = 11.9 Hz, 1H, CH₂CCl₃), 6.01 (d, *J* = 8.2 Hz, 1H, NH), 7.18 (s, 1H, H5), 8.00 (s, 1H, H2); ¹³C NMR (CDCl₃, 100 MHz) δ 27.9, 28.3, 29.6, 53.3, 74.6, 80.0, 85.7, 94.6, 114.9, 137.0, 138.2, 146.8, 155.5, 170.5; HRMS (-ESI) calcd for C₁₈H₂₆³⁵Cl₃N₃O₆ (MH⁻) 485.0887, obsd 484.9260.



Scheme 2.36: Synthesis of compound **97**

Boc-*L*-His-OTCE (**97**). A solution of DMAP (0.57 g, 4.70 mmol, 1.2 equiv.) in anhydrous CH₂Cl₂ (1.2 mL) was added dropwise to a suspension of commercially available Boc-*L*-His-OH (**103**) (1.00 g, 3.92 mmol, 1.0 equiv.) in 2,2,2-trichloroethanol (4.0 mL) under N₂. The reaction mixture was then cooled to 0 °C. A solution of EDC (0.901 g, 4.70 mmol, 1.2 equiv.) in anhydrous CH₂Cl₂

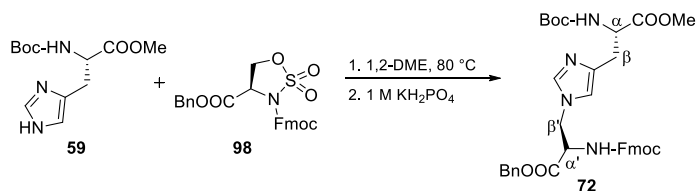
(2.8 mL) was added dropwise. The mixture was warmed to rt and stirred overnight. The solution was partitioned between H₂O (40 mL) and CH₂Cl₂ (40 mL). The layers were separated and the aqueous layer extracted further with CH₂Cl₂ (3 x 20 mL). The combined organic layers were dried over MgSO₄, filtered and concentrated. The pale yellow oil was purified by flash chromatography on silica gel, eluting with 4% MeOH in CH₂Cl₂ to give Boc-*L*-His-OTCE (**97**) as a colorless solid (1.21 g, 80%). *R_f* 0.21 (9:1 CH₂Cl₂-MeOH). [α]_D²⁵ -16.2 (*c* 1.0, CHCl₃). ¹H-NMR (400 MHz, CDCl₃) δ 1.44 (s, 9H), 3.15 (dd, *J* = 14.7, 4.8 Hz, 1H), 3.22 (dd, *J* = 14.7, 4.8 Hz, 1H), 4.63 (d, *J* = 11.9 Hz, 1H), 4.66-4.70 (m, 1H), 4.81 (d, *J* = 11.9 Hz, 1H), 6.15 (br s, 1H), 6.84 (s, 1H), 7.57 (s, 1H); ¹³C-NMR (100 MHz, CDCl₃) δ 28.3, 29.4, 53.7, 74.5, 80.1, 94.6, 115.4, 134.4, 135.3, 155.7, 170.8. HRMS (ESI+) calcd for C₁₃H₁₈Cl₃N₃O₄Na (M+Na)⁺ 408.0255, obsd 408.0243.



Scheme 2.37: Synthesis of compound **98**

Sulfamidate (**98**). Triethylamine (520 μL, 377 mg, 3.73 mmol, 3.0 equiv) was added to a stirred solution of Fmoc-*D*-Ser-OBn (**69**) (519 mg, 1.24 mmol, 1.0 equiv) in dry CH₂Cl₂ (11 mL) under N₂ at -78 °C. Distilled thionyl chloride (135 μL, 222 mg, 1.87 mmol, 1.5 equiv) was added dropwise over 5 min which turned the solution yellow. After 2 h at -78 °C, H₂O (7 mL) was added and the mixture was warmed to rt. The two layers were separated and the aqueous layer was extracted with CH₂Cl₂ (3 x 11 mL). The combined organic layers were washed with 5% citric acid (8 mL) and brine (8 mL). The organic layer was dried over MgSO₄, filtered and concentrated. The crude sulfamidite (**104**) was taken to the next step.

The residue was dissolved in MeCN (8 mL) and cooled to 0 °C. Sodium periodate (283 mg, 1.32 mmol, 1.1 equiv) was added followed by ruthenium (III) chloride (25 mg, 0.120 mmol, 0.1 equiv). Water (5 mL) was added dropwise to the solution and the mixture was left to stir vigorously for 1 h at 0 °C. The mixture was allowed to warm to rt and stirred an additional 15 min. The mixture was diluted with Et₂O (15 mL), and the two layers separated. The aqueous layer was extracted with Et₂O (3 x 15 mL) and the combined organic layers were washed with sat'd aq. NaHCO₃ (2 x 15 mL) and brine (15 mL), dried over MgSO₄, filtered and concentrated. The light yellow oil was purified by flash chromatography on silica gel, eluting with 5:1 hexanes-EtOAc \longrightarrow 3:1 hexanes: EtOAc, to give Fmoc-*D*-Ser-OBn derived sulfamidate as a colorless solid (**97**) (417 mg, 70%). *R*_f 0.34 (2:1 Hexane-EtOAc). ¹H NMR (400 MHz, CDCl₃) δ 4.26 (br s, 1H), 4.44 (t, *J* = 8.8 Hz, 1H), 4.56 (appt. t, *J* = 8.8 Hz, 1H), 4.72 (d, *J* = 8.7 Hz, 1H), 4.83 (t, *J* = 8.7 Hz, 1H), 4.87 (br s, 1H), 5.24 (d, *J* = 3.0 Hz, 2H), 7.30 – 7.37 (m, 7H), 7.41 (t, *J* = 7.4 Hz, 2H), 7.67 (br s, 2H), 7.76 (d, *J* = 7.5 Hz, 2H); ¹³C NMR (100 MHz, CDCl₃) δ 14.2, 46.5, 58.0, 60.4, 68.1, 68.7, 70.7, 120.1, 125.3, 127.4, 128.1, 128.3, 128.8, 128.9, 134.3, 141.3, 141.3, 142.8, 142.9, 149.5, 166.5; HRMS (-ESI) calcd for C₂₅H₂₀NO₇S (M-H)⁻ 478.0966, obsd 478.0958.



Scheme 2.38: Synthesis of compound **72**

τ -HAL derivative (**72**). Boc-*L*-His-OMe (**59**) (51 mg, 0.19 mmol, 3.0 equiv.) was added to a solution of sulfamidate **98** (30 mg, 0.06 mmol, 1.0 equiv.) in 1,2-DME (3 mL). This mixture was then heated at 80 °C under N₂ and allowed to stir for 5 h. 1 M potassium phosphate (6 mL) was

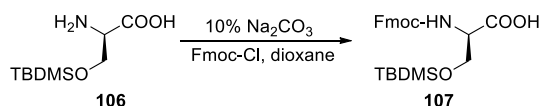
added to the mixture which then stirred at RT overnight. This mixture was partitioned between EtOAc (3 mL) and H₂O (3 mL) to dissolve the precipitate. The two layers were separated, and the aqueous layer was extracted with EtOAc (3 x 3 mL). The combined organic extracts were dried over MgSO₄, filtered and concentrated. The clear oil was subjected to flash chromatography on silica gel, eluting with 2:1 hexanes-EtOAc, to give τ -HAL (**72**) as a colorless oil (13 mg, 30%). *R_f* 0.34 (95:5 CH₂Cl₂-MeOH). ¹H NMR (CDCl₃, 400 MHz) δ 1.42 (s, 9H, ^tBu), 2.91 (dd, *J* = 14.0, 3.2 Hz, 1H, H β), 2.99 (dd, *J* = 14.0, 5.1 Hz, 1H, H' β), 3.69 (s, 3H, OMe), 4.21 (t, *J* = 6.3 Hz, 1H, Fmoc-CH), 4.29, (br s, 2H, H β '), 4.41-4.53 (m, 3H, Fmoc-CH₂, H α), 4.62 (m, 1H, H α '), 5.16 (d, *J* = 11.9 Hz, 2H, CH₂OBn), 5.26 (d, *J* = 11.9 Hz, 2H, CH₂OBn), 5.58 (d, *J* = 5.2 Hz, 1H, NH), 5.89 (d, *J* = 7.8 Hz, 1H, NH), 5.89 (d, *J* = 7.8 Hz, 1H, NH), 6.32 (s, 1H, H5), 7.16 (s, 1H, H2), 7.31 – 7.42 (m, 11 H, Fmoc-Ar, Ph-Ar), 7.58 (d, *J* = 7.2 Hz, 2H, Fmoc-Ar), 7.78 (d, *J* = 7.2 Hz, 2H, Fmoc-Ar); ¹³C NMR (CDCl₃, 100 MHz) δ 28.3 ((CH₃)₃), 30.1 (C β), 30.9, 47.1 (Fmoc-CH), 47.9 (C β '), 52.2 (OMe), 53.5 (C α), 54.8 (C α '), 67.2 (CH₂Ph), 68.2 (Fmoc-CH₂), 79.6 (4°Boc), 117.1, 120.1 (Fmoc-Ar), 125.0 (Fmoc-Ar), 125.0 (Fmoc-Ar), 127.1 (Fmoc-Ar), 127.2 (Fmoc Ar), 127.9 (Fmoc Ar), 128.5 (Ph-Ar), 128.9 (Ph-Ar), 129.0 (Ph-Ar), 129.1(Ph-Ar), 134.3 (C=C Ph), 137.5 (C5), 141.3 (C2), 143.5, 143.6, 155.6, 168.8, 172.5; HRMS (+ESI) calcd for C₃₇H₄₁N₄O₈ (M+H)⁺ 669.2919, obsd 669.2932.



Scheme 2.39: Synthesis of compound **106**

H-*D*-Ser(OTBS)-OH (**106**).²⁸ A suspension of commercially available H-*D*-Ser-OH (**105**) (1.00 g, 9.52 mmol, 1.0 equiv.) in anhydrous DMF (10 mL) was treated with imidazole (1.30 g, 19.0 mmol, 2.0 equiv.) and TBDMS-Cl (1.58 g, 10.5 mmol, 1.1 equiv.) under N₂. The solution was left

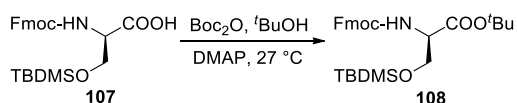
to stir at rt overnight. A biphasic solution of 1:1 H₂O:hexanes (30 mL) was added and the mixture stirred for an additional 4 h. The resulting solid was collected by filtration, rinsed with hexanes, and air dried to give H-*D*-Ser(OTBDMS)-OH (**106**) as a colorless solid (1.89 g, 90%). *R_f* 0.56 (6:4:1 CHCl₃-MeOH-H₂O). $[\alpha]_D^{20}$ 1.21 (*c* 0.174, MeOH), Lit.²⁹ *ent-X* $[\alpha]_D^{20}$ -29.3 (*c* 0.174, MeOH). ¹H NMR (CDCl₃, 400 MHz) δ 0.11 (s, 6H, CH₃Si), 0.92 (s, 9H, ^tBuSi), 3.63 (pent., *J* = 3.9 Hz, 1H, H_α), 4.00 (dd, *J* = 10.9, 5.9 Hz, 1H, H_β), 4.04 (dd, *J* = 10.8, 3.8 Hz, 1H, H_{β'}), 4.82 (br s, 2H, NH₂); ¹³C NMR (CD₃OD, 100 MHz) δ -6.8, 17.9, 25.0, 56.6, 62.2, 170.5.



Scheme 2.40: Synthesis of compound **107**

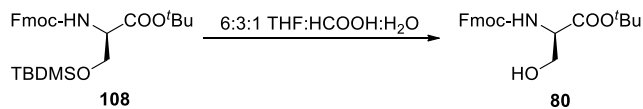
Fmoc-*D*-Ser(OTBS)-OH (**107**). 1,4-Dioxane (5 mL) was added to a cooled solution of H-*D*-Ser(OTBDMS)-OH (**106**) (1.00 g, 4.56 mmol, 1.0 equiv.) in 10% aq. Na₂CO₃ (10 mL) at 0 °C and stirred for 5 min. A solution of Fmoc-Cl (2.03 g, 9.80 mmol, 1.03 equiv.) in 1,4-dioxane (7.5 mL) was added dropwise. The mixture was stirred for 1 h at 0 °C and then allowed to warm to rt to stir overnight. The reaction mixture was concentrated to remove the dioxane, and the residual aqueous solution was acidified to pH 4 by the dropwise addition of 1 M HCl. The aqueous layer was extracted with EtOAc (3 x 50 mL). The combined extracts were washed with brine (30 mL), dried over MgSO₄, filtered and concentrated. The pale oil was purified by flash chromatography on silica gel, using a gradient system eluting first with 95:5 Hexanes-EtOAc → 10:1 Hexanes-EtOAc → 5:1 Hexanes-EtOAc → 2:1 Hexanes-EtOAc to give Fmoc-*D*-Ser(OTBDMS)-OH (**107**) as a colorless oil (1.75 g, 87%). *R_f* 0.40 (9:1 CH₂Cl₂-MeOH). ¹H NMR (CDCl₃, 400 MHz) δ 0.07 (s, 6H, CH₃Si), 0.90 (s, 9H, ^tBuSi), 3.87 (d, *J* = 6.6 Hz, 1H, H_β), 4.13 (t, *J* = 7.3 Hz, 1H, Fmoc-CH₂), 4.04

(t, $J = 6.2$ Hz, 1H, H β'), 4.40 (t, $J = 7.9$ Hz, 1H, Fmoc-CH), 4.46 (m, 1H, H α), 5.61 (d, $J = 6.8$ Hz, 1H, NH), 7.31 (t, $J = 7.1$ Hz, 2H, Fmoc-Ar), 7.40 (t, $J = 7.1$ Hz, 2H, Fmoc-Ar), 7.60 (t, $J = 7.1$ Hz, 2H, Fmoc-Ar), 7.76 (d, $J = 7.1$ Hz, 2H, Fmoc-Ar); ^{13}C NMR (CDCl₃, 100 MHz) δ -5.5, 18.2, 25.7, 47.2, 55.6, 63.3, 67.3, 120.0, 125.2, 127.1, 127.7, 141.3, 143.8, 156.1, 174.4; HRMS (ESI+) calcd for C₂₄H₃₂NO₅Si (M+H)⁺ 442.2044, obsd 442.2051.



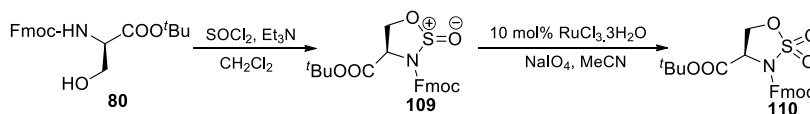
Scheme 2.41: Synthesis of compound **108**

Fmoc-*D*-Ser(OTBDMS)-O^{*t*}Bu (**108**).³¹ Fmoc-*D*-Ser(OTBDMS)-OH (**107**) (700 mg, 1.59 mmol, 1.0 equiv.) was dissolved in *tert*-butanol (16 mL) and heated gently (~27 °C) under N₂ to keep the *tert*-butanol liquid. Di-*tert*-butyl dicarbonate (1.38 g, 6.34 mmol, 4.0 equiv.) and DMAP (58 mg, 0.48 mmol, 0.3 equiv.) were added sequentially, and the solution was allowed to stir at 27 °C for 16 h. The solution was concentrated and the residue purified by flash chromatography on silica gel, eluting with 10:1 hexanes-EtOAc to give Fmoc-*D*-Ser(OTBDMS)-O^{*t*}Bu (**107**) as a pale yellow oil (670 mg, 85%). R_f 0.45 (5:1 Hexanes-EtOAc). ^1H NMR (CDCl₃, 400 MHz) δ 0.05 (s, 3H, CH₃Si), 0.06 (s, 3H, CH₃Si), 0.89 (s, 9H, ^{*t*}BuSi), 1.48 (s, 9H, O^{*t*}Bu), 3.85 (dd, $J = 9.8, 2.5$ Hz, 1H, H β), 4.04 (dd, $J = 9.8, 1.7$ Hz, 1H, H' β), 4.24 (t, $J = 7.0$ Hz, 1H, Fmoc-CH), 4.28-4.32 (m, 1H, H α), 4.36 (d, $J = 7.2$ Hz, 2H, Fmoc-CH₂), 5.62 (d, $J = 7.8$ Hz, 1H, NH), 7.30 (t, $J = 7.3$ Hz, 2H, Fmoc-Ar), 7.39 (t, $J = 7.4$ Hz, 2H, Fmoc-Ar), 7.61 (t, $J = 7.0$ Hz, 2H, Fmoc-Ar), 7.76 (d, $J = 7.5$ Hz, 2H, Fmoc-Ar); ^{13}C NMR (CDCl₃, 100 MHz) δ -5.5, 18.2, 25.7, 28.1, 30.9, 47.2, 56.4, 63.8, 67.1, 82.1, 120.0, 125.2, 127.1, 127.7, 141.3, 143.8, 144.0, 155.9, 169.5; HRMS (ESI+) calcd for C₂₈H₃₉NO₅SiNa (M+Na)⁺ 520.2490, obsd 520.2496.



Scheme 2.42: Synthesis of compound **80**

Fmoc-*D*-Ser-O^{*t*}Bu (**80**).³² A solution of Fmoc-*D*-Ser(OTBDMS)-O^{*t*}Bu (**108**) (700 mg, 1.41 mmol, 1.0 equiv.) in 6:3:1 THF-HCOOH-H₂O (125 mL) was stirred at rt for 4 h. The mixture was cooled to 0 °C and neutralized with sat'd. aqueous NaHCO₃ (125 mL). The mixture was partitioned between EtOAc (300 mL) and brine (300 mL). The aqueous layer was further extracted with EtOAc (300 mL). The combined organic layers were dried over anhydrous MgSO₄, filtered, and concentrated. The residue was purified by flash chromatography on silica gel, eluting with 5:1 hexanes-EtOAc to give Fmoc-*D*-Ser-O^{*t*}Bu as a colorless solid (448 mg, 83%). ¹H NMR and ¹³C NMR data were in good agreement with compound **80** prepared via reaction of Fmoc-*D*-Ser-OH and *tert*-butyl-2,2,2-trichloroacetimidate.

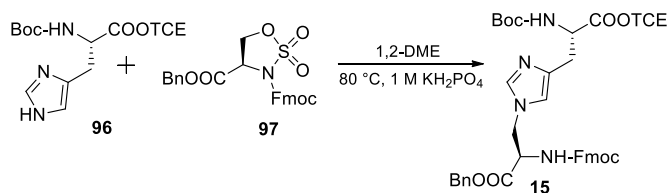


Scheme 2.43: Synthesis of compound **110**

Sulfamidate (**110**). Triethylamine (382 μ L, 277 mg, 2.7 mmol, 3.0 equiv) was added to a stirred solution of Fmoc-*D*-Ser-O^{*t*}Bu (350 mg, 0.91 mmol, 1.0 equiv) in dry dichloromethane (8 mL) under N₂ at -78 °C. Distilled thionyl chloride (99 μ L, 163 mg, 1.4 mmol, 1.5 equiv) was added dropwise over 5 min. After 1 h at -78 °C, H₂O (5 mL) was added and the mixture was warmed to rt. The two layers were separated and the aqueous layer was extracted with dichloromethane (3 x 8 mL). The combined organic layers were washed with 5% citric acid (6 mL) and brine (6

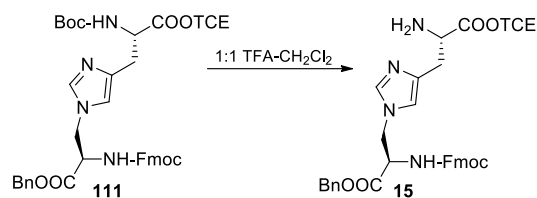
mL). The organic layer was dried over MgSO_4 , filtered and concentrated. The crude sulfamidite (**109**) was taken to the next step.

The residue was dissolved in acetonitrile (5.3 mL) and cooled to 0 °C. Sodium periodate (187 mg, 0.88 mmol, 1.1 equiv) was added followed by ruthenium (III) chloride (17 mg, 0.08 mmol, 0.1 equiv). Water (3.3 mL) was added dropwise to the solution and the mixture was left to stir for 1 h at 0 °C. The mixture was diluted with diethyl ether (10 mL), and the two layers separated. The aqueous layer was extracted with diethyl ether (3 x 10 mL) and the combined organic layers were washed with sat'd aq. NaHCO_3 (2 x 10 mL) and brine (10 mL), dried over MgSO_4 , filtered and concentrated. The light yellow oil was purified by flash chromatography on silica gel, eluting with 10:1 hexanes-EtOAc, to give Fmoc-D-Ser- O^tBu derived sulfamidate **110** as a colorless solid (284 mg, 70%). R_f 0.39 (2:1 Hexanes-EtOAc). $[\alpha]_D^{25} +15.9$ (c. 1.0, CHCl_3). ^1H NMR (400 MHz, CDCl_3) δ 1.51 (s, 9H, ^tBu), 4.35 (app. t, $J = 7.4$ Hz, 1H, $\text{H}\beta$), 4.48 (dd, $J = 10.2, 7.6$ Hz, 1H, $\text{H}'\beta$), 4.61 (dd, $J = 10.2, 7.6$ Hz, 1H, $\text{H}\alpha$), 4.72-4.77 (m, 2H, Fmoc- CH_2), 4.82-4.87 (m, 1H, Fmoc-CH), 7.34 (t, $J = 7.4$ Hz, 2H, Fmoc-Ar), 7.43 (t, $J = 7.4$ Hz, 2H, Fmoc-Ar), 7.72 (br s, 2H, Fmoc-Ar), 7.78 (d, $J = 7.5$ Hz, 2H, Fmoc-Ar); ^{13}C NMR (100 MHz, CDCl_3) δ 27.8, 46.6, 53.5, 58.5, 68.5, 70.6, 85.0, 120.1, 125.4, 127.4, 128.1, 141.3, 142.9, 143.0, 149.6, 165.6. HRMS (ESI $^+$) calcd for $\text{C}_{22}\text{H}_{23}\text{NNaO}_7\text{S}$ ($\text{M}+\text{Na}$) $^+$ 468.1087, obsd 468.1069.



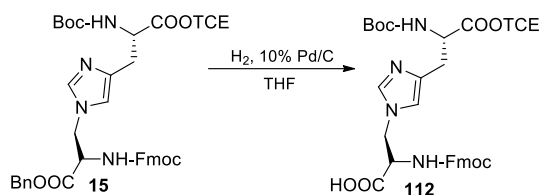
Scheme 2.44: Synthesis of compound **15**

τ -HAL (**15**). Boc-L-His-OTCE (**96**) (302 mg, 0.781 mmol, 3.0 equiv.) was added as a solid to a solution of sulfamidate (**97**) (127 mg, 0.265 mmol, 1.0 equiv.) in 1,2-DME (7.0 mL). The mixture was heated at 80 °C under N₂ and allowed to stir for 5 h. An aqueous solution of 1 M potassium dihydrogen phosphate (7.0 mL) was immediately added to the mixture and allowed to cool and stir at rt overnight. The mixture was partitioned between EtOAc (22 mL) and H₂O (7.0 mL). The two layers were separated, and the aqueous layer was extracted with EtOAc (3 x 11 mL). The combined organic extracts were dried over MgSO₄, filtered and concentrated. The clear oil was subjected to flash chromatography on silica gel, eluting with 2:1 EtOAc-Hexanes, to give τ -HAL (**15**) as a light yellow foam (105 mg, 50%). *R*_f 0.33 (95:5 CH₂Cl₂-MeOH). $[\alpha]_D^{25}$ -3.17 (c. 1.0, CHCl₃). ¹H NMR (CDCl₃, 400 MHz) δ 1.43 (s, 9H, Boc), 2.98 (dd, *J* = 14.4, 3.7 Hz, 1H, H β), 3.07 (dd, *J* = 14.4, 5.2 Hz, 1H, H' β), 4.21 (t, *J* = 6.4 Hz, 1H, Fmoc-CH), 4.28 (br s, 2H, H β '), 4.40 (appt. t, *J* = 8.6 Hz, 1H, Fmoc-CH₂), 4.52 (appt. t, *J* = 8.6 Hz, 1H, Fmoc-CH₂), 4.60–4.61 (m, 2H, H α , H α '), 4.66 (d, *J* = 11.9 Hz, 1H, CH₂TCE), 4.82 (d, *J* = 11.9 Hz, 1H, CH₂TCE), 5.16 (d, *J* = 11.8 Hz, 1H, CH₂OBn), 5.27 (d, *J* = 11.8 Hz, 1H, CH₂OBn), 5.57 (d, *J* = 5.4 Hz, 1H, NH) 6.18 (d, *J* = 7.8 Hz, 1H, NH), 6.30 (s, 1H, H5), 7.08 (s, 1H, H2), 7.30-7.43 (m, 9H, Fmoc-Ar, Ph-Ar), 7.58 (d, *J* = 7.3 Hz, 2H, Fmoc-Ar), 7.78 (d, *J* = 7.2 Hz, 2H, Fmoc-Ar); ¹³C NMR (CDCl₃, 100 MHz) δ 28.4, 29.6, 47.1, 47.8, 53.6, 54.7, 67.2, 68.3, 74.6, 79.8, 94.8, 117.1, 120.1, 125.0, 125.1, 127.1, 127.2, 127.9, 128.9, 129.1, 129.2, 134.3, 137.7, 141.4, 143.6, 155.5, 155.6, 168.8, 170.7; HRMS (ESI+) calcd for C₃₈H₄₀Cl₃N₄O₈ (M+H)⁺ 785.1912, obsd 785.1906.



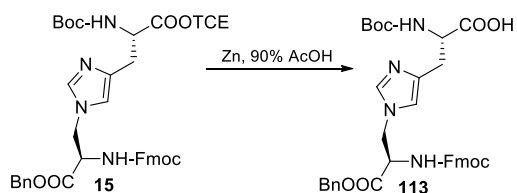
Scheme 2.45: Synthesis of compound **111**

τ -HAL [His-NH₂] (**111**). A solution of τ -HAL (**15**) (30 mg, 0.04 mmol, 1.0 equiv.) in CH₂Cl₂ (0.50 mL) was treated with TFA (0.50 mL) at 0 °C. The mixture was stirred at rt for 1 h, then quenched with a 10% triethylamine in CH₂Cl₂ solution (0.50 mL). The solution was partitioned between EtOAc (10 mL) and H₂O (10 mL). The layers were separated, and the organic layer was washed with brine (3 mL), dried over MgSO₄, and concentrated. Diethyl ether was added to the residue which was then concentrated. This was done two additional times. The residue was purified on silica gel eluting with 9:1 CH₂Cl₂-MeOH to give the free amine as a cloudy yellow oil (20 mg, 77%). *R_f* 0.21 (9:1 CH₂Cl₂-MeOH). [α]_D²⁵ -3.0 (c. 1.0, CHCl₃). ¹H NMR (DMSO-d₆, 400 MHz) δ 2.68 (dd, *J* = 13.9, 7.5 Hz, 1H, H β), 2.83 (dd, *J* = 14.3, 4.7 Hz, 1H, H' β), 3.72 (t, *J* = 5.8 Hz, 1H, H α), 4.13-4.38 (m, 5H, H β ', Fmoc-CH₂, Fmoc-CH), 4.46-4.49 (m, 1H, H α '), 4.85 (s, 2H, CH₂TCE), 5.13 (d, *J* = 12.6 Hz, 1H, CH₂OBn), 5.17 (d, *J* = 12.6 Hz, 1H, CH₂OBn), 6.93 (s, 1H, H5), 7.30 – 7.34 (m, 10H, Fmoc-Ar, Ph-Ar), 7.42 (t, *J* = 7.4 Hz, 2H, Fmoc-Ar), 7.48 (s, 1H, H2), 7.65 (t, *J* = 7.0 Hz, 2H, Fmoc-Ar), 7.90 (d, *J* = 7.4 Hz, 2H, Fmoc-Ar), 8.02 (d, *J* = 8.4 Hz, 2H, NH); ¹³C NMR (d₆-DMSO, 100 MHz) δ 33.6, 46.4, 47.0, 54.7, 55.4, 66.3, 66.9, 73.7, 95.7, 117.8, 120.6, 125.6, 127.6, 128.1, 128.3, 128.6, 128.9, 136.0, 137.6, 138.0, 141.2, 144.1, 144.2, 156.4, 170.1, 173.9. HRMS (ESI+) calcd for C₃₃H₃₁Cl₃N₄O₆ (M+H)⁺ 685.1382, obsd 685.1387.



Scheme 2.46: Synthesis of compound **112**

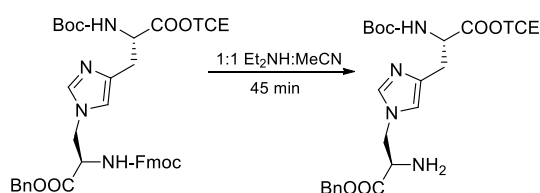
τ -HAL [Ala-OH] (**112**). τ -histidinoalanine (**15**) (30 mg, 0.04 mmol, 1.0 equiv.) was dissolved in anhydrous THF (1 mL) and 10% Pd-C (9 mg, 30% w/w) was added under N₂. The suspension was stirred at rt under an atmosphere of H₂ for 4 h. The reaction mixture was filtered through a syringe filter, and the filtrate was concentrated. The residue was purified on silica gel eluting with 20% EtOH in CH₂Cl₂ to give the free acid **112** as a colorless oil (20 mg, 77%). *R_f* 0.20 (9:1 CH₂Cl₂-MeOH). $[\alpha]_D^{25}$ -2.98 (c. 1.0, CHCl₃). ¹H NMR (DMSO-d₆, 400 MHz) δ 1.35 (s, 9H), 2.82-2.90 (m, 2H, H β), 4.11-4.24 (m, 4H, H β' , Fmoc-CH, H α'), 4.29 (t, *J* = 10.9 Hz, 2H, Fmoc-CH₂), 4.35-4.40 (m, 1H, H α), 4.82 (d, *J* = 12.3 Hz, 1H, CH₂TCE), 4.91 (d, *J* = 12.3 Hz, 1H, CH₂TCE), 6.87 (s, 1H, H5), 7.28 (d, *J* = 7.8 Hz, 1H, NH), 7.33 (t, *J* = 7.4 Hz, 2H, Fmoc-Ar), 7.41 (t, *J* = 7.4 Hz, 2H, Fmoc-Ar), 7.45 (s, 1H, H2), 7.65 (t, *J* = 12.0 Hz, 2H, Fmoc-Ar), 7.89 (d, *J* = 7.5 Hz, 3H, NH, Fmoc-Ar); ¹³C NMR (DMSO-d₆, 100 MHz) 28.6, 29.8, 47.1, 47.3, 54.1, 55.4, 66.1, 74.0, 79.0, 95.5, 118.0, 120.6, 125.6, 125.7, 127.6, 128.1, 136.9, 138.1, 141.2, 144.3, 144.4, 155.7, 156.2, 171.3, 171.6; HRMS (ESI+) calcd for C₃₁H₃₄Cl₃N₄O₈ (M+H)⁺ 695.1437, obsd 695.1426.



Scheme 2.47: Synthesis of compound **113**

τ -HAL [His-OH] (**113**). Zinc dust (125 mg, 2.00 mmol, 50.0 equiv.) was added to a solution of τ -histidinoalanine (**15**) (30 mg, 0.04 mmol, 1.0 equiv.) in glacial acetic acid (1.5 mL). The mixture

was stirred at rt for 16 h. The zinc dust and colorless precipitate that formed was filtered off. The residue was dissolved in EtOAc (5 mL) and washed with H₂O (5 mL), brine (2 x 5 mL), dried over MgSO₄, filtered, and concentrated. The residue was purified on silica gel eluting with 9:1 CH₂Cl₂:MeOH to give the free acid **113** as a cloudy pale yellow solid (15 mg, 80%). *R_f* 0.34 (9:1 CH₂Cl₂-MeOH). [α]_D²⁵ -8.12 (c. 1.0, CHCl₃). ¹H NMR (DMSO-d₆, 400 MHz) δ 1.34 (s, 9H, Boc), 2.89 (dd, *J* = 14.9, 9.5 Hz, 1H, H β), 3.02 (dd, *J* = 14.9, 4.3 Hz, 1H, H' β), 4.18-4.42 (m, 5H, H α , H β ', Fmoc-CH₂), 4.57-4.65 (m, 2H, H α ', Fmoc-CH), 5.17 (s, 2H, CH₂OBn), 7.20 (d, *J* = 8.0 Hz, 1H, NH), 7.30-7.34 (m, 10H, Fmoc-Ar, Ph-Ar, H₅, H₂), 7.42 (t, *J* = 7.5 Hz, 2H, Fmoc-Ar), 7.64 (d, *J* = 7.5 Hz, 2H, Fmoc-Ar), 7.90 (d, *J* = 7.5 Hz, 2H, Fmoc-Ar), 8.10 (d, *J* = 8.2 Hz, 2H, NH), 8.73 (br s, 1H, COOH); ¹³C NMR (d₆-DMSO, 100 MHz) δ 28.5, 29.5, 30.4, 46.4, 47.0, 54.4, 55.3, 66.3, 66.9, 78.3, 117.4, 120.6, 125.6, 127.6, 127.8, 128.1, 128.3, 128.5, 128.9, 129.4, 136.0, 137.9, 138.2, 141.2, 144.1, 144.2, 155.7, 156.4, 170.1, 174.6; HRMS (ESI+) calcd for C₃₆H₃₉N₄O₈ (M+H)⁺ 655.2762, obsd 655.2763.



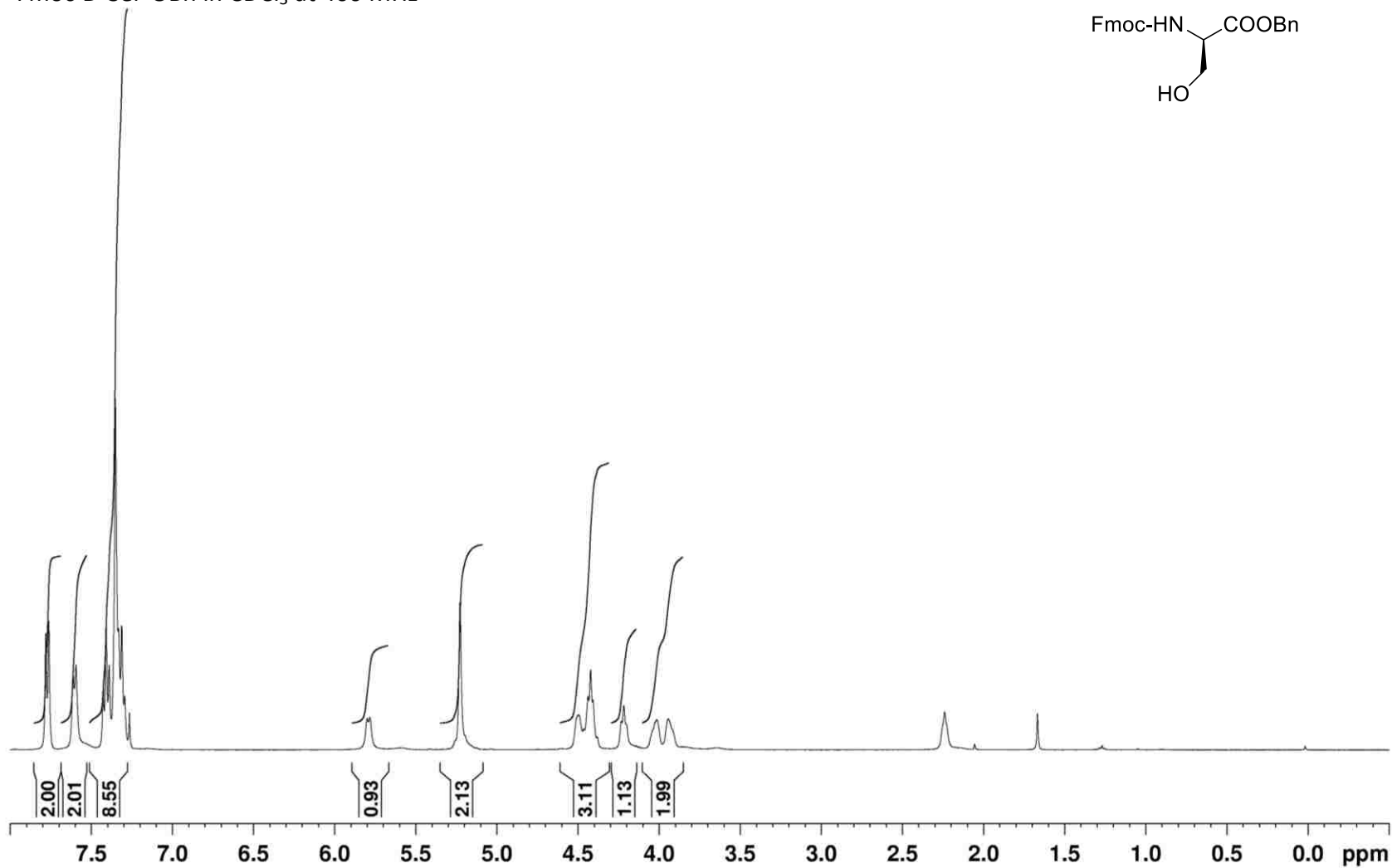
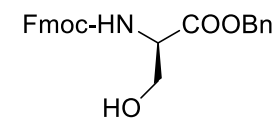
Scheme 2.48: Synthesis of compound **114**

τ -HAL [Ala-NH₂] (**114**). τ -Histidinoalanine (**15**) (45 mg, 0.06 mmol) was dissolved in a mixture of Et₂NH (0.6 mL) and MeCN (0.6 mL). The mixture was allowed to stir for 45 min, until the starting material was completely consumed. The solution was concentrated and then concentrated twice more from CH₃CN (2 x 3 mL). The residue was purified by flash chromatography on silica gel eluting with 4% MeOH in CH₂Cl₂ to give the free amine as a colorless oil (35 mg, 94%). *R_f*

0.62 (9:1 CH₂Cl₂-MeOH). [α]_D²⁵ -2.1 (c. 1.0, CHCl₃). ¹H NMR (CDCl₃, 400 MHz) δ 1.44 (s, 9H, Boc), 2.63 (br s, 2H, NH₂), 3.04 (dd, *J* = 14.7, 4.3 Hz, 1H, H β), 3.13 (dd, *J* = 14.7, 5.7 Hz, 1H, H' β), 3.82 (app. t, *J* = 4.9 Hz, 1H, H α), 4.15 (dd, *J* = 14.1, 5.7 Hz, 1H, H β '), 4.22 (dd, *J* = 14.1, 4.4 Hz, 1H, H' β '), 4.64 (d, *J* = 11.8 Hz, 1H, CH₂TCE), 4.83 (d, *J* = 11.8 Hz, 1H, CH₂TCE), 5.16 (d, *J* = 11.9 Hz, 1H, CH₂OBn), 5.21 (d, *J* = 11.9 Hz, 1H, CH₂OBn), 6.20 (d, *J* = 8.0 Hz, 1H, NH), 6.62 (s, 1H, H5), 7.35-7.41 (m, 5H, Ph-Ar), 7.46 (s, 1H, H2); ¹³C NMR (CDCl₃, 100 MHz) 28.4, 29.4, 50.3, 53.6, 55.0, 67.7, 74.5, 79.8, 94.7, 117.4, 128.8, 128.9, 134.8, 137.0, 137.6, 155.7, 170.6, 172.1; HRMS (ESI+) calcd for C₂₃H₃₀Cl₃N₄O₆ (M+H)⁺ 563.1225, obsd 563.1204.

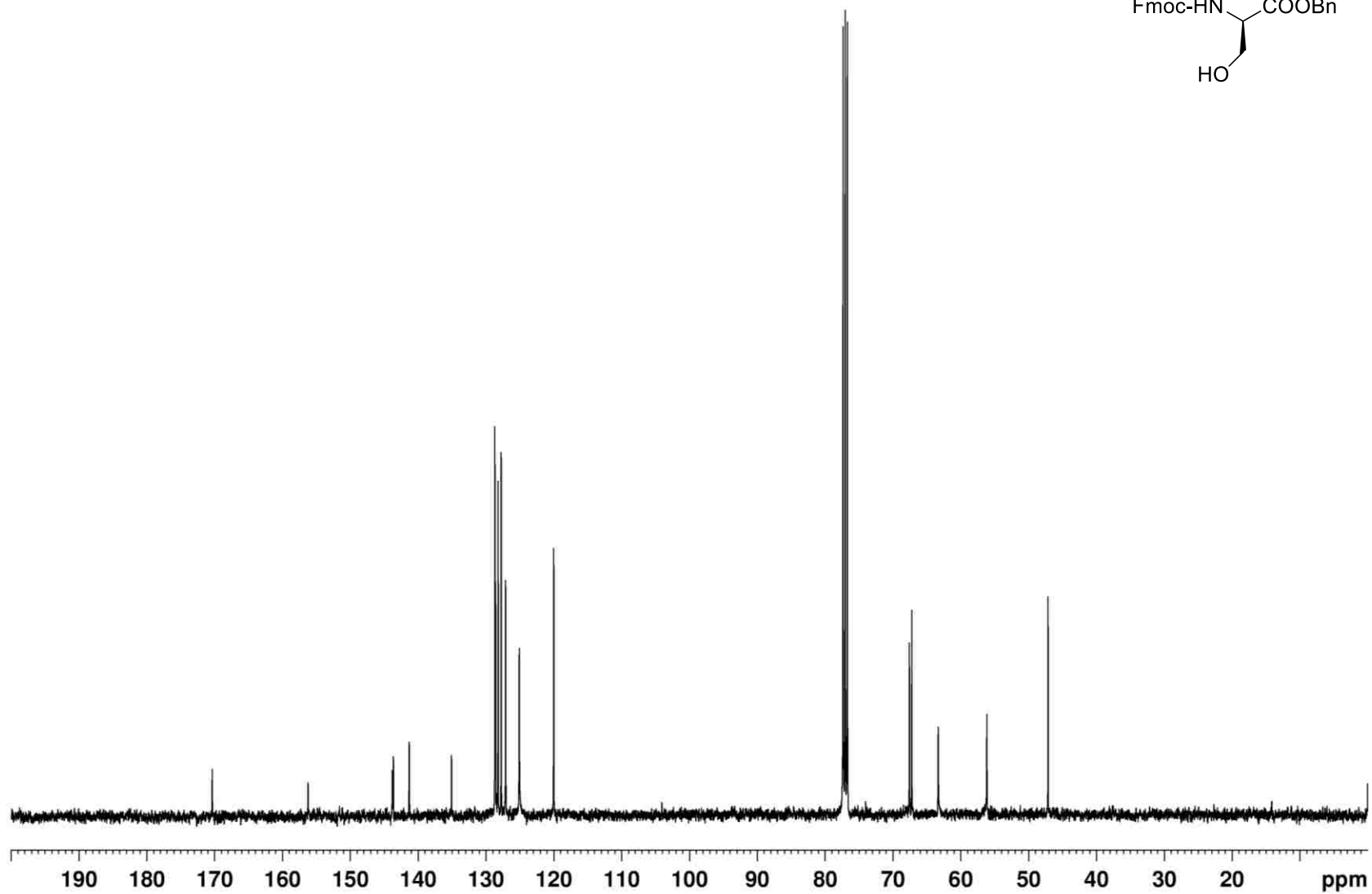
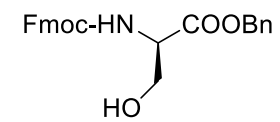
2.5.2 ^1H and ^{13}C NMR Spectra

Compound **69** (Scheme 2.20) – ^1H NMR spectrum
Fmoc-*D*-Ser-OBn in CDCl_3 at 400 MHz



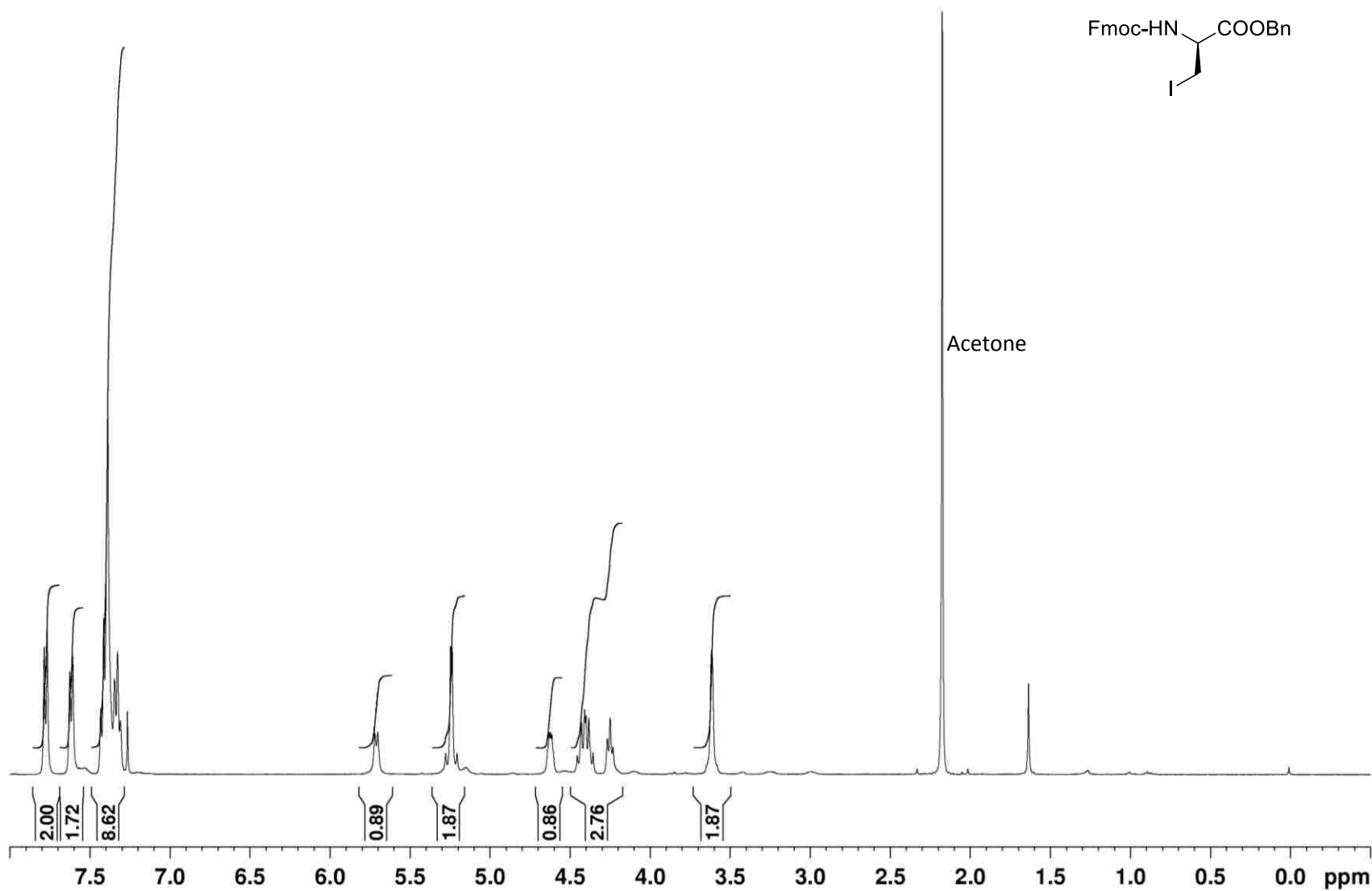
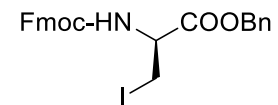
Compound **69** (Scheme 2.20) – ^{13}C NMR spectrum

Fmoc-*D*-Ser-OBn in CDCl_3 at 400 MHz



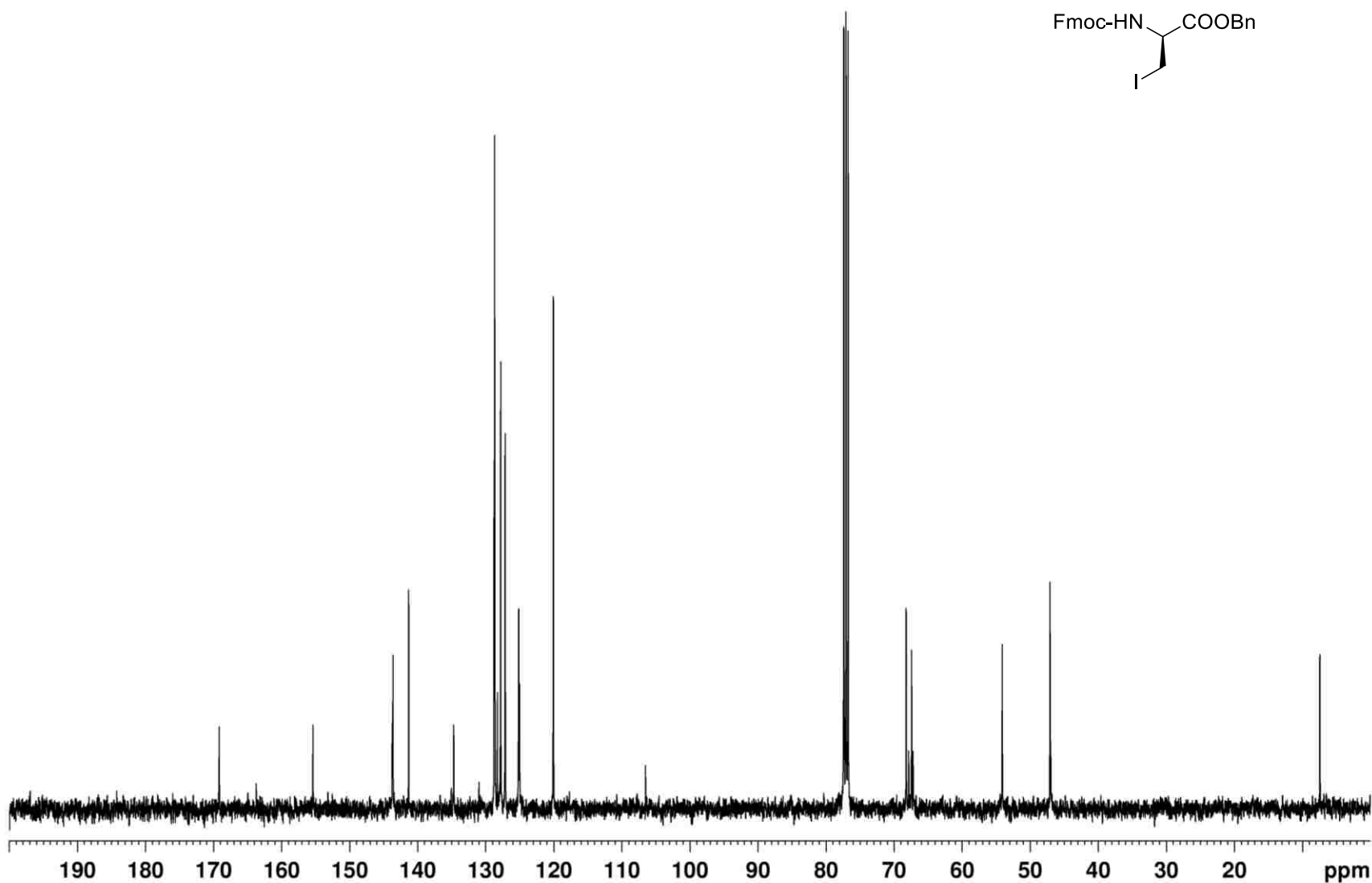
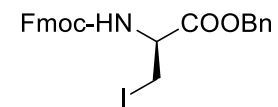
Compound **70** (Scheme 2.5) – ^1H NMR spectrum

Fmoc-D-Ser(I)-OBn in CDCl_3 at 400 MHz



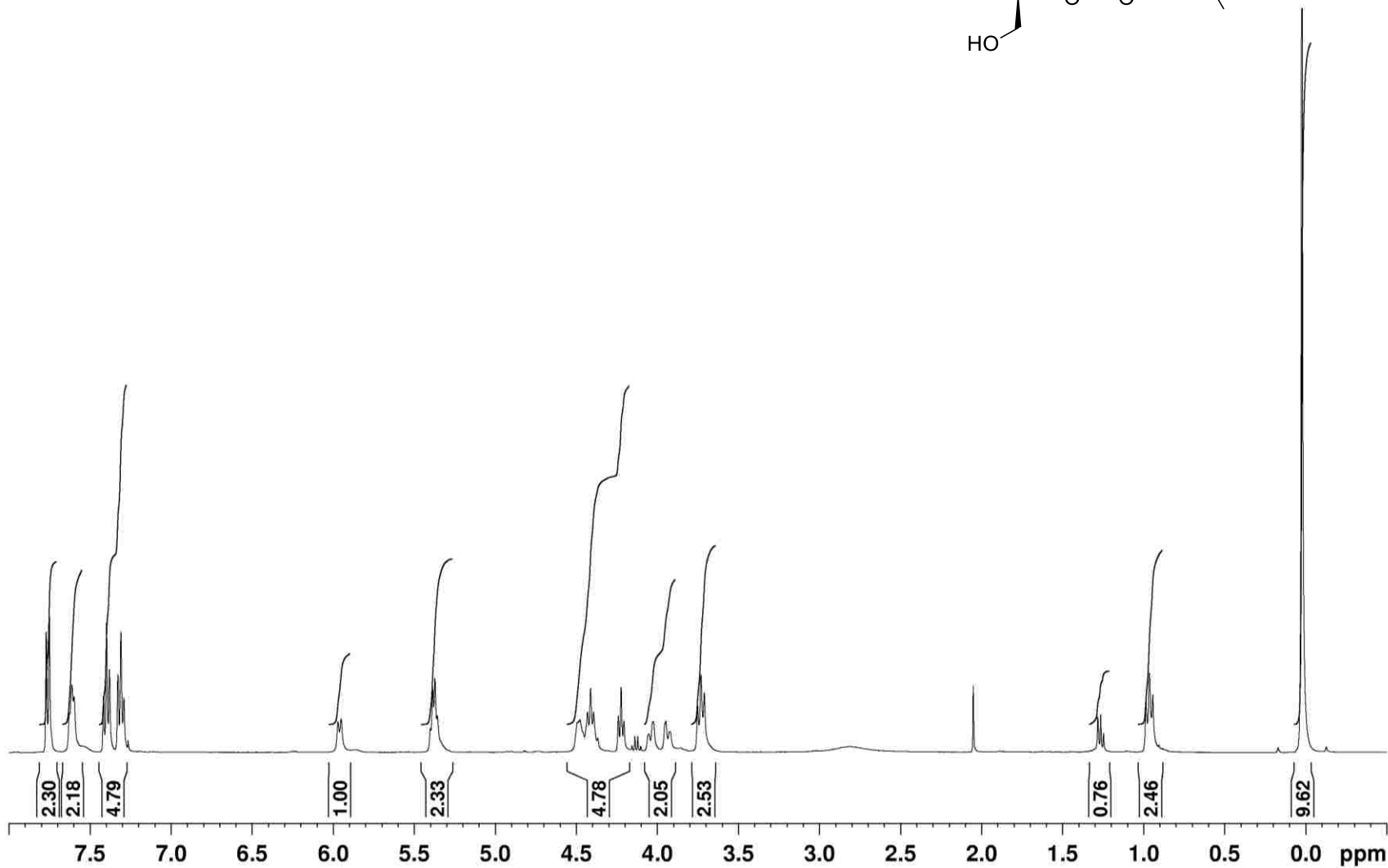
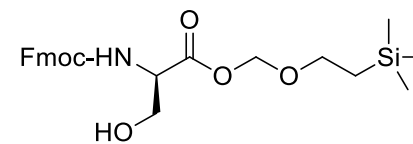
Compound **70** (Scheme 2.5) – ^{13}C NMR spectrum

Fmoc-D-Ser(I)-OBn in CDCl_3 at 400 MHz



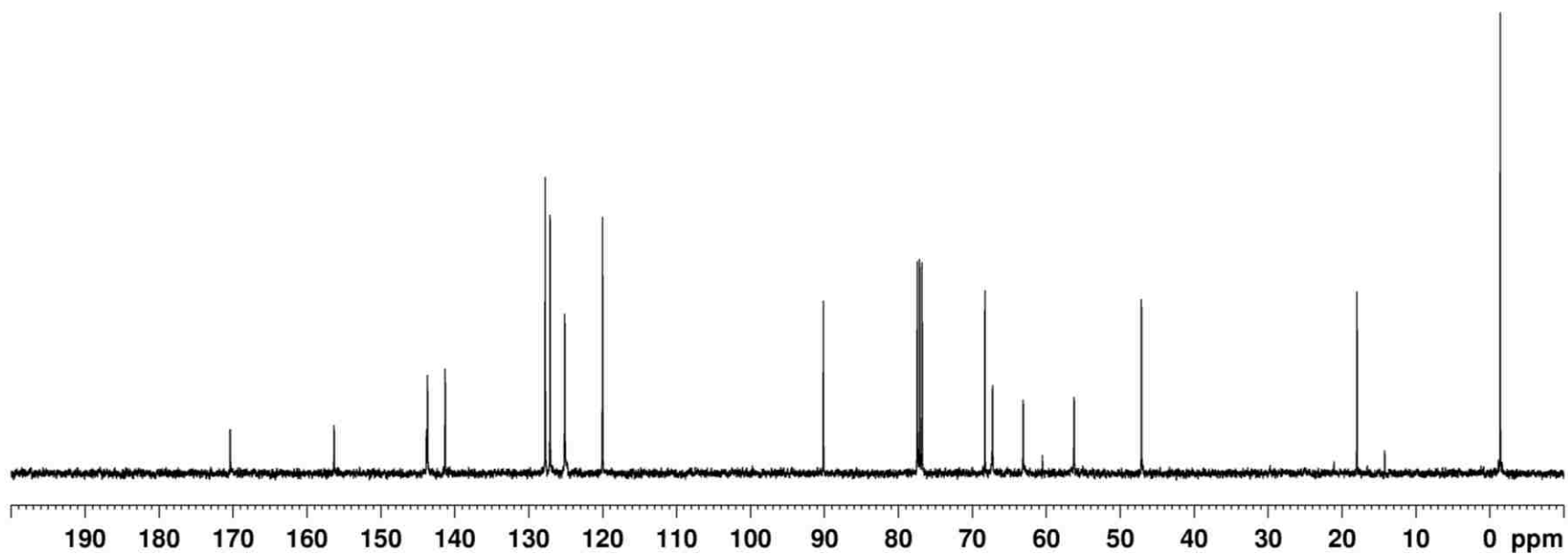
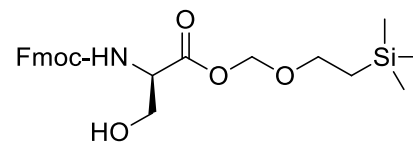
Compound **76** (Scheme 2.8) – ^1H NMR spectrum

Fmoc-*D*-Ser-OSEM in CDCl_3 at 400 MHz



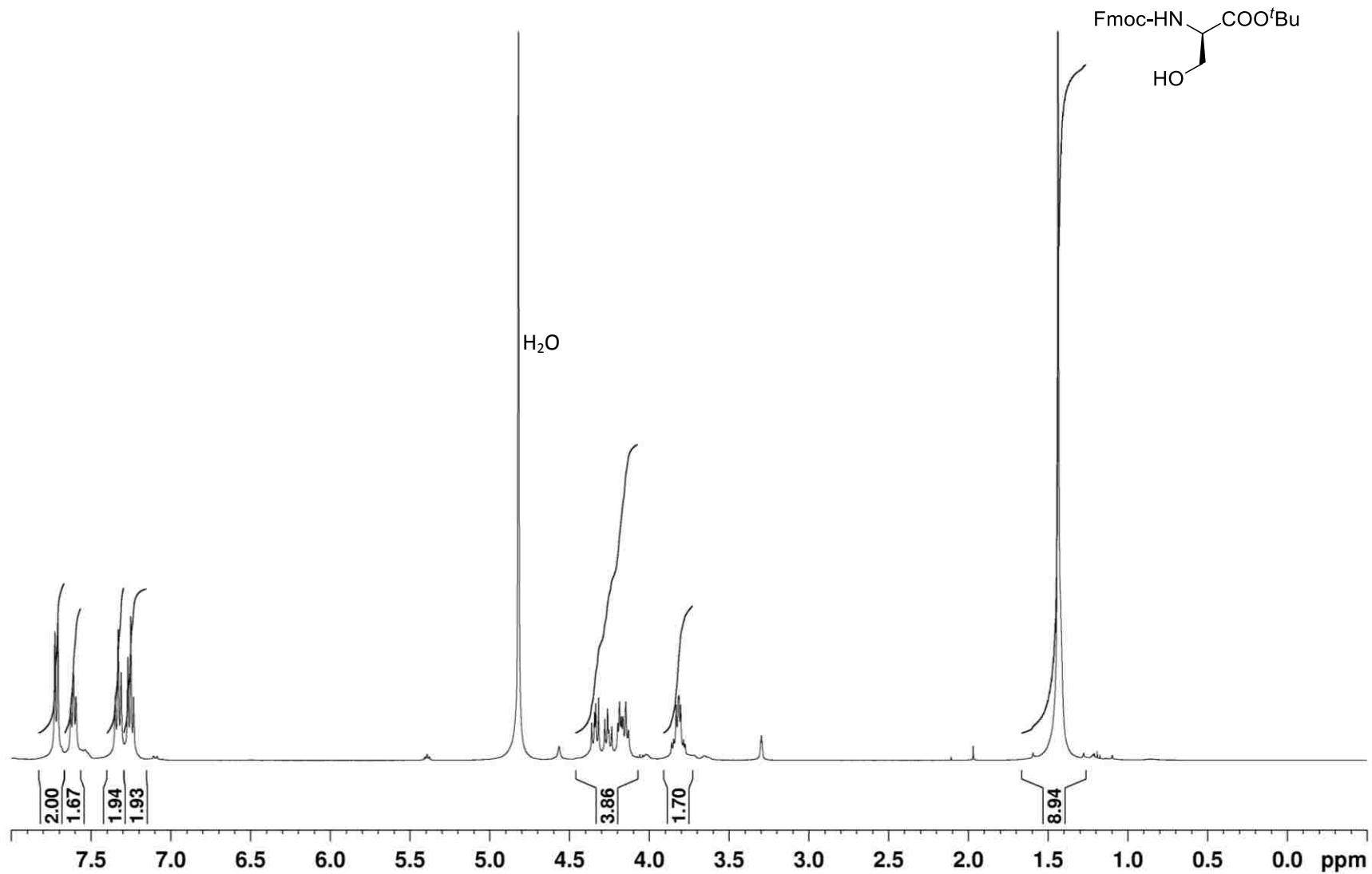
Compound **76 (Scheme 2.8)** – ^{13}C NMR spectrum

Fmoc-*D*-Ser-OSEM in CDCl_3 at 400 MHz



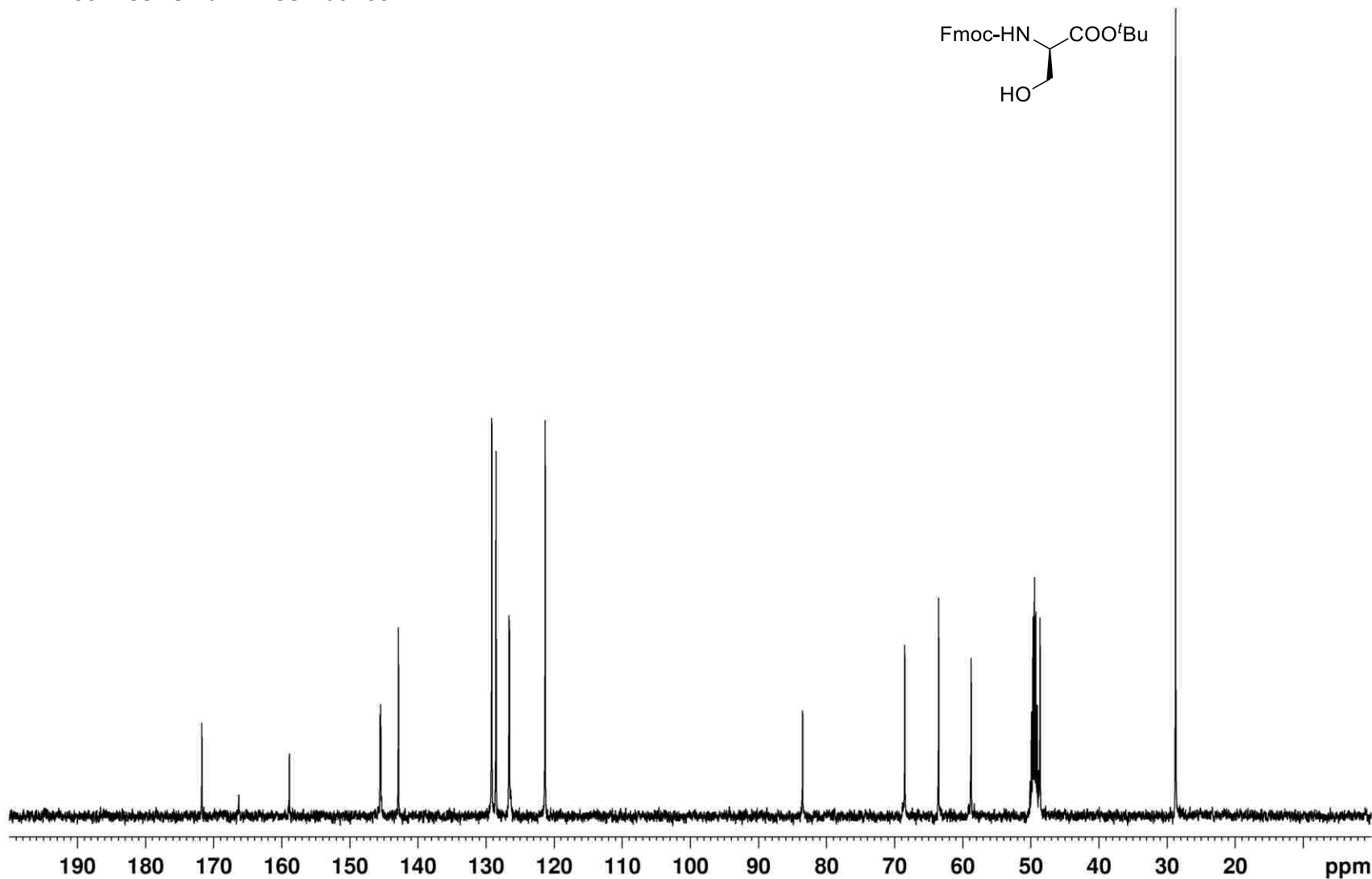
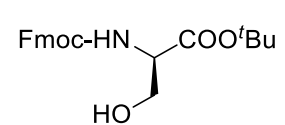
Compound **80** (Scheme 2.9) – ^1H NMR spectrum

Fmoc-*D*-Ser-O^tBu in MeOD at 400 MHz



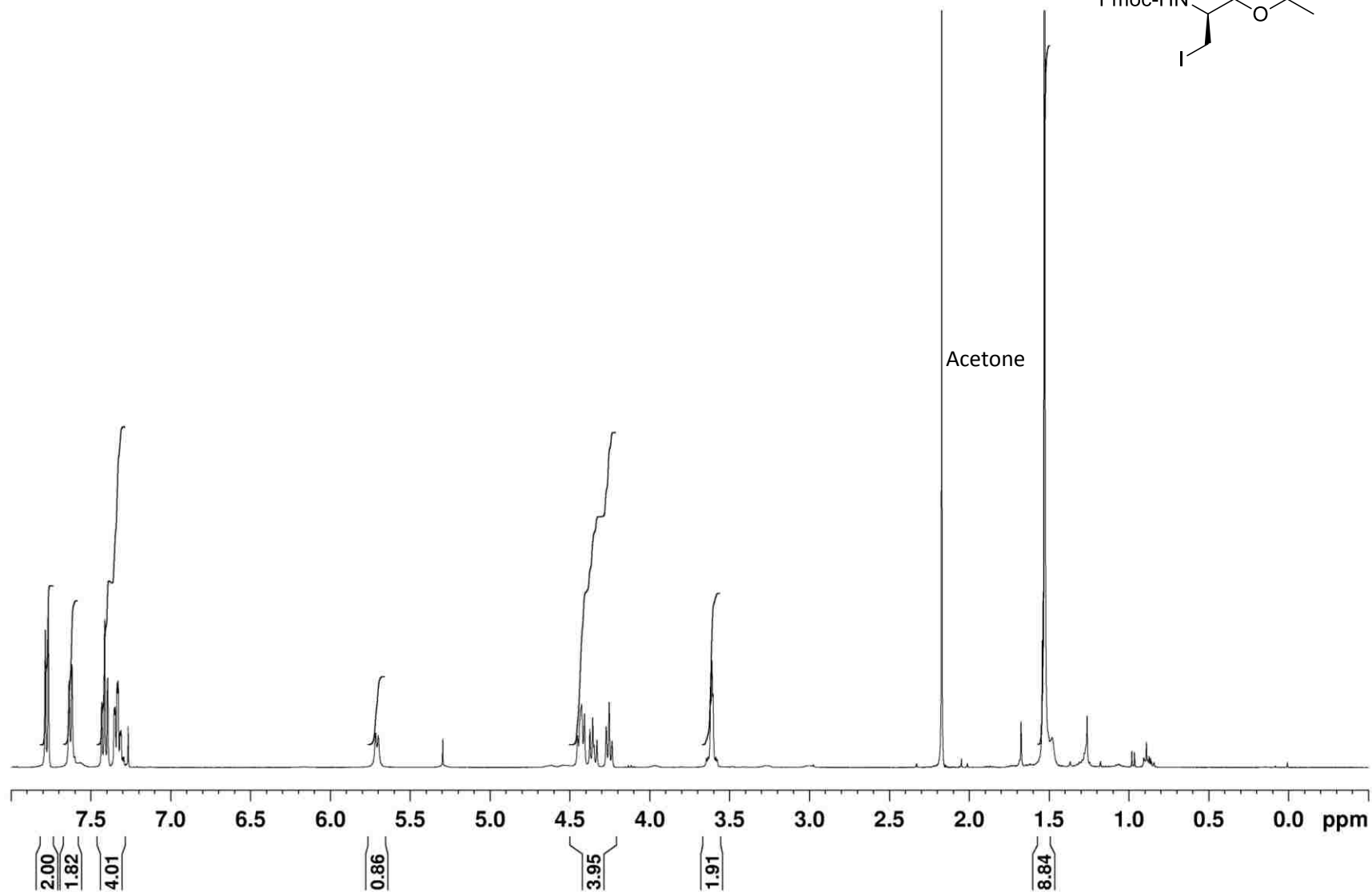
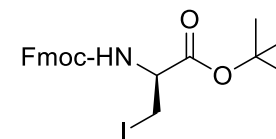
Compound **80** (Scheme 2.9) – ^{13}C NMR spectrum

Fmoc-*D*-Ser- O^tBu in MeOD at 100 MHz



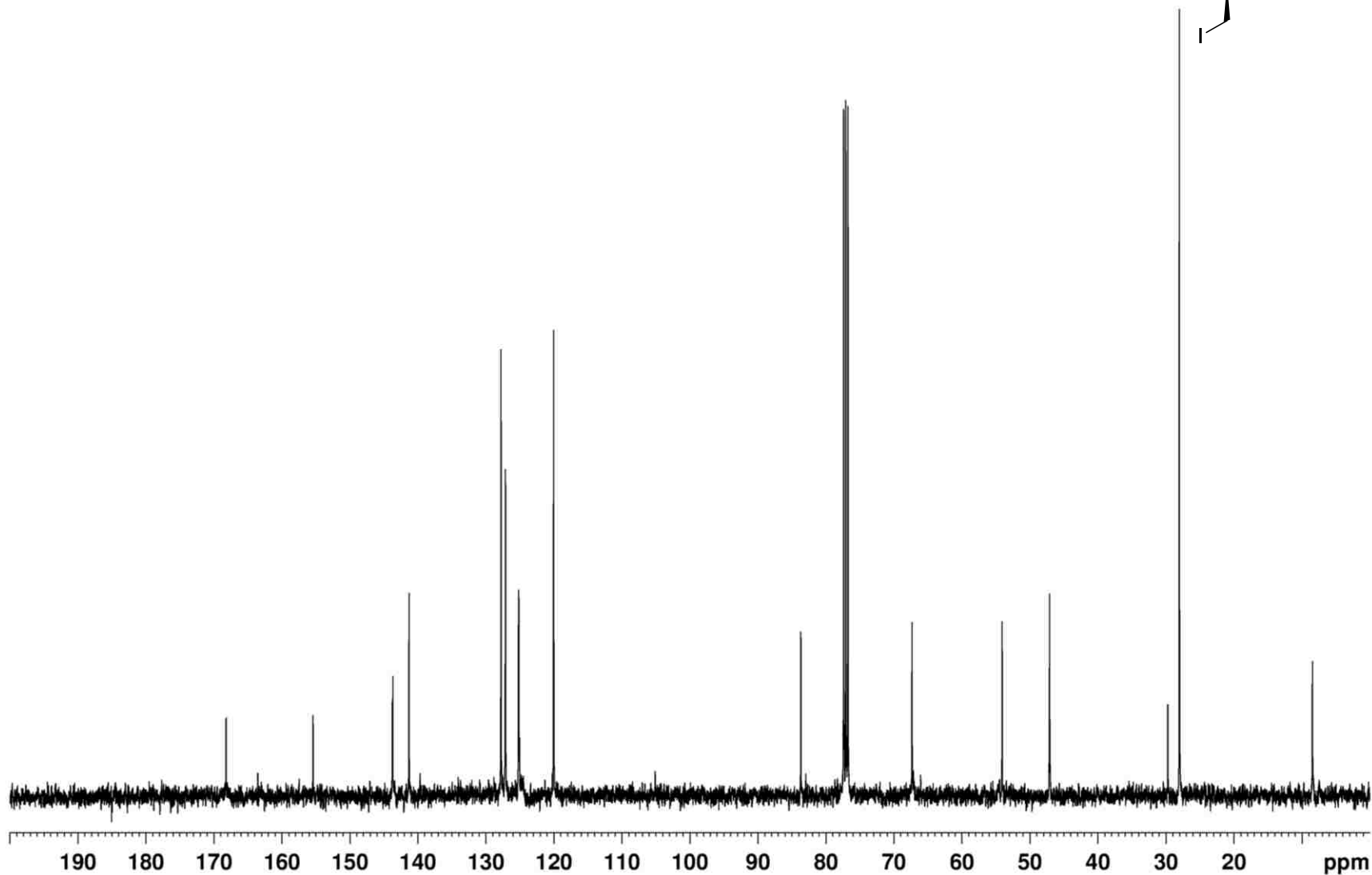
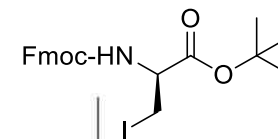
Compound **81** (Scheme 2.9) – ^1H NMR spectrum

Fmoc-D-Ser(I)-O^tBu in CDCl₃ at 400 MHz



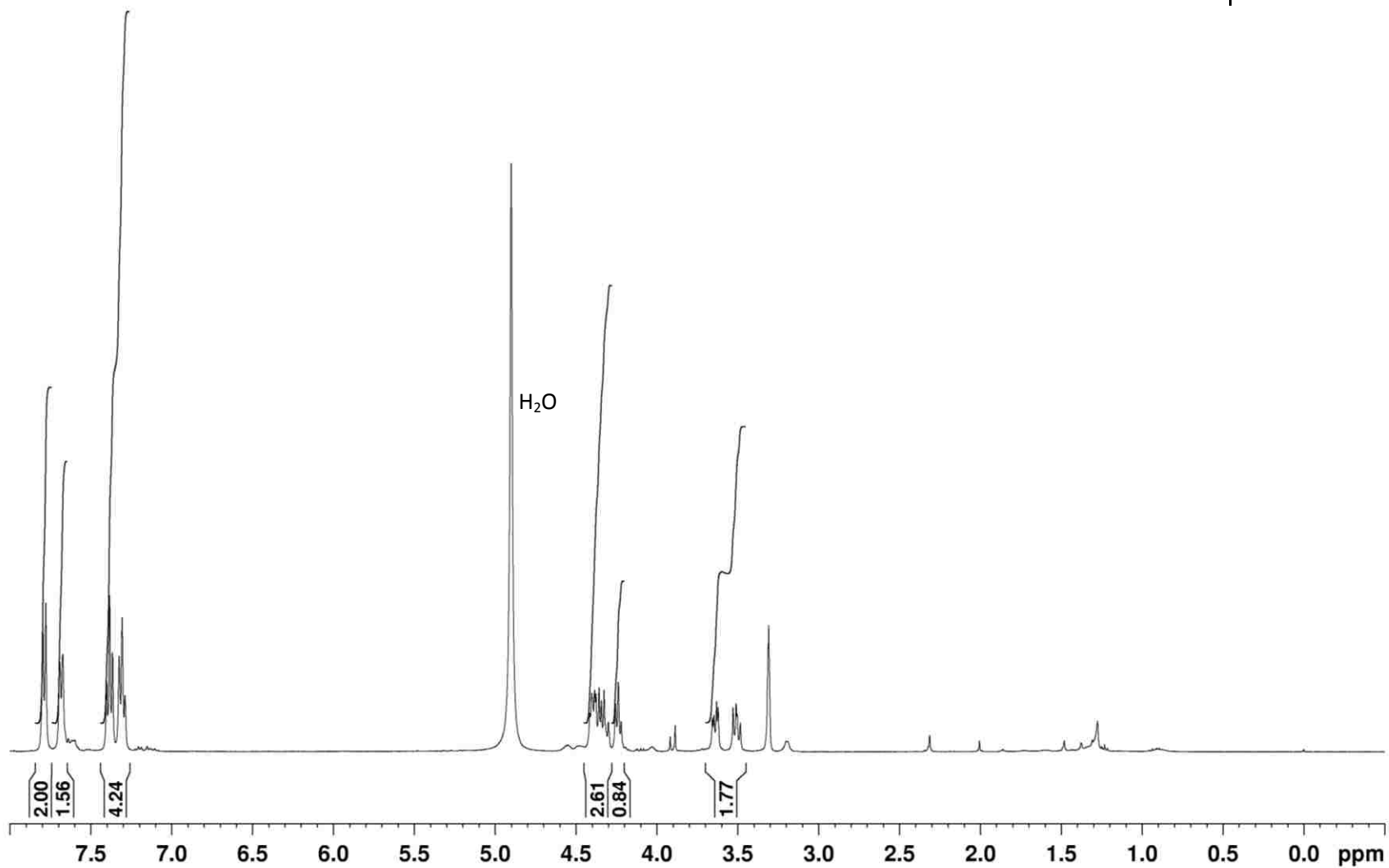
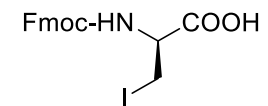
Compound **81** (Scheme 2.9) – ^{13}C NMR spectrum

Fmoc-*D*-Ser(I)-O^tBu in CDCl₃ at 400 MHz



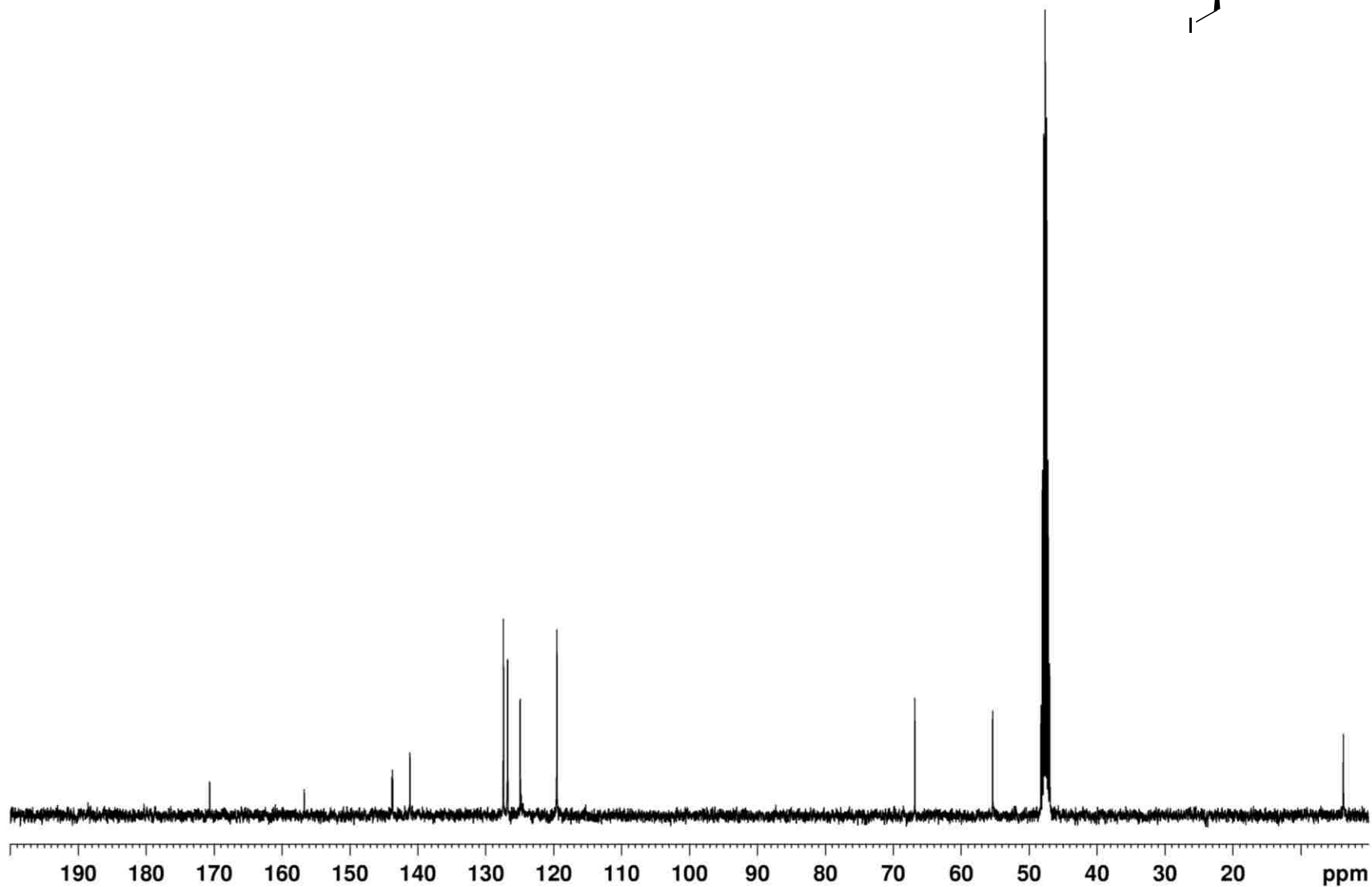
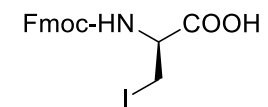
Compound **78** (Scheme 2.9) – ^1H NMR spectrum

Fmoc-*D*-Ser(I)-OH in CD_3OD at 400 MHz



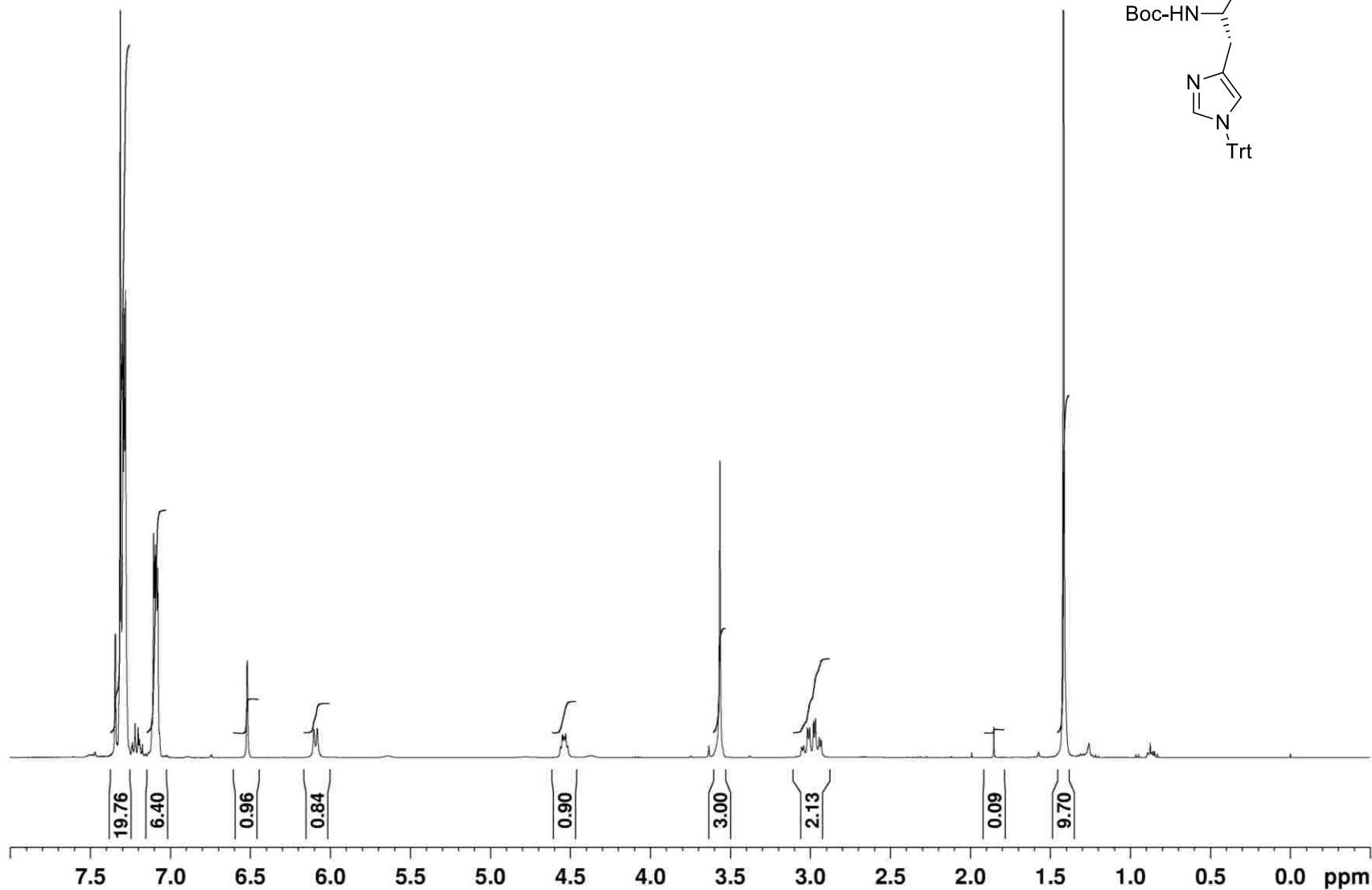
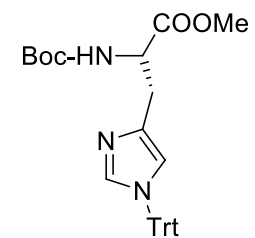
Compound **78** (Scheme 2.9) – ^{13}C NMR spectrum

Fmoc-*D*-Ser(I)-OH in CD_3OD at 400 MHz



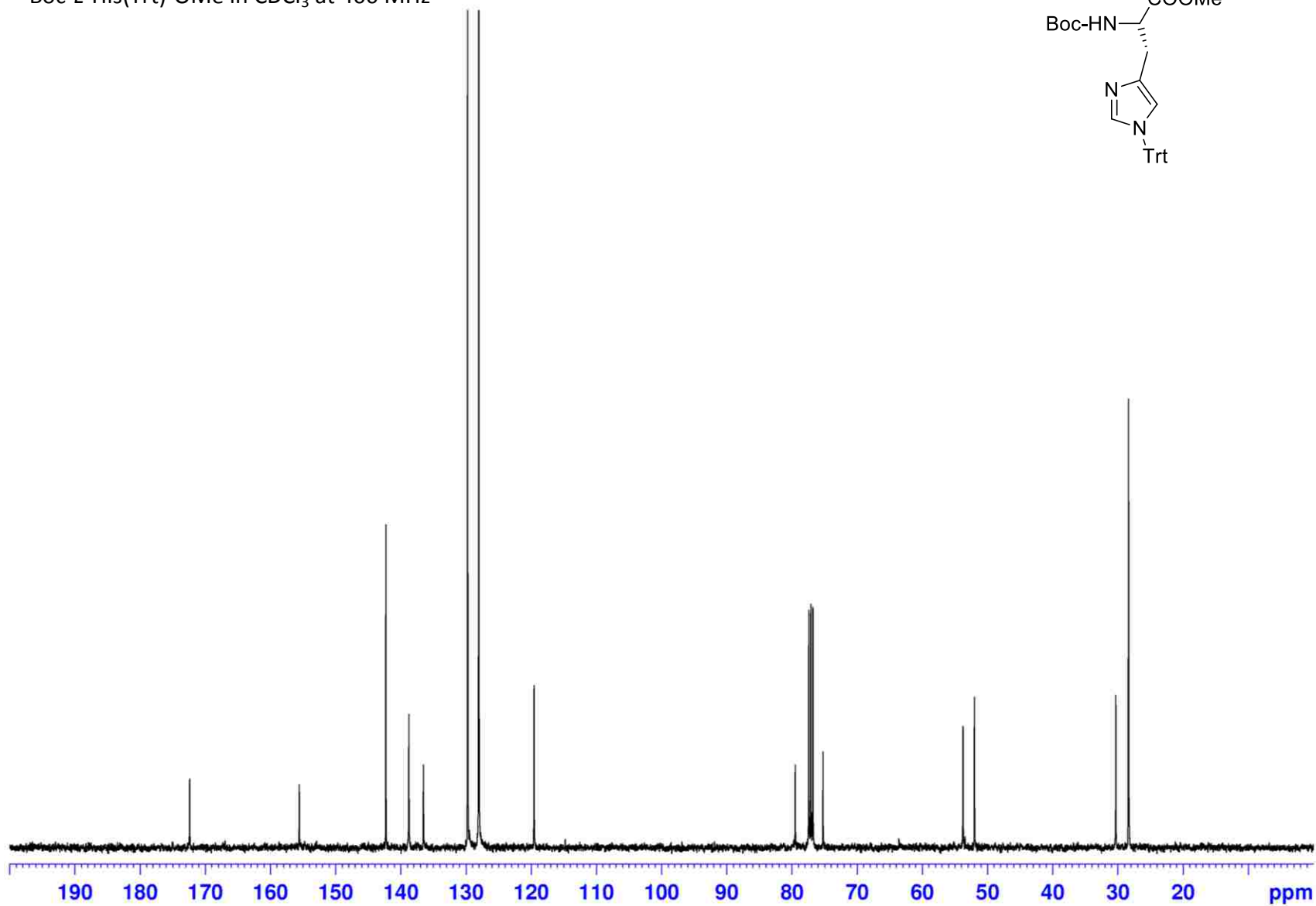
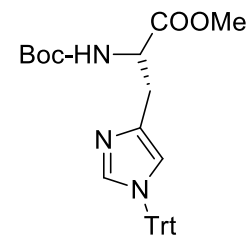
Compound **82** (Scheme 2.10) – ^1H NMR spectrum

Boc-L-His(Trt)-OMe in CDCl_3 at 400 MHz



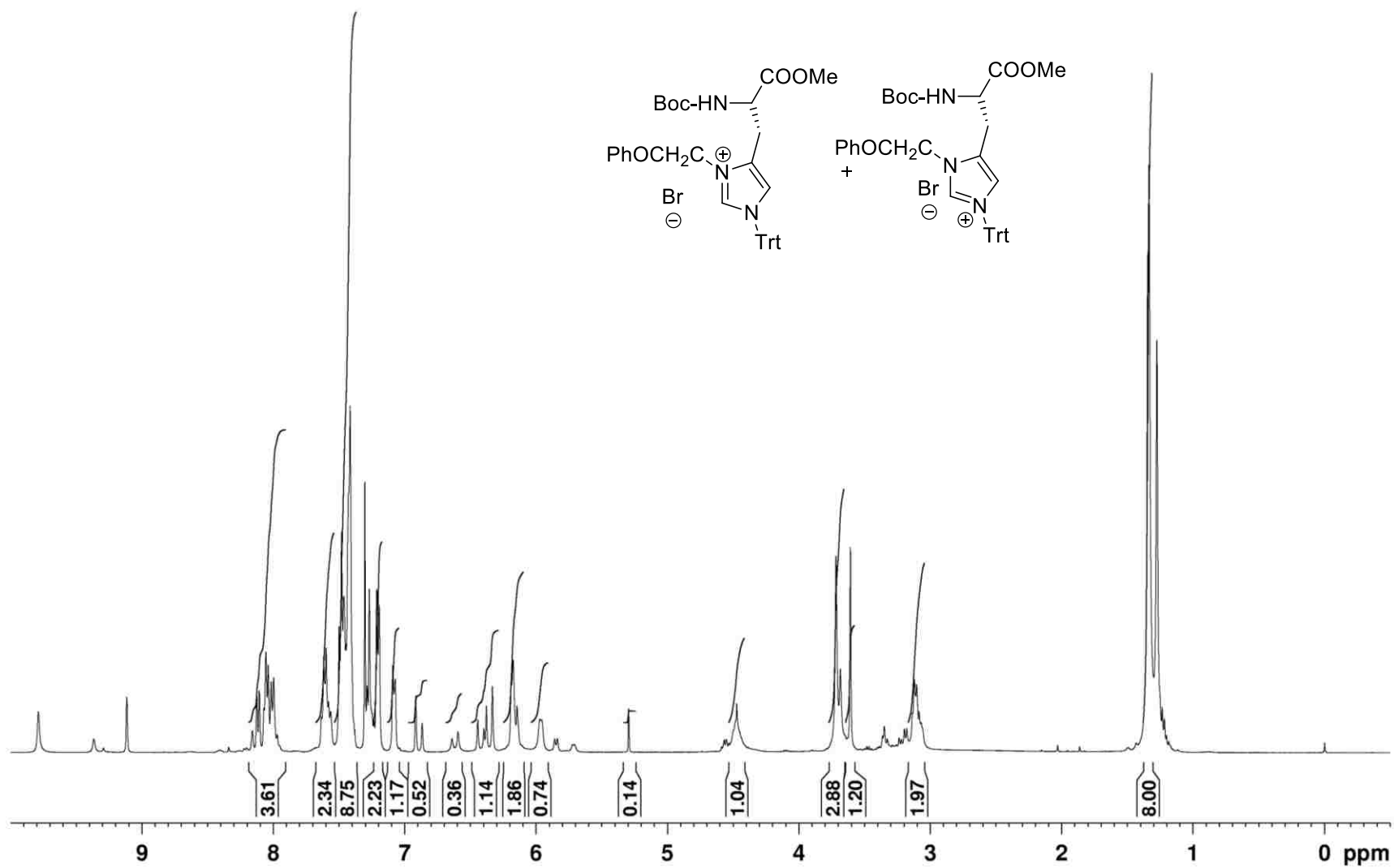
Compound **82** (Scheme 2.10) – ^{13}C NMR spectrum

Boc-*L*-His(Trt)-OMe in CDCl_3 at 400 MHz



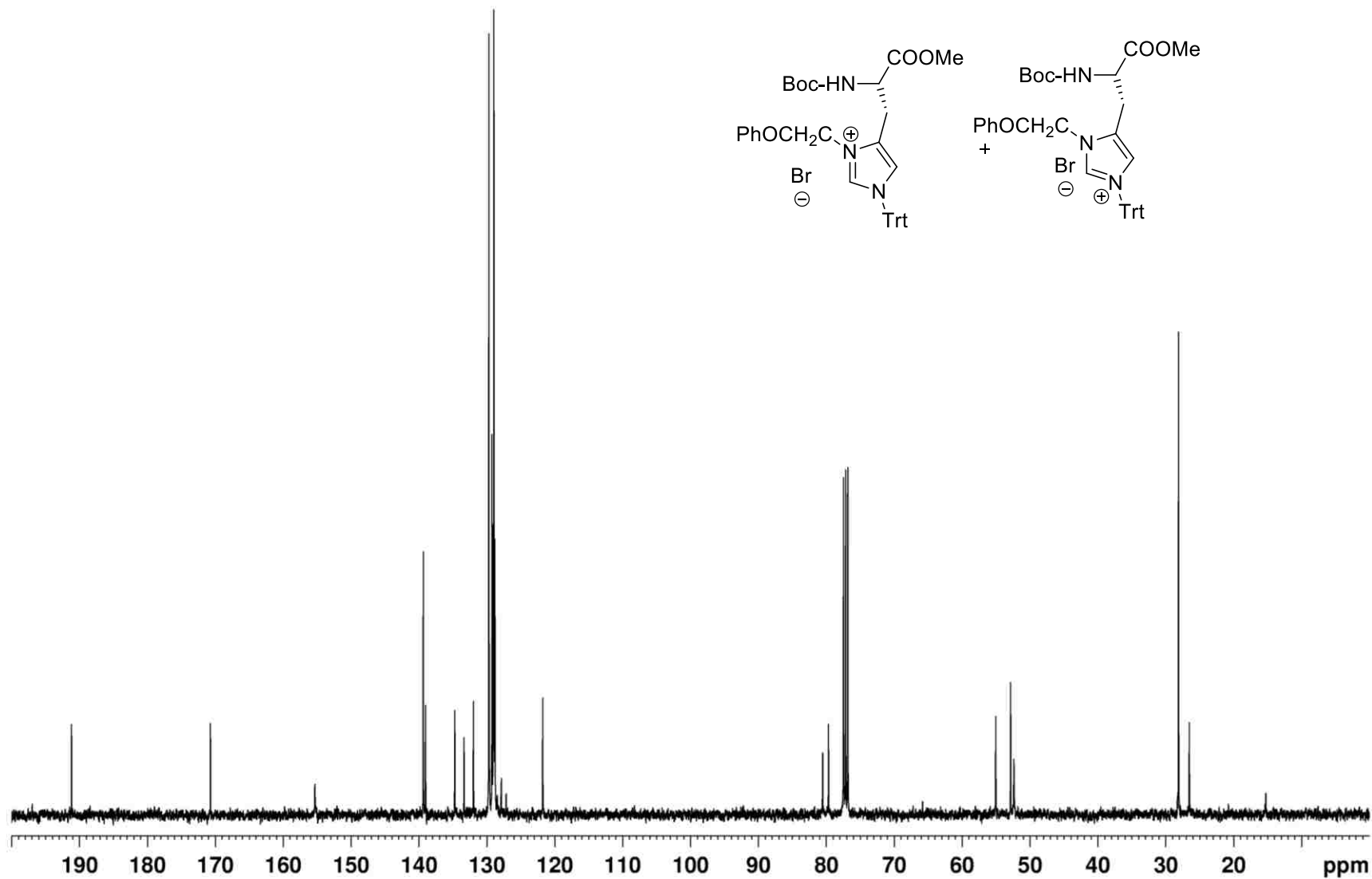
Compound **83** (Scheme 2.10) – ^1H NMR spectrum

Boc-*L*-His(π -Pac, τ -Trt)-OMe imidazolium bromine salt in CDCl_3 at 400 MHz



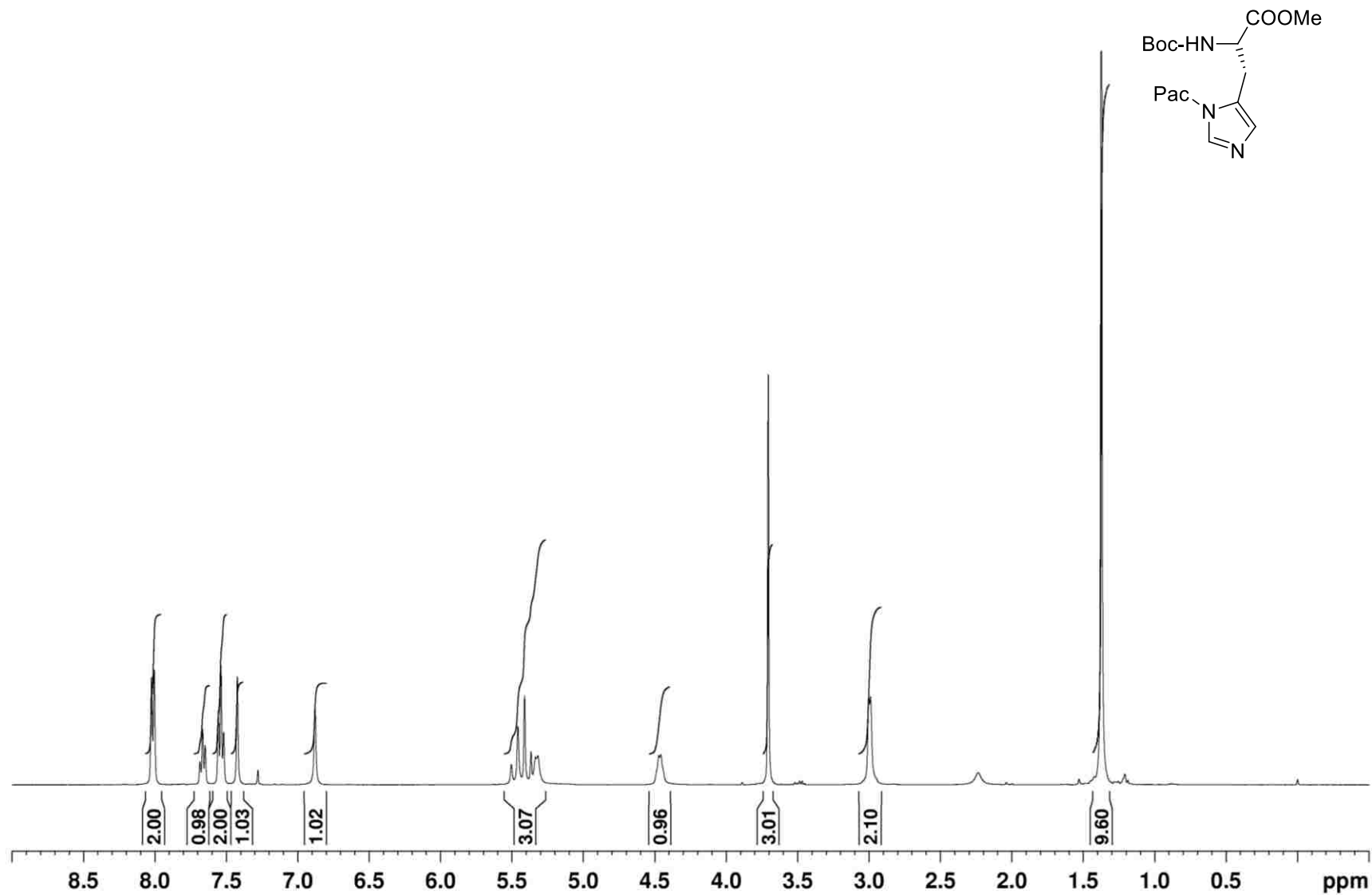
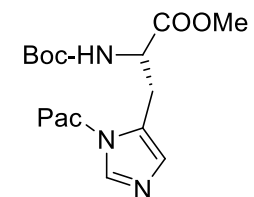
Compound **83** (Scheme 2.10) – ^{13}C NMR spectrum

Boc-*L*-His(π -Pac, τ -Trt)-OMe imidazolium bromine salt in CDCl_3 at 400 MHz



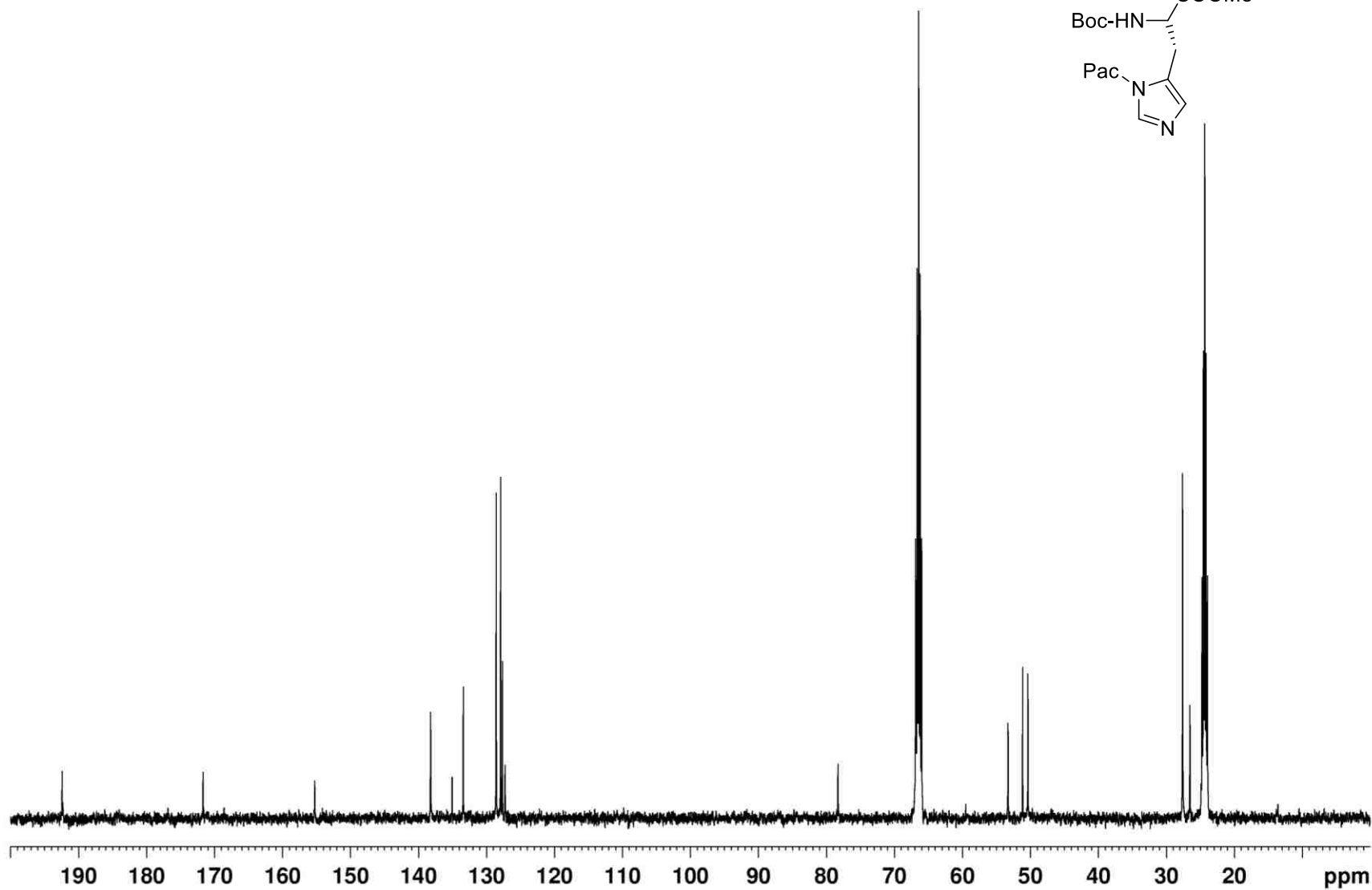
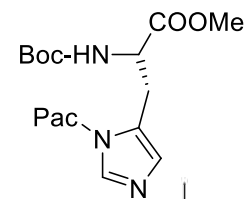
Compound **84** (Scheme 2.10) – ^1H NMR spectrum

Boc-L-His(π -Pac)-OMe in CDCl_3 at 400 MHz



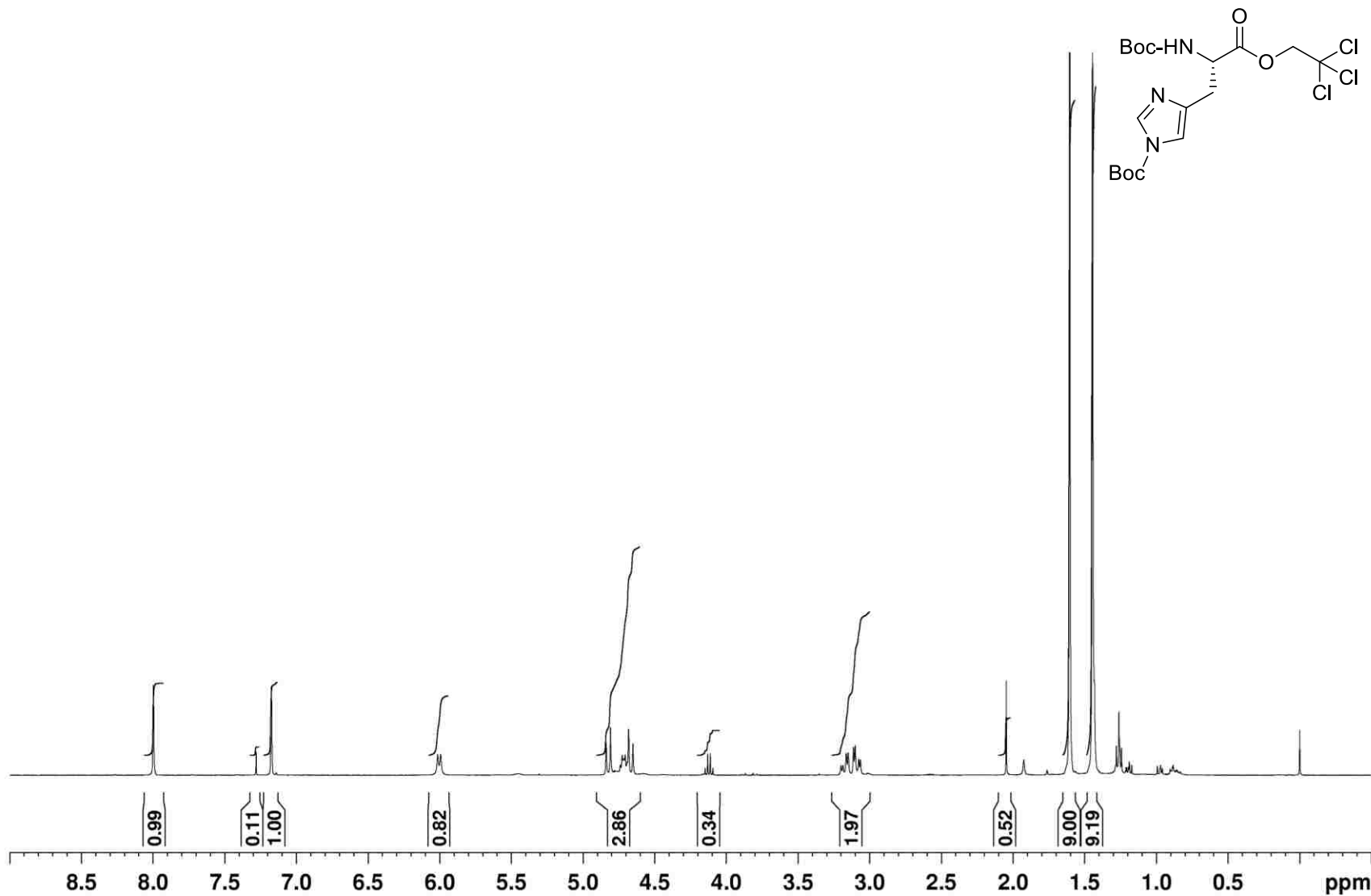
Compound **84** (Scheme 2.10) – ^{13}C NMR spectrum

Boc-L-His(π -Pac)-OMe in THF- d_8 at 400 MHz



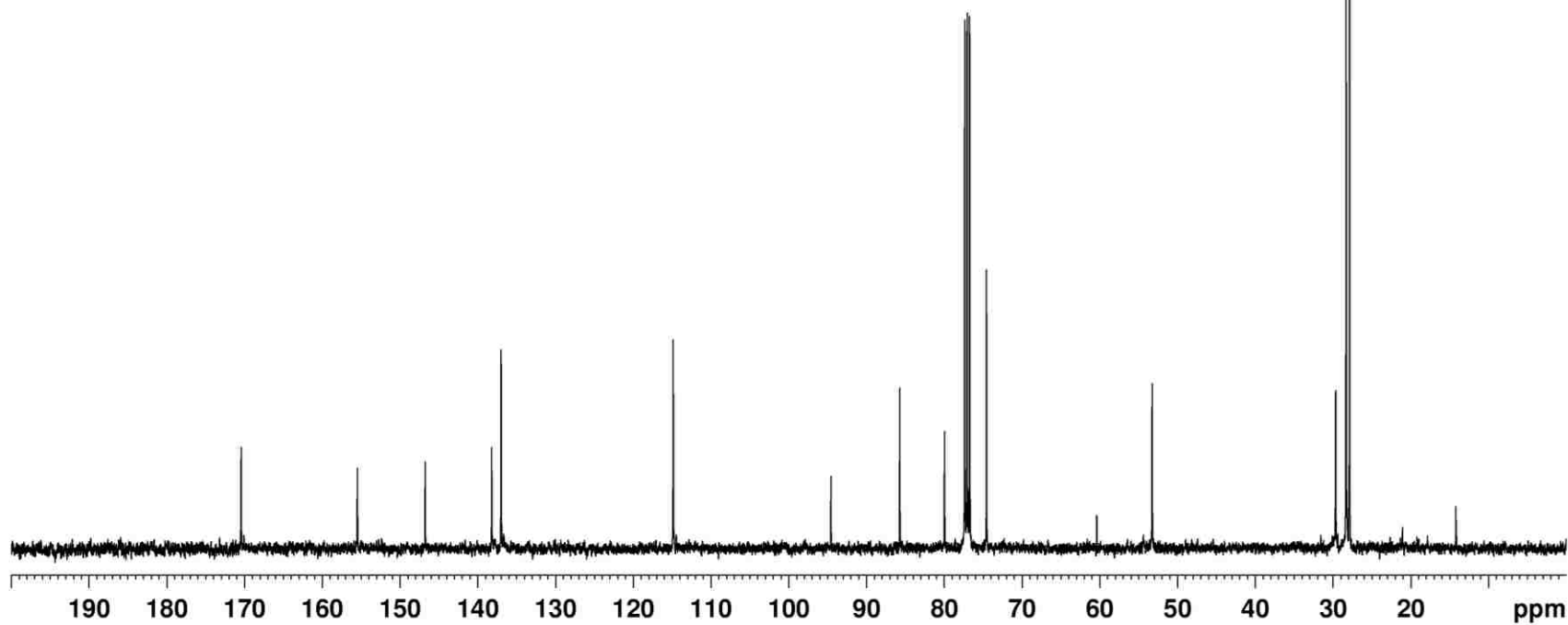
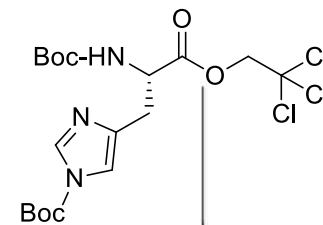
Compound **100** (Scheme 2.18) – ¹H NMR spectrum

Boc-L-His(Boc)-OTCE in CDCl₃ at 400 MHz



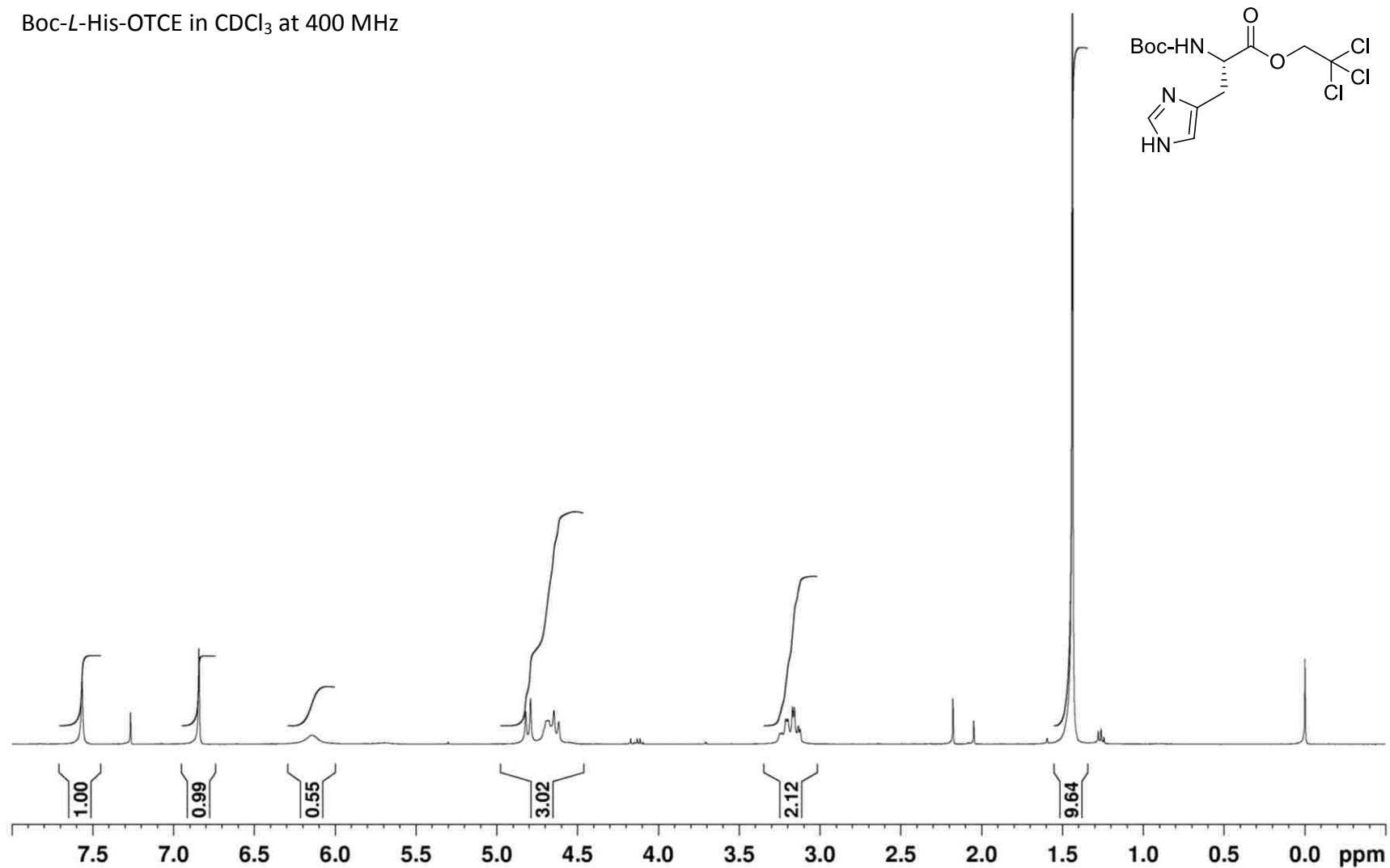
Compound **100** (Scheme 2.18) – ^{13}C NMR spectrum

Boc-*L*-His(Boc)-OTCE in CDCl_3 at 400 MHz



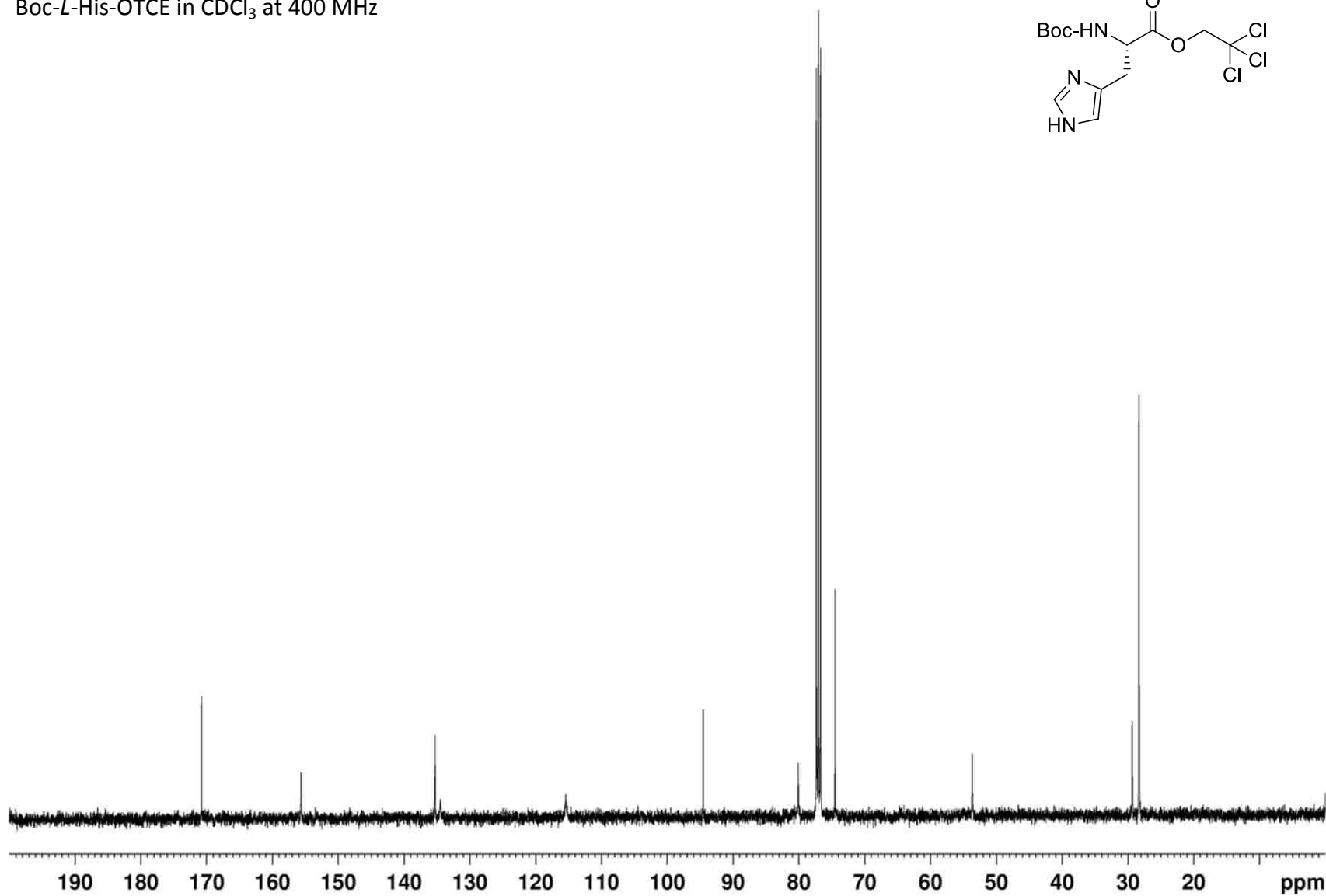
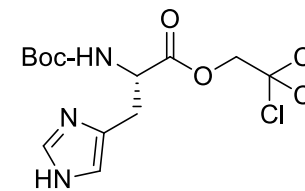
Compound **97** (Scheme 2.19) – ^1H NMR spectrum

Boc-L-His-OTCE in CDCl_3 at 400 MHz



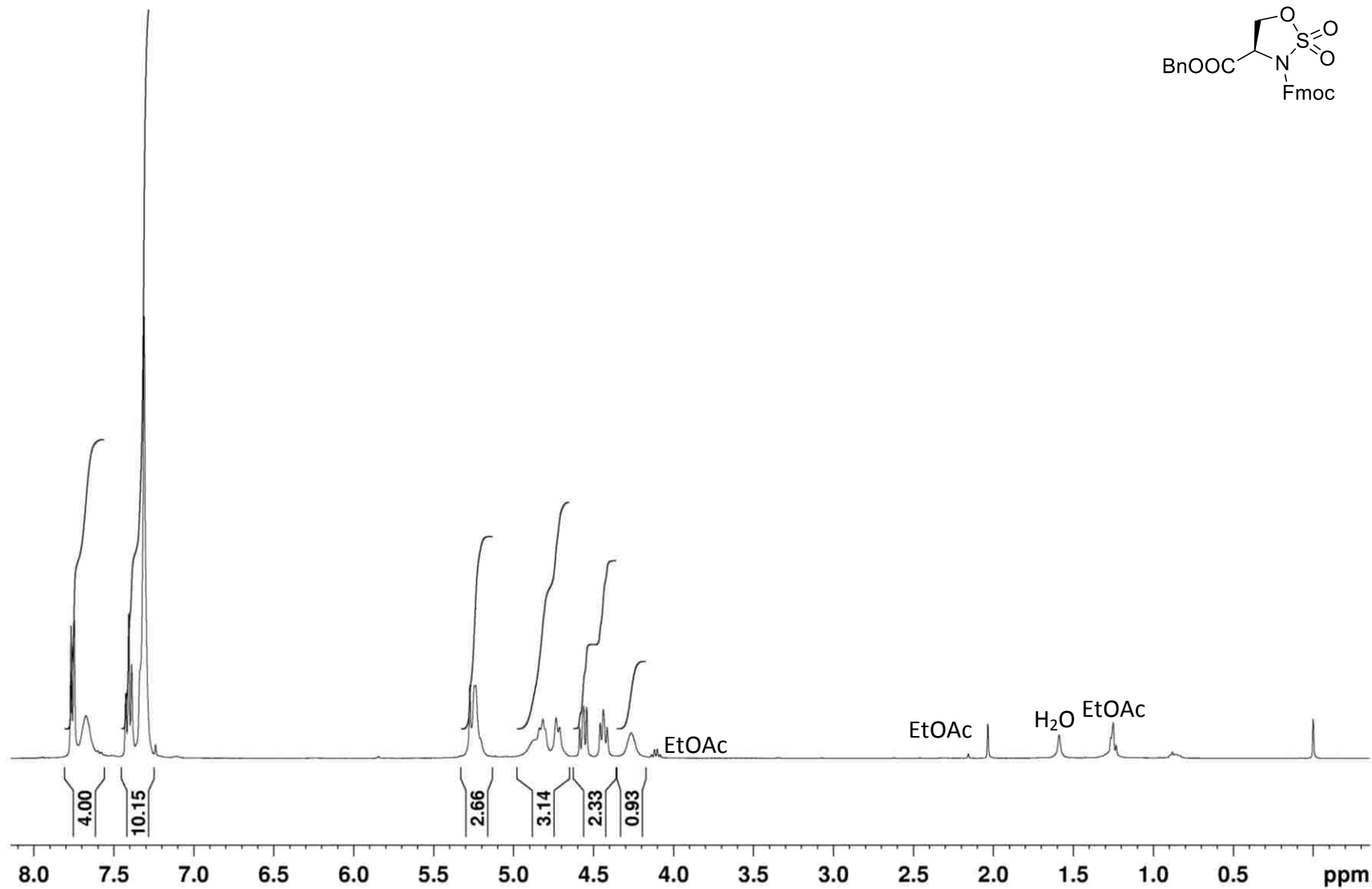
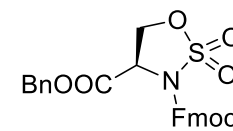
Compound **97** (Scheme 2.19) – ^{13}C NMR spectrum

Boc-L-His-OTCE in CDCl_3 at 400 MHz



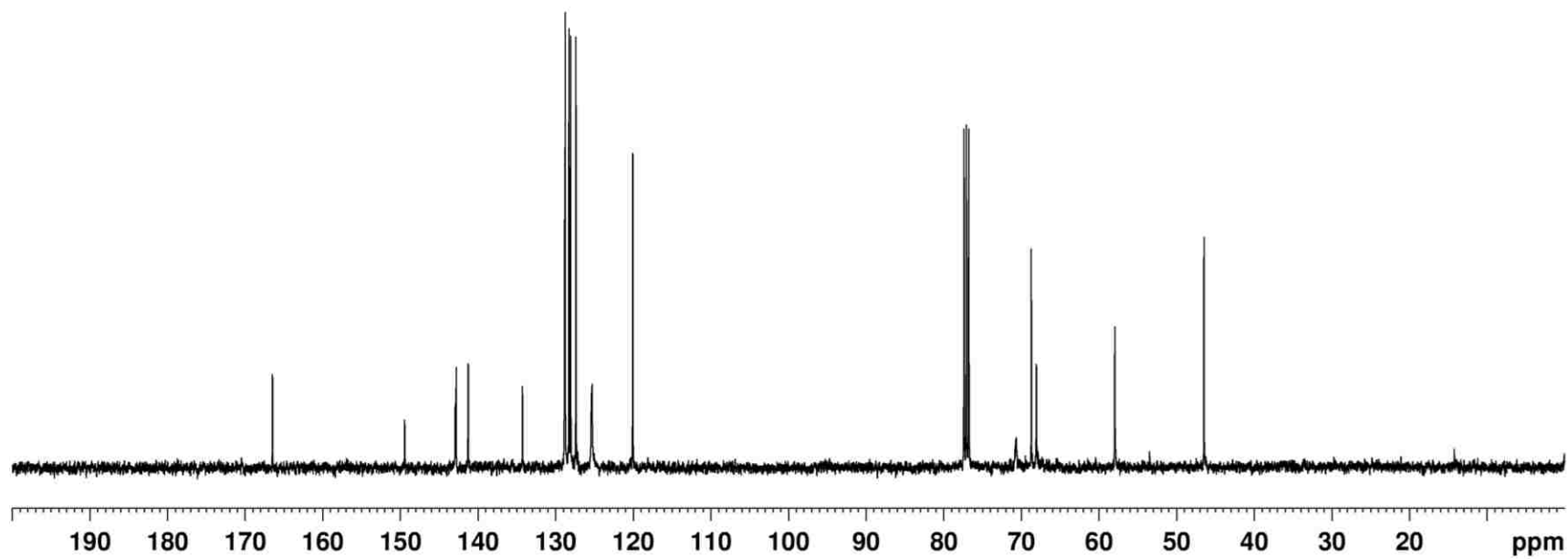
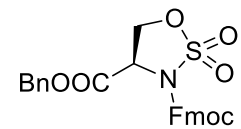
Compound **98** (Scheme 2.20) – ^1H NMR spectrum

Sulfamidate in CDCl_3 at 400 MHz



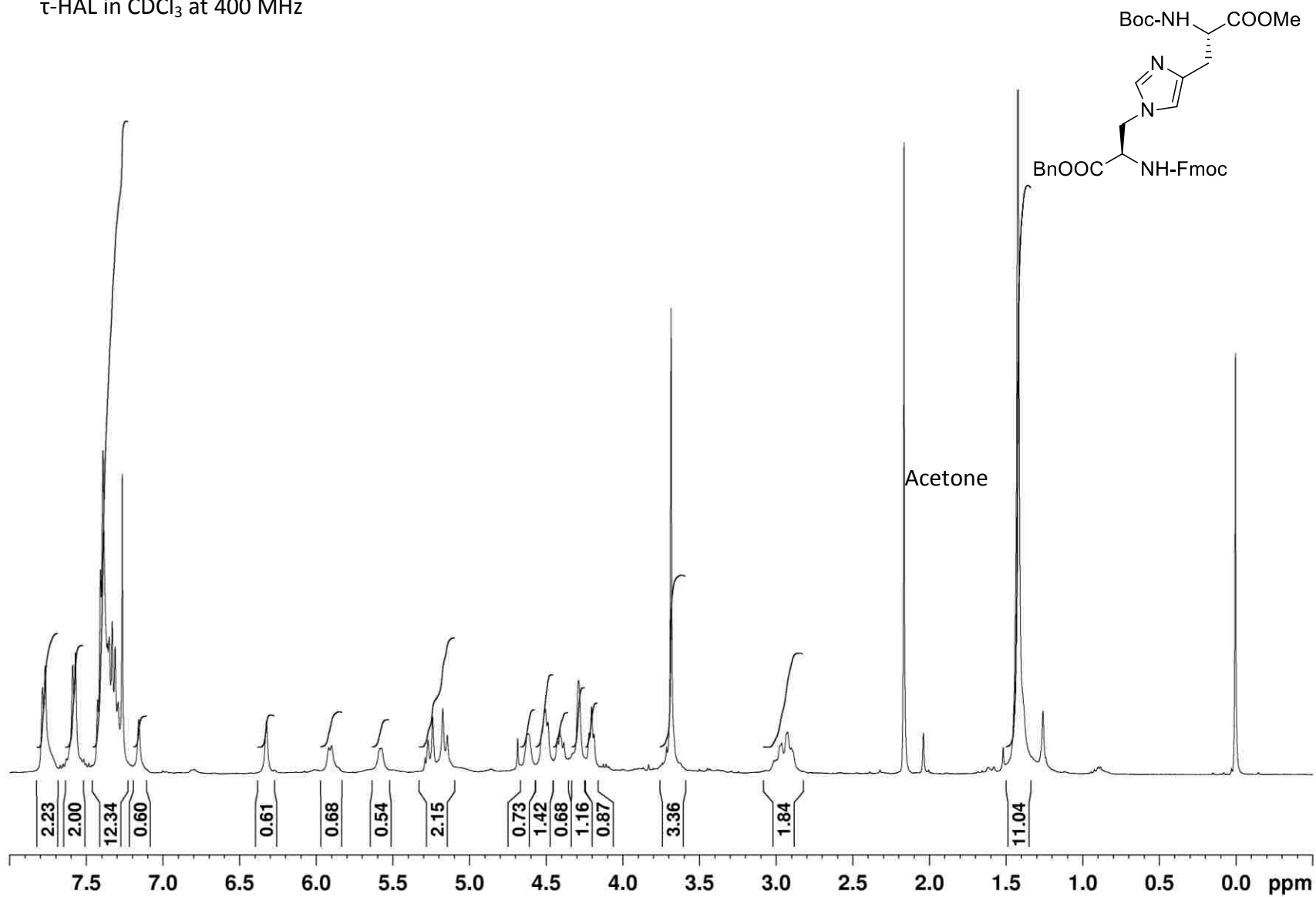
Compound **98** (Scheme 2.20) – ^{13}C NMR spectrum

Sulfamidate in CDCl_3 at 400 MHz



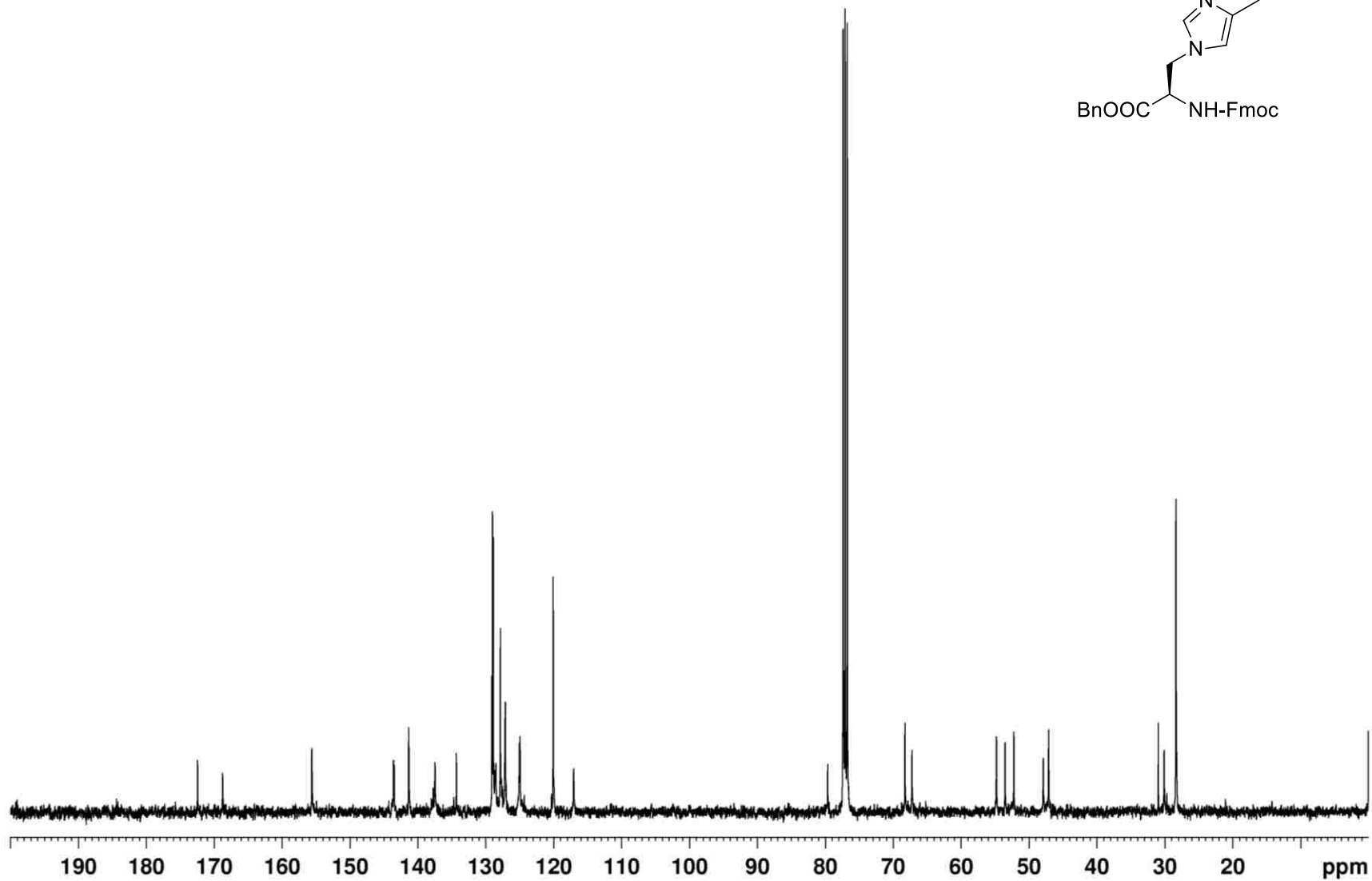
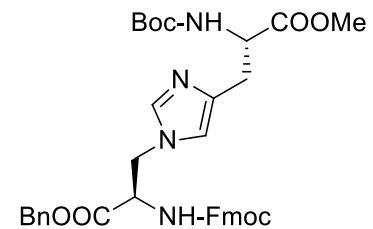
Compound **72** (Scheme 2.21) – ^1H NMR spectrum

τ -HAL in CDCl_3 at 400 MHz



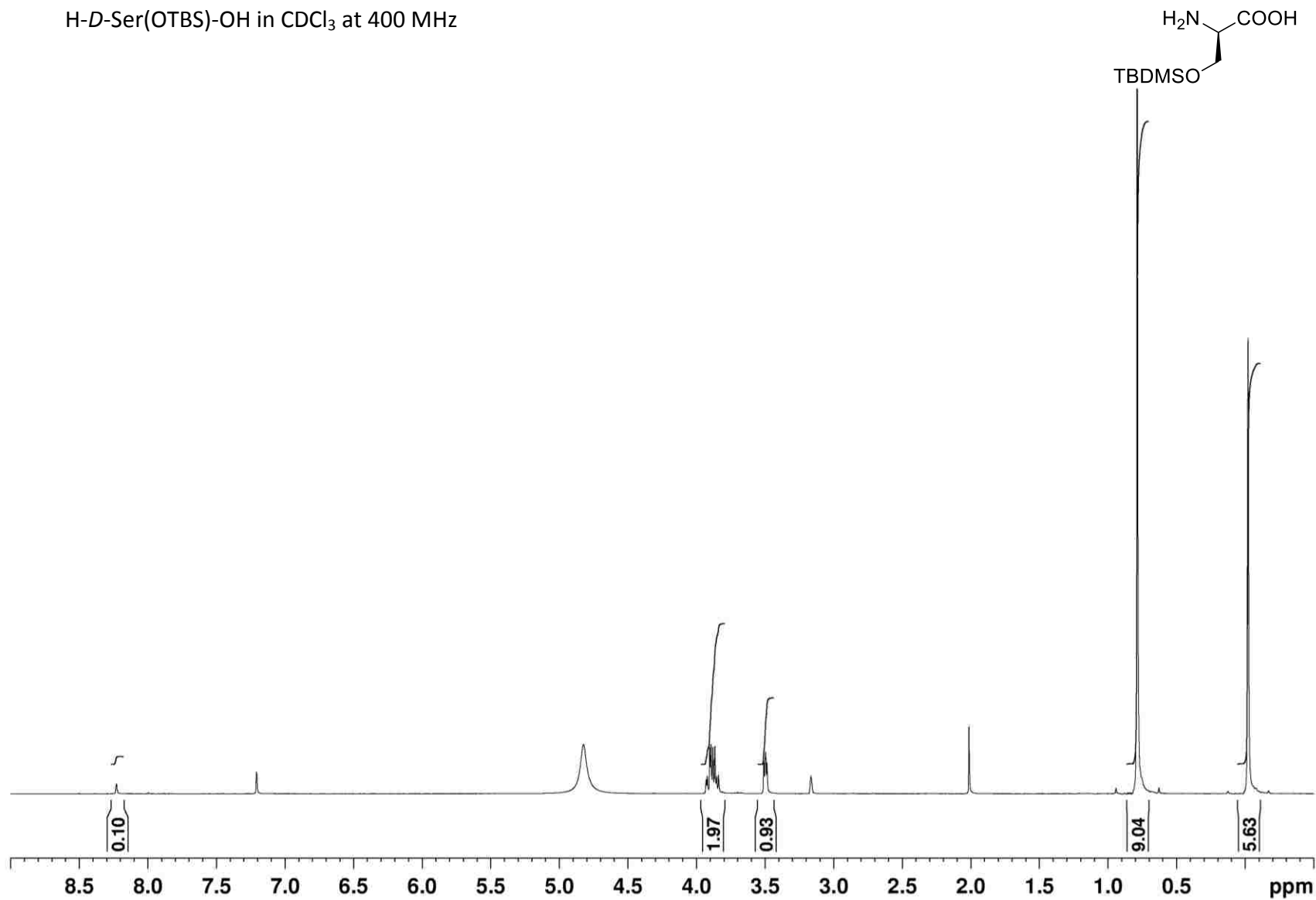
Compound 72 (Scheme 2.21) – ^{13}C NMR spectrum

τ -HAL in CDCl_3 at 400 MHz



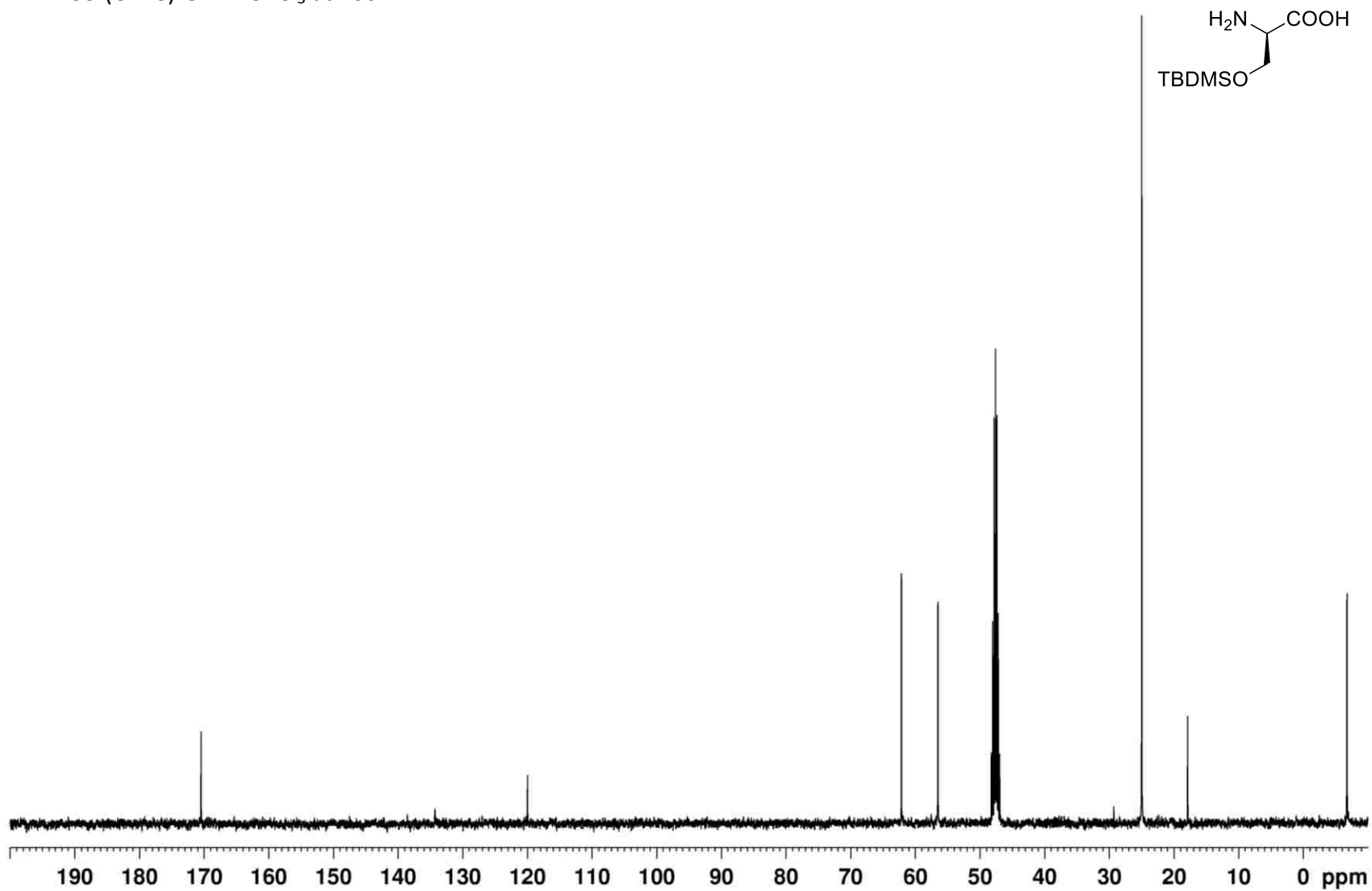
Compound **106** (Scheme 2.22) – ^1H NMR spectrum

H-*D*-Ser(OTBS)-OH in CDCl_3 at 400 MHz



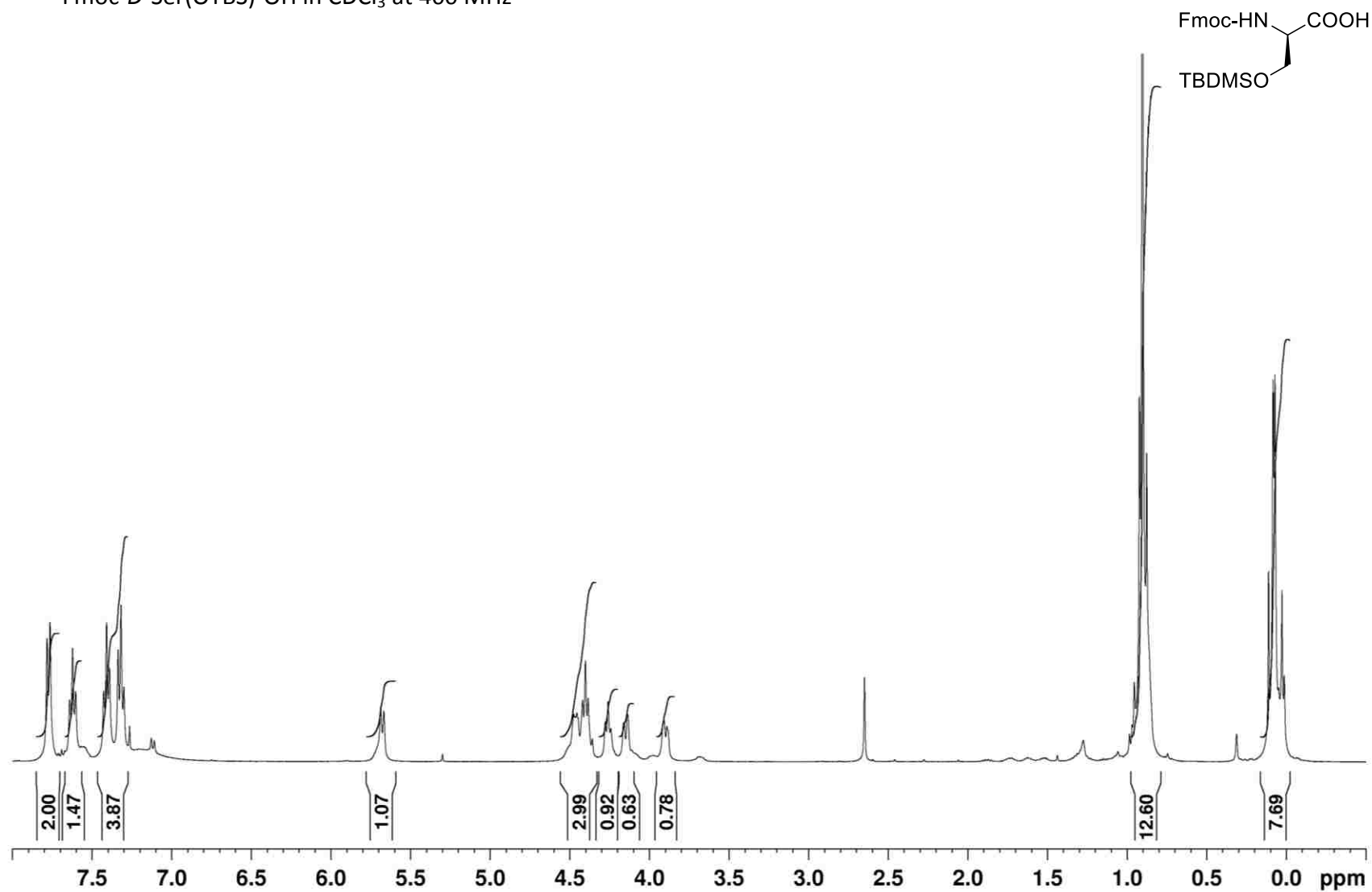
Compound **106** (Scheme 2.22) – ^{13}C NMR spectrum

H-*D*-Ser(OTBS)-OH in CDCl_3 at 400 MHz



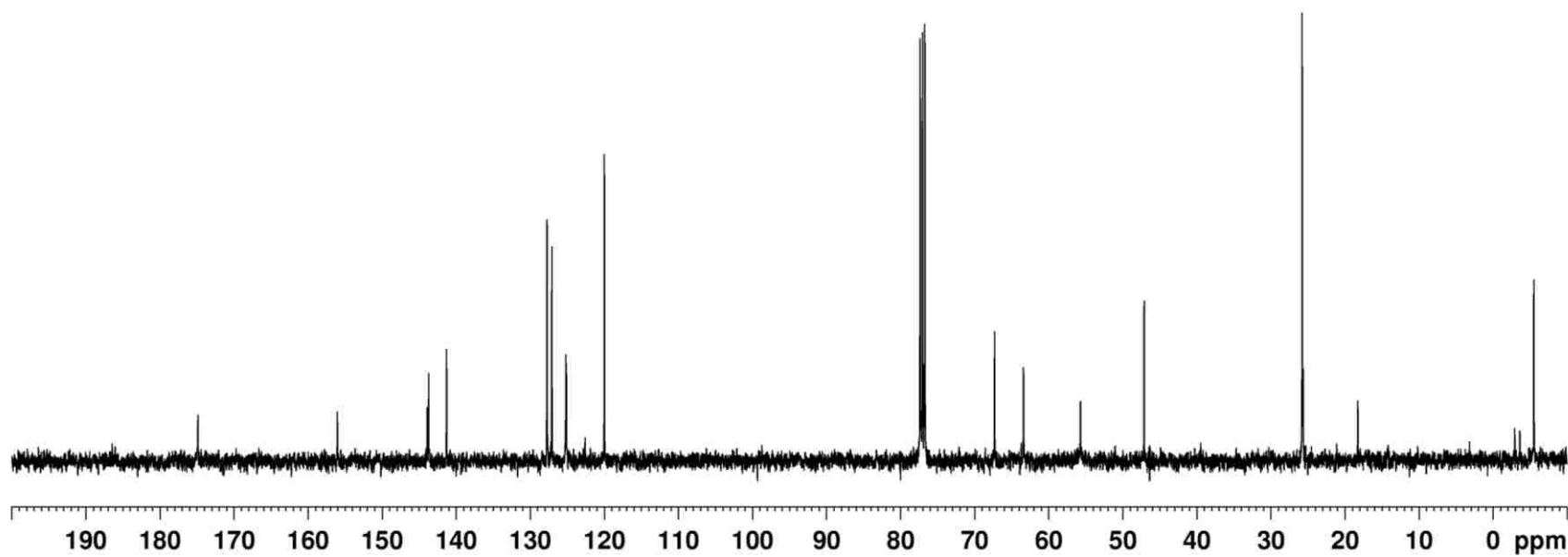
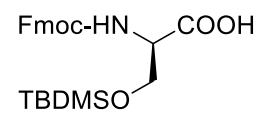
Compound **107** (Scheme 2.22) – ^1H NMR spectrum

Fmoc-D-Ser(OTBS)-OH in CDCl_3 at 400 MHz



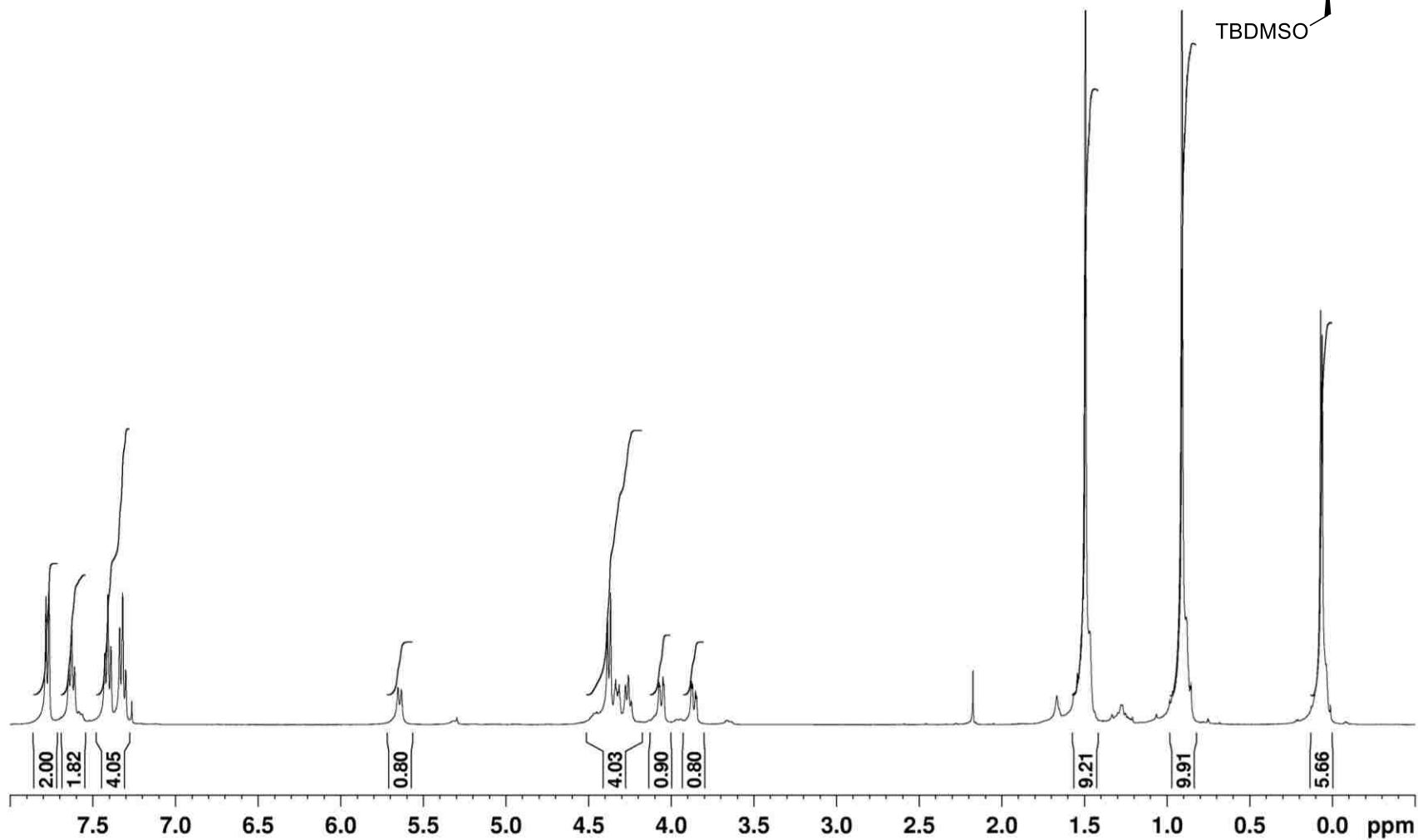
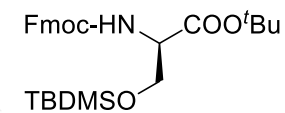
Compound **107** (Scheme 2.22) – ^{13}C NMR spectrum

Fmoc-*D*-Ser(OTBS)-OH in CDCl_3 at 400 MHz



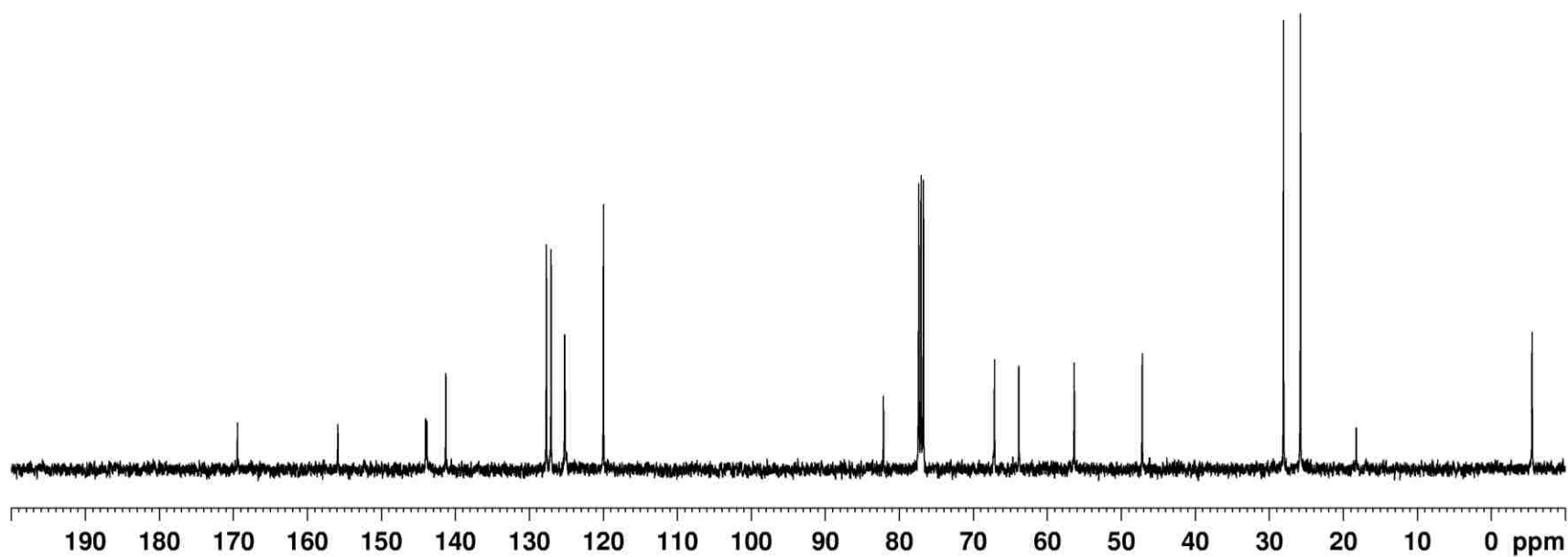
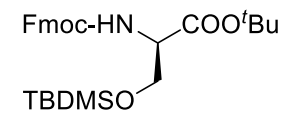
Compound **108** (Scheme 2.22) – ^1H NMR spectrum

Fmoc-*D*-Ser(OTBS)-*O*^tBu in CDCl_3 at 400 MHz



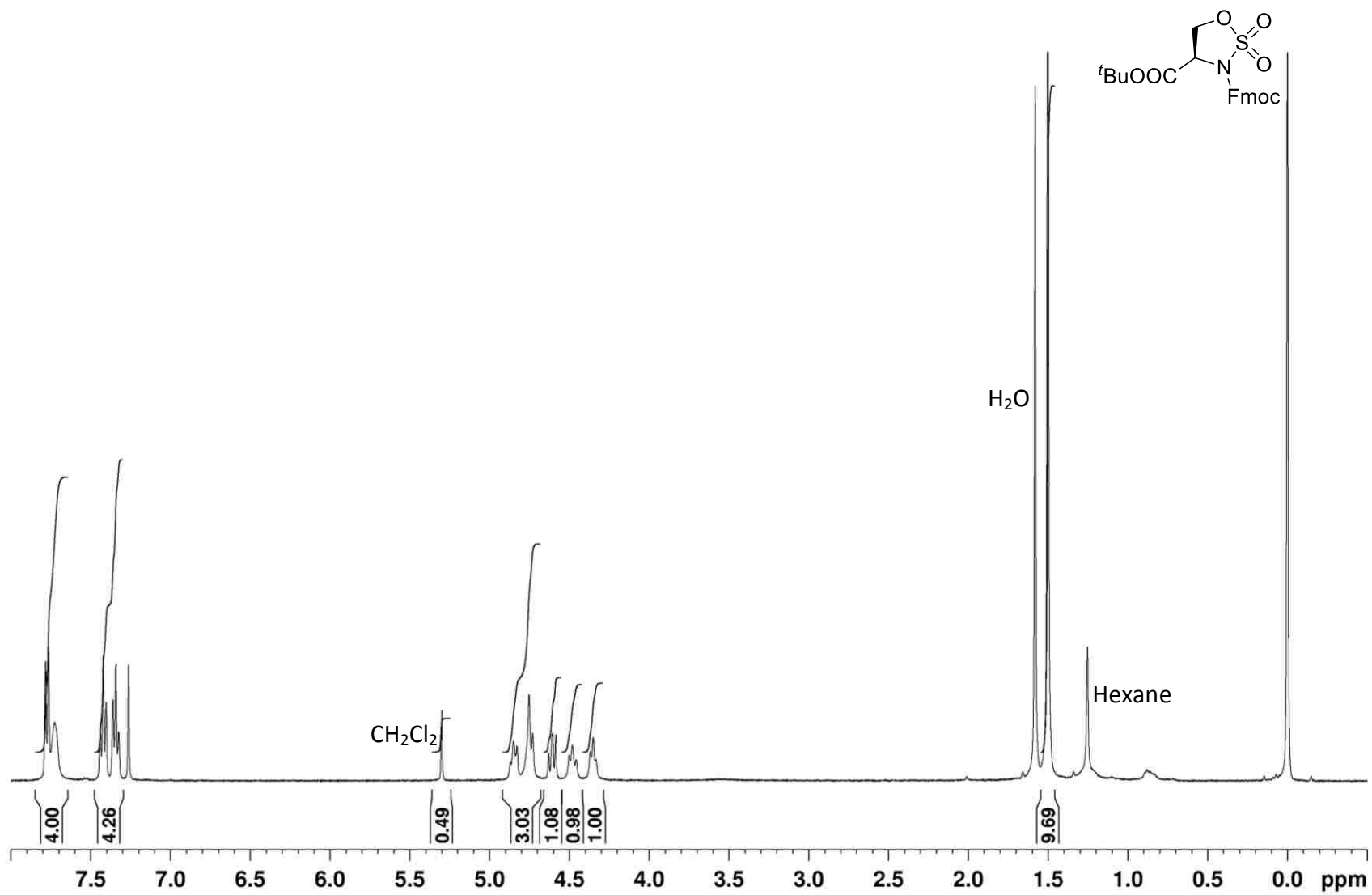
Compound **108** (Scheme 2.22) – ^{13}C NMR spectrum

Fmoc-*D*-Ser(OTBS)- O^tBu in CDCl_3 at 400 MHz



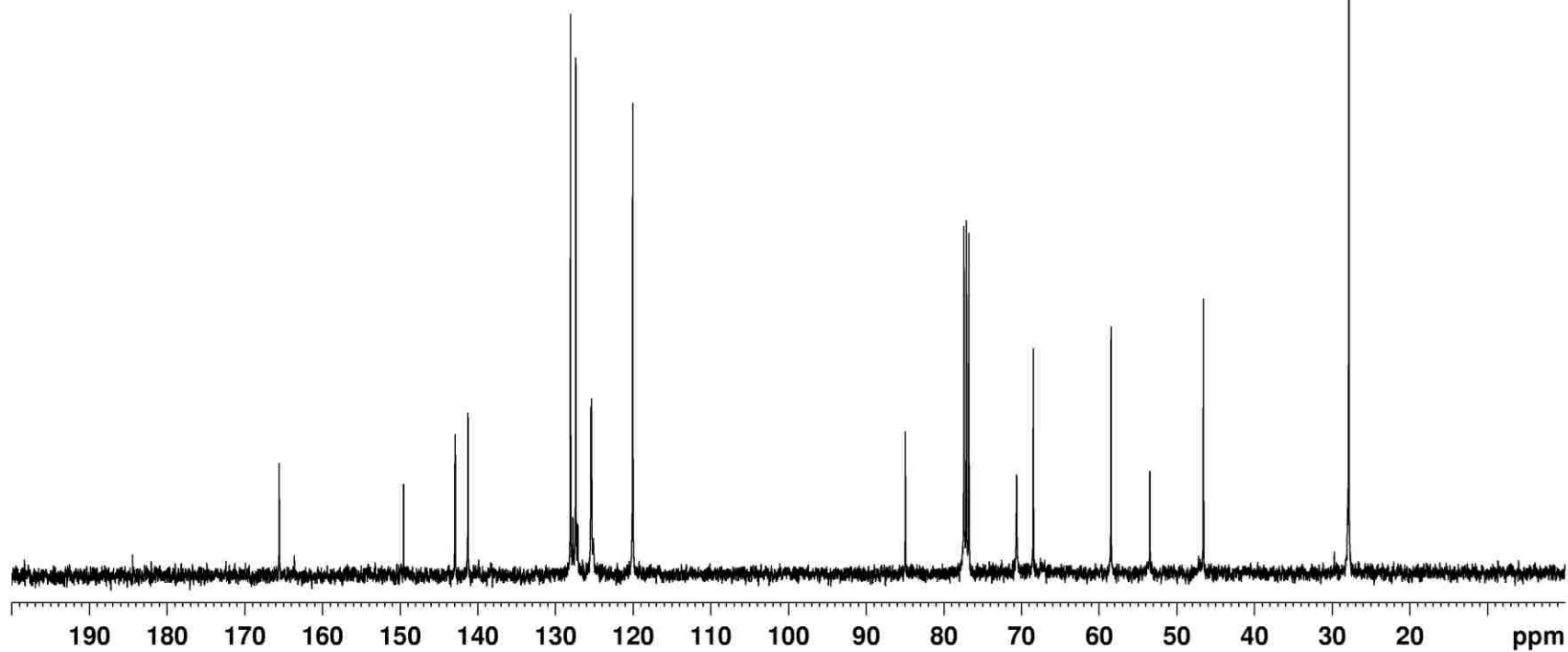
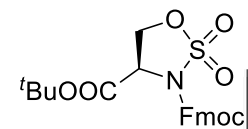
Compound **110** (Scheme 2.23) – ^1H NMR spectrum

Sulfamidate in CDCl_3 at 400 MHz



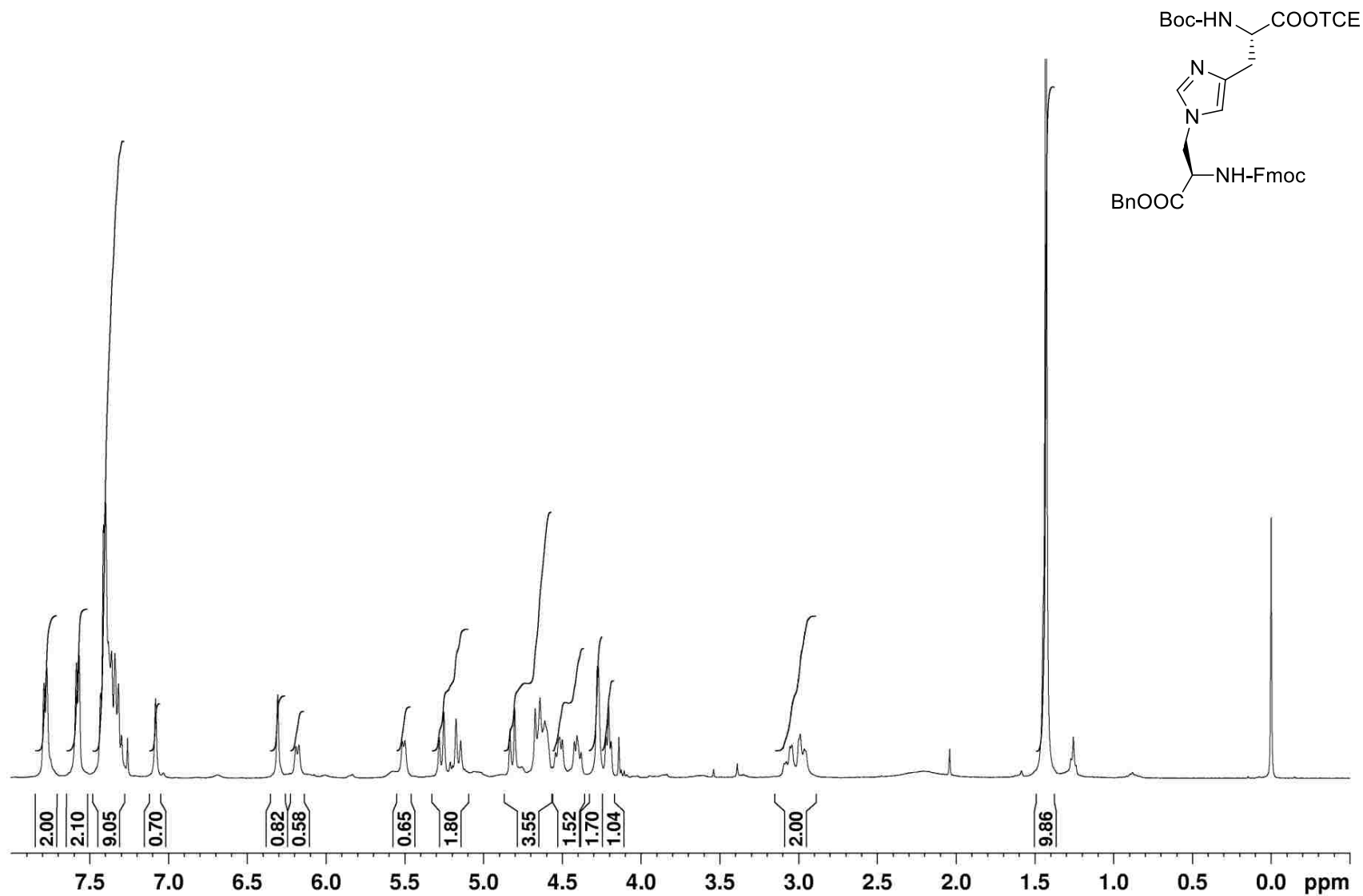
Compound **110** (Scheme 2.23) – ^{13}C NMR spectrum

Sulfamidate in CDCl_3 at 400 MHz



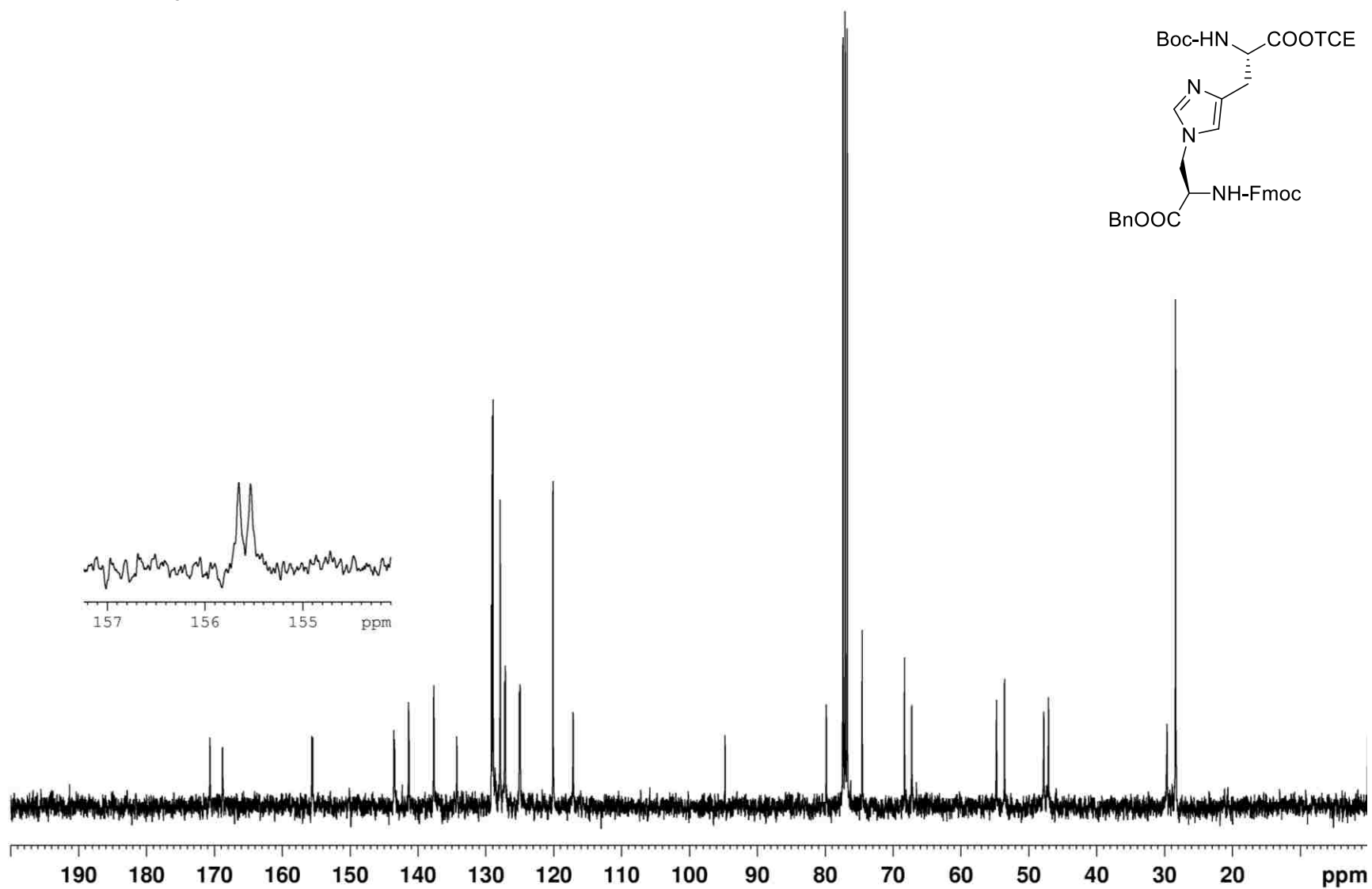
Compound 15 (Scheme 2.24) – ^1H NMR spectrum

τ -HAL in CDCl_3 at 400 MHz



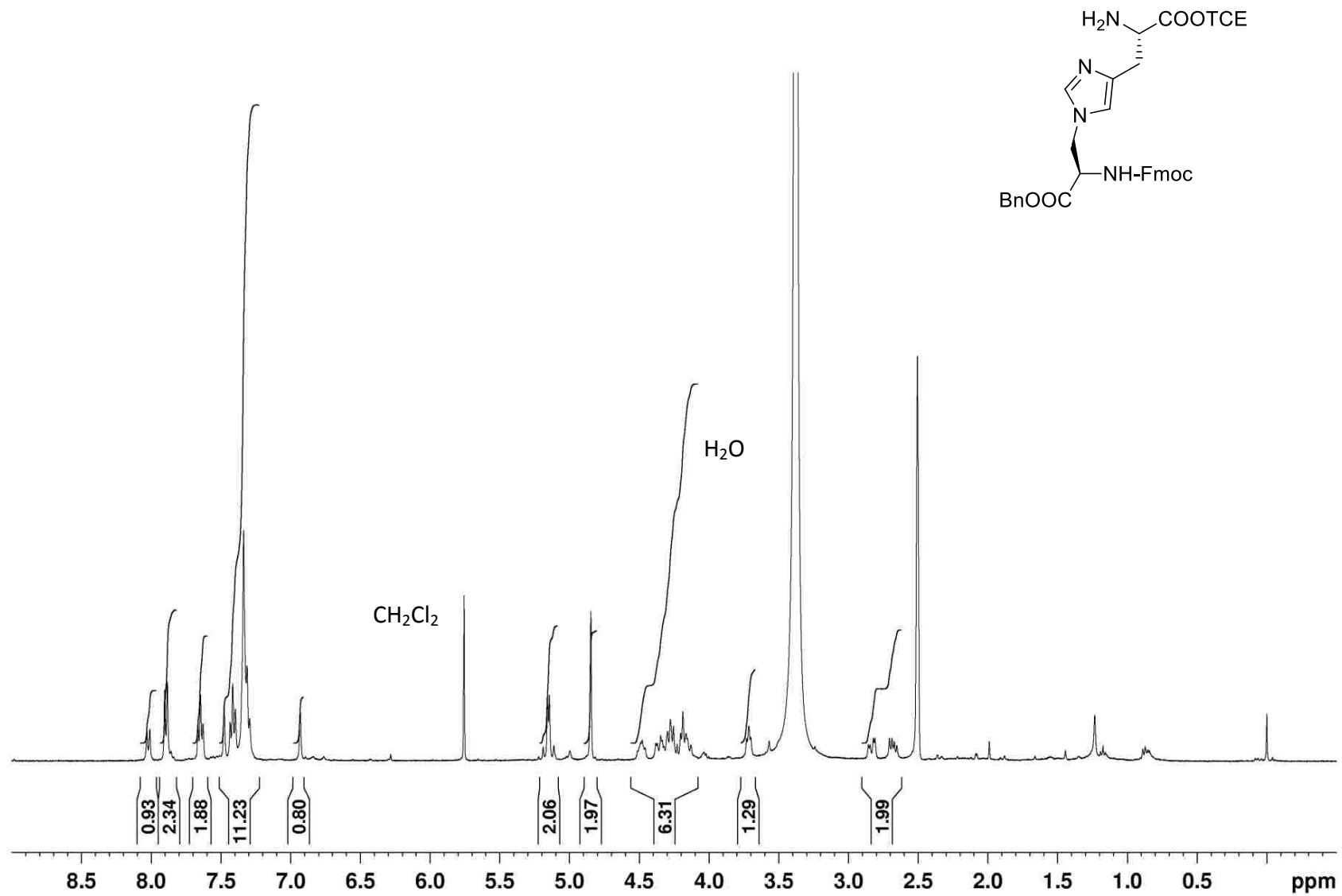
Compound 15 (Scheme 2.24) – ^{13}C NMR spectrum

τ -HAL in CDCl_3 at 400 MHz



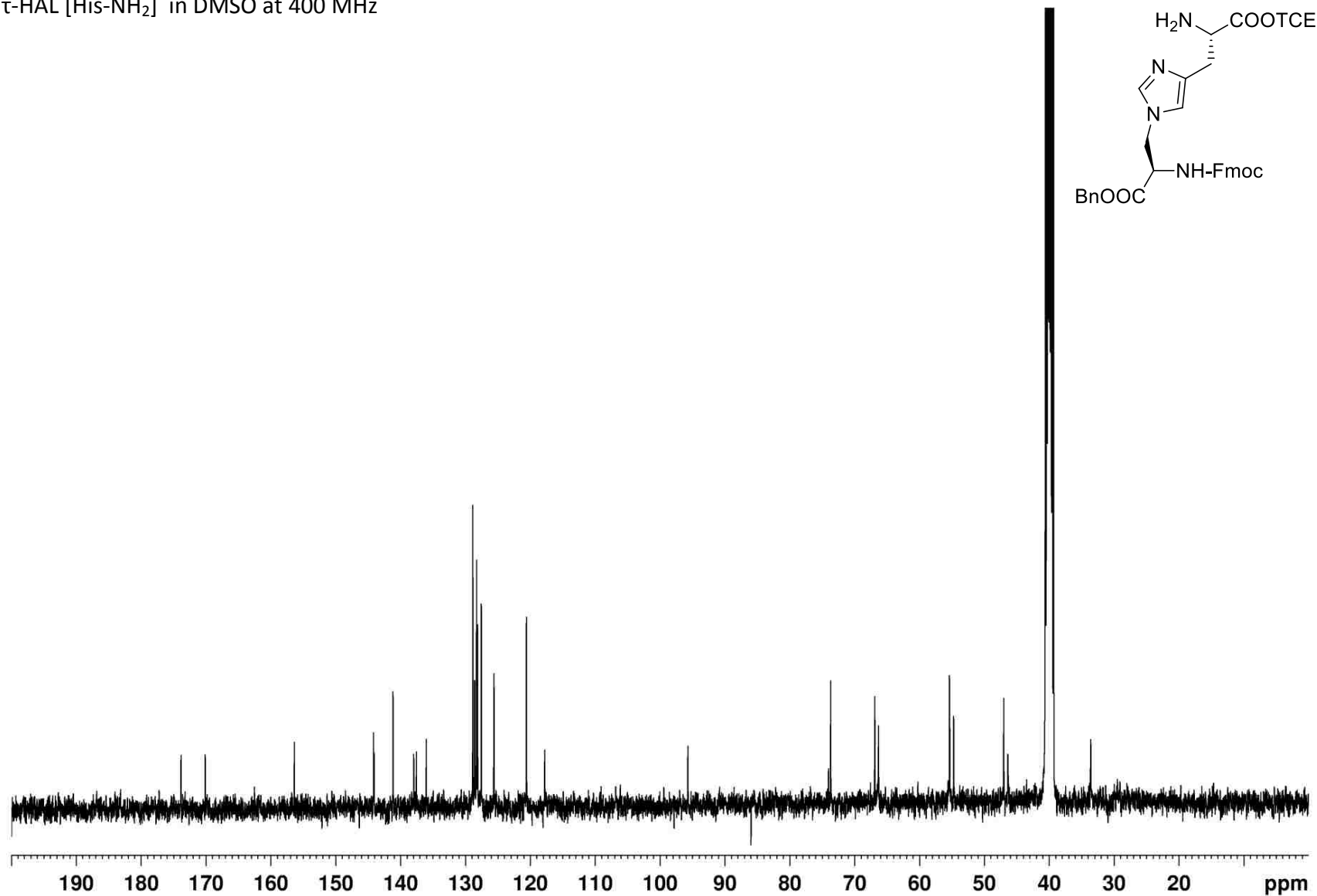
Compound **111** (Scheme 2.25) – ^1H NMR spectrum

τ -HAL [His-NH₂] in DMSO at 400 MHz



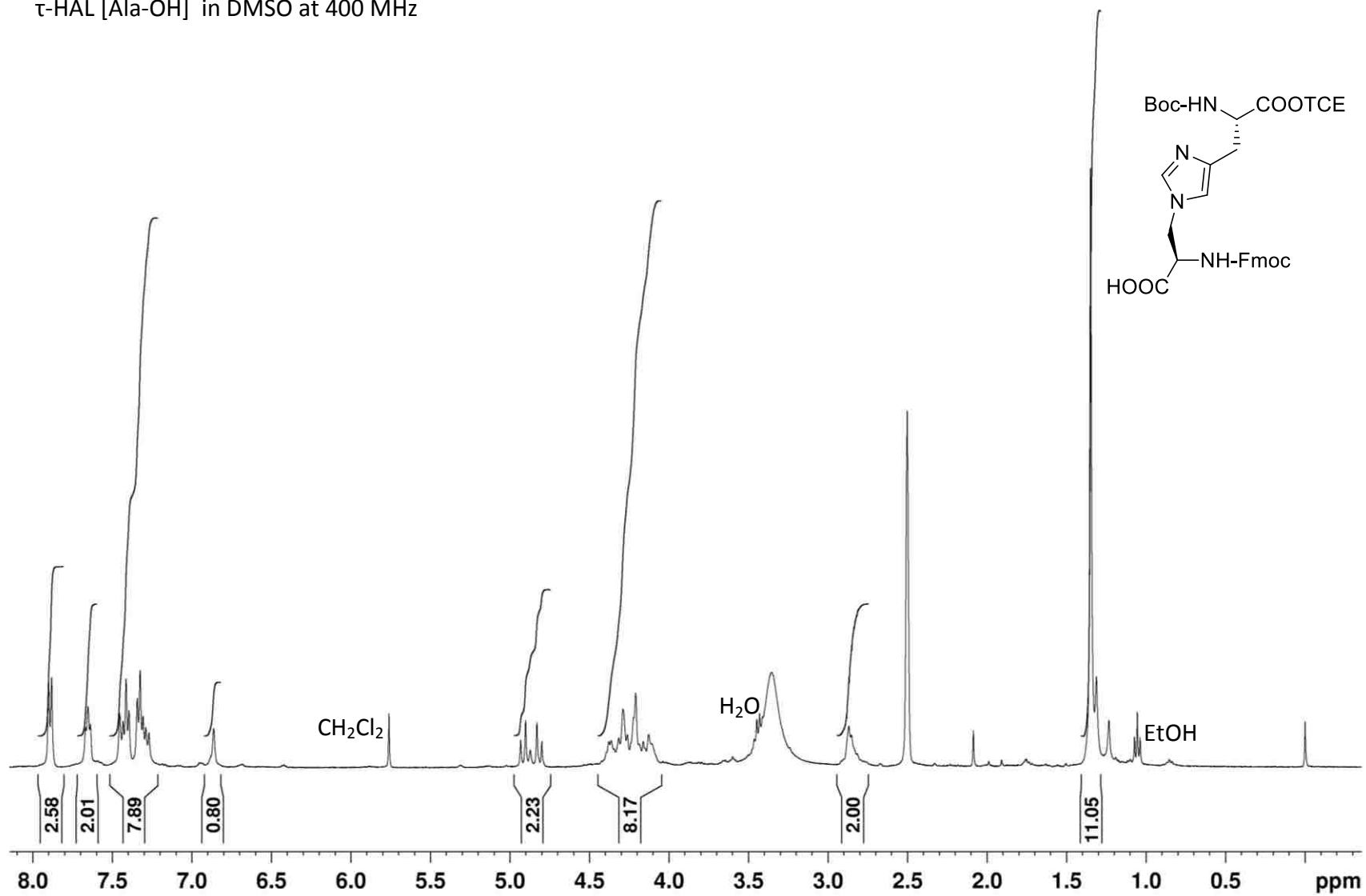
Compound **111** (Scheme 2.25) – ^{13}C NMR spectrum

τ -HAL [His-NH₂] in DMSO at 400 MHz



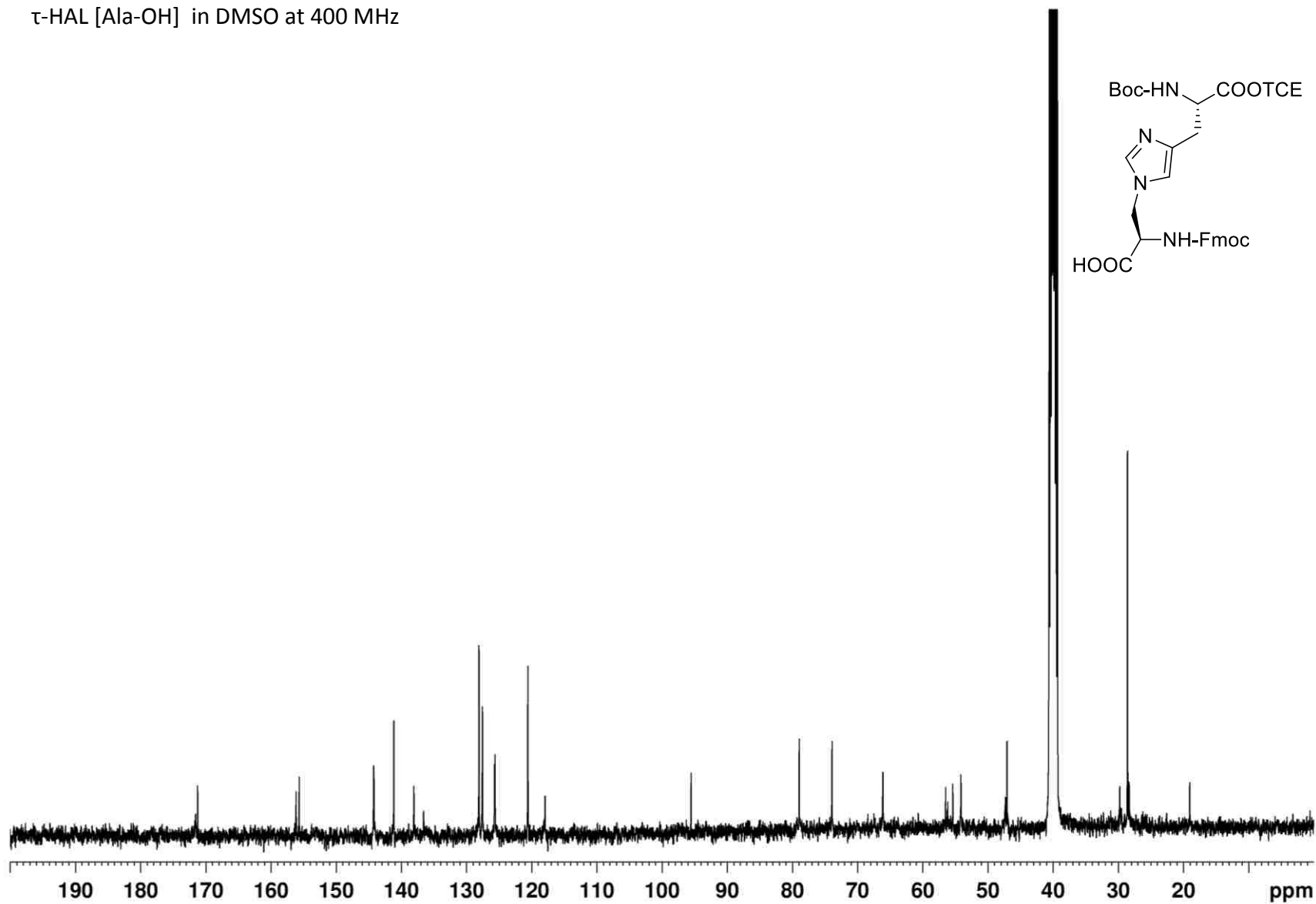
Compound (Scheme 2.25)– ^1H NMR spectrum

τ -HAL [Ala-OH] in DMSO at 400 MHz



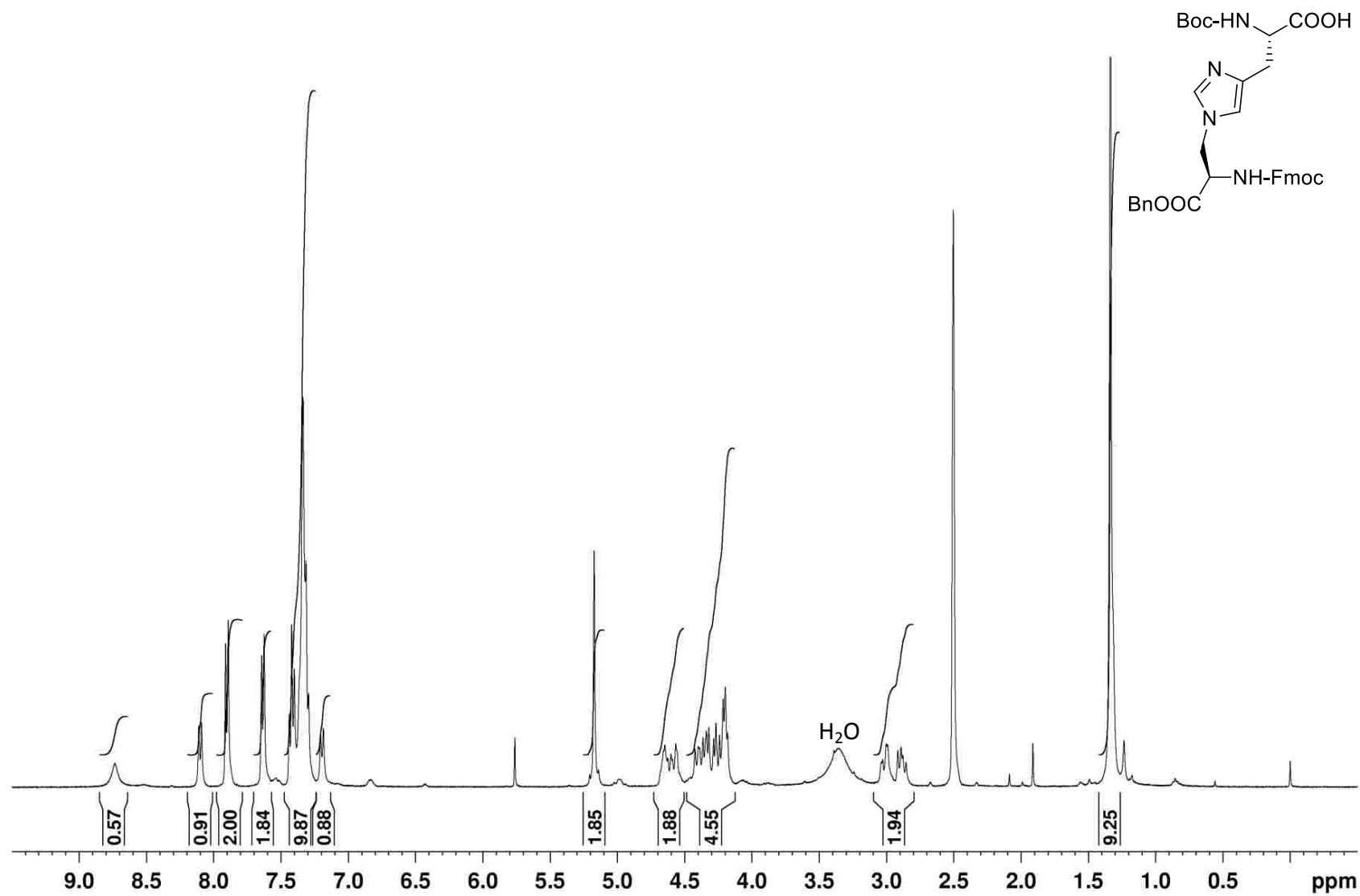
Compound **112** (Scheme 2.25) – ^{13}C NMR spectrum

τ -HAL [Ala-OH] in DMSO at 400 MHz



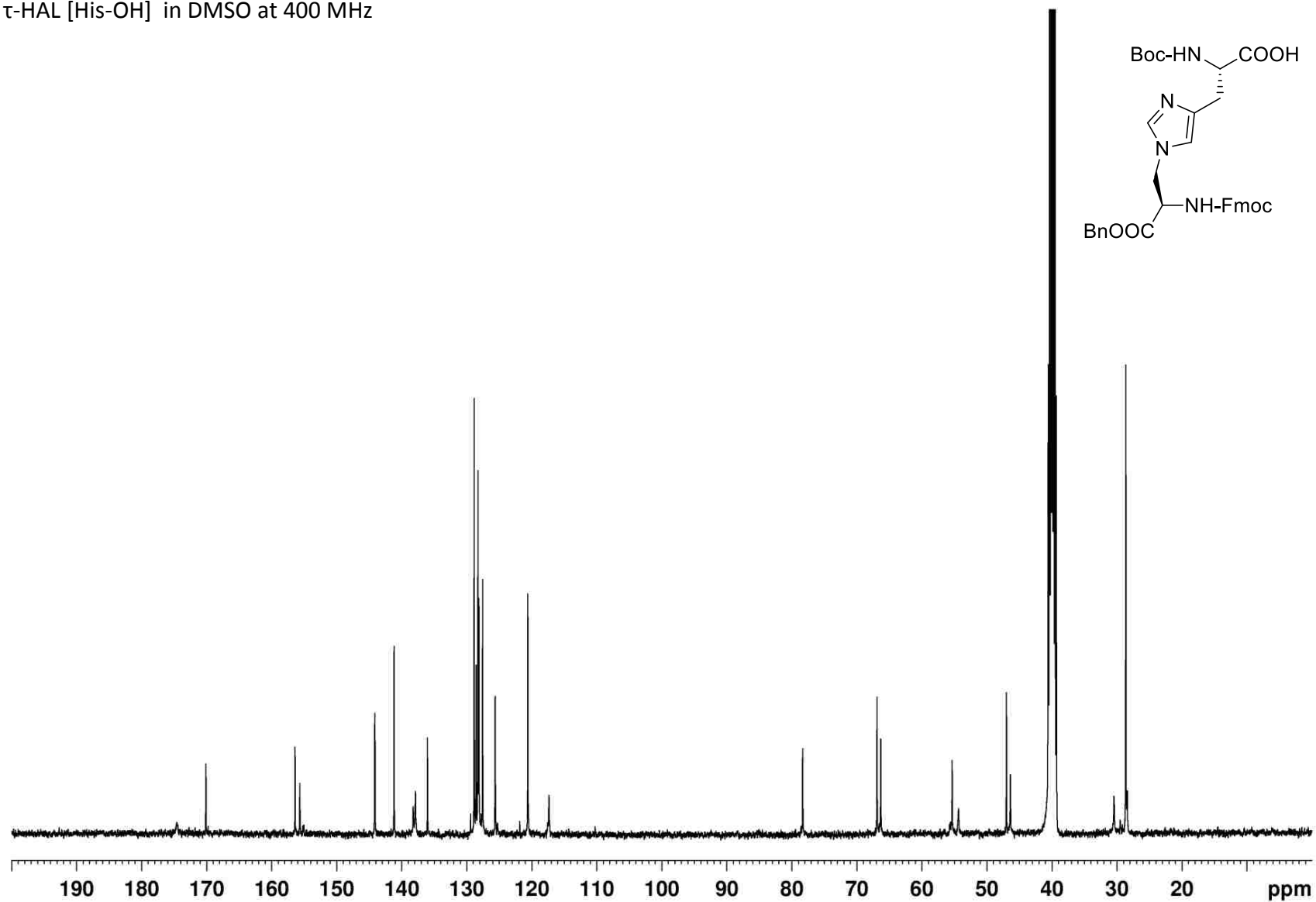
Compound **113** (Scheme 2.25) – ^1H NMR spectrum

τ -HAL [His-OH] in DMSO at 400 MHz



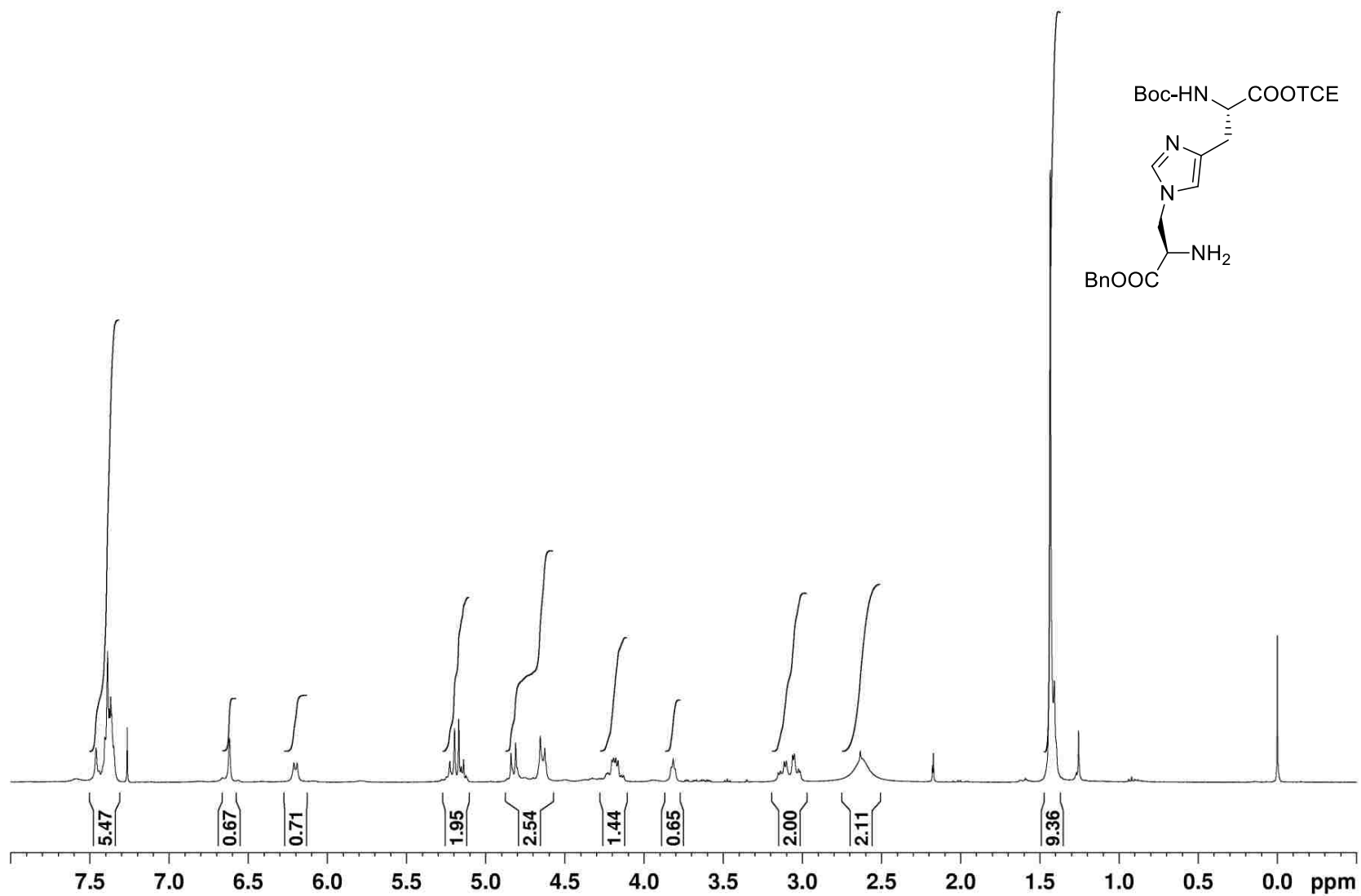
Compound **113** (Scheme 2.25) – ^{13}C NMR spectrum

τ -HAL [His-OH] in DMSO at 400 MHz



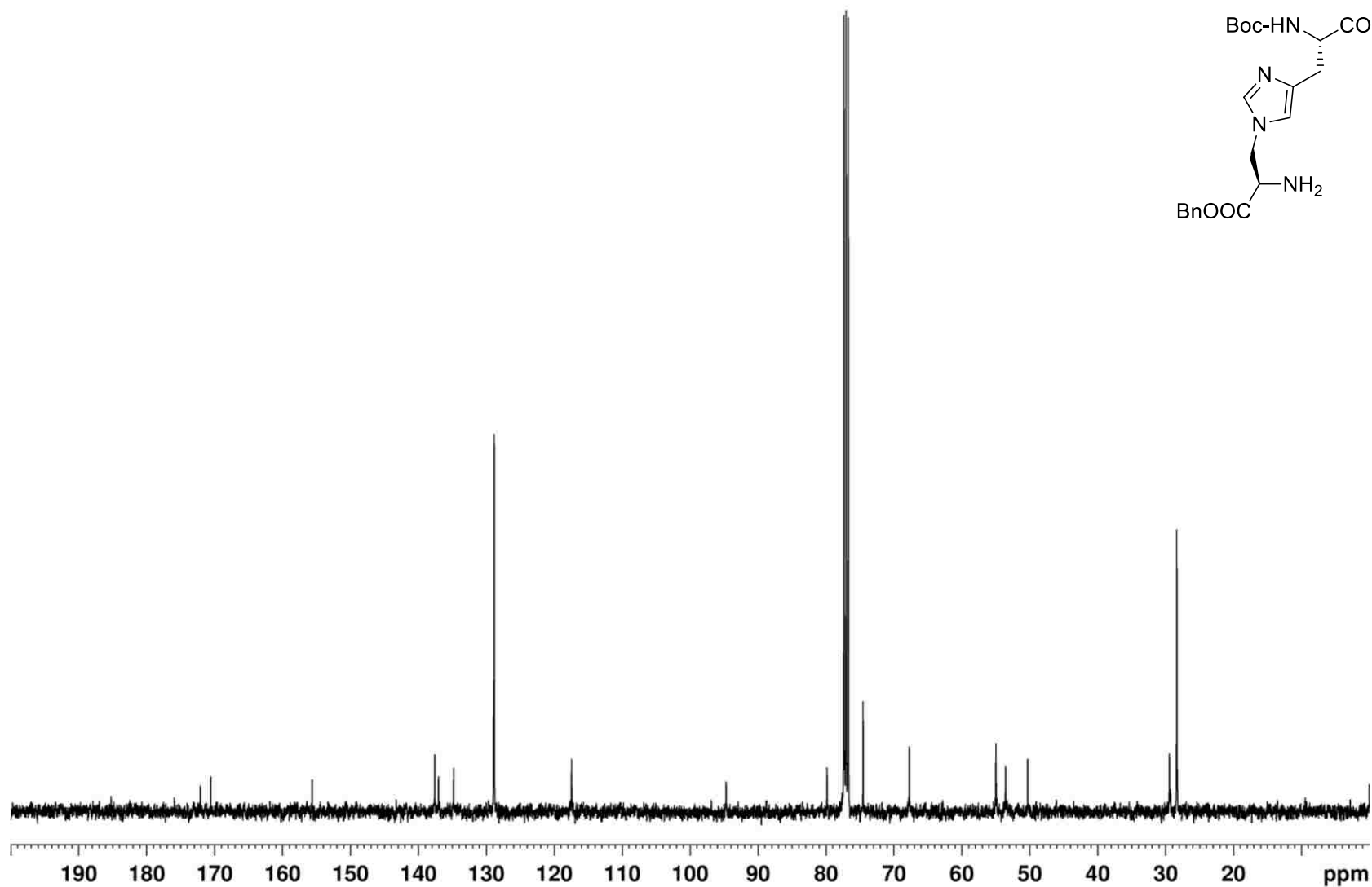
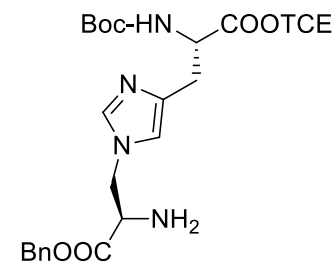
Compound **114** (Scheme 2.25) – ^1H NMR spectrum

τ -HAL [Ala-NH₂] in CDCl₃ at 400 MHz



Compound **114** (Scheme 2.25) – ^{13}C NMR spectrum

τ -HAL [Ala-NH₂] in CDCl₃ at 400 MHz



2.6 References

1. Finley, J. W., Friedman, M. "New amino acid derivatives formed by alkaline treatment of proteins" *Adv. Exp. Med. Biol.* **1977**, 86B, 123–130.
2. Henle, T., Walter, A. W., Klostermeyer, H. Z. "Detection and identification of the cross-linking amino acids $N\tau$ and $N\pi$ -(2'-amino-2'-carboxy-ethyl)-L-histidine ("histidinoalanine", HAL) in heated milk products" *Lebensm. Unters. Forsch.* **1993**, 197, 114-117.
3. a) Tohdo, K., Hamada, Y., Shioiri, T. "Synthetic study of theonellamide F" *Peptide Chemistry* **1991**, 7-12. b) Keisuke, T., Hamada, Y., Shioiri, T. "Synthesis of the southern hemisphere of theonellamide F: a bicyclic decapeptide of marine origin" *Synlett* **1994**, 4, 247-249. c) Tohdo, K., Hamada, Y., Shioiri, T. "Synthesis of the northern hemisphere of theonellamide F: a bicyclic dodecapeptide of marine origin" *Synlett* **1994**, 4, 250.
4. Rzeszotarska, B.; Masiukiewicz, E. "Arginine, histidine and tryptophan in peptide synthesis: The imidazole function of histidine," *Org. Prep. Proced. Int.* **1989**, 21, 393-450.
5. Jones, J. H., Ramage, W. I., Witty, M. J. "Mechanism of racemization of histidine derivatives in peptide synthesis" *Int. J. Peptide Protein Res.* **1980**, 15, 301-303.
6. Benoiton, N. L. *Chemistry of peptide synthesis*; Taylor & Francis: Boca Raton, 2006; pp. 169
7. Jain, R., Cohen, L. A. "Regiospecific alkylation of histidine and histamine at N-1 (τ)," *Tetrahedron* **1996**, 52, 5363-5370.
8. Pansare, S.V., Arnold, L.D., Vederas, J.C. "Synthesis of *N*-tert-butoxycarbonyl-L-serine beta-lactone and the *p*-toluenesulfonic acid salt of (*S*)-3-amino-2-oxetanone" *Org. Syn.* **1991**, 70, 10-17.
9. Kawai, Y., Ando, H., Ozeki, H., Koketsu, M., Ishihara, H. "A facile method for β -selenoglycoside synthesis using β -*p*-methylbenzoyl seleno glycoside as the selenylating unit," *Org. Lett.* **2005**, 7, 4653-4656.
10. Min, G.-H., Yim, T., Lee, H. Y., Huh, D. H., Lee, E., Mun, J., Oh, S. M., Kim, Y. G. "Synthesis and properties of ionic liquids: Imidazolium tetrafluoroborates with unsaturated side chains" *Bull. Korean Chem. Soc.* **2006**, 27, 847-852.
11. Höck, S., Marti, R., Riedl, R., Simeunovice, M. "Thermal cleavage of the Fmoc protection group," *Chimia* **2010**, 64, 200-202.
12. Chen, W.-C., Vera, M. D., Joullié, M. M. "Mild, selective cleavage of amino acid and peptide β -(trimethylsilyl)ethoxymethyl (SEM) esters by magnesium bromide," *Tetrahedron Lett.* **1997**, 38, 4025-4028.

13. Benito, J. M., Meldal, M. "Bicyclic organo-peptides as selective carbohydrate receptors: Design, solid-phase synthesis, and on-bead binding capability," *QSAR & Comb. Sci.* **2004**, *23*, 117-129.
14. Fletcher, A. R., Jones, J. H., Ramage, W. I., Stachulski, A. V. "The use of the N(π)-phenacyl group for the protection of the histidine side chain in peptide synthesis," *J. Chem. Soc. Perkin Trans. I* **1979**, 2261-2267.
15. Baldwin, J. E., Spivey, A. C., Schofield, C. J. "Cyclic sulfamidates: New synthetic precursors for β -functionalized α -amino acids," *Tetrahedron Asymm.* **1990**, *1*, 881-884.
16. Wei, L., Lubell, W. D. "Scope and limitations in the use of N-(PhF)-serine-derived cyclic sulfamidates for amino acid synthesis," *Can. J. Chem.* **2001**, *79*, 94-104.
17. Taylor, C. M., Thabrew De Silva, S. "Synthesis of histidinoalanine: a comparison of β -lactone and sulfamidate electrophiles," *J. Org. Chem.* **2011**, *76*, 5703-5708.
18. Mata, L., Jimenez-Oses, G., Avenoza, A., Busto, J. H., Peregrina, J. M. "Stereocontrolled ring-opening of a hindered sulfamidate with nitrogen-containing aromatic heterocycles: Synthesis of chiral quaternary imidazole derivative," *J. Org. Chem.* **2011**, *76*, 4034-4042.
19. Ogrel, A. A.; Zvonkova, E. N.; Gafurov, R. G. "Octadecyl esters of modified histidine and 3-(1,2,4-triazol-3-yl)alanine. Synthesis and plant growth regulating activity," *Bioorganicheskaya Khimiya* **1993**, *19*, 880-888.
20. Jamieson, A. G., Boutard, N., Beauregard, K., Bodas, M. S., Ong, H., Quiniou, C., Chemtob, S., Lubell, W. D. *J. Am. Chem. Soc.* **2009**, *131*, 7917-7927.
21. Le Corre, L., Gravier-Pelletier, C., Le Merrer, Y., "Towards new MraY inhibitors: a serine template for uracil and 5-amino-5-deoxyribosyl scaffolding," *Eur. J. Org. Chem.* **2007**, 5386-5394.
22. Knerr, P. J., Van Der Donk, W. A. "Chemical synthesis and biological activity of analogues of the lantibiotic epilancin 15X" *J. Am. Chem. Soc.* **2012**, *134*, 7648 - 7651.
23. Kim, B. M., Sharpless, K. B. "Cyclic sulfates containing acid-sensitive groups and chemoselective hydrolysis of sulfate esters" *Tetrahedron Lett.* **1989**, *30*, 655-658.
24. Malkinson, J. P., Anim, M. P., Zloh, M.; Searcey, M. "Efficient solid-phase-based total synthesis of the bisintercalator TANDEM," *J. Org. Chem.* **2005**, *70*, 7654-7661.
25. Jobron, L., Hummel, G. "Solid-phase synthesis of new S-glycoamino acid building blocks," *Org. Lett.* **2000**, *2*, 2265-2267.

26. Deboves, H. J. C., Montalbetti, C. A. G. N., Jackson, R. F. W. "Direct synthesis of Fmoc-protected amino acids using organozinc chemistry: application to polymethoxylated phenylalanines and 4-oxoamino acids" *J. Chem. Soc. Perkin Trans. 1*, **2001**, *16*, 1876-1884.
27. Losse, G., Krychowski, U. "New histidine derivatives for solid-phase peptide synthesis," *J. Prakt. Chemie.* **1970**, *312*, 1097-1104.
28. Luo, Y., Evindar, G., Fishlock, D., Lajoie, G. A. "Synthesis of N-protected N-methyl serine and threonine" *Tetrahedron Lett.* **2001**, *42*, 3807-3809.
29. Wu, X., Jiang, Z., Shen, H-M., Lu, Y. "Highly efficient threonine-derived organocatalysts for direct asymmetric aldol reactions in water" *Adv. Synth. Catal.* **2007**, *349*, 812-816.
30. Bionda, N., Cudic, M., Barisic, L., Stawikowski, M., Stawikowska, R., Binetti, D., Cudic, P. "A practical synthesis of $N\alpha$ -Fmoc protected *l*-threo- β -hydroxyaspartic acid derivatives for coupling via α - or β -carboxylic group" *Amino Acids* **2012**, *42*, 285-293.
31. Takeda, K., Akiyama, A., Nakamura, H., Takizawa, S., Mizuno, Y., Takayanagi, H., Harigaya, Y. "Dicarbonates: convenient 4-dimethylaminopyridine catalyzed esterification reagents" *Synthesis* **1994**, *10*, 1063-1066.
32. Kende, A. S., Liu, K., Kaldor, I., Dorey, G., Koch, K. "Total synthesis of the macrolide antitumor antibiotic Lankacidin C" *J. Am. Chem. Soc.* **1995**, *117*, 8258-8270.

CHAPTER 3: NEAR-INFRARED NANOGUMBOS PRODRUG DELIVERY SYSTEM


3.1 Cancer: An Overview

Cancer is the unregulated growth of genetically-mutated cells that form masses called tumors over time. These tumors eventually become malignant, or mobile, in advanced stages of cancer through metastasis and migrate to other parts of the body and form new tumors. The rapidly growing cells eventually displace normal cells and disrupt function of the infected tissues and organs.

There are over 100 different forms of cancer, with 14 types making up over 80% of all cases diagnosed. Cancer cells can develop in any of our tissues, but are most commonly found in epithelial (carcinomas), connective (sarcomas), and blood-forming (leukemias) tissues. It is noteworthy that more than 90% of all human cancers are carcinomas.¹

It is estimated that over 1.6 million people in the United States will be diagnosed with some form of cancer in 2014, with prostate cancer being the leader for men at 27% of cases and breast cancer for women at 29% (Table 3.1).²

Table 3.1: Ten leading cancer types for estimated new cancer cases in 2014 by sex in the United States, adapted with permission.²

Estimated New Cancer Cases in 2014*							
				Males	Females		
Prostate	233,000	27%		Breast	232,670	29%	
Lung and Bronchus	116,000	14%		Lung and Bronchus	108,210	13%	
Colon and Rectum	71,830	8%		Colon and Rectum	65,000	8%	
Urinary Bladder	56,390	7%		Uterine Corpus	52,630	6%	
Melanoma of the Skin	43,890	5%		Non-Hodgkin Lymphoma	32,530	4%	
Kidney and Renal Pelvis	39,140	5%		Melanoma of the Skin	32,210	4%	
Leukemia	30,100	4%		Ovary	21,980	3%	
Oral Cavity and Pharynx	30,220	4%		Thyroid	47,790	6%	
Pancreas	23,530	3%		Pancreas	22,890	3%	
All Sites	855,220	100%		All Sites	810,320	100%	

* American Cancer Society

If these numbers are extrapolated globally, the estimated number grows to over 14 million.^{3,4} Developed countries have traditionally had the highest incidences of cancer; more recently, developing countries in Africa, South America, and Asia make up over 70% of all new reported cases. The cancer epidemic is a worldwide problem and adversely affects everyone.

3.1.1 Chemotherapy

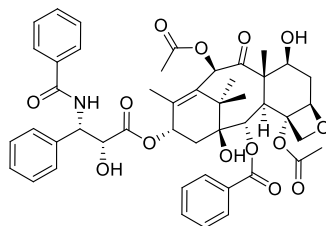
The complexity of cancer, with the ability of cancer cells to adapt, has resulted in a myriad of cancer therapies including: surgery, chemotherapy, radiation therapy, hyperthermia, and photodynamic therapy. Most therapies can be divided into two major groups: preventative therapies aimed at identifying and eradicating cancer cells before they become malignant, and therapies that contain the spread of cancer cells before metastasis. All cancer therapies try to target characteristics that are unique to cancer cells so as not to damage normal cells, however the amount of success in that endeavor is dependent on the treatment.

Surgery and radiation therapy are most effective during the early stages of cancer before metastasis. They operate at the point of origin, removing and killing tumors with the hope that all cancer cells are eradicated and have not spread. In a lot of cases, this has proven adequate treatment for the cancer to not return. However, if even one errant cell escapes, the process starts over again. This is where chemotherapy is most effective, as it acts systematically with the chemotherapeutic drugs distributed throughout the entire body.

3.2 Paclitaxel

Paclitaxel (Figure 3.1) was isolated from the bark of the Pacific yew tree, *Taxus brevifolia* by Monroe Wall and Mansukh Wani in 1967.⁵ Commercially known as TaxolTM, this potent chemotherapeutic agent, by way of inhibition of mitosis, is used clinically to treat non-small cell

lung, ovarian, and breast tumors. Systematic toxicity, poor aqueous solubility, and drug resistance have marred drug development and to some extent delayed widespread clinical usage.



Paclitaxel (Taxol)
115

Figure 3.1: Structure of Paclitaxel

3.2.1 Paclitaxel Mode of Action

Taxol™ belongs to a class of cancer compounds called taxanes. Taxanes inhibit mitosis by acting on tubulin, specifically interfering with polymerization of microtubulins. Microtubules are derived from polymerized heterodimers of α and β -tubulin proteins. These proteins are found in eukaryotic cells where they facilitate intracellular trafficking of macromolecules and organelles, along with regulating maintenance of cell shape, motility, and cell division (mitosis).⁶ Taxol™ binds stoichiometrically to the β -tubulin subunit in malignant cells, stabilizing the microtubule and suppressing disassembly. This over-stabilization prevents cell proliferation and ultimately results in apoptotic cell death.⁷ Unfortunately, this mechanism proves to be non-discriminating, also affecting normal cells, manifesting in bone marrow suppression (myelosuppression), reducing the overall efficacy of the drug.⁸

3.2.2 Taxol Solubility in Aqueous Media

Taxol™ suffers from poor solubility in water (less than 0.03 mg/mL), and by proxy, in biological systems.⁹ Clinically, Taxol™ is administered intravenously in a 1:1 solution of ethanol and Cremophor EL (polyethoxylated castor oil, CrEL).¹⁰ Small doses are administered over a long

period of time to suppress acute toxicity due to overdose and poor permeability. This formulation has proven to have many side effects including hypersensitivity, nephrotoxicity and neurotoxicity. Most of these effects stem from the CrEL vehicle.¹¹ Precipitation of the formulation upon aqueous dilution has also been reported.¹²

Alternative formulations of TaxolTM have been developed to eliminate usage of the CrEL drug delivery vehicle by increasing aqueous solubility, which will also increase bioavailability. The use of co-solvents and emulsions have markedly increased TaxolTM solubility in aqueous media¹³ but do not address systematic toxicity associated with prolonged local drug delivery. Drug delivery vehicles such as liposomes, prodrugs, and nanoparticle encapsulation have been used to increase Taxol solubility through varying mechanisms, and could be effective systems in preventing multidrug resistance.

3.2.3 Multidrug Resistance

Multidrug resistance (MDR) arises when cancer cells exhibit reduced sensitivity to structurally and functionally different chemotherapeutic agents, and is a major factor in the reduced effectiveness of many forms of chemotherapy.¹⁴ Tumor environments consist of mixed populations of drug-sensitive and drug-resistant malignant cells. Inadequate drug exposure and treatment-free periods due to intermittent chemotherapy select for drug-resistant cancer cells, resulting in new tumors that are resistant to traditional chemotherapy.¹⁵

Various mechanisms by which cancer cells can acquire MDR have been identified; however the most common is over-expression of the plasma membrane drug efflux transporter, P-glycoprotein (P-gp). P-Glycoprotein belongs to the ATP-binding cassette family of ABC transporters that facilitate intra- and extra-cellular trafficking of molecules across

membranes.¹⁶ This protein behaves like a “pump” in drug-resistant cells, actively expelling chemotherapeutic agents from the cell (Figure 3.2). Long-term drug exposure induces overexpression of P-gp, effectively converting cancer cells into the drug-resistant type.¹⁷

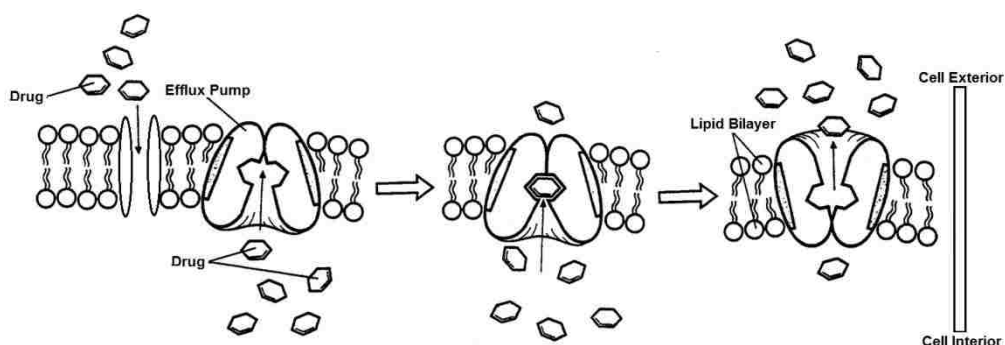


Figure 3.2: Drug-resistant cell expelling chemotherapeutic agents via P-gp efflux pump. Adapted with permission.

A series of studies conducted by the Piquette-Miller group have demonstrated increased tumor responsiveness to chemotherapeutic agents administered at a low-dosage on a more frequent, prolonged or sustained schedule.¹⁸ These studies were corroborated by Ho *et al.* who reported that ovarian cancer tumors exposed to sustained delivery of Taxol™ did not induce P-gp overexpression compared to traditional intermittent chemotherapy, which saw significant downregulation.

A recent report by Pierre *et al.* reported significant cellular uptake of olivacine derivative S16020-2 in cells *in vitro* and *in vivo* that exhibit resistance mediated by the MDR-1 phenotype (Figure 3.3).¹⁹ This may be a result of the rapid uptake of the compound which bypasses the P-gp, leading to its high intracellular accumulation and effectiveness.

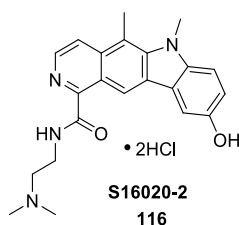


Figure 3.3: S16020-2

With the ability of cancer cells to develop resistance to drugs that once proved effective, it becomes imperative that we focus our efforts on how to administer these drugs more effectively, specifically targeting drug delivery systems that can administer a drug's dosage rapidly and efficiently at the site of interest over a sustained period of time. This system would ideally eradicate cancer cells faster than they could develop resistance. Carrier-linked vehicles, or prodrugs, seem to meet these criteria.²⁰

3.3 Prodrugs

“Drugs need to be designed with delivery in mind.” - Takeru Higuchi²¹

The last couple of decades have seen exponential growth in the research and development of prodrugs (Chart 3.1).

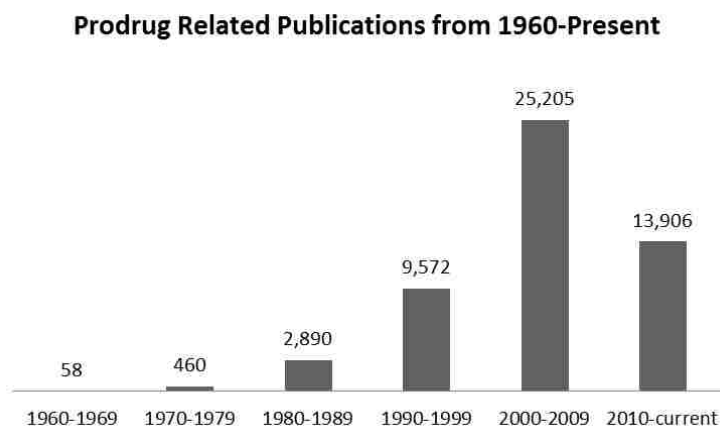


Chart 3.1: Plot of published journal articles, reviews, patents, conference proceedings, and clinical trials using the search term prodrugs according to Sci-Finder Scholar Database

Prodrugs currently account for 10% of globally marketed drugs, with 2008 being a highlight year where one-third of all approved small molecular weight drugs were prodrugs.²²

Prodrugs are biologically inactive precursors to therapeutic agents that undergo enzymatic or chemical transformation *in vivo* to release a bioactive drug. They are designed to increase the efficacy of a parent drug through optimization of a drug's ADMET (absorption, distribution, metabolism, excretion, and unwanted toxicity) properties. Although design-dependent, prodrugs can be very effective in addressing many of the stability, solubility, permeability and targeting problems that plague drug discovery and development, and is often a more practical solution than searching for new therapeutic agents that meet ADMET criteria.²³

Mechanistically, prodrugs work through modification of a functional group that is responsible for biological activity, temporarily masking the chemical reactivity of the active compound. Functional groups that are amenable to prodrug design include carboxylate, hydroxyl, amine, thiol, phosphate/phosphonate and carbonyl groups.

There are two main classes of prodrugs: carrier-linked prodrugs, and bioprecursor prodrugs. Carrier-linked prodrugs bond the parent drug to a promoiety (carrier) either directly or through a linker via a bioreversible covalent linkage in the form of esters, carbonates, carbamates, amides, phosphates and oximes.²⁴ Biotransformation of the prodrug through hydrolysis, oxidation, or reduction releases the parent drug and the carrier (Figure 3.4). Macromolecular prodrugs (macromolecular promoiety), and drug-antibody conjugates (antibody promoiety) can be classified as carrier-linked prodrugs.²⁵ Bioprecursor prodrugs do not contain a promoiety but result from a molecular modification of the active compound itself.

Biotransformation of the bioprecursor prodrug occurs metabolically or chemically by hydration, oxidation, or reduction. Examples of these prodrug classes are given throughout the chapter.

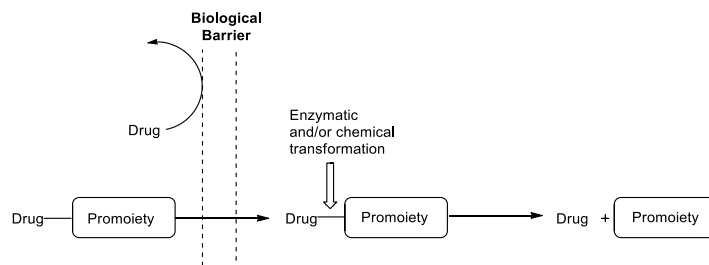
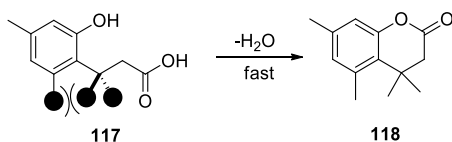


Figure 3.4: Biotransformation of prodrug into parent molecule

3.3.1 Trimethyl Lock – Kinetics and Application

Many groups have successfully incorporated TaxolTM into prodrug systems, reporting improvements such as increased water solubility, reduced cytotoxicity, and enhanced permeability. The trimethyl lock carrier-linked prodrug is a great example of this system used to solvate TaxolTM.

The coumarin-based promoiety, *i.e.* *o*-hydroxydihydrocinnamic lactone derivatives, have found use as a versatile prodrug carrier due to their tunable “trimethyl lock” motif. The name is derived from unfavorable steric interactions between three pendant methyl groups which encourage rapid lactonization to form a dihydrocoumarin derivative (Scheme 3.1).



Scheme 3.1: Rapid lactonization to hydrocoumarin facilitated by the trimethyl lock phenomenon.

The trimethyl lock (TML) system was first investigated by Louis A. Cohen who found that substituted phenol acid derivatives undergo spontaneous lactonization in mild biological

systems.²⁶ The rate constant for lactonization of **117** was found experimentally to exceed that of the non-methylated version by a factor of $3 \times 10^{15} \text{ M}^3$. Cohen postulated this was due to a “relief-of-strain”. This was further corroborated by a study that replaced all the methyl hydrogens with deuterium, decreasing the lactonization rate by 10%, presumably because deuterium-carbon bonds are shorter.

The trimethyl lock system is a viable prodrug strategy for alcohols, but also makes amines accessible as well. Usually amines aren't utilized in prodrug systems because they hydrolyze too slowly to be useful, however, when installed in a trimethyl lock system, lactams form at similar rates to the analogous lactones.²⁷

This system is highly tunable and can be modified to address different physicochemical properties of cancer therapeutic drugs. If the aromatic ring is phosphorylated it can enhance water solubility of historically insoluble drugs such as TaxolTM. The Borchardt group employed this technique, incorporating TaxolTM into a trimethyl lock prodrug moiety that had been phosphorylated. They observed markedly increased solubility in water [$>10 \text{ mg/mL}$ at $37 \text{ }^\circ\text{C}$] compared to free Taxol [$\sim 2 \text{ } \mu\text{g/mL}$] (Figure 3.5, **121-122**). They also reported that derivative **122** was as potent as TaxolTM in an M109 mouse xenograft model, requiring no solubilizing agents for *in vivo* studies.²⁸ In contrast, attempts to increase solubility by phosphorylation of the hydroxyl groups positioned at C7 or C2' of free TaxolTM by the Doyle group were unsuccessful. They found that although water solubility did increase for the phosphorylated derivatives, the phosphoryl groups could not be hydrolyzed in plasma or by alkaline phosphatase (Figure 3.5).²⁹

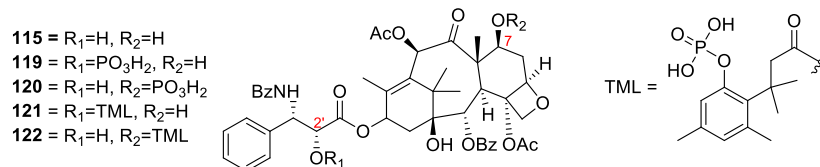
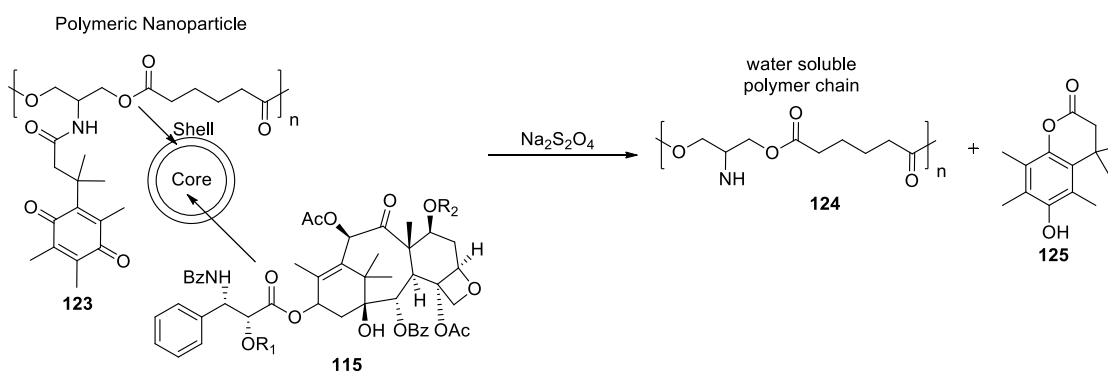


Figure 3.5: Structures of TaxolTM (**115**), phosphorylated TaxolTM derivatives (**119-120**), and trimethyl lock-based TaxolTM prodrugs (**121-122**)

If the TML motif is embedded in a quinone precursor, reduction triggers aromatization and lactonization. This increases the system's site-selectivity as tumors have high levels of reductase enzymes and low oxygen tension. Cho *et al.* demonstrated this in their preparation of polymeric nanoparticles composed of the shell: a biodegradable polymer, which was conjugated to the trimethyl lock-based benzoquinone via an amide linkage, and a TaxolTM core (Scheme 3.2).³⁰ Upon reduction of the quinone moiety to a free phenol by sodium dithionite, the encapsulated Taxol was released after spontaneous lactonization, producing a water soluble polymer and a biocompatible dihydrocoumarin derivative as byproducts. About 52% of the TaxolTM was released *in vitro* within three hours of sodium dithionite treatment.



Scheme 3.2: Reduction of benzquinone-based trimethyl lock prodrug by sodium dithionite to release TaxolTM, and dihydrocoumarin-derivative and a water soluble polymer chain as byproduct

The findings of Cho *et al.* highlight a shift towards using nanoparticles as prodrug delivery vehicles “to enhance storage stability, modulate prodrug release, enhance tumor-

targeting, and protect against enzymatic attack”.³¹ Efficiency of the drug carrier is crucial for optimal employment of prodrug’s ADMET enhancing properties.

3.4 Nanomaterials

A diverse range of nanomaterials has been developed to address rapid deactivation, poor solubility, and biodistribution challenges. These include inorganic materials (quantum dots, metal oxides, gold nanoparticles, carbon nanotubes), and organic materials (liposomes, natural and synthetic polymers, dendrimers) (Figure 3.6).³² Drugs can be attached, encapsulated, absorbed, entrapped, or dissolved in these materials rendering them as drug delivery vehicles.

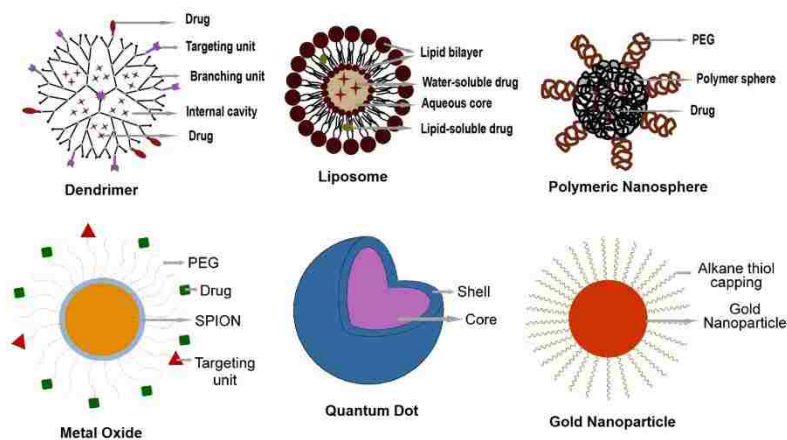


Figure 3.6: Selected examples of organic and inorganic nanoparticles. Reprinted with permission.³¹

Many of these materials are biocompatible, and biodegradable, breaking down to form benign species. They range from 10-100nm in scale, small enough to penetrate capillaries and be taken up by malignant tissues, but large enough to target and deliver at specified sites via the enhanced permeation and retention (EPR) effect. The EPR effect is due to the anatomic and pathophysiological differences between tumors and normal tissues (Figure 3.7). Angiogenesis,

which is the ability for tumors to develop nerve systems, leads to high vascular density which causes large gaps in the endothelial cells in tumor blood vessels. This allows for enhanced drug uptake in tumor tissue instead of normal tissues.

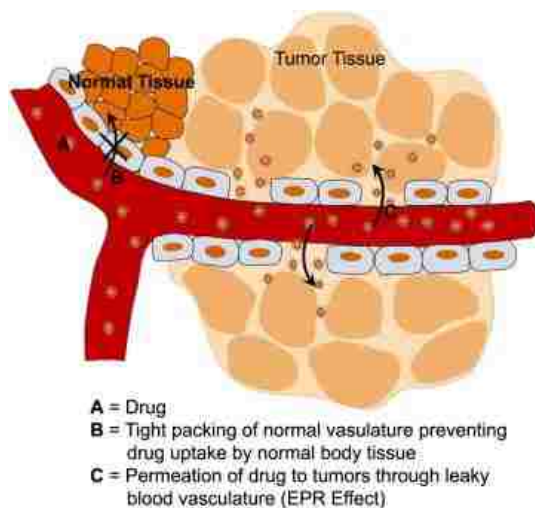


Figure 3.7: Tumor uptake of nanoscale drug carriers via the EPR effect. Reprinted with permission.³²

A polymeric nanoparticle, with prostate-specific membrane antigen (PSMA) targeting properties is currently in clinical trials.³³ This nanoparticle, which contains Docetaxal, another member of the taxane family, attributed its enhanced tumor accumulation and prolonged tumor growth suppression in part due to the EPR effect. This accumulation was not seen with solvent-based Docetaxal formulations.

3.4.1 Targeted Drug Delivery

Although traditional prodrug strategies have helped to improve physiochemical properties of chemotherapeutic agents, allowing for enhanced permeability, targeting, and overall increased effectiveness, they didn't address dosage. They only allowed for a slower release of the drug at a predetermined rate. There has been increasing interest in developing

methods where drug release can be controlled directly. These remote control systems could dictate the timing, duration, dosage, and location of drug release.

There have been many recent reports of new materials that have been designed with specific sensitivity to visible light, near-infrared (NIR) light, ultrasound, and magnetic fields making these viable triggers for on-demand drug delivery. To be an effective trigger, the system must allow for precise control of the timing, duration, and magnitude of drug release.³⁴

Ultraviolet and visible light are strongly absorbed by the skin and tissue and cannot be utilized in applications that require activation deep into skin tissue. However, one of the advantages of using light in the NIR region, ca. 650-900 nm is its minimal absorbance by skin and tissue. At the low end of this region, hemoglobin absorbs light (650 nm) while at the high end the absorbance of water (900 nm) (Figure 3.8).

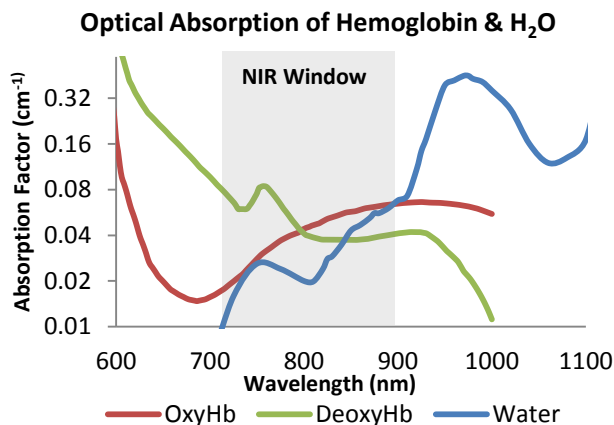


Figure 3.8: NIR Therapeutic Optical Window.³⁵

The ANSI (American National Standards Institute) has given maximum exposure values for human tissue using a 700 nm light from a continuous wave source to be between 200 mW cm⁻² for long exposure and as high as 10 W cm⁻² for no longer than a second. NIR triggers more specifically also have the added benefit of photothermal application, where absorption in the

NIR region of specific materials often leads to a thermally induced change. Remotely triggered drug delivery systems are most ideally suited for nanoscale applications as they can take advantage of the EPR effect.³²

3.4.2 NanoGUMBOS: NIR-based Targeted Drug Delivery Application

Not all nanomaterials are biocompatible, and frequently some materials are thought to be non-toxic only to be revealed to be cytotoxic upon further studies. Carbon nanotubes, silver nanoparticles, and quantum dots are examples of nanomaterials that have been proposed as drug delivery vehicles that can assist with permeation,³⁶ but are known for their acute toxicity in biological systems.³⁷ Ionic liquid-based nanoparticles are a promising alternative to these existing inorganic nanomaterials.

Ionic liquids are organic salts with melting points below 100 °C. They can be divided into two categories, room temperature ionic liquids (RTIL), which are ionic liquids that are in the liquid state at room temperature, and frozen ionic liquids, which are solid above room temperature. Their low melting point stems from the asymmetry of the ion pairs, preventing stable crystal lattice stacking.³⁸ Ionic liquids usually contain a 1:1 ratio of an organic cation and an inorganic or organic anion. Some common anion and cation combinations are outlined in Figure 3.9.

Ionic liquids have powerful solvent capabilities due to their diverse ion pairings. Although the concept of ionic liquids is not new, suspending them as nanoparticles is fairly recent. The Warner group has pioneered these ionic liquid-based nanoparticles giving them the portmanteau GUMBOS or (groups of uniform materials based on organic salts).³⁹

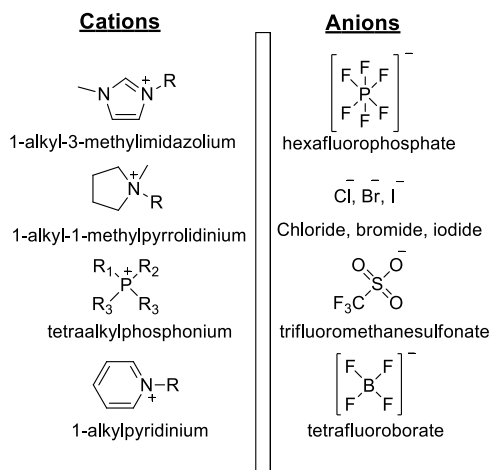
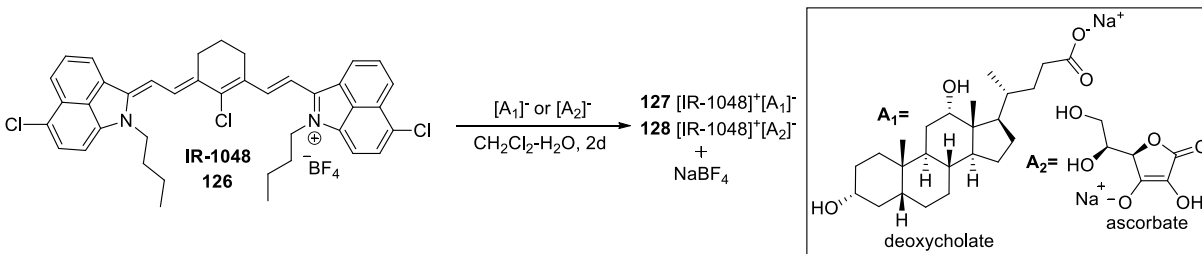


Figure 3.9: Common cations and anions used in ionic liquids.

What distinguishes these materials from traditional nanoparticles, is that nanoGUMBOS can be designed for specific uses, rather than simply adapted for a particular use after being synthesized. The myriad of different ion combinations available make these nanomaterials extremely tunable. They can be prepared from biologically safe compounds and depending on the application and ion pairs used, can increase permeability through biological membranes, add optimal site-selectivity, and minimize non-specific cytotoxicity. Their high melting points versus traditional ionic liquids lend them thermal stability.

Dumke *et al.* recently demonstrated the high photothermal stability of near-infrared-based GUMBOS (NIR-nanoGUMBOS).⁴⁰ They paired an organic NIR-absorbing laser dye (IR-1048, IR-1061 not shown) with either deoxycholate or ascorbate (Scheme 3.3). They prepared the bulk GUMBOS using the ion exchange method, which is the process of mixing two charged species, each introduced with a inorganic ion, in a biphasic system (*i.e.* water and dichloromethane) resulting in migration of the formed inorganic salt to the aqueous layer, and the organic salt to the organic layer.



Scheme 3.3: Ion exchange of NIR laser dye IR-1048 and deoxycholate or ascorbate.

Initial photothermal response of the solid bulk GUMBOS under continuous irradiation at 1000 mW led to heat generation within seconds upon excitation, reaching temperatures as high as 500 °C (Figure 3.10, A). In contrast, when the bulk GUMBOS were suspended in aqueous media as nanoGUMBOS, excitation led to more reasonable temperatures between 40-50 °C (Figure 3.10, B).

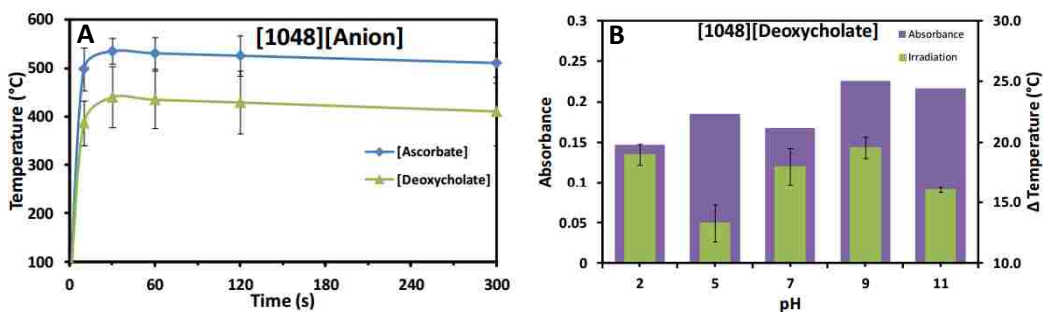


Figure 3.10: Photothermal profile of 4 mg bulk GUMBOS and nanoGUMBOS samples under continuous NIR irradiation for five minutes at a 1000 mW. Reprinted with permission.⁴⁰

The purpose of this study was to introduce nanoGUMBOS as novel materials for NIR-laser-triggered hypothermia cancer therapy. These nanoGUMBOS can be prepared using biocompatible compounds (*e.g.* vitamins, amino acids, organic acids) which would assist in tumor targeting. Their “nano” size (10-100 nm) enables the rapid uptake in cellular membranes and increased permeability. Preliminary results with these NIR-based nanoGUMBOS in experiments with malignant MDA-MB-231 and non-malignant HS-578-BST epithelial human breast cells demonstrate the ability of the particles to reach the temperature threshold

necessary for cancer cell apoptosis.⁴¹ These results make nanoGUMBOS a promising candidate for use as a drug delivery system. Ideally, a chemotherapeutic agent could be incorporated into NIR-based nanoGUMBOS and, due to their powerful solvent properties and high temperature threshold, would lend stability at high temperatures and increased solubility.

3.5 Drug Delivery System Overview

We demonstrate in the next chapter our proposed nano-mediated prodrug system that attempts to address the aforementioned limitations of drug delivery by focusing on transporter-mediated delivery of cancer agents to help permeate membranes, and exploring an alternative prodrug “trigger”. Because of GUMBOS’ inherent stability at high temperatures, they should also exhibit better control of photothermal destruction of cancerous tissues. Prodrugs that could take advantage of the high temperature threshold of the GUMBOS by using indirect heat generated from light absorption of organic NIR absorbing dyes as a trigger, combined with ease of permeability via nanoparticles would make an innovative drug delivery system.

We ultimately want to attach a full TaxolTM moiety to a trimethyl lock-based prodrug conjugate, and subsequently convert the system into NIR-based GUMBOS (Figure 3.11). This will be achieved by giving the prodrug an anionic functionality. Synthesis of the drug delivery system will focus on four main goals: 1) Synthesis of a model prodrug system with Taxol sidechain, 2) rearrangement studies in different solvent systems, 3) synthesis of NIR-GUMBOS/nanoGUMBOS derivatives of model produg, and 4) rearrangment studies of NIR-GUMBOS in the presence of laser irradiation.

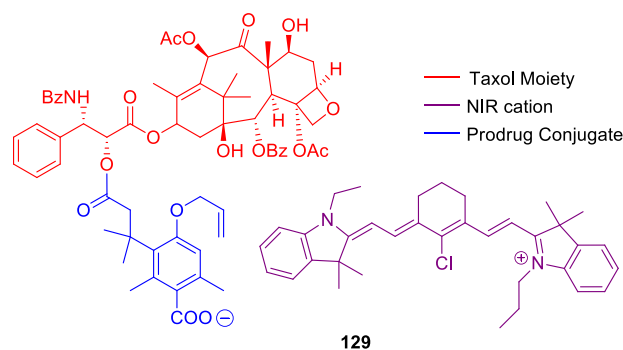


Figure 3.11: Trimethyl lock-based Taxol™ prodrug incorporated into NIR-absorbing nanoGUMBOS

3.6 References

1. Panno, J. *Cancer: the role of genes, lifestyle, and environment*; Facts on File: New York, 2005; pp. 1-18
2. American Cancer Society. *Cancer Facts & Figures 2014*. Atlanta: American Cancer Society; 2014
3. Bray, F., Ren J. S., Masuyer E., Ferlay J. "Estimates of global cancer prevalence for 27 sites in the adult population in 2008" *Int. J. Cancer*. **2013**, *132*, 1133-1145.
4. American Cancer Society. *Global Cancer Facts & Figures 2nd Edition*. Atlanta: American Cancer Society; 2011.
5. Wani, M. C., Taylor, H. L., Wall M. E., Coggon, P., McPhail, A. T. *J. Am. Chem. Soc.* **1971**, *93*, 2325-2327.
6. Xiao, H., Verdier-Pinard, P., Fernandez-Fuentes, N., Burd, B., Angeletti, R., Fiser, A., Horwitz, S. B., Orr, G. A. "Insights into the mechanism of microtubule stabilization by Taxol" *PNAS* **2006**, *103*, 10166-10173.
7. Yvon, A-M. C., Wadsworth, P., Jordan, M. A. "Taxol suppresses dynamics of individual microtubules in living human tumor cells" *Mol. Biol. Cell*, **1999**, *10*, 947-959.
8. Gascoigne, K. E., Taylor, S. S. "How do anti-mitotic drugs kill cancer cells?" *J. Cell Sci.* **2009**, *122*, 2579-2585.
9. Dordunoo S. K., Burt H. M. "Solubility and stability of taxol: effects of buffers and cyclodextrins" *Int. J. Pharm.* **1996**, *133*, 191-201.
10. Rowinsky, E. K., Cazenave, L. A., Donehower, R. C. "Taxol: a novel investigational antimicrotubule agent" *J. Natl. Cancer. Inst.* **1990**, *82*, 1247-1259.

11. Gelderblom, H., Verweij, J., Nooter, K., Sparreboom, A. "Cremophor EL: the drawbacks and advantages of vehicle selection for drug formulation" *Eur. J. Cancer* **2001**, *37*, 1590-1598.
12. Singla, A. K., Garg, A., Aggarwal, D. "Paclitaxel and its formulations" *Int. J. Pharm.* **2002**, *235*, 179-192.
13. Tarr, B. D., Yalkowsky, S. H., "A new parenteral vehicle for the administration of some poorly soluble anti-cancer drugs" *J. Parental. Sci. Technol.* **1987**, *41*, 31-33.
14. Persidis, A. "Cancer multidrug resistance" *Nature Biotechnology* **1999**, *17*, 94-95.
15. Lage, H. "An overview of cancer multidrug resistance: A still unsolved problem" *Cell. Mol. Life Sci.* **2008**, *65*, 3145–3167.
16. Breier, A., Gibalova, L., Seres, M., Barancik, M., Sulova, Z. "New insight into P-glycoprotein as a drug target" **2013**, *13*, 159-170.
17. Zahedi, P., De Souza, R., Huynh, L., Piquette-Miller, M., Allen, C. "Combination drug delivery strategy for the treatment of multidrug resistant ovarian cancer" *Mol. Pharmaceutics* **2011**, *8*, 260–269.
18. a) Vassileva, V., Allen, C. J., Piquette-Miller, M. "Effects of sustained and intermittent paclitaxel therapy on tumor repopulation in ovarian cancer" *Mol. Cancer Ther.* **2008**, *7*, 630–637 b) De Souza, R., Zahedi, P., Moriyama, E. H., Allen, C. J., Wilson, B. C., Piquette-Miller, M. "Continuous docetaxel chemotherapy improves therapeutic efficacy in murine models of ovarian cancer" *Mol. Cancer Ther.* **2010**, *9*, 1820–1830.
19. Pierré, A., Léonce, S., Pérez, V., Atassi, G. "Circumvention of P-glycoprotein-mediated multidrug resistance by S16020-2: kinetics of uptake and efflux in sensitive and resistant cell lines" *Cancer Chemother. Pharmacol.* **1998**, *42*, 454-460.
20. Jiang, D., Sui, M., Zhong, W., Huang, Y., Fan, W. "Different administration strategies with paclitaxel induce distinct phenotypes of multidrug resistance in breast cancer cells" *Cancer Letters*, **2013**, *335*, 404-411.
21. Stella, V. J. "Prodrugs: some thoughts and current issues" *J. Pharm. Sci.*, **2010**, *99*, 4755–4765.
22. Huttunen, K. M., Raunio, H., Rautio, J. "Prodrugs – from serendipity to rational design" *Pharm. Rev.* **2011**, *63*, 750-771.
23. Rautio, J., Kumpulainen, H., Heimbach, T., Oliyai, R., Oh, D., Järvinen, T., Savolainen, J. "Prodrugs: design and clinical applications" *Nat. Rev. Drug Discov.* **2008**, *7*, 255-270.

24. Zawilska, J. B., Wojcieszak, J., Olejniczak, A. B. "Prodrugs: A challenge for the drug development" *Pharmalogical Reports* **2013**, *65*, 1-14.
25. Huttunen, K. M., Rautio, J. "Prodrugs – An efficient way to breach delivery and targeting barriers" *Curr. Top. Med. Chem.* **2011**, *11*, 2265-2287.
26. Milstien, S., Cohen, L. Stereopopulation control. I. Rate enhancement in the lactonizations of *o*-hydroxyhydrocinnamic acids *J. Am. Chem. Soc.* **1972**, *94*, 9158-9156.
27. Levine, M. N., Raines, R. T. "Trimethyl lock: a trigger for molecular release in chemistry, biology, and pharmacology" *Chem Sci.* **2012**, *3*, 2412–2420.
28. Nicolaou, M. G., Yuan, C., Borchardt, R. T. "Phosphate prodrugs for amines utilizing a fast intramolecular hydroxy amide lactonization" *J. Org. Chem.* **1996**, *61*, 8636–8641.
29. Vyas D. M., Wong H., Crosswell A. R., Casazza A. M., Knipe J. O., Mamber S. W., Doyle T. W. *Bioorg. Med. Chem. Lett.* **1993**, *3*, 1357–1360.
30. Cho, H., Bae, J., Garripelli, V. K., Anderson, J. M., Jun, H. W., Jo, S. "Redox-sensitive polymeric nanoparticles for drug delivery" *Chem. Commun.* **2012**, *48*, 6043-6045.
31. Fang, J.-Y., Al-Suwayeh, S. A. "Nanoparticles as delivery carriers for anticancer prodrugs" *Expert Opin. Drug. Deliv.* **2012**, *9*, 657-669.
32. Nazir, S., Hussain, T., Ayub, A., Rashid, U., MacRobert, A. J. "Nanomaterials in combating cancer: therapeutic applications and developments" *Nanomedicine: NBM* **2014**, *10*, 19-34.
33. Hrkach, J., Von Hoff, D., Ali, M., Andrianova, E., Auer, J., Campbell, T., De Witt, D., Figa, M., Figueiredo, M., Horhota, A., Low, S., McDonnell, K., Peeke, E., Retnarajan, B., Sabnis, A., Schnipper, E., Song, J. J., Song, Y. H., Summa, J., Tompsett, D., Troiano, G., Van Geen Hoven, T., Wright, J., LoRusso, P., Kantoff, P. W., Bander, N. H., Sweeney, D., Farokhzad, O. C., Langer, R., Zale, S. "Preclinical development and clinical translation of a PSMA-targeted Docetaxel nanoparticle with a differentiated pharmacological profile" *Sci. Transl. Med.* **2012**, *4*, 128ra39.
34. Timko, B. P., Dvir, T., Kohane, D. S. "Remotely triggerable drug delivery systems" *Adv. Mater.* **2010**, *22*, 4925-4943.
35. a) Hale, G., Query, M. "Optical constants of water in the 200-nm to 200- μ m wavelength region" *Appl. Opt.* **1973**, *12*, 555-563.
36. Suri, S. S., Fenniri, H., Singh, B. "Nanotechnology-based drug delivery systems" *J. Occ. Med. Toxicology* **2007**, *2*, 16-21.
37. Dhawan, A., Sharma, V. "Toxicity assessment of nanomaterials: methods and challenges" *Anal. Bioanal. Chem.* **2010**, *398*, 589-605.

38. Feng, R., Zhao, D., Guo, Y. "Revisiting characteristics of ionic liquids: a review for further application development" *Journal of Environmental Protection*, **1**, **2010**, 95-104.
39. Tesfai, A., El-Zahab, B., Kelley, A. T., Li, M., Garno, J. C., Baker, G. A., Warner, I. M. "Magnetic and non-magnetic nanoparticles from a group of uniform materials based on organic salts" *ACS Nano*. **2009**, **3**, 3244-3250.
40. Dumke, J. C., Qureshi, A., Hamdan, S., El-Zahab, B., Das, S., Hayes, D. J., Boldor, D., Rupnik, K., Warner, I. M. "Photothermal response of near-infrared-absorbing nanoGUMBOS" *Appl. Spectrosc.* **2014**, **68**, 340-352.
41. Dumke, J. C., Qureshi, A., Hamdan, S., Rupnik, K., El-Zahab, B., Hayes, D. J., Warner, I. M. "In vitro activity studies of hyperthermal near-infrared nanoGUMBOS in MDA-MB-231 breast cancer cells" *Photochem. Photobiol. Sci.* **2014**, **13**, 1270-1280.

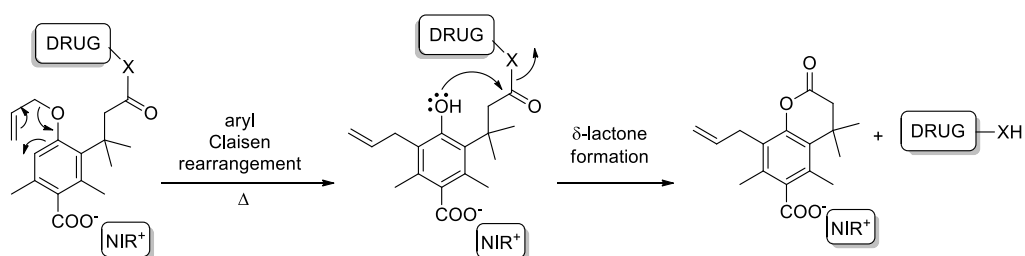
CHAPTER 4: SYNTHESIS OF ALLYL AND PRENYL ETHERS AND INVESTIGATION OF THE TANDEM CLAISEN REARRANGEMENT-LACTONIZATION REACTIONS

4.1 Drug Delivery System: Mechanism of Action

Our thermally-induced prodrug drug delivery system involves two reactions (Scheme 4.1):

1) Upon heating, a [3,3]-sigmatropic rearrangement (aromatic Claisen rearrangement) will occur, followed by tautomerism, revealing the free phenol.

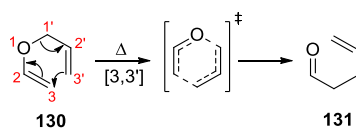
2) Spontaneous lactonization based on the well-established “trimethyl lock” (TML) motif previously discussed in Chapter 3 would then release the drug molecule.



Scheme 4.1: Ionic liquid-based prodrug drug delivery system. NIR⁺ = cationic near-infrared laser dye

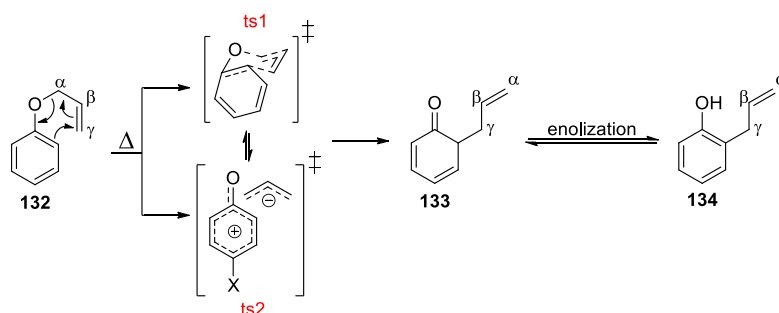
4.2 Claisen Rearrangement: A [3,3']-Sigmatropic Rearrangement

Since its discovery in 1912 by Ludwig Claisen, the Claisen rearrangement and its many variations has become a significant stereoselective carbon-carbon-bond forming reaction.¹ Originally, the Claisen rearrangement was described as “the thermal isomerization of an allyl aryl ether” and was eventually expanded to include rearrangements of allyl vinyl ethers into unsaturated carbonyl compounds, which were then classified as [3,3']-sigmatropic rearrangements (Scheme 4.2).²



Scheme 4.2: [3,3]-Sigmatropic rearrangement of allyl vinyl ether

It is generally accepted that the aromatic Claisen rearrangement proceeds through a concerted pericyclic reaction (Scheme 4.3, ts1).³ Upon heating, the allyl ether moiety undergoes a [3,3'] shift resulting in bond formation between the γ -carbon of the allyl group and the carbon on the aromatic ring at the *ortho*-position to the ether, generating the trienone intermediate (**133**, Scheme 4.3). If there are no substituents present at the *ortho* position, the dienone intermediate undergoes rapid enolization to re-establish aromaticity to generate the *ortho* allyl phenol product (**134**, Scheme 4.3).



Scheme 4.3: Aromatic Claisen rearrangement mechanism with alternative transition state

Theoretical and experimental studies have been ongoing to elucidate the mechanism for the Claisen rearrangement.⁴ A number of reports attempted to clarify the geometry of the transition state. Most groups agree that the Claisen rearrangement proceeds via a favorable six-membered ring chair-like transition state (Scheme 4.3, *ts1*), however there have been alternative transition states proposed. One proposal suggests the formation of “ion pairs”(Scheme 4.3, *ts2*) as an intermediate step between the allyl aryl ether and the dienone. The allyl group will ionize as an anion and the aromatic moiety as a cation.⁵ The true nature of the transition state probably lies between these two scenarios, and is likely substrate dependent.

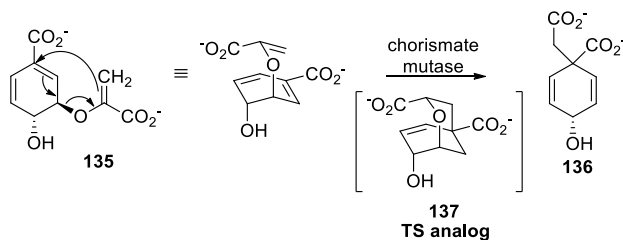
4.2.1 Aromatic Claisen Rearrangement: Solvent Effects

Under standard conditions, the aromatic Claisen rearrangement proceeds at high temperatures, between 180°C-225 °C, in a hydrocarbon solvent. It has been established experimentally that the reaction rate increases marginally in protic solvents; the more polar the solvent, the faster the reaction rates.⁶ This marginal increase in rate has resulted in the exploration of catalysts for milder conditions. Water has been shown to accelerate Claisen rearrangements, lowering the temperature required.⁷ Rearrangements that can occur at temperatures below 70 °C are important in order for this reaction to be feasible in physiological systems.

4.2.2 Water Promoted Claisen Rearrangement: Mechanistic Studies

Deducing the mechanism behind the water-induced acceleration of the Claisen rearrangement has proven difficult. Early on, this was mostly due to the false assumption that all variations of the Claisen rearrangement were generally resistant to solvent effects.⁸ As more studies appeared, detailing the accelerating effects of hydrogen-bonding solvents on the pericyclic rearrangement, interest grew in understanding the mechanism. Early theories hinted at the importance of hydrogen bonding,⁹ at first contested,¹⁰ but eventually corroborated by an enlightening study done by two groups out of Cornell and Indiana universities in the late 80's.¹¹ They were studying solvent effects on the non-enzymatic Claisen rearrangement of chorismate. Chorismate (**135**) is the anionic form of chorismic acid, which is an important biological precursor to aromatic amino acids such as tryptophan, phenylalanine, and tyrosine, as well as the precursor to the biosynthesis of folate and Vitamin K in plants, and ubiquinone.¹² Chorismate mutase catalyzes the rearrangement of chorismate to prephenate in biological

media (Scheme 4.4). Rearrangement of chorismate represents one of few examples of pericyclic reactions in nature.



Scheme 4.4: Chorismate rearrangement to prephenate ion catalyzed by chorismate mutase

Surprisingly, the rearrangement of dimethyl chorismate in an aqueous methanolic solution was only 18 times faster than that of allyl vinyl ether in the same solution.¹¹ They concluded that the ability of chorismate to rapidly rearrange in biological media at room temperature was largely due to the presence of an aqueous environment, and not by the unusual structural motif as previously thought.

A Monte Carlo simulation done by Severance and Jorgenson further explored this hydration theme in an effort to understand the role of enhanced solvent hydrogen bonding in accelerating the rate of Claisen rearrangements.¹³ They concluded that “with hydrogen bonding increasing as the reactant moves towards the transition state, $n \rightarrow \pi^*$ conjugation in the vinyl ether ground state is disrupted,” stabilizing the transition state and lowering the activation barrier for rearrangement (Figure 4.1).⁴

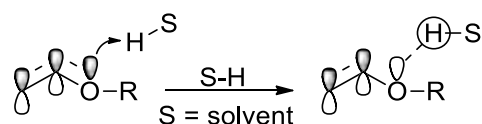


Figure 4.1: Solvent hydrogen bonding in vinyl ether transition state

High-resolution X-ray structures of the *N*-terminal domain of the *E. Coli* enzyme chorismate mutase prephenate dehydratase (EcCM)¹⁴ and the monofunctional *B. subtilis*

chorismate mutase (BsCM)¹⁵ provided real mechanistic insight into the role water plays in this biologically relevant Claisen rearrangement.

Both BsCM and EcCM structures were solved as complexes with a chorismate-type intermediate **137** (Figure 4.2). The Ganem group, who reported the X-ray structure of EcCM, postulated that adjacent, positively charged active site residues exert conformational control by locking the reoriented chorismate ion in the requisite chair conformer for rearrangement. This stabilizes the transition state in a network of hydrogen bonds which reduces the activation enthalpy for rearrangement. Of particular importance are the Lys39 and Gln88 residues in the EcCM enzyme and arginine residue 90 in the BsCM enzyme which forms two hydrogen bonds with the enol ether group of the chorismate ion that further promotes the pericyclic rearrangement.

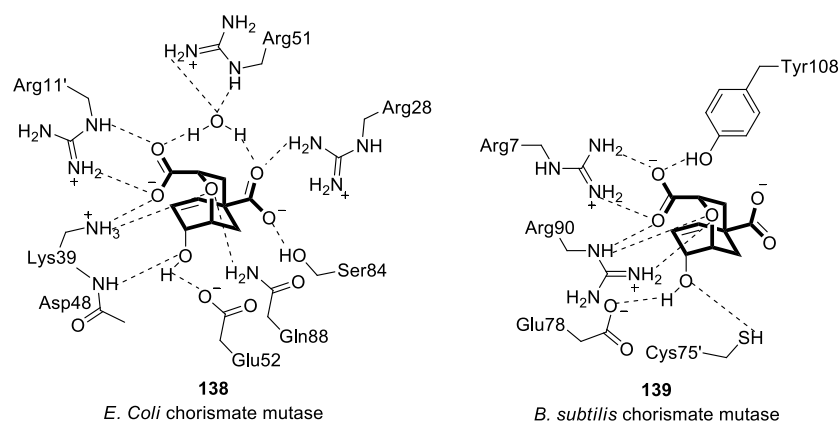


Figure 4.2: Amino acid residues of active site in EcCM and BsCM complexed with dianionic competitive inhibitor **137**

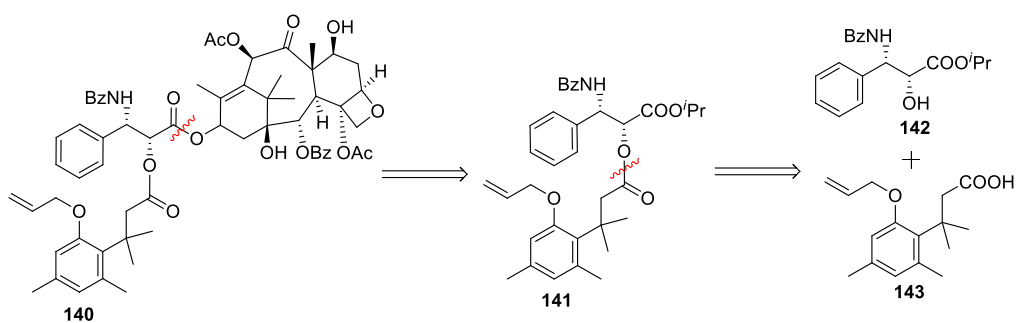
4.3 Synthesis of Prodrug Conjugate Model System

On the basis of this background information on Claisen rearrangements, specifically acceleration in aqueous solutions, we sought to apply this reaction to our prodrug project. As TaxolTM has precedent for successful incorporation into prodrugs, it will serve as our target drug

for drug release.¹⁶ TaxolTM's amino alcohol sidechain provides the opportunity to conjugate via an ester linkage, and cleavage of that bond will be the focus of our prodrug model system. Because there is a proven, established linkage site, we can focus our efforts on the thermal release of the drug.

4.3.1 Retrosynthetic Analysis

Scheme 4.5 outlines our approach to the assembly of the prodrug model system. To test the feasibility of the system, we opted to synthesize a model system that will mimic TaxolTM drug release (Scheme 4.5, **141**). Structure-activity relationship studies determined that the bulk of TaxolTM's biological activity is centered on the amido alcohol sidechain, particularly the hydroxyl group.¹⁷ If this group is masked, in our case as an ester, the biological activity will be severely reduced. Because of this, we have opted to synthesize the Taxol sidechain **142** as a simplified representative for the drug molecule. This will then be conjugated to the allyl ether trimethylock linker **143**.

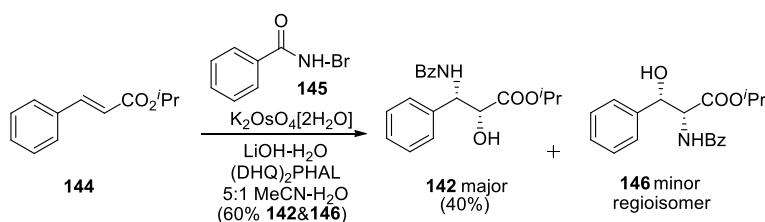


Scheme 4.5: Retrosynthetic analysis of prodrug model system **140**

4.3.2 Previous Synthesis of Taxol Sidechain Amino Alcohol

In 1999, the Choi group published the highly enantioselective one-step synthesis of the paclitaxel side chain precursor, (2*R*,3*S*)-isopropyl 3-benzamido-2-hydroxy-3-phenylpropionate (**142**).¹⁸ This was achieved through Sharpless asymmetric aminohydroxylation of isopropyl

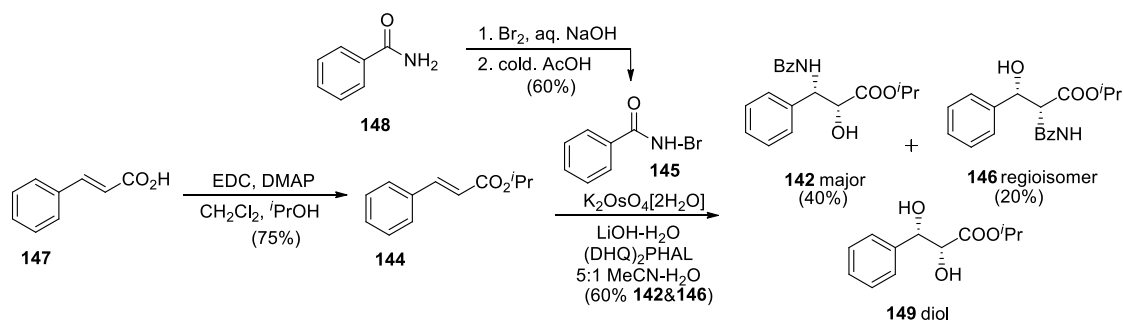
trans-cinnamate. Through careful optimization of the chiral ligands, solvent choice, and mole ratio of ligand to oxidant they were able to synthesize the amino alcohol in 40% yield with 97% e.e. Although there are other reported syntheses of amido alcohol **142**,¹⁹ the convenience of a one-step asymmetric synthesis with high enantioselectivity offsets the poor yield.



Scheme 4.6: Asymmetric aminohydroxylation of isopropyl *trans*-cinnamate

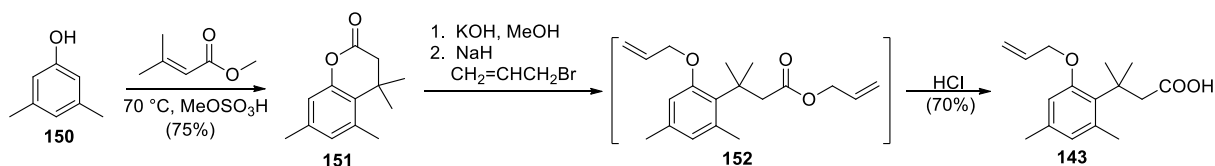
Preparation of TaxolTM sidechain **142** is outlined in Scheme 4.7. Bromobenzamide (**145**) was prepared via bromination of benzamide in moderate yield. Synthesis of bromobenzamide was not trivial and required interpretation of dated literature procedures²⁰ and optimization of the purification step. Bromobenzamide cannot be stored at room temperature, or exposed to light for long periods of time as it degrades back to its parent compound benzamide. It also reacts rapidly when in solution, preventing purification by column chromatography. Fortunately, recrystallization from chloroform-hexanes, provided colorless crystals that could be stored indefinitely at 0 °C.

Trans-cinnamic acid **147** was protected as the isopropyl ester using standard EDC coupling conditions in good yield. The *trans*-cinnamate ester was subjected to Sharpless conditions for amino hydroxylation giving a mixture of products. While the two regioisomers **142** and **146** could be separated by flash column chromatography, **142** was contaminated with diol **149**. Removal of the diol was achieved using HPLC.



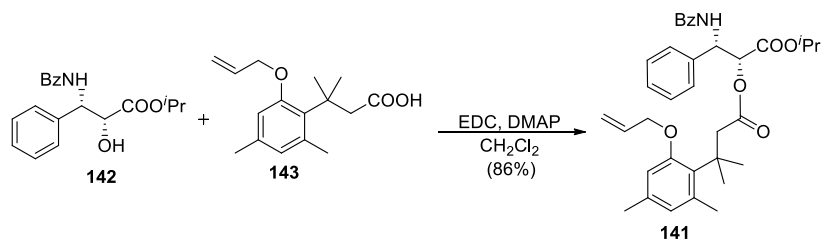
Scheme 4.7: Synthesis of Taxol amido alcohol sidechain

With the purified TaxolTM side-chain fragment in hand, we turned our attention to the allyl ether trimethyl lock reaction partner (Scheme 4.8). 3,5-Dimethylphenol was converted to lactone **151** via acid catalyzed aromatic alkylation in good yield.²¹ The lactone was then opened with one equivalent of potassium hydroxide. The phenol is deprotonated with sodium hydride, and the resulting salt is reacted with allyl bromide to give intermediate **152**. The allyl ester is then removed by hydrolysis to furnish compound **143** in moderate yield. Monoallylation is not possible due to the trimethyllock effect. If the phenol is left unprotected, spontaneous lactonization will occur, cleaving the allyl ester.



Scheme 4.8: Synthesis of allyl ether trimethyllock linker **143**

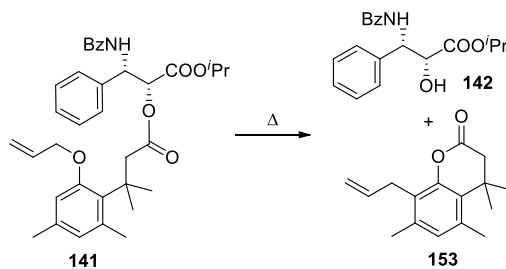
Next, amido alcohol **142** was coupled to the acid **143** using procedures based on those of Tsuchiya and coworkers, EDC/DMAP, to give the prodrug model system **141** in good yield (Scheme 4.9).²² Surprisingly the bulkiness of the *gem*-dimethyl group did not seem to impede the coupling of the two reaction partners.



Scheme 4.9: Coupling of amido alcohol **142** and acid **143** to give prodrug model system **141**

4.4 Rearrangement Studies

With the model system prepared, we turned our efforts towards studying solvent effects on the rearrangement of model system **141** (Scheme 4.10). We were specifically searching for a solvent system that would give us efficient rearrangement at the lowest possible temperature (Table 4.1), as this system will eventually be used under physiological conditions.



Scheme 4.10: Thermal rearrangement of prodrug model system **141**

We first explored the time required for rearrangement in a traditional hydrocarbon solvent to establish a “baseline”. Our findings are summarized in Table 4.1. Although TLC confirmed the disappearance of compound **141** and the emergence of lactone **153** and amido alcohol **142**, continued heating for complete disappearance of starting material led to degradation of both products. We next tested ethylene glycol, a moderately polar compound that should decrease the time required for maximum rearrangement. To reduce the risk of product degradation, the reaction was stopped after 24 hours. Product isolated was not positively identified from the mixture. It was apparent that the high temperatures were having

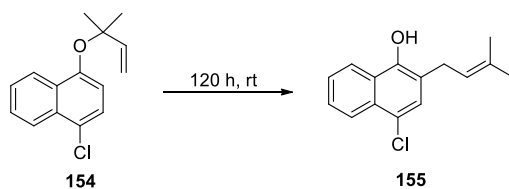
undesired consequences on the rearrangement products. We next moved to aqueous solutions, first attempting water as the sole solvent. All attempts to promote rearrangement were unsuccessful; it seems that the presence of a co-solvent (MeOH) was needed to realize the rate accelerating effects of water. We can only conclude that to promote rearrangement in pure water, vigorous stirring that promotes universal contact between both hydrophobic and hydrophilic layers is crucial.

Table 4.1: Various solvents, temperatures, and reaction times for thermal Claisen rearrangement trials of model system **141**. Yields are given.

Trial	Solvent	Temp. (°C)	Reaction Time (h)	Disappearance 141 (%)
1	Xylenes	100-140	16 h – 72	100 (loss of 141)
2	Ethylene Glycol	110	24	30
3	H ₂ O	rt – 100	24 h – 48	0 – trace
4	3:1 EtOH:H ₂ O	100	24	67

4.5 “On-Water” Claisen Rearrangement

A report by the Sharpless group detailed the enhanced reactivity of pericyclic reactions in aqueous suspensions,²³ in particular, they demonstrated an aromatic Claisen rearrangement in various solvents at room temperature, noting 100% conversion using solely water after 120 hours (Scheme 4.11, Table 4.2). This was of interest to us, as previously stated, we were not able to lower the temperature required for rearrangement under 100 °C. Upon closer inspection, the only distinguishing feature was the presence of a *gem*-dimethyl group on the allyl moiety. There was no discussion on why this particular substrate was chosen for rearrangement studies. This 1,1-dimethylallyl group (DMA), is also known as a “reverse” prenyl group.



Scheme 4.11: Aromatic Claisen rearrangement of 1-(4-chloronaphthyl)-1,1-dimethylallyl ether at room temperature

Table 4.2: Comparison of solvents for aromatic Claisen rearrangement of 1-(4-chloronaphthyl)-1,1-dimethylallyl ether and associated yields.²³

Solvent	Yield [%]
Toluene	16
DMF	21
CH ₃ CN	27
MeOH	56
Neat	73
“On H ₂ O”	100

4.6 Prenyl Moiety and its Derivatives

The prenyl group (3-methyl-but-2-en-1-yl) and its derivatives 1,1-dimethylallyl, geranyl (*E*-3,7-dimethyl-2,6-octadienyl), and lavandulyl (5-methyl-2-isopropenyl-hex-4-enyl) are hydrophobic moieties derived from isoprene (Figure 4.3).

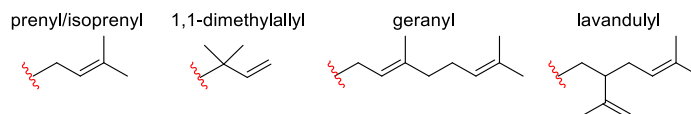


Figure 4.3: Prenyl group and its derivatives

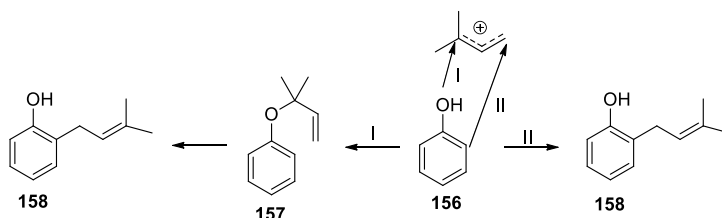
Prenyl groups in the form of prenylated proteins were first identified by the Harker group during a study of the effects of plasma lipoproteins on smooth muscle cells.²⁴ During preparation of the lipoproteins, the centrifuge process to extract and separate the lipoproteins from blood cells inadvertently separated the lipoproteins from platelets and a then-unknown growth factor. This growth factor, which was later identified as platelet-derived growth factor (PDGF), was purified and used to stimulate Swiss 3T3 cells which were used in mevalonic acid-

based DNA synthesis studies. The Harker group observed cellular uptake of the acid into cell proteins which was regulated by prenyl containing proteins.²⁴ Since then over 100 prenyl transferases have been identified as a result of posttranslational modification of proteins in eukaryotic cells.

The prenyl structural motif can be found in many natural products including flavonoids, xanthenes, and cyanobactins. Each of these families represents a diverse group of compounds that are known to have anti-malarial, anti-cancer, anti-oxidant, anti-bacterial, and anti-inflammatory properties. These properties are often attributed to the lipophilic nature of the prenyl moiety, which facilitates transmembrane transport, and may increase biological activity.

4.6.1 Claisen Rearrangement: Is There An Enzyme In Nature?

The aforementioned natural products all undergo electrophilic alkylation via a prenyl transferase enzyme. These enzymes install the prenyl group as a fixed moiety, where it is not altered after installation. In general, it has been established that aromatic prenyl transferases attach prenyl groups at the *ortho*-position via electrophilic aromatic substitution (Scheme 4.12, Pathway II).²⁵



TruLy1:MGSSHHHHHSSGLVPRGSHMNKKNILPQLGQPVIRLTAGQLSSQLAELSEEALGGVDASTLPVPTLCSYDGVDAVCMPCYPSYDD
159

Scheme 4.12: 1) Mechanism of action for LynF demonstrated on tyrosine (Pathway I) 2) LynF enzyme sequence 159 3) Traditional prenyl transferase mechanism of installation of prenyl group *ortho* to the phenol

However, with the recent characterization of the enzyme LynF (**159**, Scheme 4.12), isolated from the marine cyanobacterium *Lyngbya aestuarii*, may challenge that assumption.²⁶

LynF, from the TruF family, represents the first prenyl transferase enzyme characterized that leads to the synthesis of ribosomal peptide natural products. Most dimethylallyl pyrophosphate (DMAPP) based transferases functionalize single amino acids or small dipeptides. LynF acts by a novel mechanism in that it *O*-prenylates (reverse and forward) tyrosine, serine, and threonine residues in polypeptides, specifically cyanobactins, after the leader sequence and recognition elements have been removed. This is a deviation from the traditional ribosomal peptide natural product synthesis model which requires a leader sequence to direct post-translational modifications. The proposed mechanism of action of LynF is *O*-prenylation, and then a Claisen rearrangement, that happens at physiological temperature to give C-prenylation (Scheme 4.12, Pathway I).

Scientists have been unclear as to how prenylation occurs on peptides made by ribosomes. It was suggested as early as the 1970's that some natural products could arise by a Claisen rearrangement, but experimental evidence for the proposal was lacking until now. The LynF enzyme's amino acid sequence is completely different from that of other prenyl-transferring enzymes.

4.6.2 Computational Studies of Water-Accelerated *gem*-Dimethyl Allyl Ether Rearrangement

Cramer and Truhlar proposed that acceleration of Claisen rearrangements in aqueous systems is caused by electrostatic polarization and first-hydration-shell hydrophilic effects. As stated earlier Jorgenson and Severance used QM calculations to show that two water molecules hydrogen-bond with the ether oxygen atom in the transition state and accelerate the

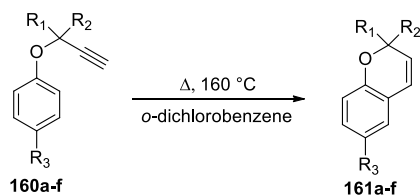
reaction. Calculations by the Hillier group with two explicit solvent water molecules have been used to explain the decrease in the activation energy due to solvation.

The Houk group developed a computation design of a biocatalyst for the Claisen rearrangement of prenyl coumaryl ethers. They first conducted benchmark test on traditional Claisen rearrangement substrates (*i.e.* aryl allyl ethers) where the activation enthalpy is known, and then applied these calculations to the rearrangement of *O*-prenylated tyrosine.²⁷

They calculated the aromatic Claisen rearrangement to be slower than its alkyl counterpart, which agrees with experimental data. The activation energy was computed to be 5.6-7.1 kcal/mol higher in energy than the prototypical alkyl Claisen rearrangement. The larger enthalpy of activation is due to the loss of aromaticity in the aromatic-Claisen TS. When these same calculations were applied to the *O*-prenylated tyrosine, they found that explicit solvation was necessary for acceleration of the Claisen rearrangement, and for lowering the activation barrier. Hydrogen bonding plays a significant role, especially between protic solvents and the TS, resulting in a lower barrier to activation.

4.6.3 Experimental Evidence of *gem*-Dimethyl Allyl Ether Rearrangement

Literature evidence for rate-acceleration of Claisen rearrangements by *gem*-dimethyl substituents is scarce. Harfenist and Thom demonstrated the rate-acceleration of propargyl aryl ethers in *o*-dichlorobenzene in 1972 (Scheme 4.13).²⁸ They found, during rearrangement studies, that the addition of one methyl substituent at the α -position increases the Claisen-like cyclization by a factor of 10. A second methyl group increases the rate by a factor of 1000 (Table 4.3).



Scheme 4.13: Relative rates of cyclization and chemical yields of propargyl aryl ether derivatives in *o*-dichlorobenzene

Table 4.3: Relative rates of cyclization and chemical yields of propargyl aryl ether derivatives in *o*-dichlorobenzene

Propargyl ether	R ₁	R ₂	R ₃	<i>k</i> rel ^a	Yield (%)
160a	H	H	NO ₂	1	46
160b	H	Me	NO ₂	9.1	84
160c	Me	Me	NO ₂	1400	75
160d	H	H	CN	1	
160e	H	Me	CN	10	99
160f	Me	Me	CN	1000	100

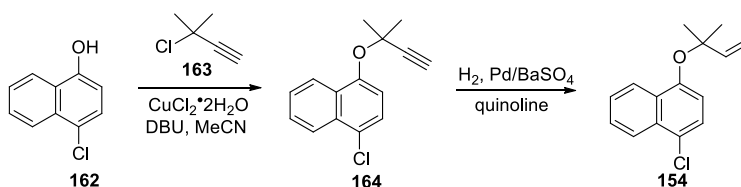
^a Data were extrapolated to 161.6 °C.

This experimental data suggests that the *gem*-dimethyl group is the sole determining factor in the rate acceleration of the Claisen rearrangement. To our knowledge, there haven't been any studies concerning the rate acceleration properties of the 1,1-dimethylallyl group on regular Claisen rearrangements nor rate acceleration kinetics.

4.7 Synthesis of *O*-Prenylated Derivatives

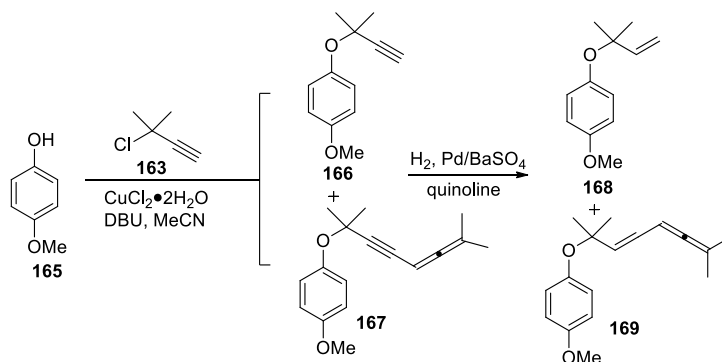
With the realization that the “reverse” prenyl group has rate accelerating properties, we set out to synthesize a library of aryl DMA ethers with different substituents on the aromatic ring (*i.e.* electron donating, electron withdrawing) to first demonstrate the rate-accelerating effect of the *gem*-dimethyl group on the aromatic Claisen rearrangement and then to study substituent effects on the rate acceleration of *gem*-dimethyl aryl allyl ethers compared to traditional aryl allyl ethers.

Naturally, we revisited the reported procedures for dimethylallylation of 4-chloro-1-naphthol by the Sharpless group.²³ They prepared compound **164** by installing a dimethylpropargyl group on the hydroxyl group, followed by reduction of the triple bond in the presence of barium sulfate to give the 1,1-dimethylallyl naphthyl ether **154** (Scheme 4.14).



Scheme 4.14: Sharpless and coworkers synthesis of 4-chloro-1,1-dimethylallyl naphthyl ether **154**

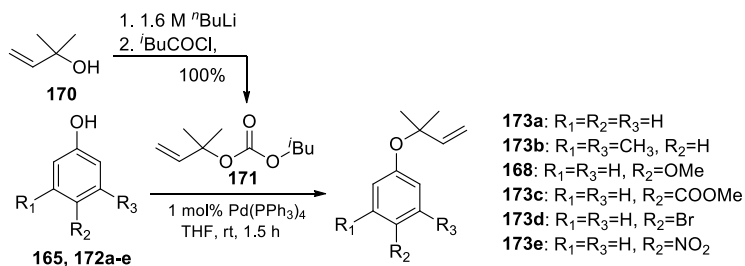
We attempted to prepare **168** by analogy to Scheme 4.14. Transformation to ether **166**, which is mediated by copper chloride, proceeded smoothly, but is accompanied by formation of an expected side product, allene **167** (Scheme 4.15). Compounds **166** and **167** could not be separated by flash chromatography or HPLC. Reduction of the mixture of **166** and **167** led to a mixture of **168** and **169**, from which **168** could now be partially purified by HPLC. Due to the tedious purification for both steps, a more efficient route to dimethylallyl ethers was sought.



Scheme 4.15: Attempted synthesis of aryl prenyl ether **168**

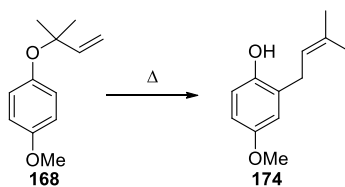
An alternative approach to prenylate heteroatoms is the use of allylic carbonates and $\text{Pd}(\text{PPh}_3)_4$. The DMA carbonate was prepared using *n*-butyllithium, 1,1-dimethylallyl alcohol,

and isobutyl chloroformate in quantitative yield. Using isobutyl prenyl carbonate (**171**) compounds **168**, and **173a-e** were prepared in very high yields (85-90%) (Scheme 4.16).



Scheme 4.16: Synthesis of 1,1-dimethylallyl ether derivatives

After preparation of the library of DMA aryl ether derivatives, we turned to rearrangement studies (Scheme 4.17). Substrate **168** was chosen as the prototype for a survey of potential solvents for the reaction. Table 4.3 summarizes our findings. It was observed that the DMA group does accelerate the Claisen rearrangement relative to prodrug model system **141** (Scheme 4.9) enough to facilitate rearrangement at 70 °C. Rearrangement at lower temperatures was observed, but required longer time for complete conversion. It seems that with the *gem*-dimethyl group present, the rearrangement is stunted in hydrocarbon solvents but greatly accelerated in polar solvents. This was an interesting finding as traditional Claisen rearrangements require high boiling hydrocarbon solvents for rearrangement. Another point of interest was the rapid rearrangement of the prenylated ether (**168**) on pure water. The non-polar nature of the DMA group rendered the compounds volatile liquids at room temperature. On the positive side, this low viscosity enabled effective mixing of the hydrophobic and hydrophilic layers.



Scheme 4.17: Thermal rearrangement of aryl prenyl ether **168**

Table 4.4: Comparison of solvents and reaction times for the aromatic claisen rearrangement of aryl prenyl ether **168** and associated yields.

Trial	Solvent	Temperature (°C)	Reaction Time (h)	Yield (%)
1	Neat	70	15	70
2	Xylenes	100-140	16 – 72	Trace-10
3	Ethylene Glycol	70	24	56
4	H ₂ O	70	3	quantitative
5	3:1 EtOH:H ₂ O	70	9	95

Since this project is focusing on rearrangement in aqueous solutions, the rest of the derivatives underwent rearrangement in the EtOH:H₂O solvent system and were compared to the *p*-OMe derivative to see any trends. In essence, the electron donating groups at the *para* position on the ring led to rearrangement at a faster rate than electron withdrawing groups, which is a trend that has been observed in other systems.²⁹ Although “on-water” conditions led to the fastest reaction time and highest yield, subsequent trials were not reproducible due to difficulty in achieving a consistent uniform dispersion of a heterogeneous mixture.

4.8 Synthesis of Second Generation Prodrug Model System: Preliminary Results

Now that rearrangement at acceptable temperatures has been achieved, the synthesis of the second generation of the prodrug model system (**175**, Figure 4.5) was the next step. Due to the nature of the installation of the DMA group via the allylic carbonate, it wasn't feasible to use this same method in conjugation with the prodrug model system (Scheme 4.16). Excess base is present when lactone **151** is opened, and the resultant nucleophiles could compete with

the Pd(0) to give isobutyl alkylation instead of prenyl alkylation. Our goal was to synthesize this second generation model system in an efficient manner.

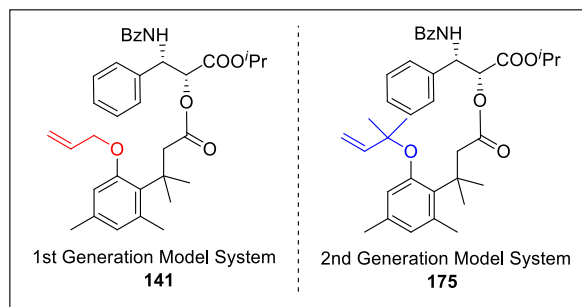
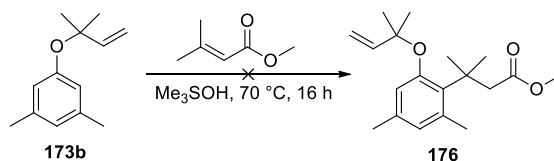


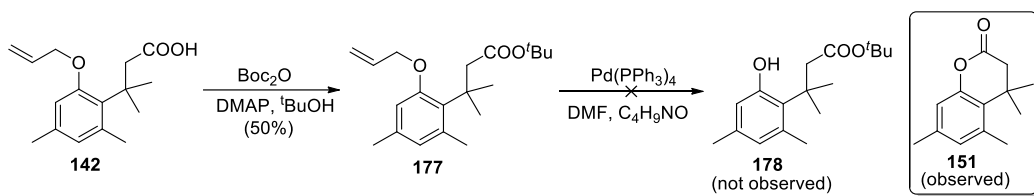
Figure 4.4: 1st and 2nd generation prodrug model systems

Our first approach was a direct alkylation of DMA derivative **173b** with dimethyl acrylate, analogous to the preparation of the lactone precursor **151** (*vide supra*, Scheme 4.8). Unfortunately, many byproducts were formed including the rearranged product, and subsequent lactonization of the free phenol. Methanesulfonic acid appears to be too acidic for the DMA group.



Scheme 4.18: Attempted aromatic alkylation of aryl prenyl ether **173b**

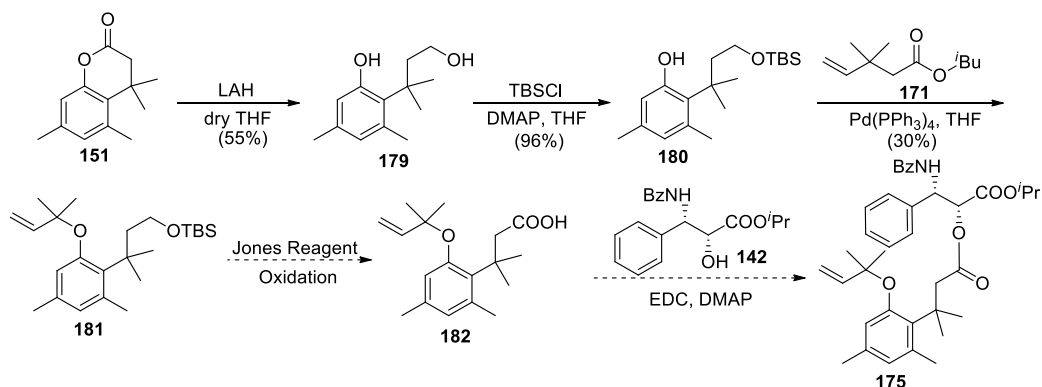
A less direct approach involved converting the acid in compound **142** to a *tert*-butyl ester (Scheme 4.19). We postulated that the bulky ester would prevent the lactonization upon liberation of the phenol. Steric hindrance around the acid is known to disfavor bulky alkylation.³⁰ Deallylation of the allyl ether proceeded smoothly by TLC, but subsequent NMR of the recovered product revealed the lactone **151** as the major product.



Scheme 4.19: Attempted synthesis of compound **178**

It appeared that a straightforward, short synthesis of the DMA prodrug model system was not going to be possible. There were a few relevant reports that reduced the acid to a primary alcohol, effectively eliminating the problematic spontaneous lactonization. This gives us the opportunity to install the DMA group on the phenol without interference.

Thus, synthesis of model system **175** begins with LAH reduction of lactone **151** to give diol **179** in modest yield (Scheme 4.20). The primary alcohol was then protected as a TBDMS group in excellent yield. Initially, we attempted to install the DMA ether using the established procedures. However, the bulkiness of the TBS group, and the *gem*-dimethyl groups of the substituent *ortho* to the phenol were hindering alkylation. Longer reaction times and heat (50 °C) were needed to get some conversion to the DMA ether. Oxidation with Jones Reagent, cleaving the TBDMS group *in situ*, will furnish free acid **182**. Standard coupling using EDC/DMAP gives DMA prodrug model system **175**.

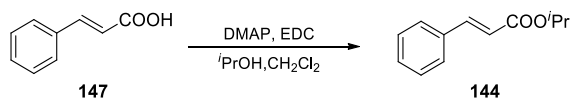


Scheme 4.20: Proposed synthesis of second generation prodrug model system **175**

4.9 Experimental Section

General Methods: All reactions were performed under a dry nitrogen atmosphere unless otherwise noted. All chemicals and reagents were purchased from Sigma-Aldrich, Fisher, and Acros and used without further purification. Triethylamine and diethylamine were dried and distilled from CaH₂ and stored over KOH pellets. Dry methanol was distilled from Mg turnings and stored over 3Å molecular sieves. Flash chromatography was performed using 230-400 mesh silica gel (40-63 μm) from Sigma-Aldrich. Reactions were followed by thin layer chromatography (TLC) on pre-coated aluminum-backed 60 F254 silica plates from EMD Chemicals, Inc. Compounds were visualized under UV fluorescence or by staining with KMnO₄, or an acidic, ethanolic solution of ninhydrin. ¹H and ¹³C NMR spectra were recorded at room temperature on a Bruker AV-400 or Bruker Nanobay-400 and are reported in parts per million (ppm) on the δ scale relative to residual CHCl₃ or CH₃OH in deuterated solvents or tetramethylsilane as an internal standard. Coupling constants (*J*) are reported in Hertz (Hz). High resolution mass spectrometry (HRMS) was carried out using an Agilent 6210 electrospray ionization-time-of-flight (ESI-TOF) mass spectrometer. Optical rotations were recorded under the specified conditions.

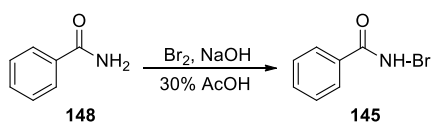
4.9.1 Procedures



Scheme 4.21: Synthesis of compound **144**

Isopropyl *trans*-cinnamate (**144**).³¹ A solution of DMAP (495 mg, 4.05 mmol, 1.2 equiv.) in anhydrous CH₂Cl₂ (0.9 mL) was added dropwise to a suspension of *trans*-cinnamic acid (**147**) (500 mg, 3.37 mmol, 1.0 equiv.) in isopropyl alcohol (3.4 mL) under N₂. The reaction mixture

was cooled to 0 °C. A solution of EDC (776 mg, 4.05 mmol, 1.2 equiv.) in anhydrous CH₂Cl₂ (2.4 mL) was added dropwise. The mixture was warmed to rt and stirred overnight. The solution was partitioned between H₂O (34 mL) and CH₂Cl₂ (34 mL). The layers were separated and the aqueous layer extracted further with CH₂Cl₂ (3 x 17 mL). The combined organic layers were dried over MgSO₄, filtered and concentrated. The pale yellow oil was purified by flash chromatography on silica gel, eluting with 2:1 hexanes:EtOAc to give isopropyl *trans*-cinnamate as a light yellow viscous oil (490 mg, 76%). *R*_f 0.21 (9:1 CH₂Cl₂-MeOH). ¹H-NMR (400 MHz, CDCl₃) δ 1.31 (d, *J* = 6.2 Hz, 6H, CHMe₂), 5.14 (septet, *J* = 6.2 Hz, 1H, ^{*i*}Pr-CH), 6.42 (d, *J* = 16.0 Hz, 1H, CH=CH-Ph), 7.36-7.38 (m, 3H, Ar-H), 7.52 (d, *J* = 3.3 Hz, 2H, Ar-H), 7.67 (d, *J* = 16.0 Hz, 1H, CH=CH-Ph); ¹³C-NMR (100 MHz, CDCl₃) δ 22.0, 67.8, 118.8, 128.0, 128.9, 130.1, 134.6, 144.3, 166.5.

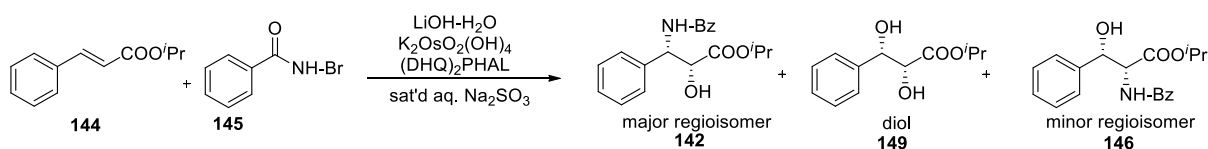


Scheme 4.22: Synthesis of compound **145**

N-Bromobenzamide (**145**).²⁰ Benzamide (**148**) (1.0 g, 8.3 mmol, 1.0 equiv.) was added to a vigorously stirred solution of freshly prepared sodium hypobromite* (15 mL) at 0 °C. After 10 min, the solution was rapidly filtered, and the filtrate was collected in a flask containing an aqueous solution of acetic acid (30%, 4 mL). The filtrate was discarded. The orange-yellow precipitate that formed was then filtered, and washed with water that had been cooled to 0 °C. The precipitate was dried under N₂ and then vacuum to remove all water. The crude precipitate (1.5 g) was dissolved in chloroform (25 mL) and heated at reflux. Immediately after the solid had dissolved, the solution was transferred to an Erlenmeyer flask. This solution was treated

with hexanes (~35 mL), and as the solution cooled, a colorless precipitate formed. The solid was collected by filtration and washed with hexanes to give *N*-bromobenzamide as a colorless solid (952 mg, 58%). R_f 0.50 (9:1 CH₂Cl₂-MeOH). The compound was stored in an amber vial at 0 °C to avoid degradation back to benzamide.

*Sodium hypobromite was prepared by dissolving NaOH pellets (920 mg, 23.0 mmol, 2.80 equiv.) in H₂O (14.4 mL) for a total volume of 15 mL. The solution was cooled to 0 °C. Bromine (462 μL, 1.44 g, 9.01 mmol, 1.09 equiv.) was added dropwise and the solution was stirred for 10 min during which time it turned a bright yellow.



Scheme 4.23: Synthesis of compound **142**, **149**, and **146**

Amido alcohol (**142**).¹⁸ K₂OsO₂(OH)₄ (12 mg, 0.032 mmol, 0.04 equiv.) was added to an aqueous solution of LiOH-H₂O (7.1 mg, 0.30 mmol, 2.4 mL). After addition of MeCN (9.5 mL), (DHQ)₂PHAL (123 mg, 0.158 mmol, 0.20 equiv.) was added, and the mixture stirred for 10 min giving a transparent solution. Water (2.4 mL) was added, and the mixture cooled to 0 °C. After addition of isopropyl *trans*-cinnamate (**144**) (150 mg, 0.788 mmol, 1.00 equiv.), *N*-bromobenzamide (**145**) (315 mg, 1.580 mmol, 2.00 equiv.) was added in one portion, and the mixture stirred vigorously at 0 °C for 10 h. The reaction color changed from deep green to yellow. The reaction was quenched by the addition of sat'd aq. Na₂SO₃ (~2-3 mL) and stirred for an additional hour at 0 °C. The phases were separated, and the aqueous layer extracted with ethyl acetate (3 x 5 mL). The combined organic layers were washed with 3 M HCl (5 mL) to

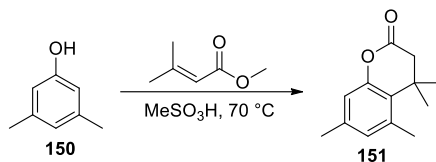
recover the ligand, H₂O (5 mL), brine (5 mL), dried over MgSO₄, filtered and concentrated. The residue was purified by flash chromatography on silica gel eluting with 3:1 hexanes:EtOAc to yield a mixture of amido alcohol **142** and diol **149** as a colorless solid (155 mg, 60%). Followed by the regioisomeric amido alcohol **146** (20%). Compounds **142** and **149** were separated by HPLC using a Alltima 10 μ 10mm x 20mm silica column eluting with 20% EtOAc in hexanes at 5 mL/min. Absorbance was detected at 254 and 218 nm.

(2*R*,3*S*)-Isopropyl 3-benzamido-2-hydroxy-3-phenylpropionate (**142**): *R_f* 0.34 (9:1 CH₂Cl₂-MeOH). Lit.¹⁸ [α]_D¹⁶ -24.7 (c 0.618, CHCl₃). ¹H-NMR (400 MHz, CDCl₃) δ 1.26 (d, *J* = 6.3 Hz, 3H, ^{*i*}PrCH₃), 1.31 (d, *J* = 6.3 Hz, 3H, ^{*i*}PrCH₃), 3.32 (br s, 1H, OH), 4.60 (app. s, 1H, CH-OH), 5.12 (sept., *J* = 6.3 Hz, 1H, ^{*i*}PrCH), 5.77 (dd, *J* = 9.2, 1.7 Hz, 1H, CH-NH), 7.01 (d, *J* = 9.1 Hz, 1H, NH), 7.28-7.53 (m, 8H, Ar-H), 7.76 (d, *J* = 7.9 Hz, 2H, Ar-H); ¹³C-NMR (100 MHz, CDCl₃) δ 21.6, 21.7, 54.6, 71.1, 73.4, 126.9, 127.0, 127.9, 128.7, 131.7, 134.3, 138.8, 166.7, 172.5.

Diol **149**: *R_f* 0.35 (9:1 CH₂Cl₂-MeOH). ¹H-NMR (400 MHz, CDCl₃) δ 1.21 (d, *J* = 6.2 Hz, 3H, ^{*i*}PrCH₃), 1.26 (d, *J* = 6.2 Hz, 3H, ^{*i*}PrCH₃), 2.86 (br s, 1H, OH), 3.20 (br s, 1H, OH), 4.31 (app. s, 1H, CH-OH), 4.95 (app. s, 1H, CH-OH), 5.12 (sept., *J* = 6.2 Hz, 1H, ^{*i*}PrCH), 7.30-7.39 (m, 5H, Ar-H); ¹³C-NMR (100 MHz, CDCl₃) δ 21.6, 21.7, 70.2, 74.7, 74.7, 126.3, 128.0, 128.4, 140.0, 172.3.

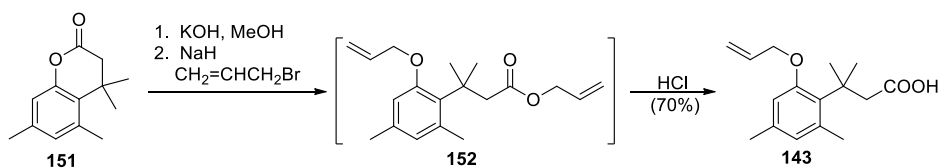
(2*R*,3*S*)-Isopropyl 3-hydroxy-2-benzamido-3-phenylpropionate (**146**): *R_f* 0.30 (9:1 CH₂Cl₂-MeOH). Lit.¹⁸ [α]_D¹⁶ 28.02 (c 0.760, CHCl₃). ¹H-NMR (400 MHz, CDCl₃) δ 1.18 (d, *J* = 6.3 Hz, 3H, ^{*i*}PrCH₃), 1.27 (d, *J* = 6.3 Hz, 3H, ^{*i*}PrCH₃), 2.97 (d, *J* = 3.8 Hz, 1H, OH), 5.02 (dd, *J* = 8.5, 3.7 Hz, 1H, CH-NH), 5.06 (sept., *J* = 6.3 Hz, 1H, ^{*i*}PrCH), 5.32 (t, *J* = 3.7 Hz, 1H, CH-OH), 6.87 (d, *J* = 8.1 Hz, 1H, NH), 7.29 (d, *J* = 7.1 Hz, 1H, Ar-H), 7.34 (t, *J* = 7.3 Hz, 2H, Ar-H), 7.40-7.44 (m, 2H, Ar-H), 7.49-7.52 (m,

2H, Ar-H), 7.71 (d, $J = 8.4$ Hz, 2H, Ar-H); $^{13}\text{C-NMR}$ (100 MHz, CDCl_3) δ 21.6, 21.8, 58.7, 69.8, 74.4, 126.0, 127.1, 128.3, 128.5, 128.6, 131.8, 133.8, 139.6, 167.7, 169.9.



Scheme 4.24: Synthesis of compound **151**

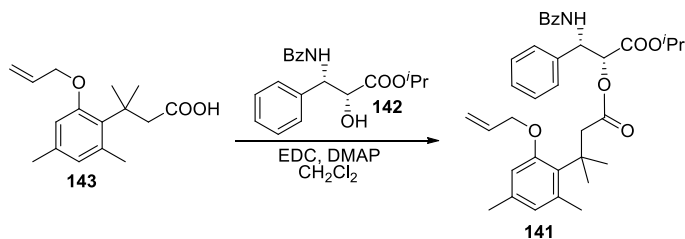
4,4,5,7-Tetramethylchroman-2-one (**151**).²¹ Methyl-3,3-dimethylacrylate (289 mg, 313 μL , 2.25 mmol, 1.1 equiv.) was added to a solution of 3,5-dimethylphenol (**150**) (250 mg, 2.05 mmol, 1.0 equiv.) in methanesulfonic acid (0.25 mL). The reaction was heated to 70 °C and stirred for 14 h. The mixture was diluted with water (35 mL) and extracted with CH_2Cl_2 (3 x 10 mL). The combined organic layers were washed with sat'd. aq. NaHCO_3 (2 x 5 mL), brine (2.5 mL), then dried over MgSO_4 , filtered and concentrated. The dark orange oil was purified by flash chromatography on silica gel, eluting with 30% CH_2Cl_2 in hexanes to give 4,4,5,7-tetramethylchroman-2-one (**151**) as a light brown solid (380 mg, 91%). R_f 0.21 (5:1 hexanes-EtOAc). $^1\text{H-NMR}$ (400 MHz, CDCl_3) δ 1.43 (s, 6H, CMe_2), 2.27 (s, 3H, Ar- CH_3), 2.46 (s, 3H, Ar- CH_3), 2.58 (s, 2H, CH_2), 6.73 (s, 1H, Ar-H), 6.74 (s, 1H, Ar-H); $^{13}\text{C-NMR}$ (100 MHz, CDCl_3) δ 20.6, 23.1, 27.8, 35.0, 45.7, 116.1, 126.6, 129.5, 136.1, 137.6, 151.1, 168.5.



Scheme 4.25: Synthesis of compound **143**

Allyl aryl ether **143**.³² 4,4,5,7-Tetramethylchroman-2-one (**151**) (500 mg, 2.45 mmol, 1.00 equiv.) was added to a solution of KOH (143 mg, 2.55 mmol, 1.04 equiv.) in MeOH (4 mL), and

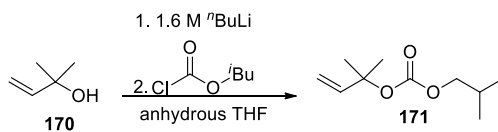
left to stir at rt for 3 h under N₂. The mixture was concentrated and redissolved in anhydrous CH₃CN (15 mL) and cooled to 0 °C. Sodium hydride (141 mg, 5.87 mmol, 60% dispersion in mineral oil, 2.4 equiv.) was added in one portion, and the mixture stirred for 10 min at 0 °C before allyl bromide (508 μL, 711 mg, 5.87 mmol, 2.4 equiv.) was added dropwise. The reaction was warmed to rt and stirred overnight. The solution was cooled to 0 °C, and H₂O (2.5 mL) was added dropwise. The solution was warmed to rt and allowed to stir for 5 h, and then acidified with 2 M HCl to pH 3. Acetonitrile was removed under reduced pressure, and the aqueous layer extracted with CH₂Cl₂ (3 x 3 mL). The combined organic extracts were washed with H₂O (3 mL), dried over MgSO₄, filtered, and concentrated. The residue was purified by flash chromatography on silica gel eluting with 7:1 hexanes:EtOAc to yield the allyl aryl ether **143** as a colorless oil (591 mg, 85%). *R_f* 0.21 (5:1 hexanes-EtOAc). ¹H-NMR (400 MHz, CDCl₃) δ 1.61 (s, 6H, CMe₂), 2.22 (s, 3H, Ar-CH₃), 2.50 (s, 3H, Ar-CH₃), 3.03 (s, 2H, CH₂COOH), 4.52 (d, *J* = 5.2 Hz, 2H, CH₂OPh), 5.26 (d, *J* = 10.5 Hz, 1H, allyl-H_c), 5.39 (d, *J* = 17.3 Hz, 1H, allyl-H_b), 6.10 (ddt, *J* = 17.3, 10.5, 5.2 Hz, 1H, allyl-H_a), 6.53 (s, 1H, Ar-H), 6.56 (s, 1H, Ar-H); ¹³C-NMR (100 MHz, CDCl₃) δ 20.8, 25.6, 31.6, 39.6, 46.8, 69.6, 85.9, 112.4, 117.4, 127.5, 130.0, 133.6, 136.1, 137.6, 157.9, 176.7; HRMS (ESI+) calcd for C₁₆H₂₂O₃Na (M+Na)⁺ 285.1461, obsd 285.1458.



Scheme 4.26: Synthesis of compound **141**

Compound **141**. Acid **143** (19.2 mg, 0.07 mmol, 1.20 equiv.) was added to a solution of amido alcohol **142** (20.0 mg, 0.06 mmol, 1.00 equiv.) in anhydrous CH₂Cl₂ (1 mL) under N₂. 4-

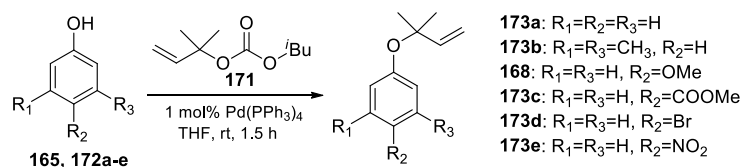
Dimethylaminopyridine (10.4 mg, 0.09 mmol, 1.40 equiv.) and EDC (16.4 mg, 0.09 mmol, 1.40 equiv.) were added sequentially, and the reaction was allowed to stir at rt overnight. The solution was concentrated and the product isolated by flash chromatography on silica gel, eluting with 3:1 hexanes:EtOAc to give the ester **141** as a colorless oil (25 mg, 86%). R_f 0.34 (3:1 Hexanes-EtOAc). $^1\text{H-NMR}$ (400 MHz, CDCl_3) δ 1.16 (d, $J = 6.2$ Hz, 3H, $^i\text{PrCH}_3$), 1.23 (d, $J = 6.2$ Hz, 3H, $^i\text{PrCH}_3$), 1.49 (s, 3H, CH_3), 1.60 (d, 3H, CH_3), 2.03 (s, 3H, $\text{CH}_3\text{-Ar}$), 2.46 (s, 3H, $\text{CH}_3\text{-Ar}$), 2.82 (d, $J = 15.1$ Hz, 1H, CH_2COOR), 3.43 (d, $J = 15.1$ Hz, 1H, CH_2COOR), 4.30 (dd, $J = 12.2, 4.1$ Hz, 1H, CH_2OPh), 4.36 (dd, $J = 12.2, 4.1$ Hz, 1H, CH_2OPh), 5.04 (sept., $J = 6.0$ Hz, 1H, $^i\text{PrCH}$), 5.20 (d, $J = 10.5$ Hz, 1H, allyl- H_c), 5.30-5.33 (m, 2H, CHCOO^iPr , allyl- H_b), 5.71 (d, $J = 9.2$ Hz, 1H, CH-NH), 5.98 (ddt, $J = 17.3, 12.2, 4.1$ Hz, 1H, allyl- H_a), 6.26 (s, 1H, Ar-H), 6.43 (d, $J = 9.2$ Hz, 1H, NH), 6.46 (s, 1H, Ar-H), 7.08 (d, $J = 6.4$ Hz, 2H, Ar-H), 7.26-7.30 (m, 3H, Ar-H), 7.49 (t, $J = 7.2$ Hz, 2H, Ar-H), 7.57 (t, $J = 7.2$ Hz, 1H, Ar-H), 7.71 (d, $J = 7.2$ Hz, 2H, Ar-H); $^{13}\text{C-NMR}$ (100 MHz, CDCl_3) δ 20.6, 21.5, 21.7, 25.6, 31.3, 39.7, 47.4, 53.3, 69.3, 70.0, 74.2, 112.4, 117.4, 126.5, 127.3, 127.55, 127.62, 128.4, 128.6, 130.3, 131.7, 133.5, 134.6, 135.9, 137.2, 137.5, 157.8, 167.5, 167.6, 172.1.



Scheme 4.27: Synthesis of compound **171**

Isobutyl prenyl carbonate (**171**).³³ A solution of 1.6 M $^n\text{BuLi}$ in hexanes (8.0 mL, 5.42 g, 84.6 mmol, 7.3 equiv.) was added dropwise to a clear solution of 1,1-dimethyl prop-2-en-1-ol (**170**) (1.2 mL, 1.00 g, 11.6 mmol, 1.0 equiv.) in dry THF (20 mL) under N_2 at 0 °C. After 30 min at 0 °C, isobutyl chloroformate (2.3 mL, 2.38 g, 17.4 mmol, 1.5 equiv.) was added dropwise to the clear yellow mixture. The reaction was allowed to gradually warm to rt and stirred for an additional 4

h. The cloudy solution was partitioned between brine (20 mL) and ether (20 mL). The layers were separated and the aqueous layer extracted further with ether (3 x 10 mL). The combined organic layers were dried over MgSO_4 , filtered and concentrated. Traces of ether were removed under a stream of nitrogen to give the isobutyl prenyl carbonate (**171**) as a volatile colorless liquid (2.16 g, 100%). No further purification was needed. R_f 0.21 (15:1 hexanes-EtOAc). $^1\text{H-NMR}$ (400 MHz, CDCl_3) δ 0.93 (d, $J = 1.0$ Hz, 3H, $^i\text{BuCH}_3$), 0.95 (d, $J = 1.0$ Hz, 3H, $^i\text{BuCH}_3$), 1.56 (s, 6H, CMe_2), 1.96 (septet, $J = 6.7$ Hz, 1H, $^i\text{BuCH}$), 3.85 (dd, $J = 6.7, 1.0$ Hz, 2H, $^i\text{BuCH}_2$), 5.13 (d, $J = 10.9$ Hz, 1H, $\text{HC}=\text{CH}_2$ -cis), 5.22 (d, $J = 17.5$ Hz, 1H, $\text{HC}=\text{CH}_2$ -trans), 6.11 (ddd, $J = 17.5, 10.9, 0.9$ Hz, 1H, $\text{HC}=\text{CH}_2$); $^{13}\text{C-NMR}$ (100 MHz, CDCl_3) δ 19.0, 26.2, 27.8, 73.3, 82.0, 113.5, 141.8, 153.6; MS (EI, 70 eV) calcd for $\text{C}_{10}\text{H}_{18}\text{O}_3$ (M) $^+$ 187.1, obsd 187.2.



Scheme 4.28: Synthesis of aryl prenyl ether derivatives

Aryl Prenyl Ether **173b**: $\text{Pd}(\text{PPh}_3)_4$ (18.4 mg, 0.02 mmol, 0.01 equiv.) was added to a solution of phenol **172b** (150 mg, 1.59 mmol, 1.0 equiv.) and isobutyl prenyl carbonate (534 mg, 2.87 mmol, 1.8 equiv.) in THF (10 mL) under N_2 at rt. The mixture was stirred at rt for 1.5 h and then partitioned between CH_2Cl_2 (10 mL) and brine (10 mL). The aqueous layer was further extracted with EtOAc (5 mL). The organic layers were combined, dried over MgSO_4 , filtered, and concentrated. The yellow liquid was purified on silica gel eluting with 50:1 hexanes:EtOAc, to give **173b** as a colorless liquid (210 mg, 90%). R_f 0.61 (5:1 hexanes-EtOAc). $^1\text{H-NMR}$ (400 MHz, CDCl_3) δ 1.43 (s, 6H, CMe_2), 2.24 (s, 6H, Ar- CH_3), 5.11 (d, $J = 10.9$ Hz, 1H, $=\text{CH}_2$ -cis), 5.16 (d, $J =$

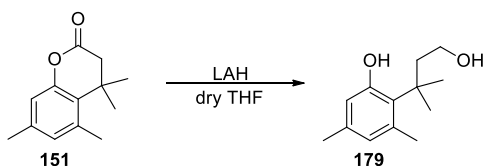
17.6 Hz, 1H, =CH₂-trans) 6.13 (dd, *J* = 17.6, 10.9 Hz, 1H, HC=), 6.61 (s, 2H, Ar-H), 6.63 (s, 1H, Ar-H); ¹³C-NMR (100 MHz, CDCl₃) δ 19.0, 21.4, 27.1, 79.1, 113.1, 119.4, 124.0, 138.4, 144.7, 156.0; MS (EI, 70 eV) calcd for C₁₃H₁₈O (M)⁺ 190.1, obsd 190.0.

173a: prepared by analogy to **173b** on a scale of 1.59 mmol to give an extremely volatile colorless liquid (195 mg, 95%). *R_f* 0.59 (5:1 Hexanes-EtOAc). ¹H-NMR (400 MHz, CDCl₃) δ 1.43 (s, 6H, ^{*i*}PrCH₃), 5.09-5.17 (m, 2H, =CH₂), 6.13 (dd, *J* = 17.6, 10.8 Hz, 1H, HC=), 6.95-6.99 (m, 3H, Ar-H), 7.19 (d, *J* = 7.1 Hz, 1H, Ar-H), 7.21 (d, *J* = 7.1 Hz, 1H, Ar-H); ¹³C-NMR (100 MHz, CDCl₃) δ 27.1, 79.4, 113.4, 121.8, 122.3, 128.8, 144.5, 156.0.

168: prepared by analogy to **173b** on a scale of 1.21 mmol to give a colorless liquid (223 mg, 96%). *R_f* 0.51 (5:1 Hexanes-EtOAc). ¹H-NMR (400 MHz, CDCl₃) δ 1.39 (s, 6H, ^{*i*}PrCH₃), 3.75 (s, 3H, OMe), 5.09 (d, *J* = 10.8 Hz, 1H, =CH₂), 5.12 (d, *J* = 17.6 Hz, 1H, =CH₂) 6.10 (dd, *J* = 17.6, 10.8 Hz, 1H, HC=), 6.75 (d, *J* = 9.1 Hz, 2H, Ar-H), 6.91 (d, *J* = 9.1 Hz, 2H, Ar-H); ¹³C-NMR (100 MHz, CDCl₃) δ 26.7, 55.5, 79.3, 113.7, 123.9, 144.3, 149.1, 155.3; HRMS (ESI⁺) calcd for C₁₂H₁₇O₂ (M+H)⁺ 193.1223, obsd 193.1213.

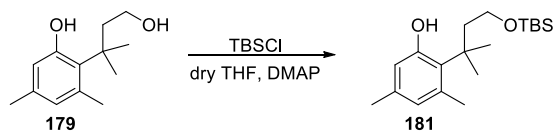
173c: prepared by analogy to **173b** on a scale of 1.05 mmol to give colorless oil (195 mg, 84%). *R_f* 0.42 (10:1 Hexanes-EtOAc). ¹H-NMR (400 MHz, CDCl₃) δ 1.50 (s, 6H, CH₃×2), 3.87 (s, 3H, OMe), 5.18 (d, *J* = 10.9 Hz, 1H, HC=CH₂), 5.22 (d, *J* = 17.6 Hz, 1H, HC=CH₂), 6.13 (dd, *J* = 17.6, 10.9 Hz, 1H, CH=CH₂), 7.00 (d, *J* = 8.9 Hz, 2H, Ar-H), 7.90 (d, *J* = 8.9 Hz, 2H, Ar-H); ¹³C-NMR (100 MHz, CDCl₃) δ 27.2, 51.8, 80.2, 114.0, 119.5, 123.0, 130.9, 143.8, 160.6, 166.9; HRMS (ESI⁺) calcd for C₁₃H₁₇O₃ (M+H)⁺ 221.1172, obsd 221.117.

173d: prepared by analogy to **173b** on a scale of 1.45 mmol to colorless liquid (314 mg, 90%). R_f 0.36 (10:1 Hexanes- CH_2Cl_2). $^1\text{H-NMR}$ (400 MHz, CDCl_3) δ 1.43 (s, 6H, $\text{CH}_3 \times 2$), 5.12-5.17 (m, 2H, $=\text{CH}_2$), 6.09 (dd, $J = 17.6, 10.9$ Hz, 1H, $\text{CH}=\text{CH}_2$), 6.86 (d, $J = 8.9$ Hz, 2H, Ar-H), 7.31 (d, $J = 8.9$ Hz, 2H, Ar-H); $^{13}\text{C-NMR}$ (100 MHz, CDCl_3) δ 26.9, 79.9, 113.9, 114.8, 123.4, 131.7, 143.9, 155.1.



Scheme 4.29: Synthesis of compound **179**

Diol **179**. Lithium aluminum hydride (52.0 mg, 1.36 mmol, 1.5 equiv.) was added in a single portion to a solution of 4,4,5,7-tetramethylchroman-2-one (**151**) (185 mg, 0.91 mmol, 1.0 equiv.) in anhydrous THF (4 mL) under N_2 at 0 °C. The solution was allowed to warm to rt and stirred for 8 h. Saturated aq. NH_4Cl (1-2 mL) was added dropwise to quench excess LAH. The mixture was filtered, and the solid was washed with THF (3 x 5mL). The filtrate and combined washings was concentrated, and the oily yellow residue was purified by flash chromatography on silica gel eluting with 5:1 hexanes:EtOAc \longrightarrow 1:1 hexanes:EtOAc to give the diol **179** as a colorless solid (100 mg, 56%). R_f 0.21 (3:1 hexane-EtOAc). $^1\text{H-NMR}$ (400 MHz, CDCl_3) δ 1.53 (s, 6H, CMe_2), 1.89 (br s, 1H, OH), 2.15 (s, 3H, Ar- CH_3), 2.23 (t, $J = 7.2$ Hz, 2H, CH_2OH), 2.46 (s, 3H, Ar- CH_3), 3.61 (t, $J = 7.6$ Hz, 2H, CH_2CMe_2), 6.31 (s, 1H, Ar-H), 6.34 (s, 1H, Ar-OH), 6.46 (s, 1H, Ar-H); $^{13}\text{C-NMR}$ (100 MHz, CDCl_3) δ 20.3, 25.6, 31.9, 39.5, 44.9, 61.5, 116.3, 126.9, 128.6, 136.2, 137.8, 155.5.



Scheme 4.30: Synthesis of compound **180**

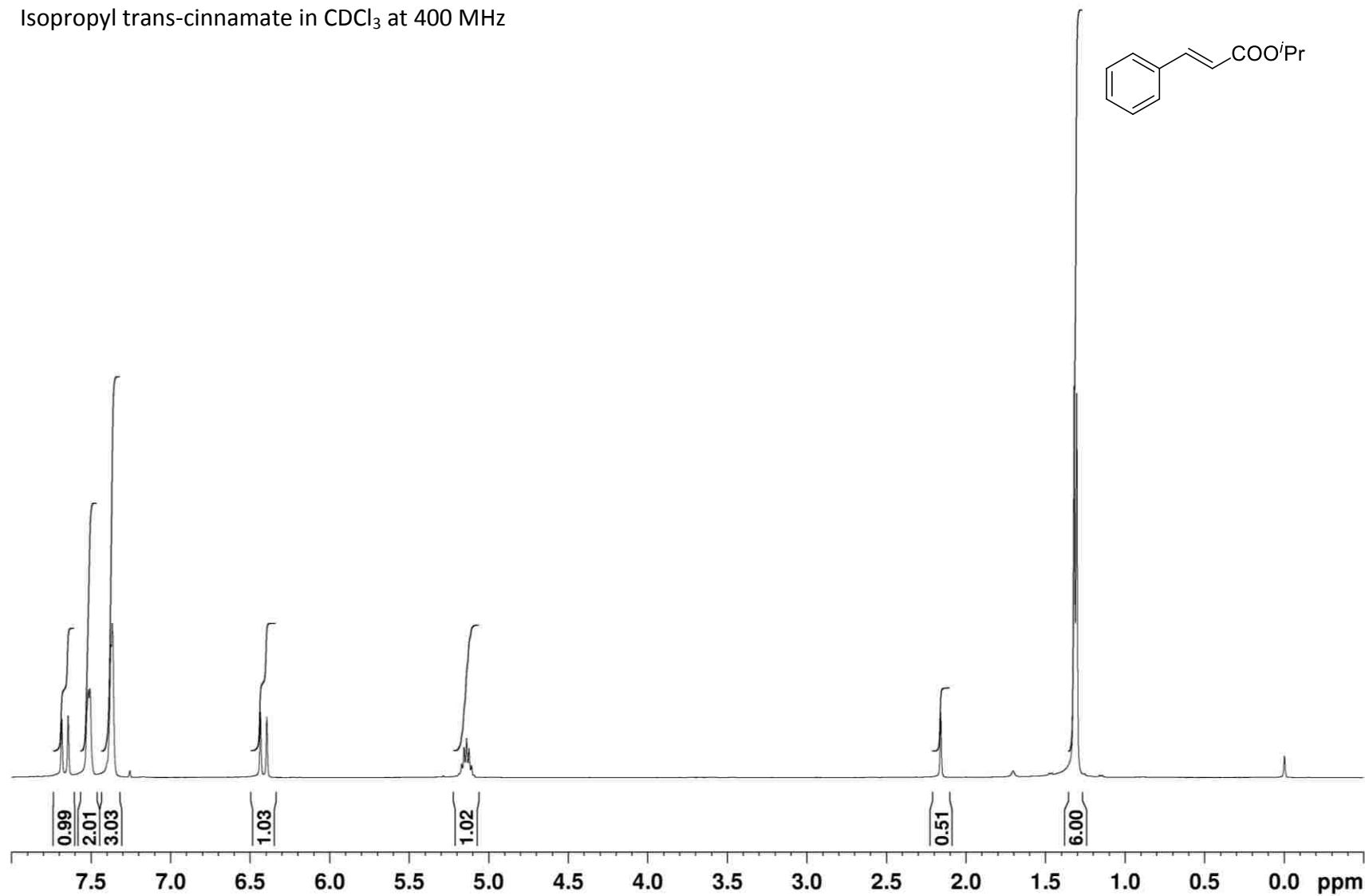
2-((4-tert-Butyldimethylsilyloxy)-2-methylbutan-2-yl)-3,5-dimethylphenol (**181**).

4-Dimethylaminopyridine (80.1 mg, 0.66 mmol, 1.57 equiv.) was added in one portion to a solution of diol **179** (87.0 mg, 0.42 mmol, 1.00 equiv.) in anhydrous THF (1 mL). *tert*-Butyldimethylsilyl chloride (71.0 mg, 0.47 mmol, 1.13 equiv) was added and the reaction was cooled to 0 °C and left to stir at this temp. overnight. Ethyl acetate (10 mL) was added and the mixture was washed with water (5 mL), brine (3 x 5 mL), dried over MgSO₄, filtered, and concentrated. The residue was purified by flash chromatography on silica gel, eluting with 5:1 hexanes:EtOAc to give the TBS ether **180** as a colorless solid (111 mg, 82%). *R_f* 0.31 (10:1 hexanes:EtOAc). ¹H-NMR (400 MHz, CDCl₃) δ 0.04 (s, 6H, Si(CH₃)₂), 0.89 (s, 9H, ^tBuSi), 1.56 (s, 6H, CMe₂), 2.15 (t, *J* = 7.1 Hz, 2H, CH₂CMe₂), 2.19 (s, 3H, Ar-CH₃), 2.47 (s, 3H, Ar-CH₃), 3.61 (t, *J* = 7.1 Hz, 2H, CH₂OTBS), 5.83 (s, 1H, Ar-OH), 6.41 (s, 1H, Ar-H), 6.49 (s, 1H, Ar-H); ¹³C-NMR (100 MHz, CDCl₃) δ -5.3, 18.3, 20.2, 25.5, 26.0, 32.1, 39.3, 45.0, 61.8, 116.8, 126.8, 129.2, 135.9, 137.7, 155.5.

4.9.2 ^1H and ^{13}C -NMR Spectra

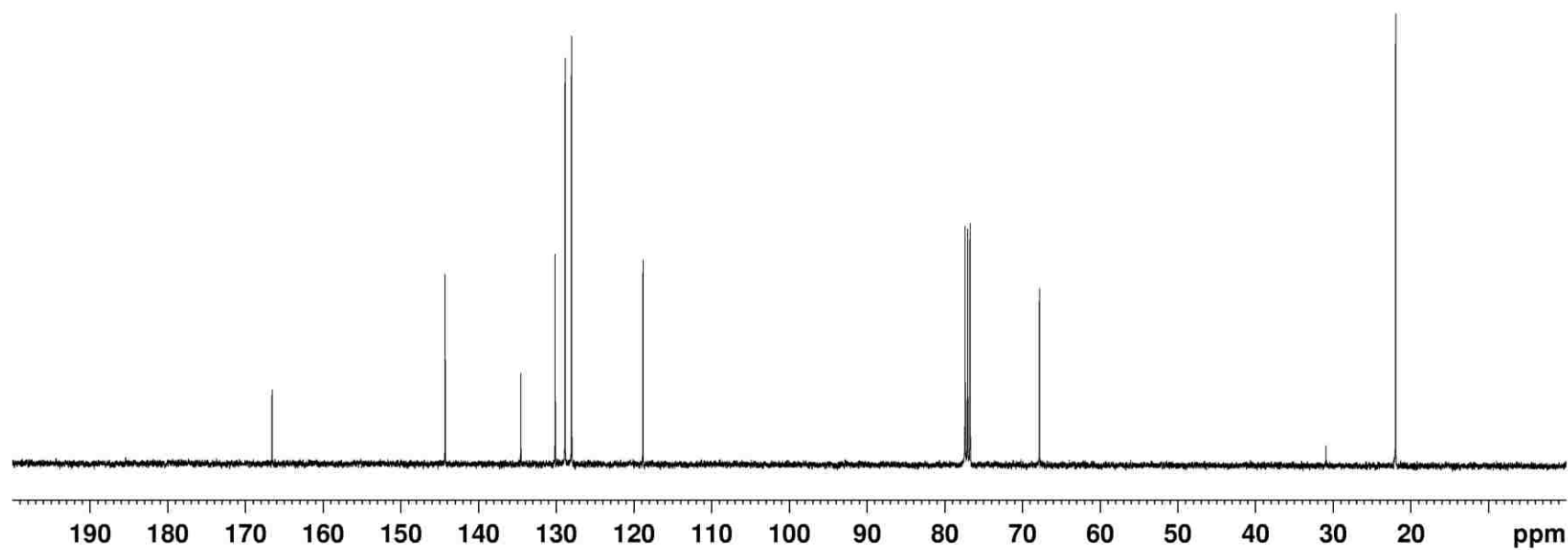
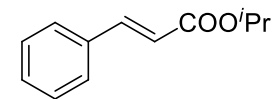
Compound **144** (Scheme 4.7) – ^1H NMR spectrum

Isopropyl trans-cinnamate in CDCl_3 at 400 MHz



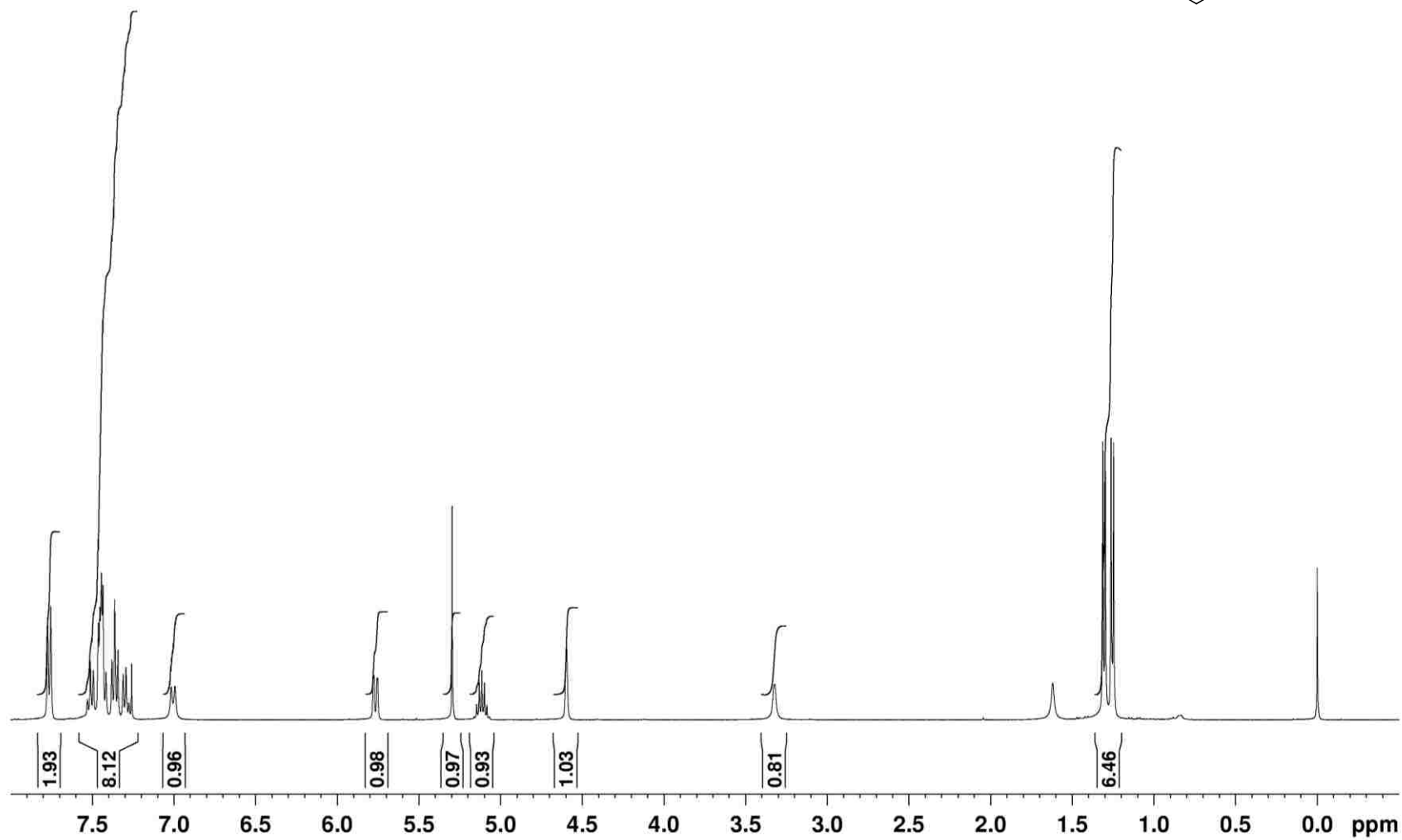
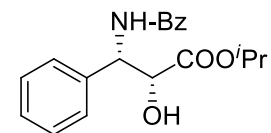
Compound **144** (Scheme 4.7) – ^{13}C NMR spectrum

Isopropyl trans-cinnamate in CDCl_3 at 100 MHz



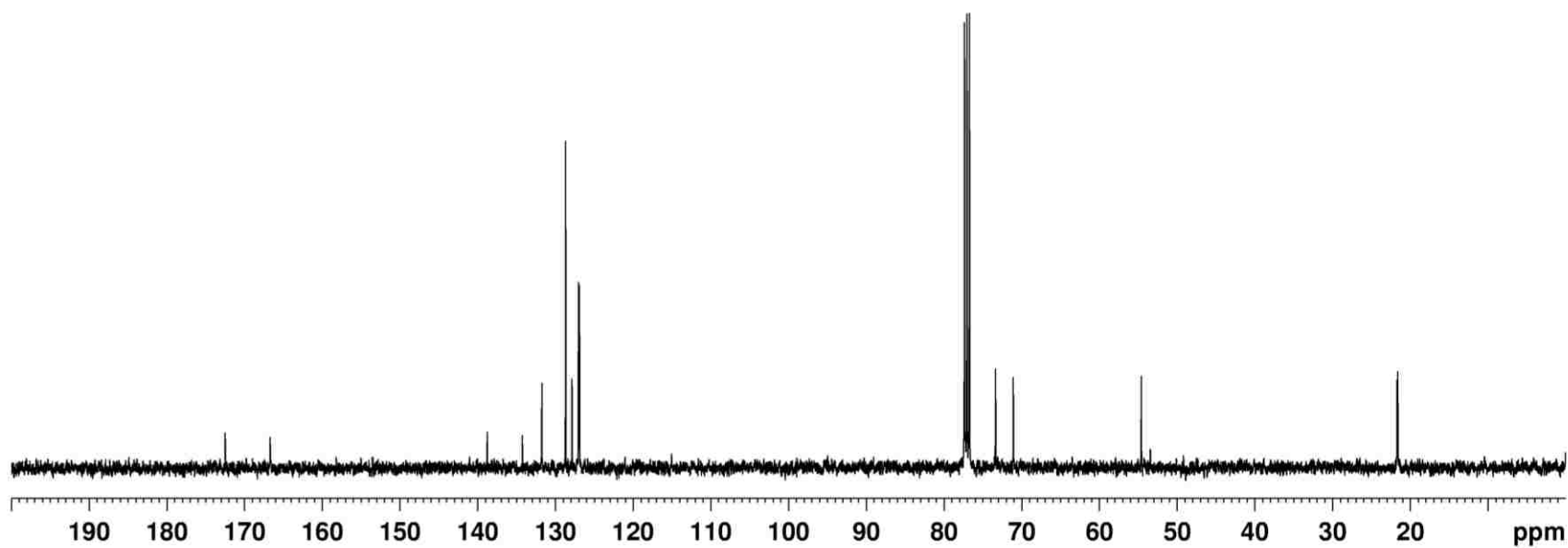
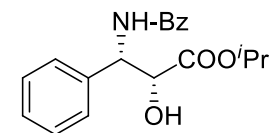
Compound **142** (Scheme 4.7) – ^1H NMR spectrum

Taxol amido alcohol sidechain (major) in CDCl_3 at 400 MHz



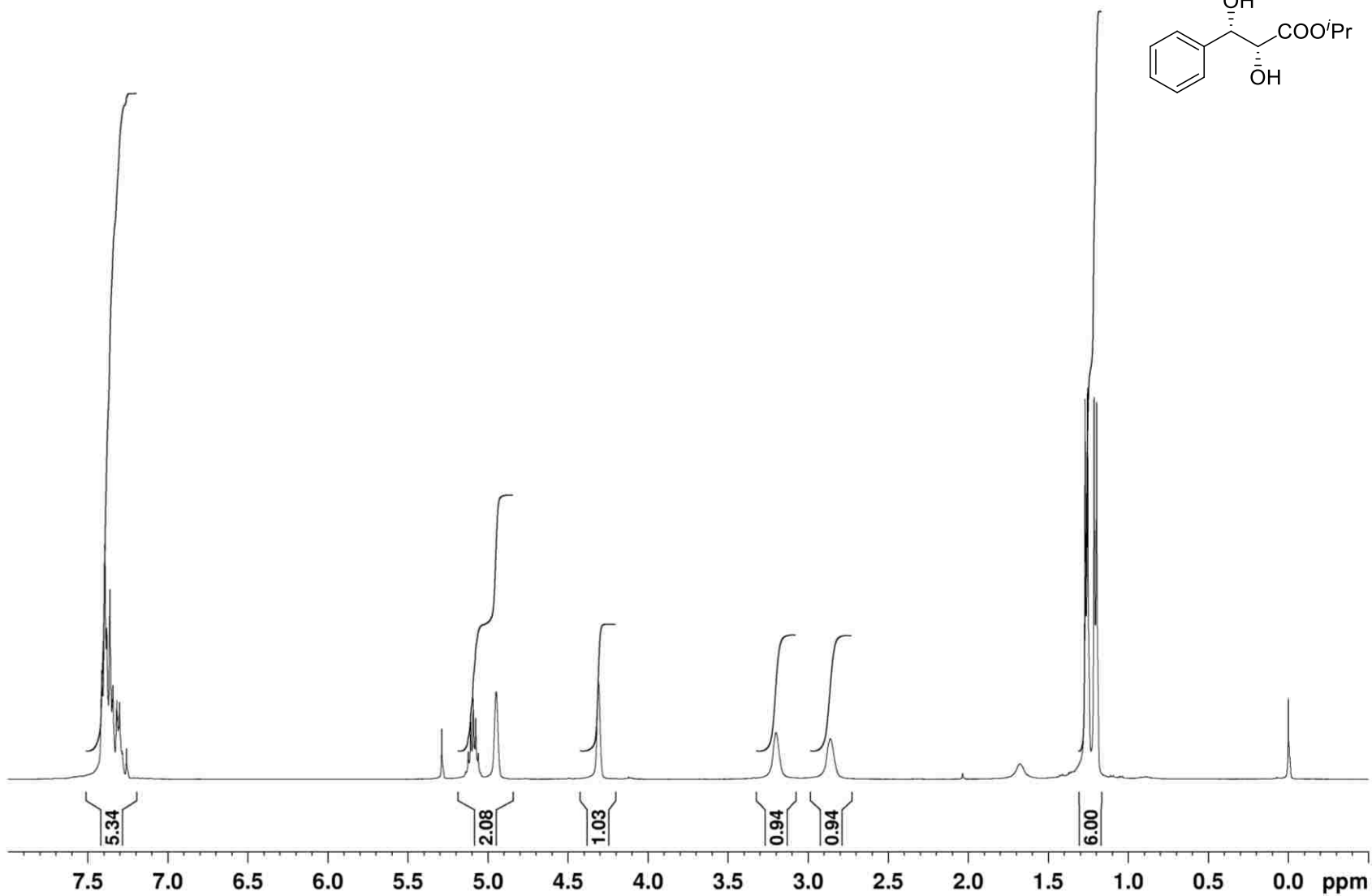
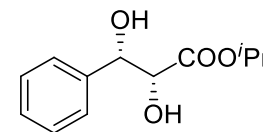
Compound **142** (Scheme 4.7) – ^{13}C NMR spectrum

Taxol amido alcohol sidechain (major) in CDCl_3 at 100 MHz



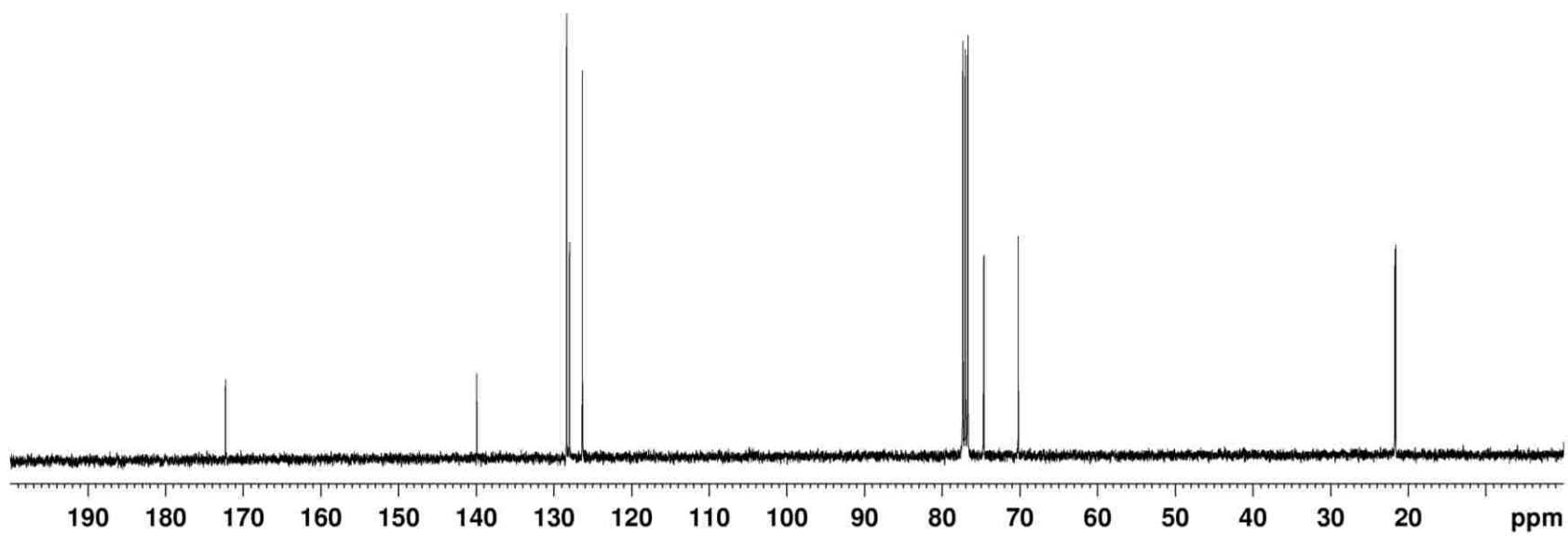
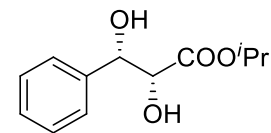
Compound **149** (Scheme 4.7) – ^1H NMR spectrum

Diol in CDCl_3 at 400 MHz



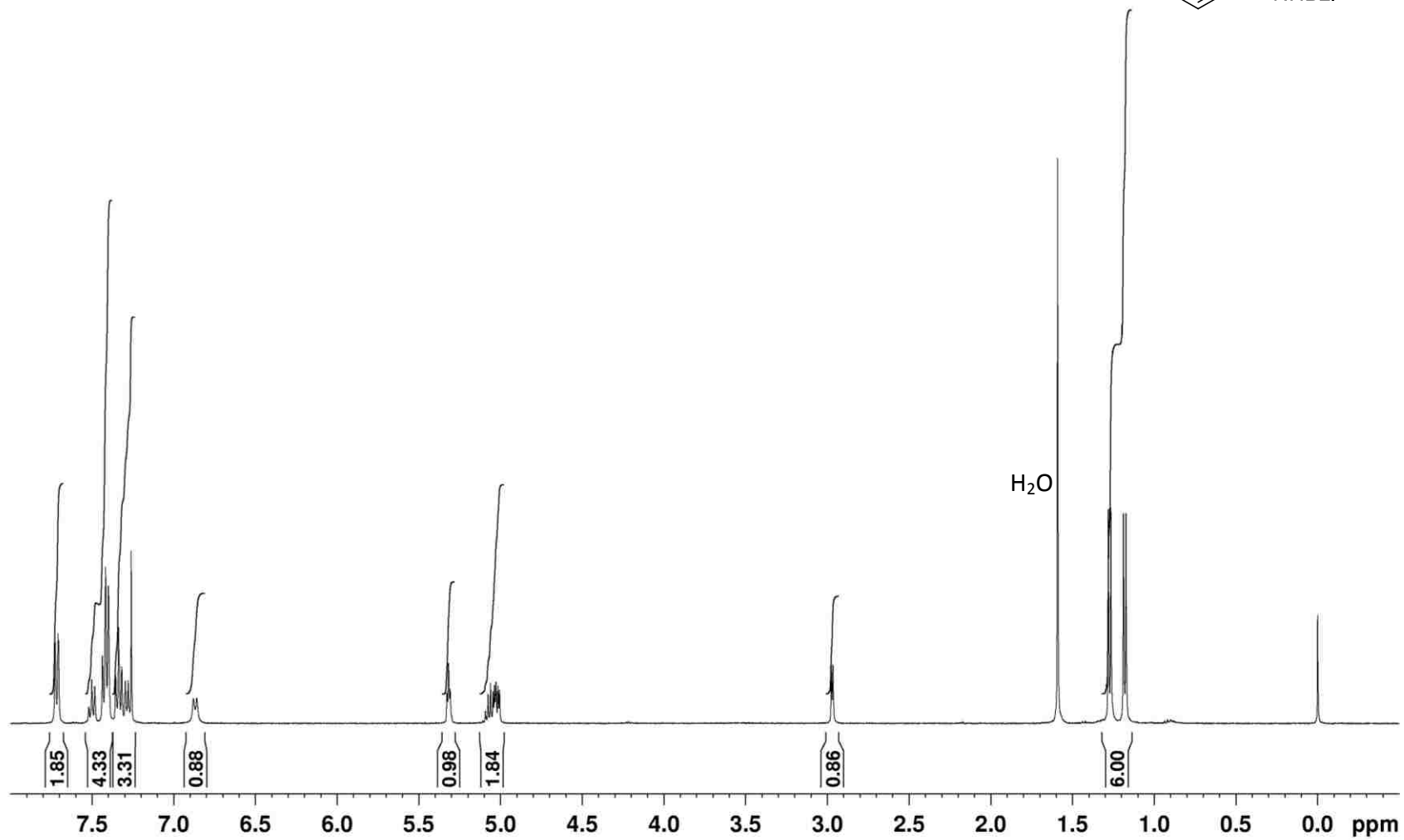
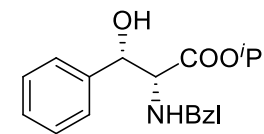
Compound **149** (Scheme 4.7) – ^{13}C NMR spectrum

Diol in CDCl_3 at 100 MHz



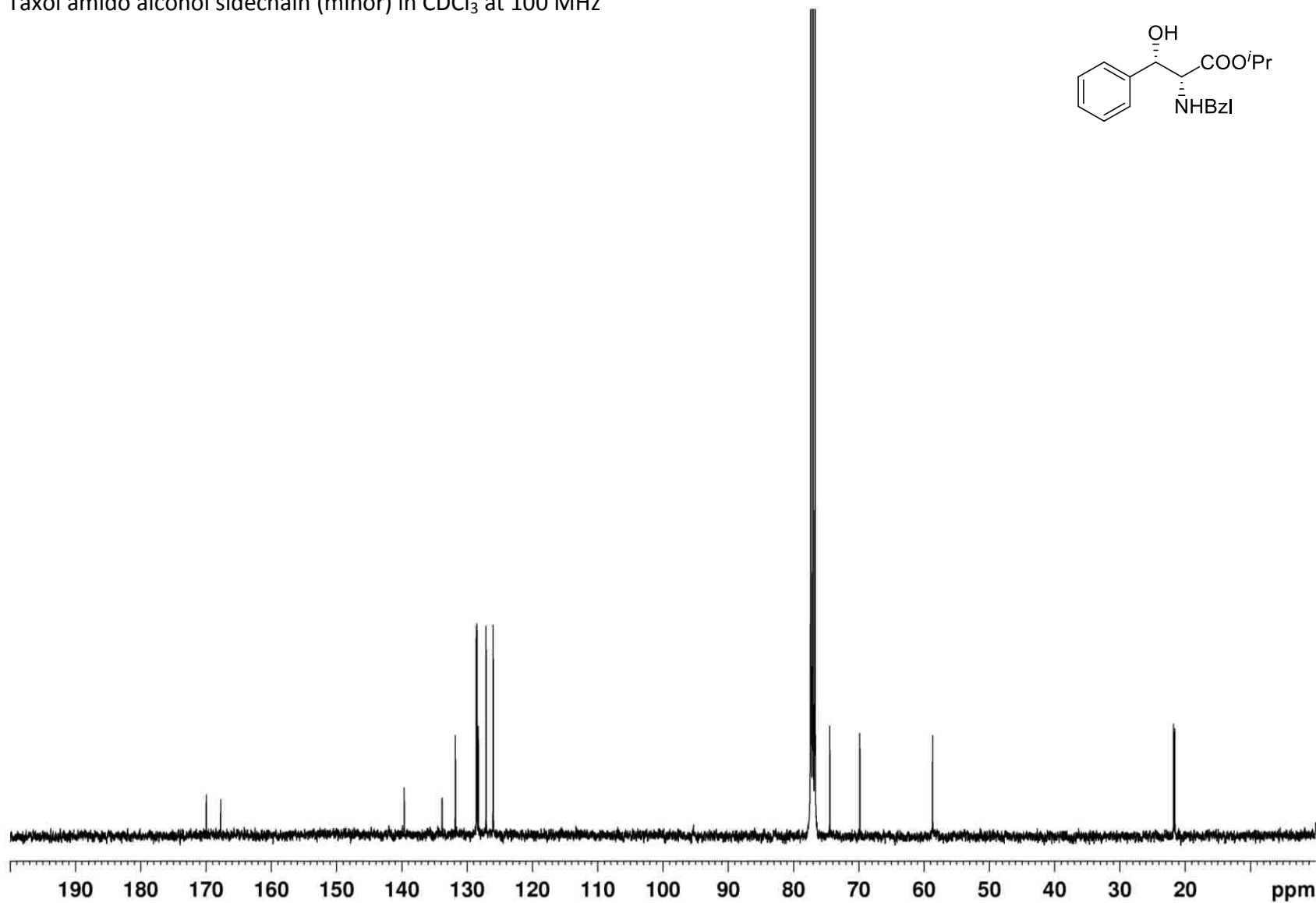
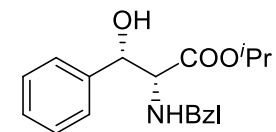
Compound **146** (Scheme 4.7) – ^1H NMR spectrum

Taxol amido alcohol sidechain (minor) in CDCl_3 at 400 MHz



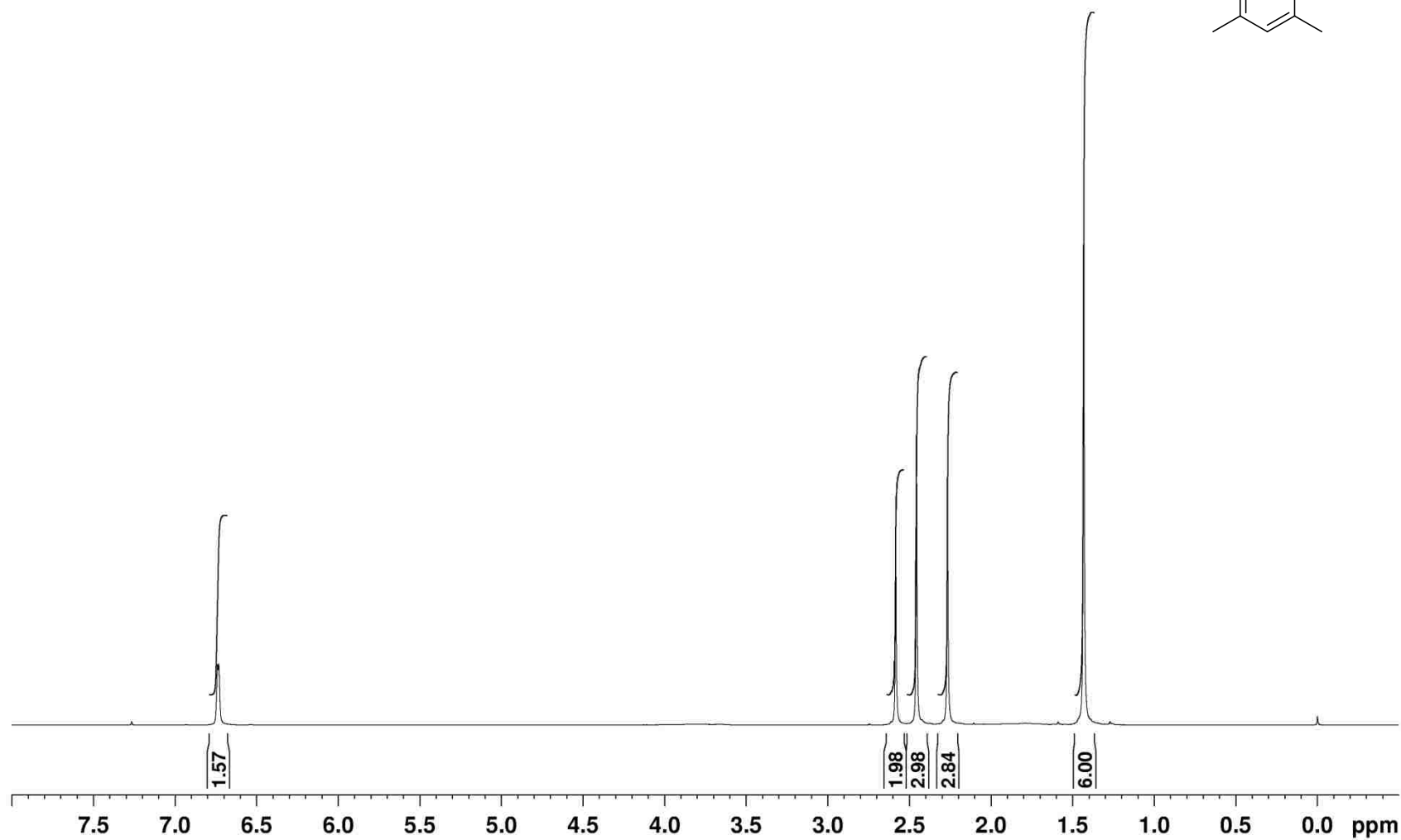
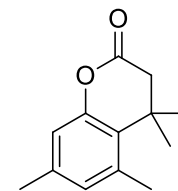
Compound **146** (Scheme 4.7) – ^{13}C NMR spectrum

Taxol amido alcohol sidechain (minor) in CDCl_3 at 100 MHz



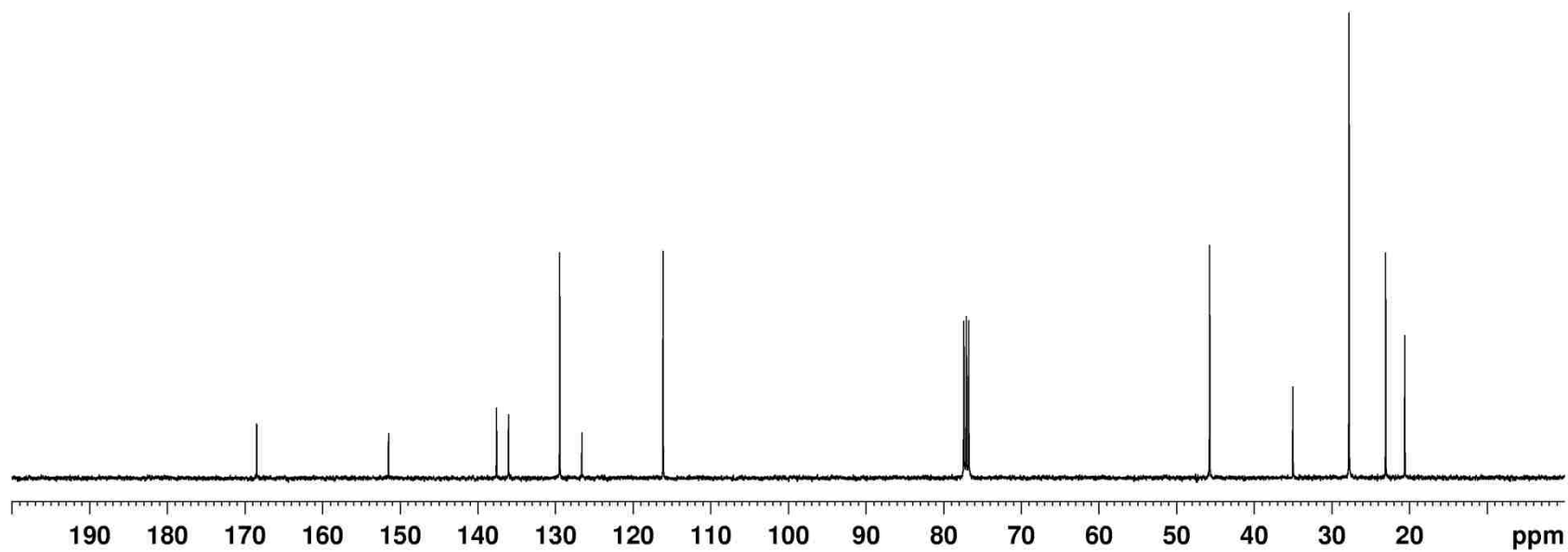
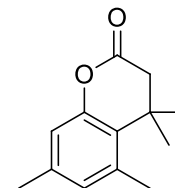
Compound **151** (Scheme 4.8) – ^1H NMR spectrum

4,4,5,7-tetramethylchroman-2-one in CDCl_3 at 400 MHz



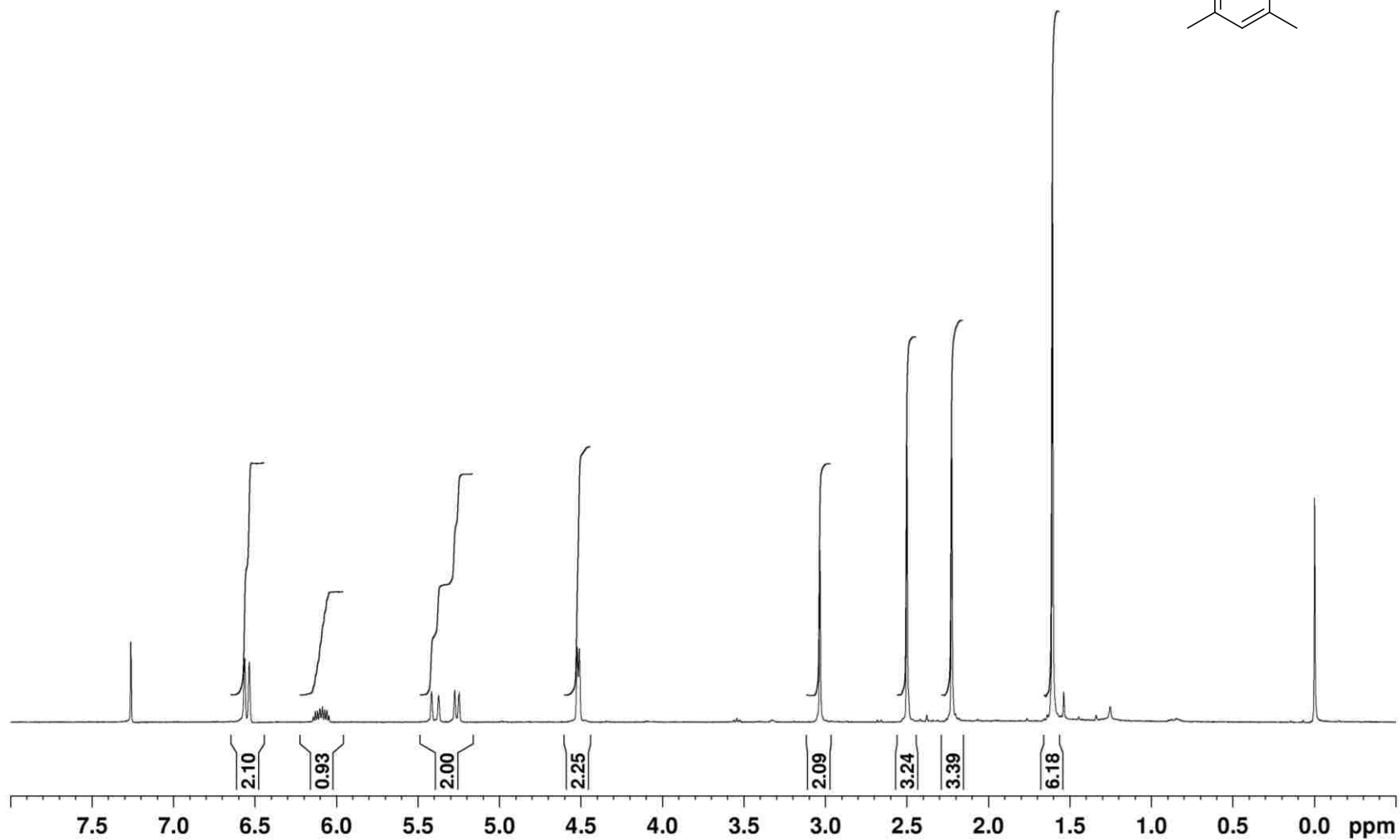
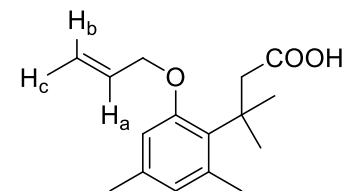
Compound **151** (Scheme 4.8) – ^{13}C NMR spectrum

4,4,5,7-tetramethylchroman-2-one in CDCl_3 at 100 MHz



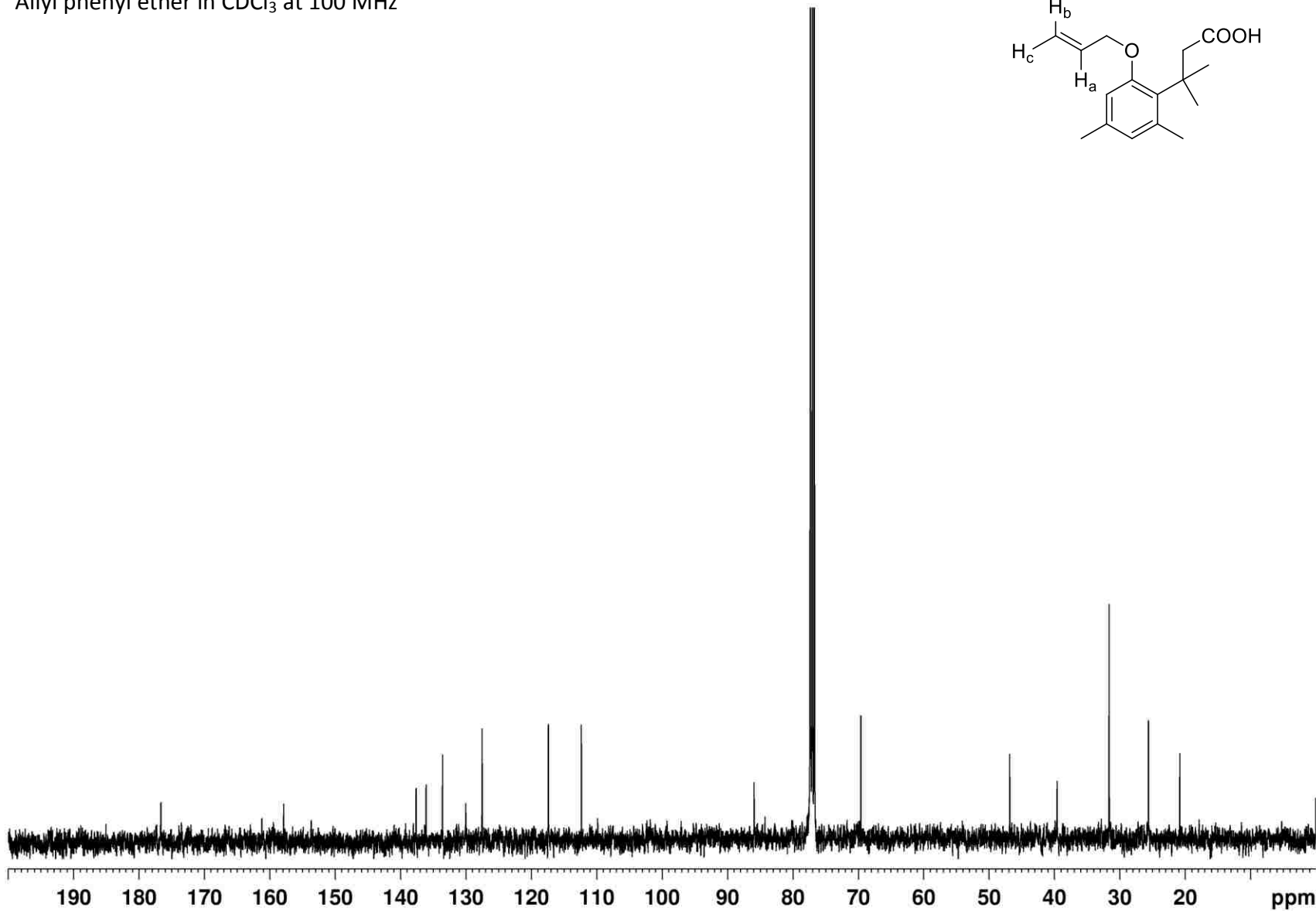
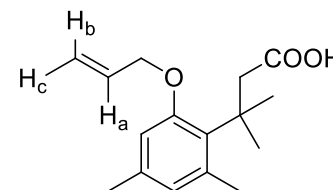
Compound **143** (Scheme 4.8) – ^1H NMR spectrum

Allyl phenyl ether in CDCl_3 at 400 MHz



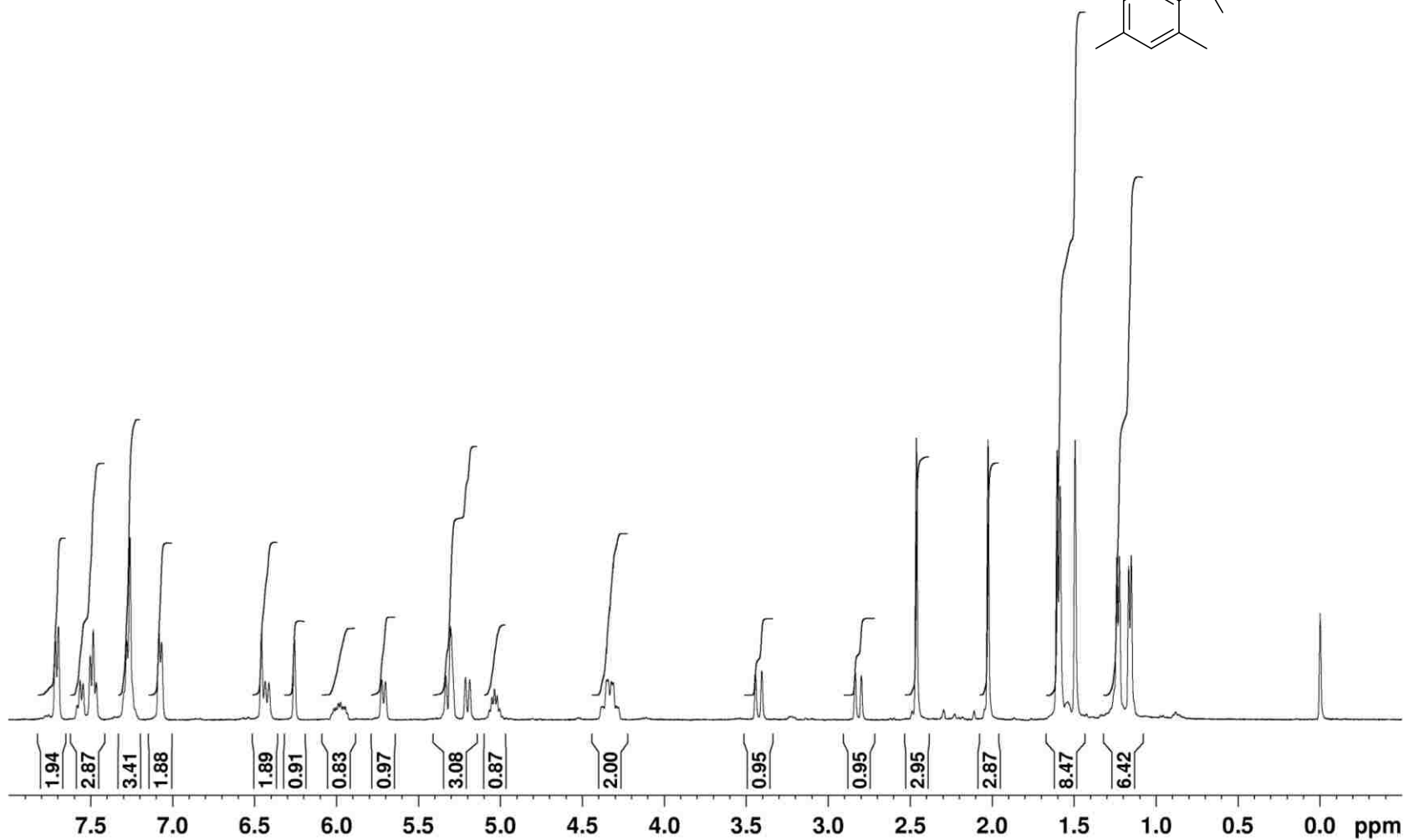
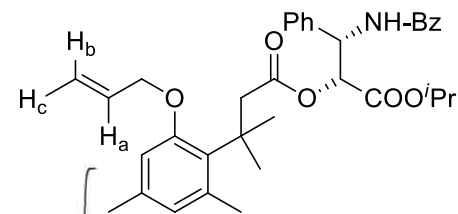
Compound **143** (Scheme 4.8) – ^{13}C NMR spectrum

Allyl phenyl ether in CDCl_3 at 100 MHz



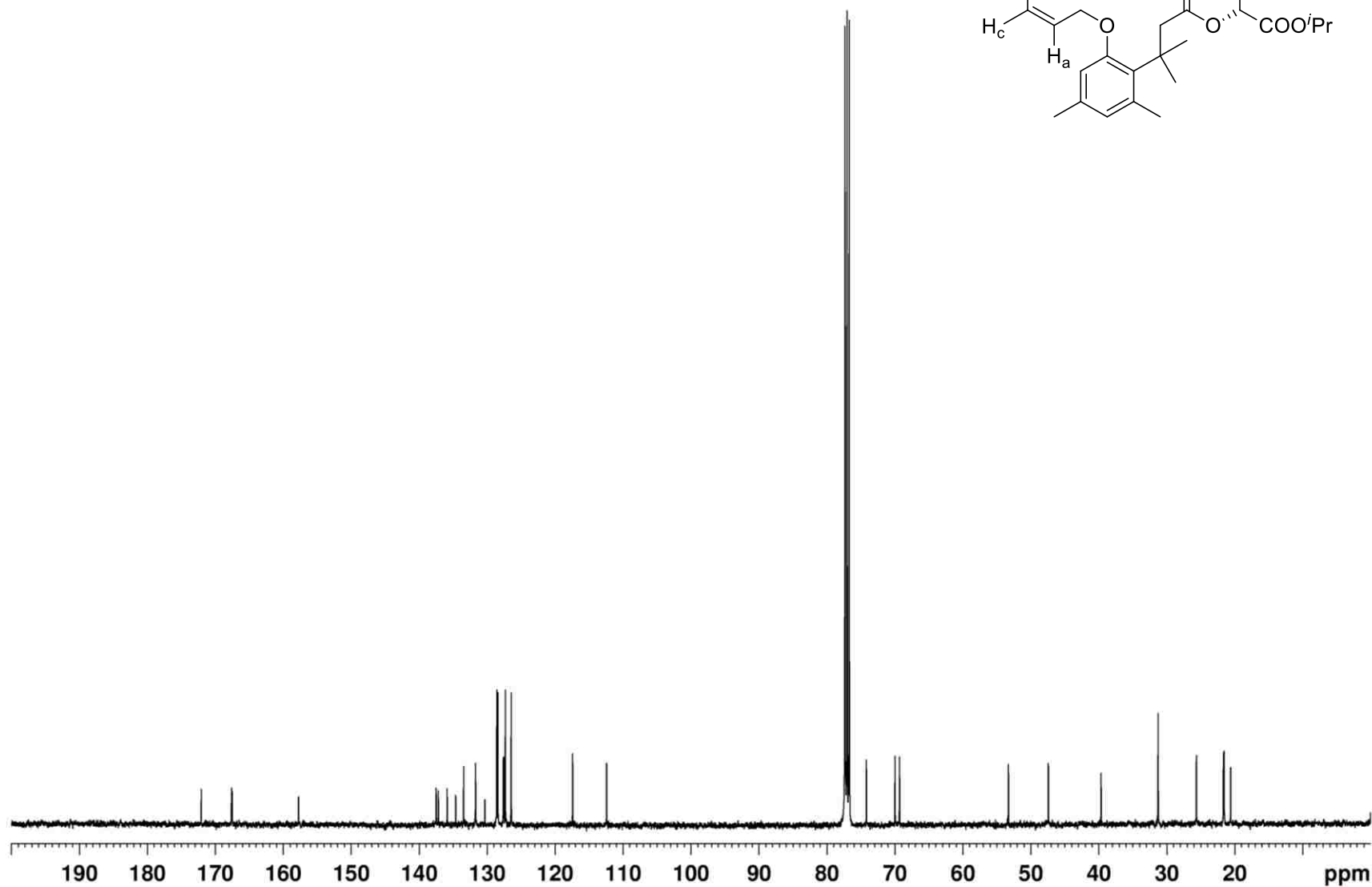
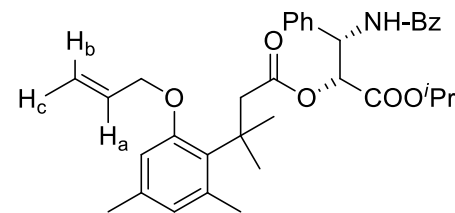
Compound **141** (Scheme 4.9) – ^1H NMR spectrum

Allyl Model System in CDCl_3 at 400 MHz



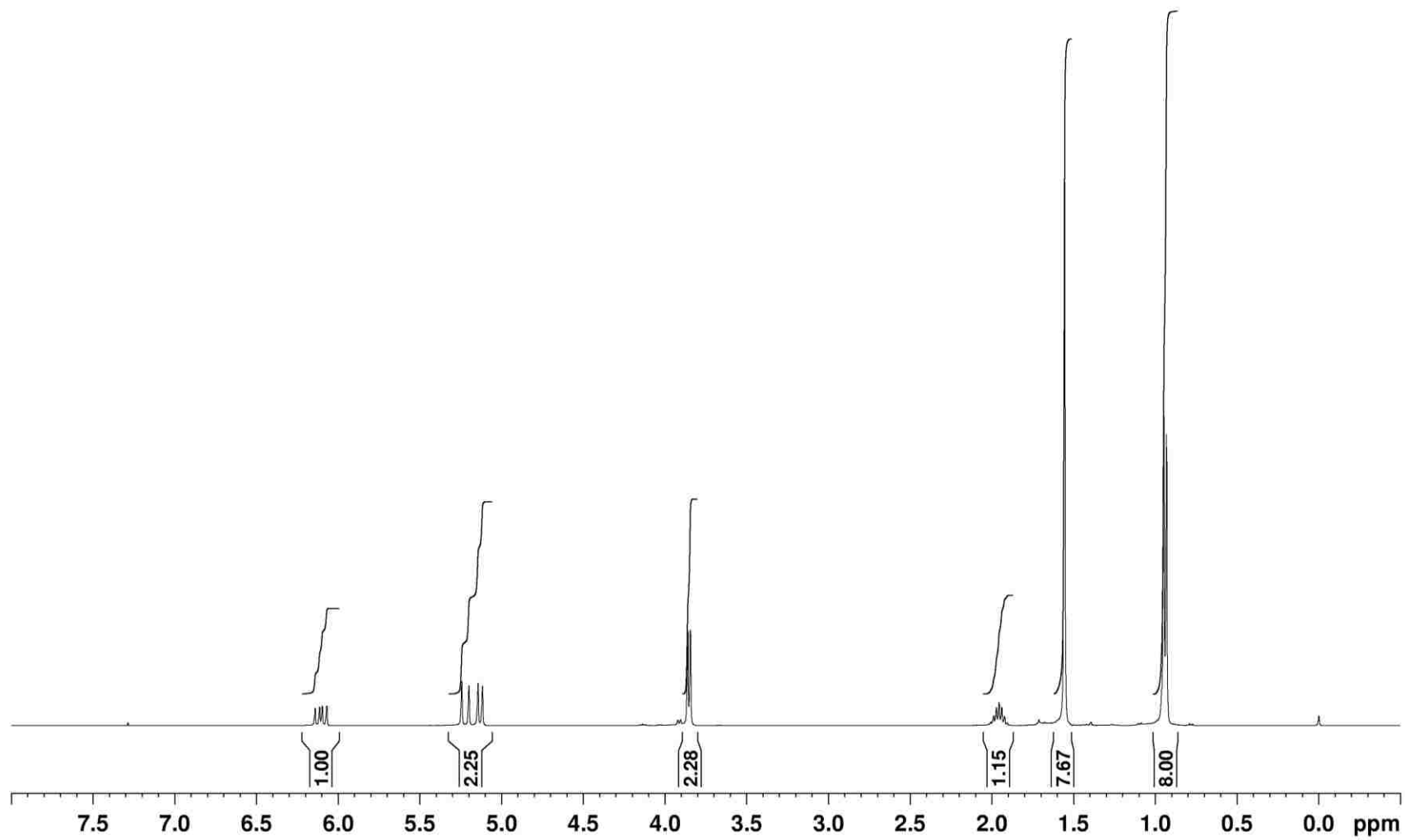
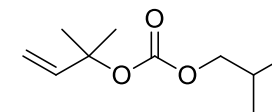
Compound **141** (Scheme 4.9) – ^{13}C NMR spectrum

Allyl Model System in CDCl_3 at 100 MHz



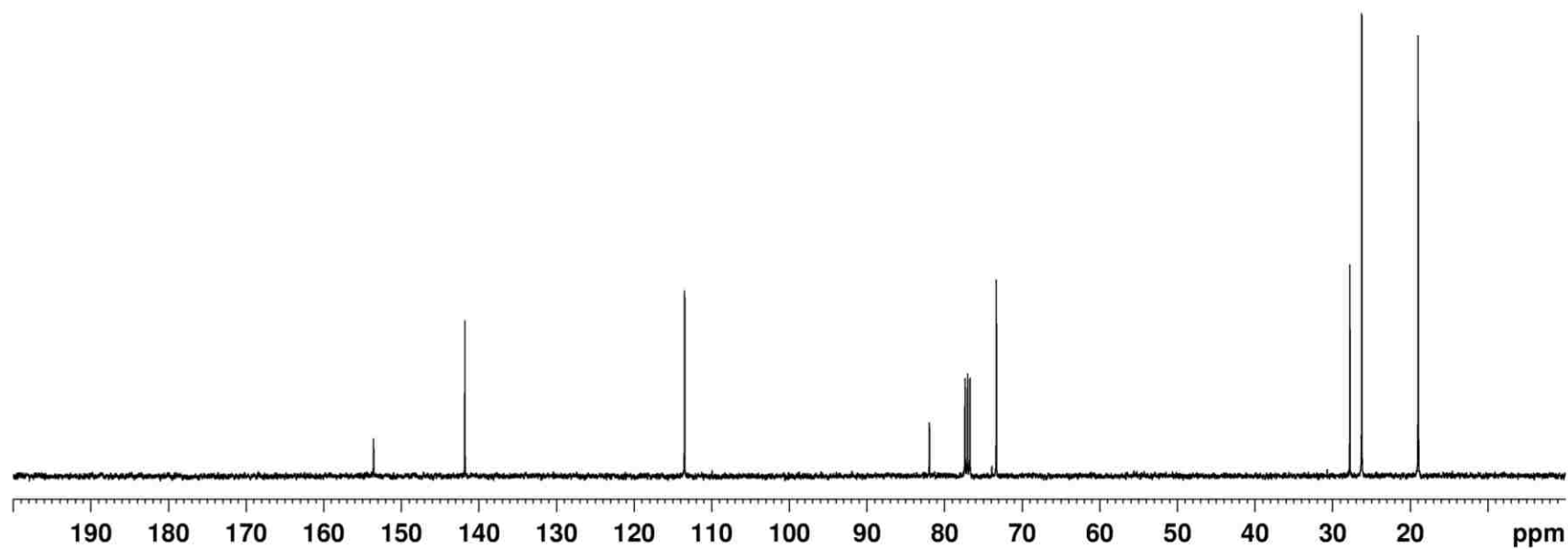
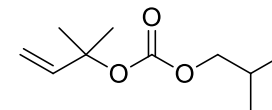
Compound **171** (Scheme 4.16) – ^1H NMR spectrum

Isobutyl prenyl carbonate in CDCl_3 at 400 MHz



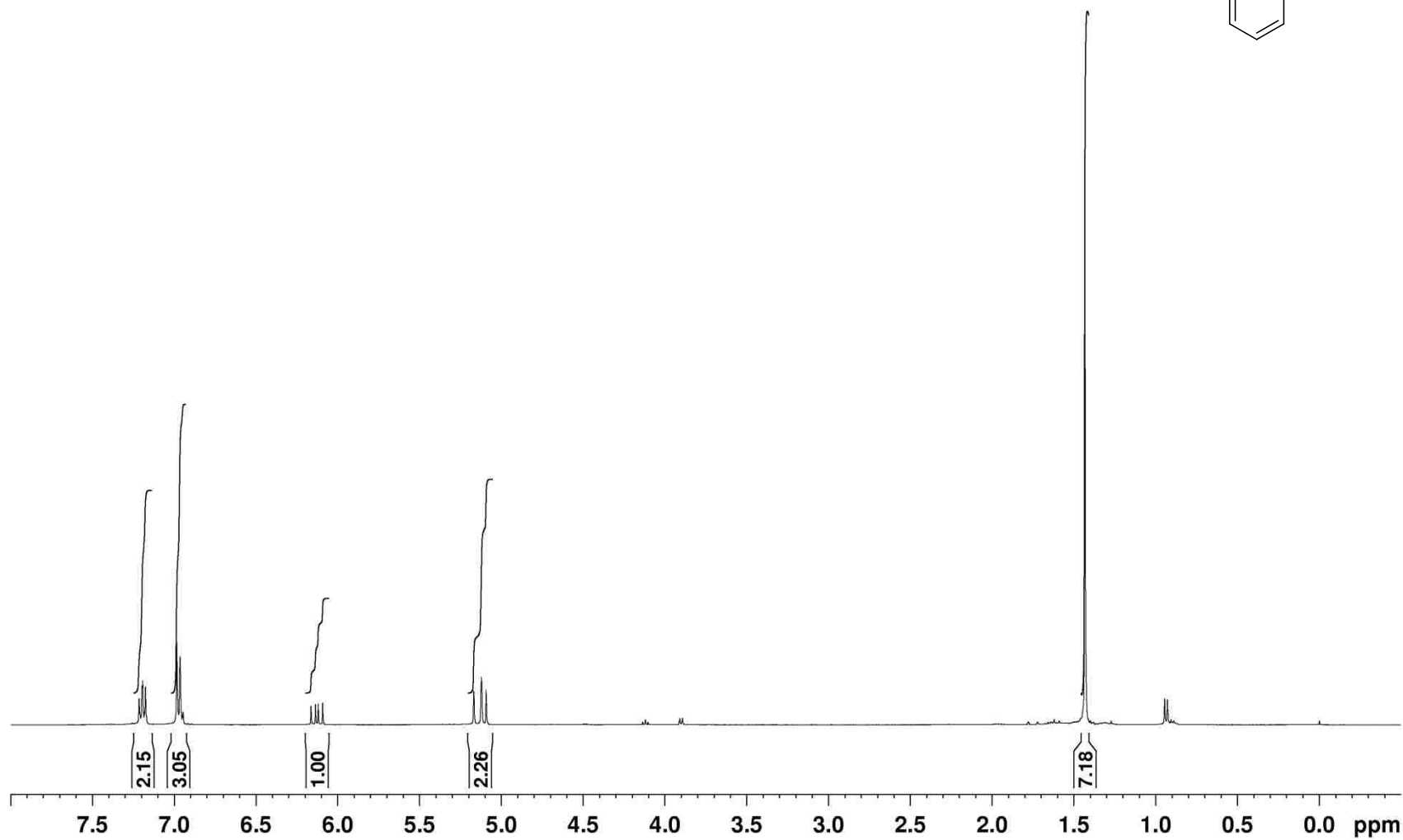
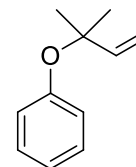
Compound **171** (Scheme 4.16) – ^{13}C NMR spectrum

Isobutyl prenyl carbonate in CDCl_3 at 100 MHz



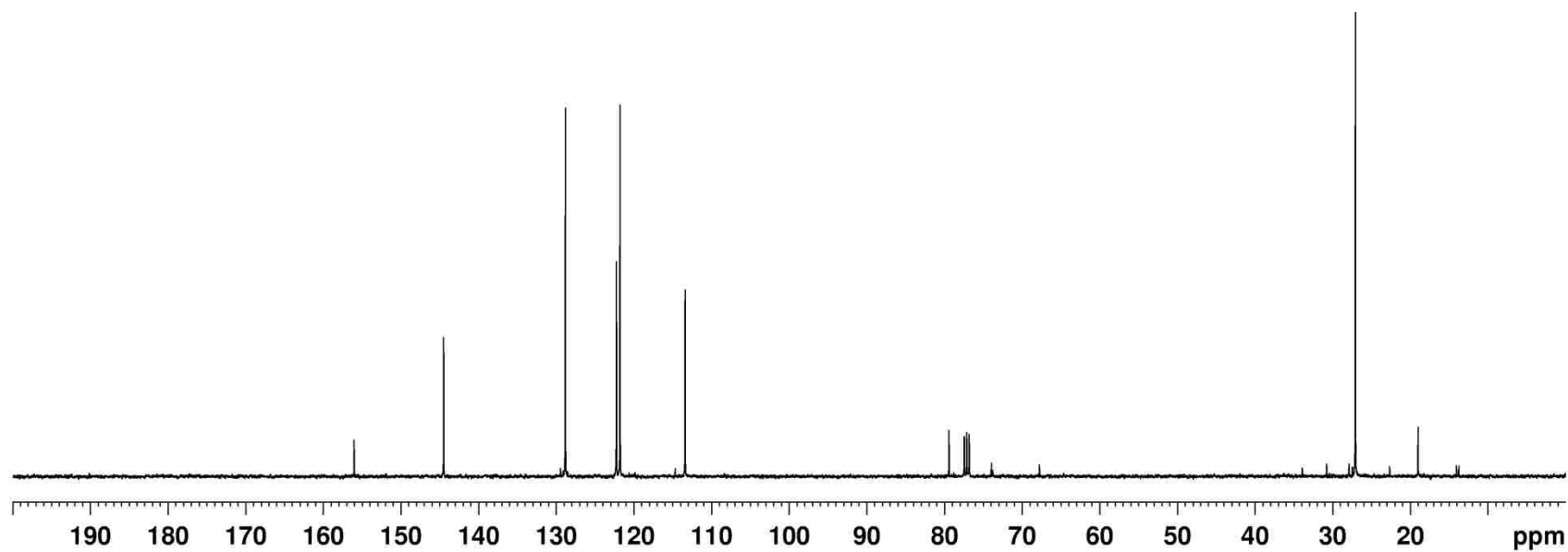
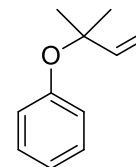
Compound **173a** (Scheme 4.16) – ^1H NMR spectrum

Aryl prenyl ether in CDCl_3 at 400 MHz



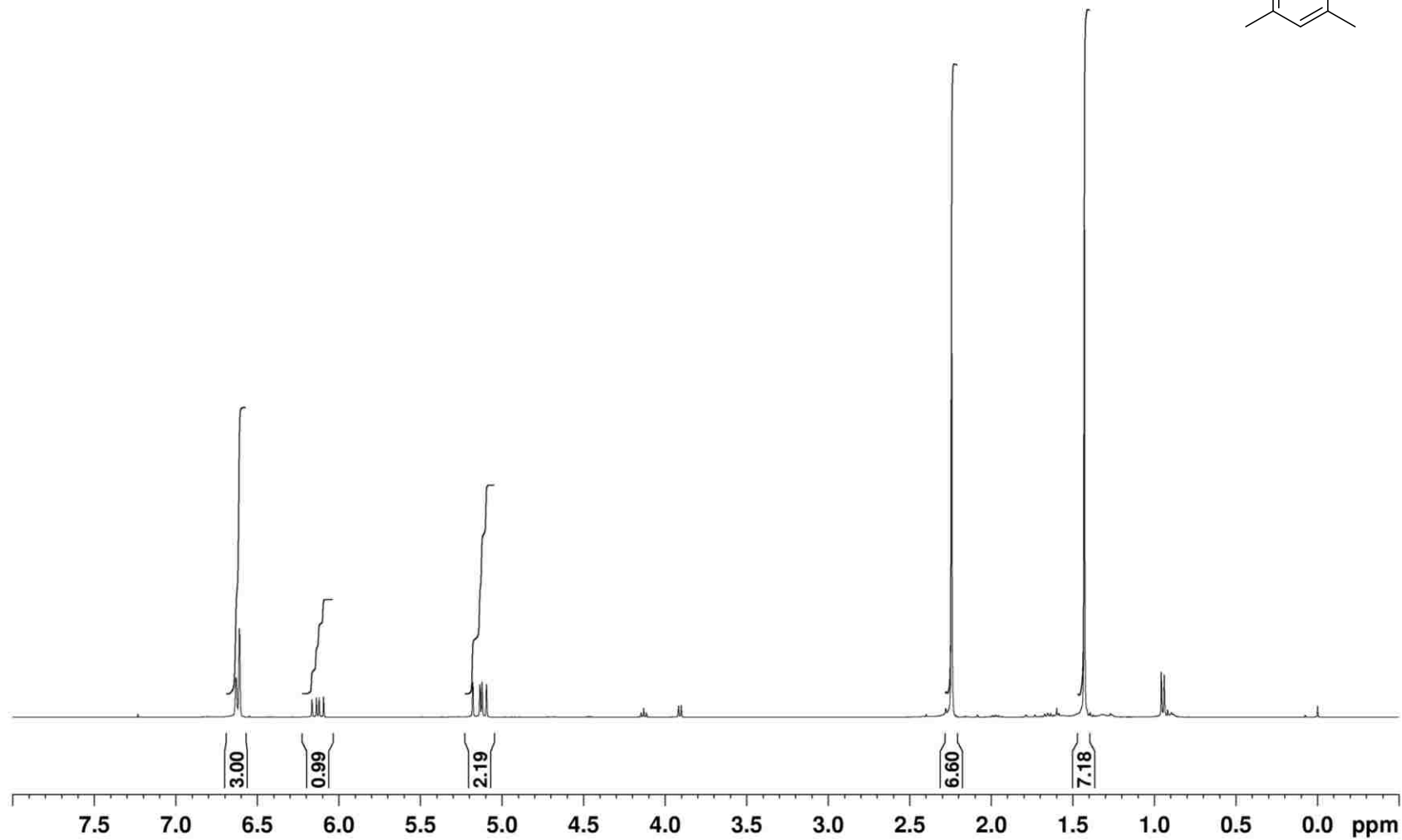
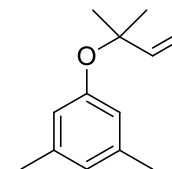
Compound **173a** (Scheme 4.16) – ^{13}C NMR spectrum

Aryl prenyl ether in CDCl_3 at 100 MHz



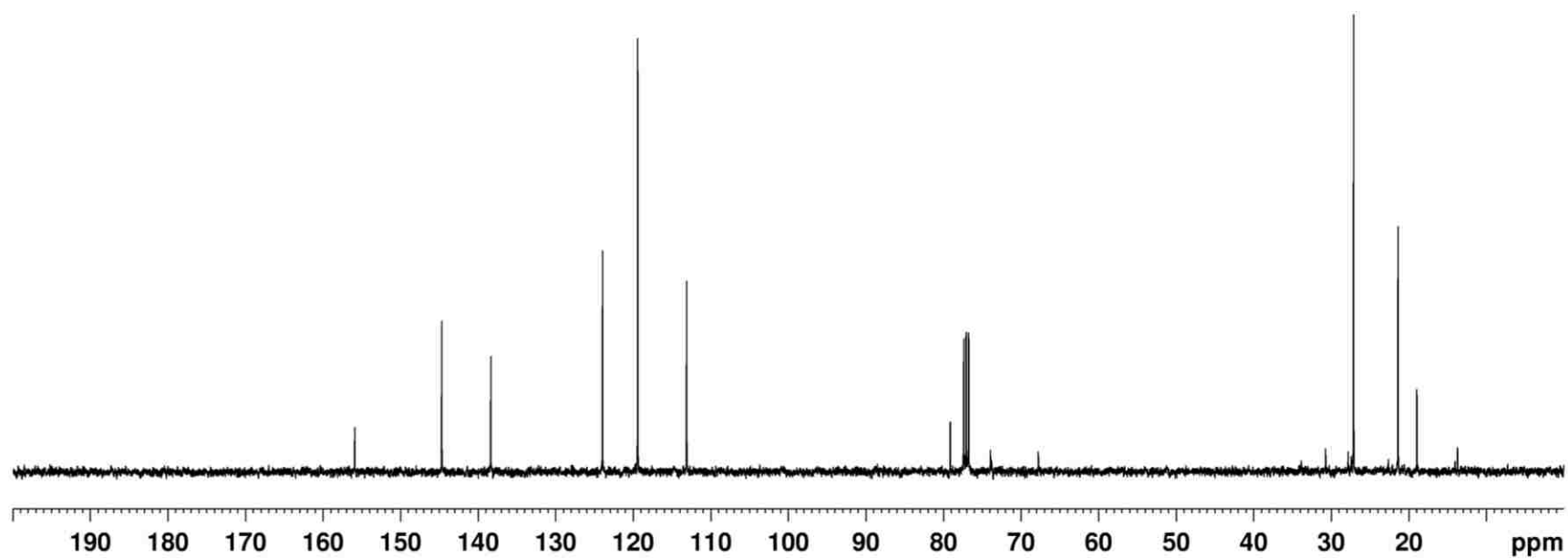
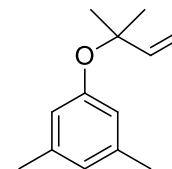
Compound **173b** (Scheme 4.16) – ^1H NMR spectrum

Aryl prenyl (*m*-3,5-dimethyl) ether in CDCl_3 at 400 MHz



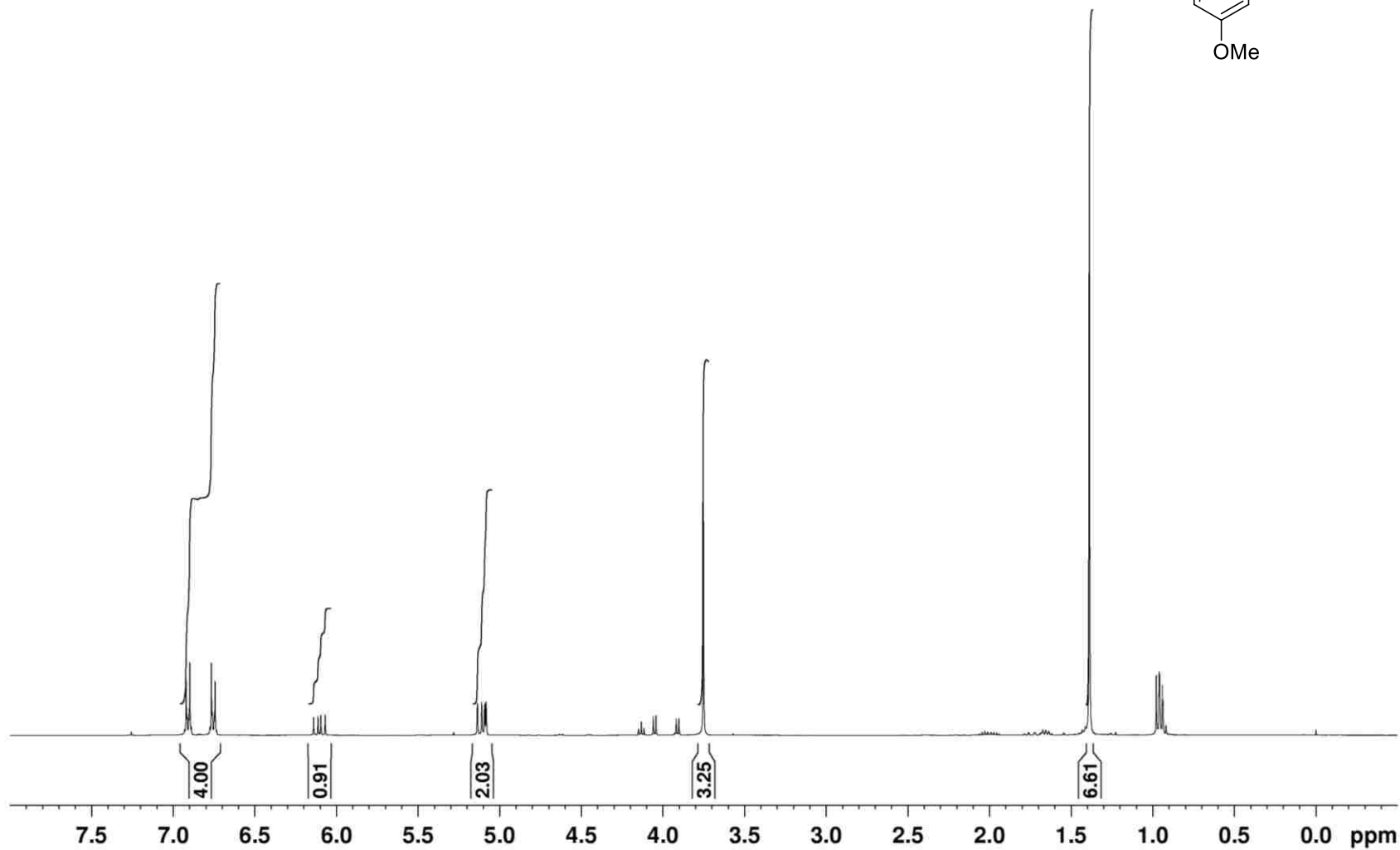
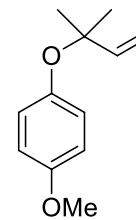
Compound **173b** (Scheme 4.16) – ^{13}C NMR spectrum

Aryl prenyl (*m*-3,5-dimethyl) ether in CDCl_3 at 100 MHz



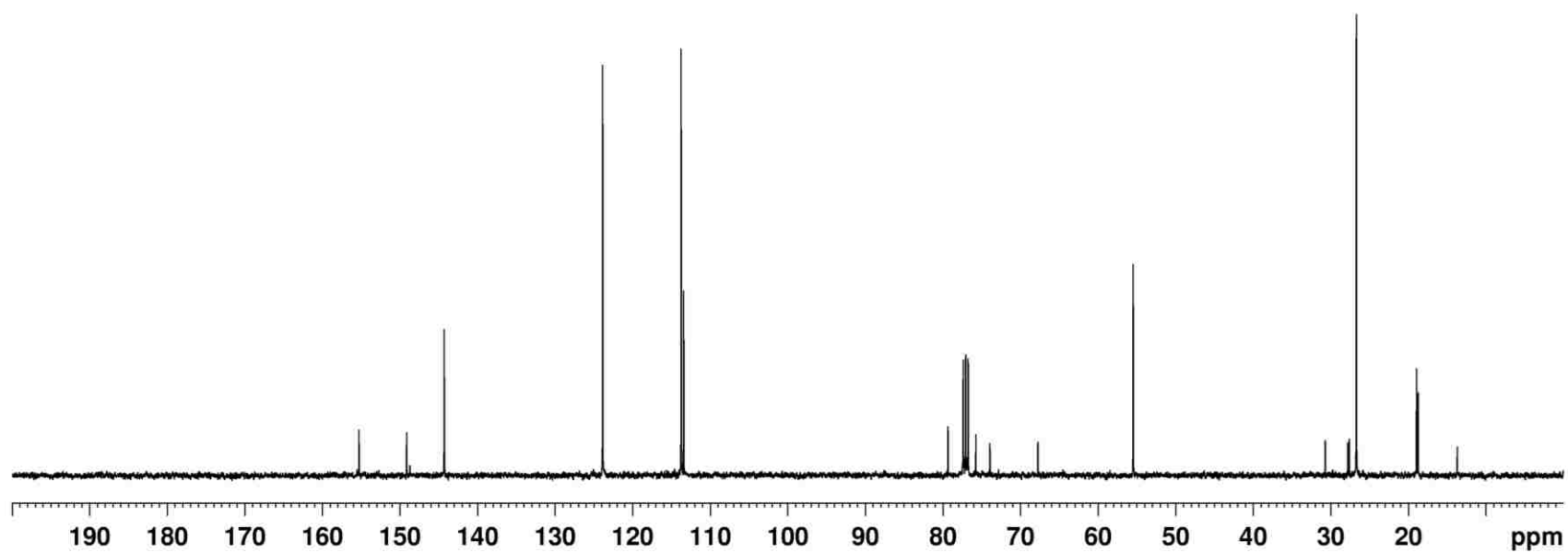
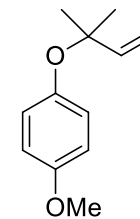
Compound **168** (Scheme 4.16) – ^1H NMR spectrum

Aryl prenyl (*p*-OMe) ether in CDCl_3 at 400 MHz



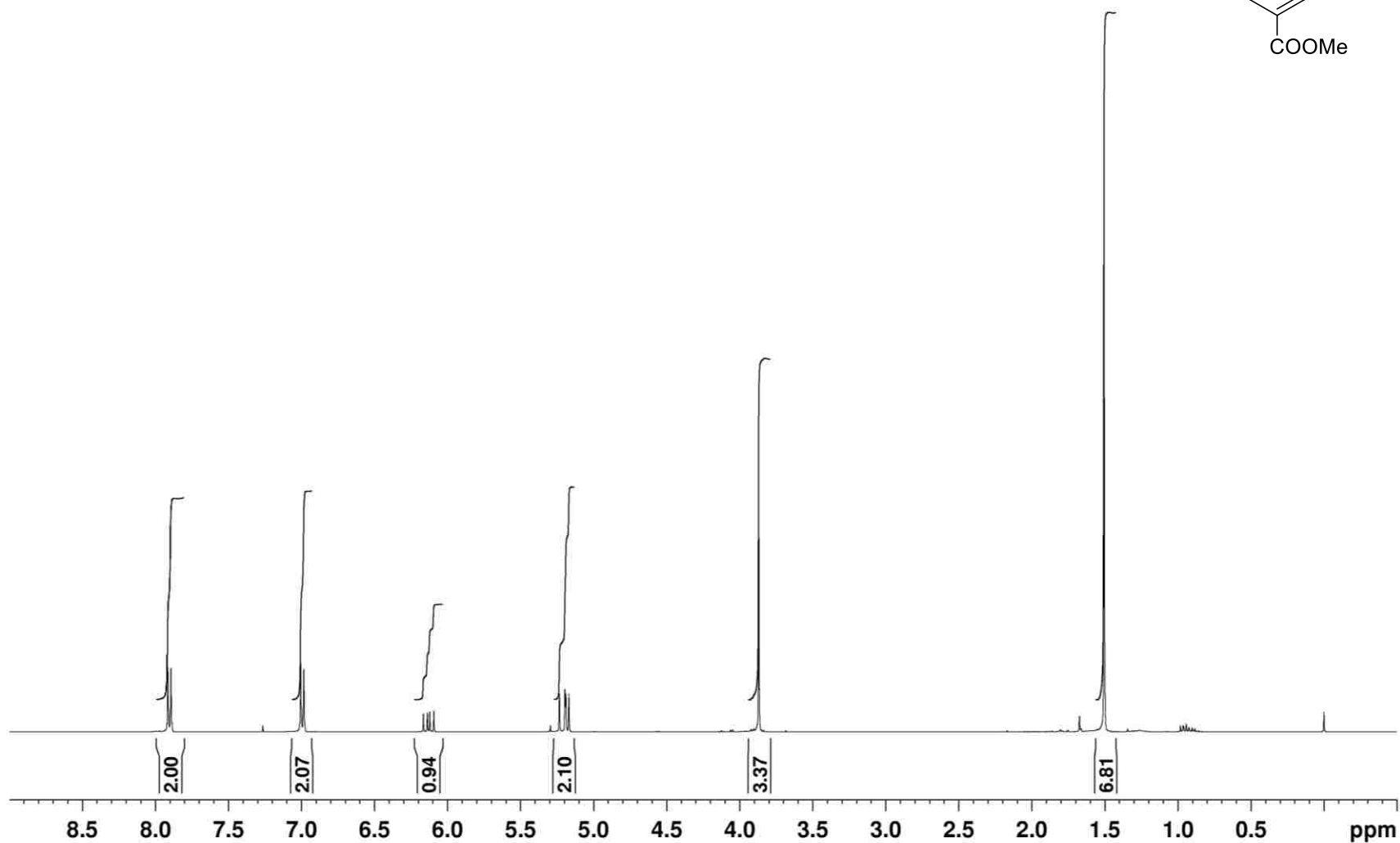
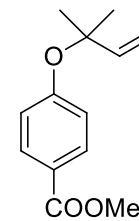
Compound **168** (Scheme 4.16) – ^{13}C NMR spectrum

Aryl prenyl (*p*-OMe) ether in CDCl_3 at 100 MHz



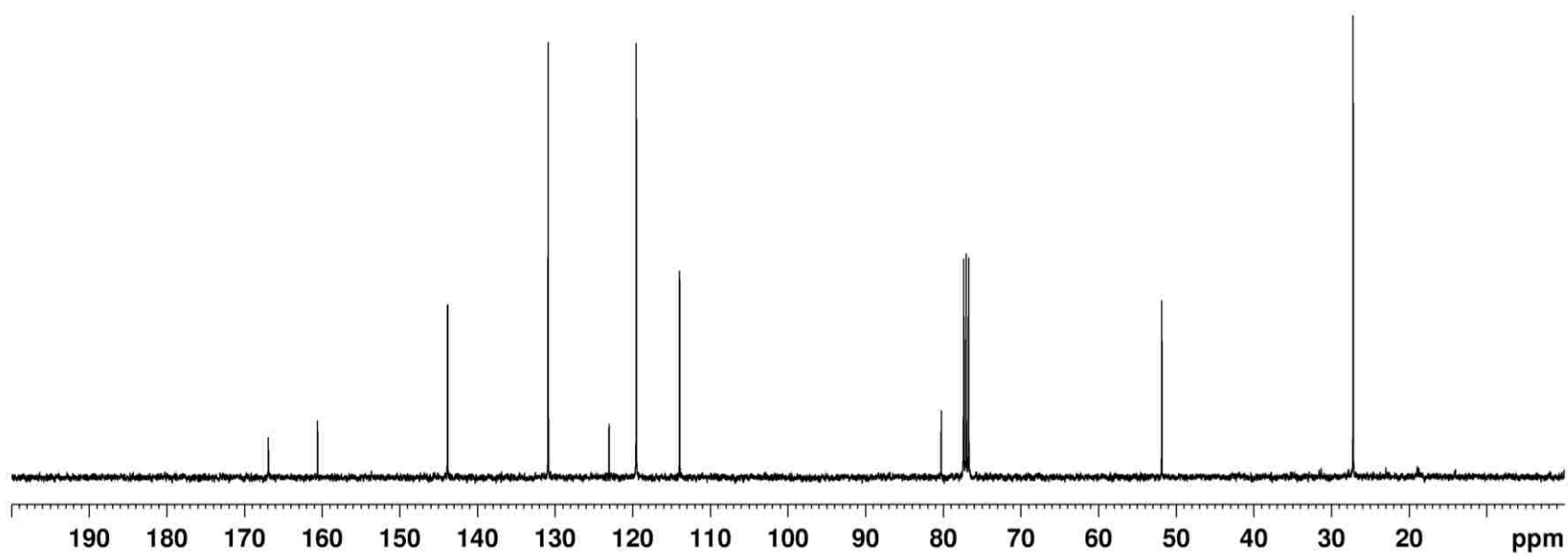
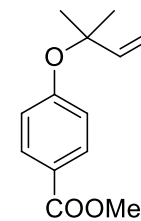
Compound **173c** (Scheme 4.16) – ^1H NMR spectrum

Aryl prenyl (*p*-COOMe) ether in CDCl_3 at 400 MHz



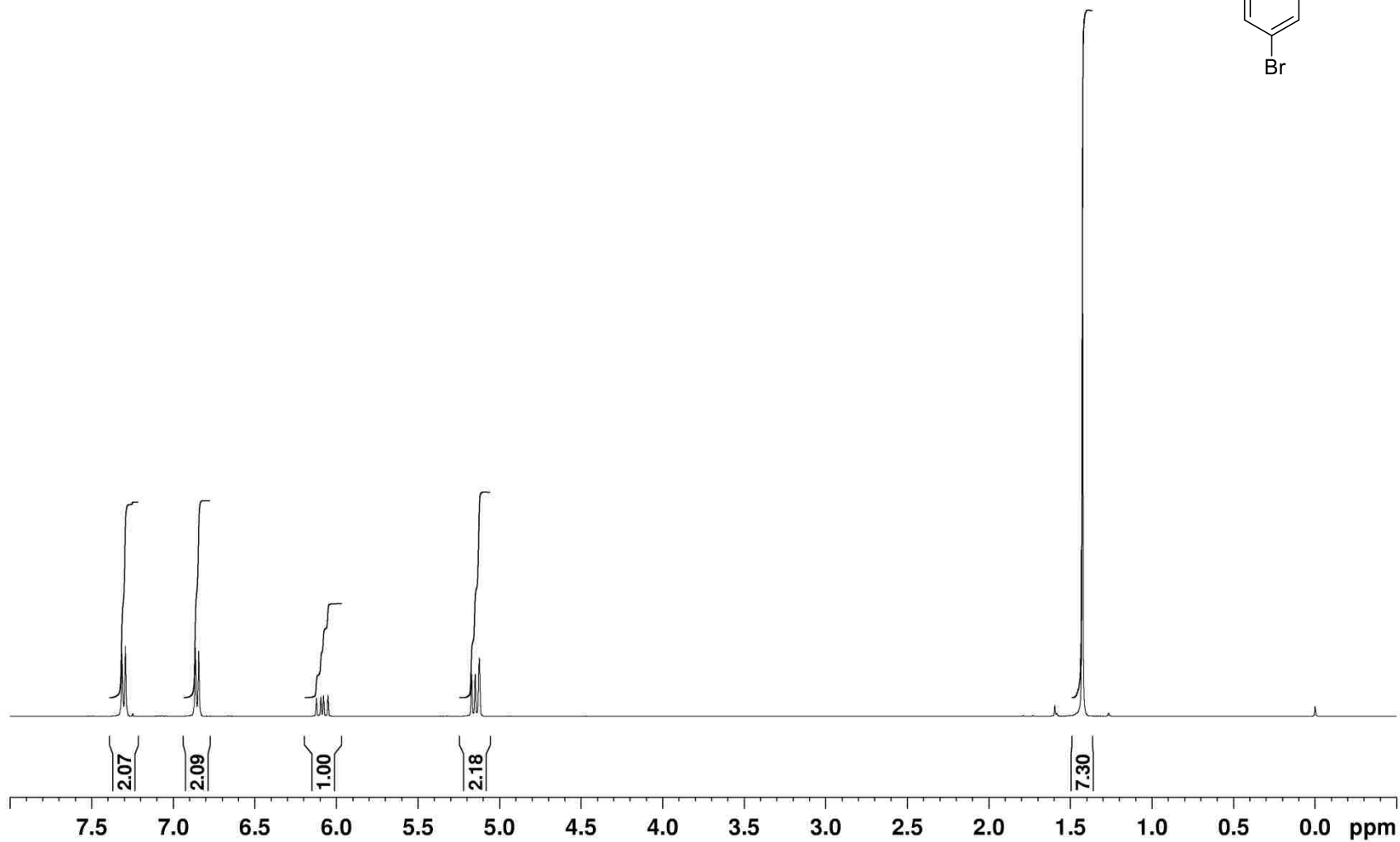
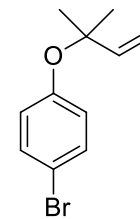
Compound **173c** (Scheme 4.16) – ^{13}C NMR spectrum

Aryl prenyl (*p*-COOMe) ether in CDCl_3 at 100 MHz



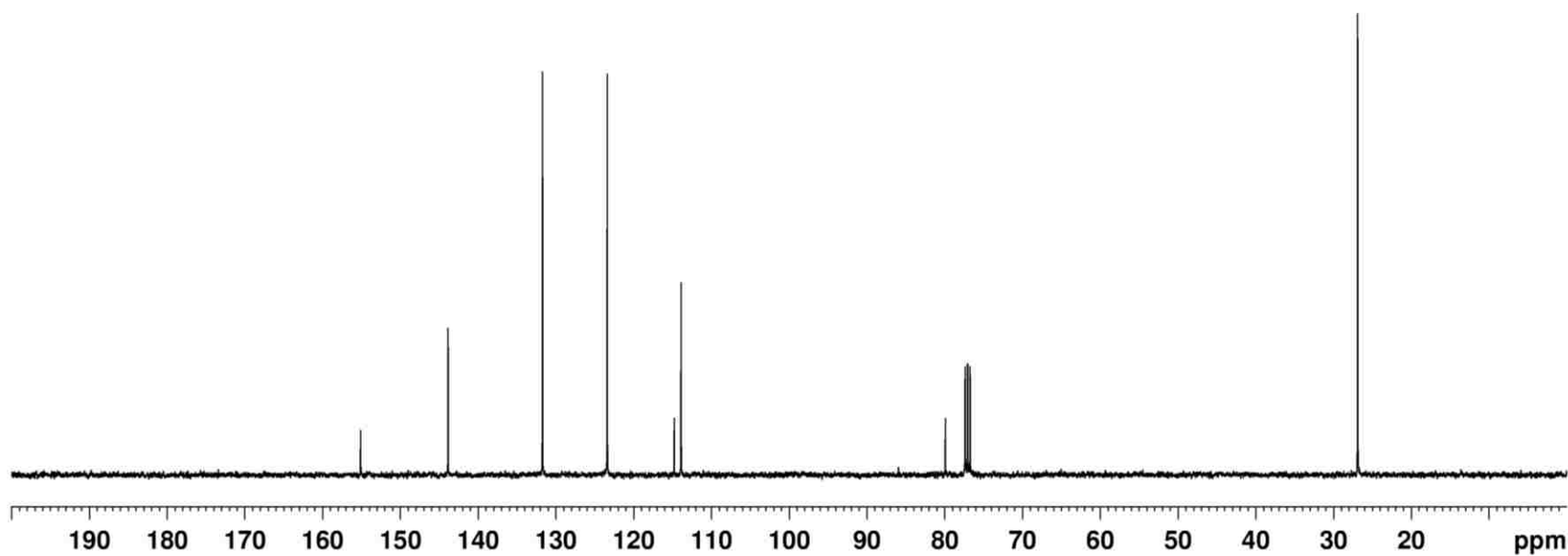
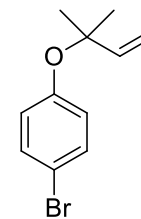
Compound **173d** (Scheme 4.16) – ^1H NMR spectrum

Aryl prenyl (*p*-Br) ether in CDCl_3 at 400 MHz



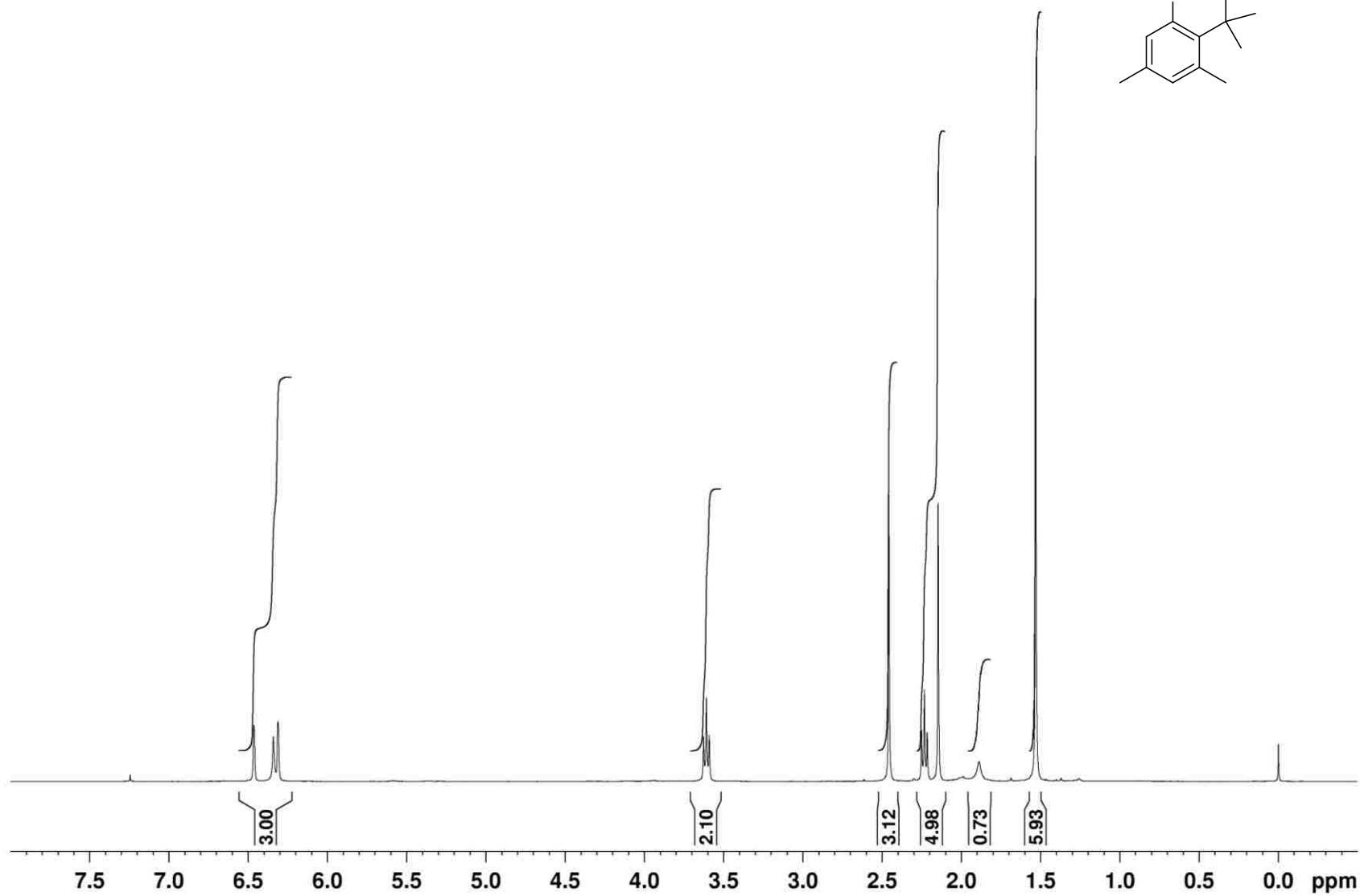
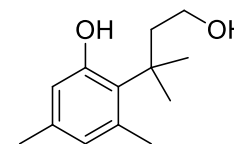
Compound **173d** (Scheme 4.16) – ^{13}C NMR spectrum

Aryl prenyl (*p*-Br) ether in CDCl_3 at 100 MHz



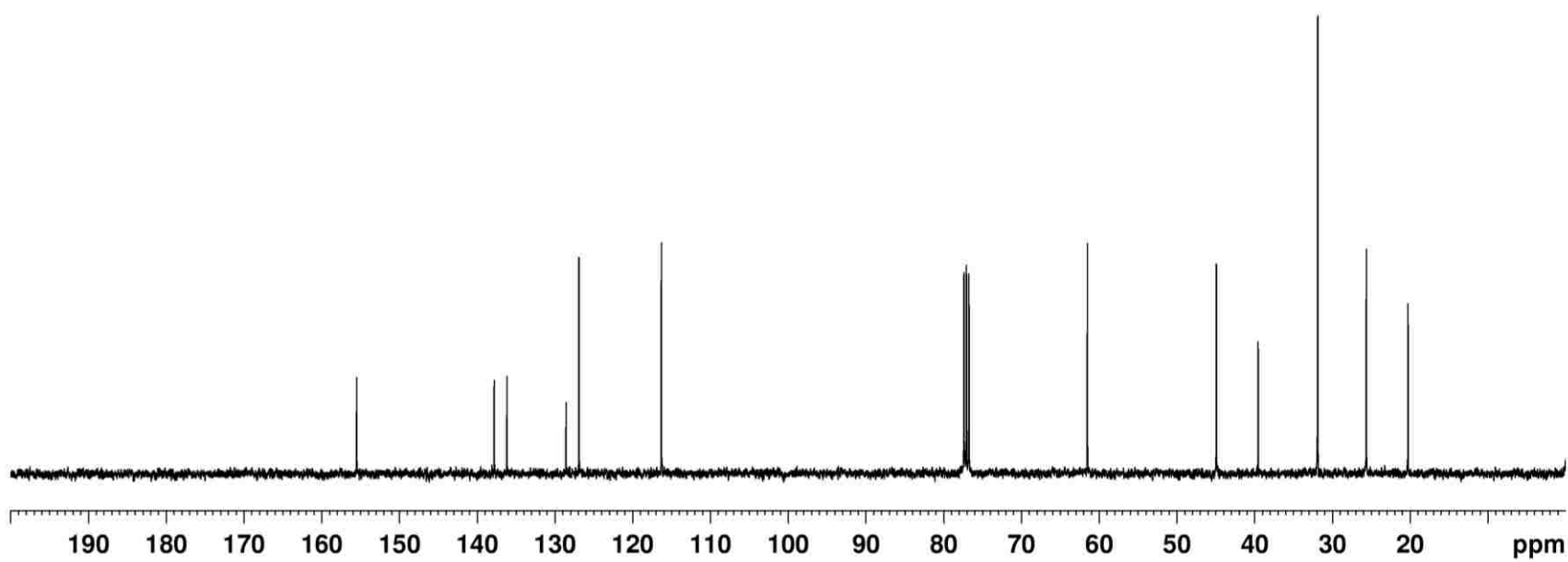
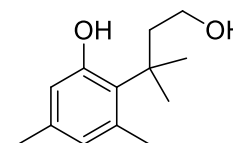
Compound **179** (Scheme 4.20) – ^1H NMR spectrum

3,5-dimethyldiol in CDCl_3 at 400 MHz



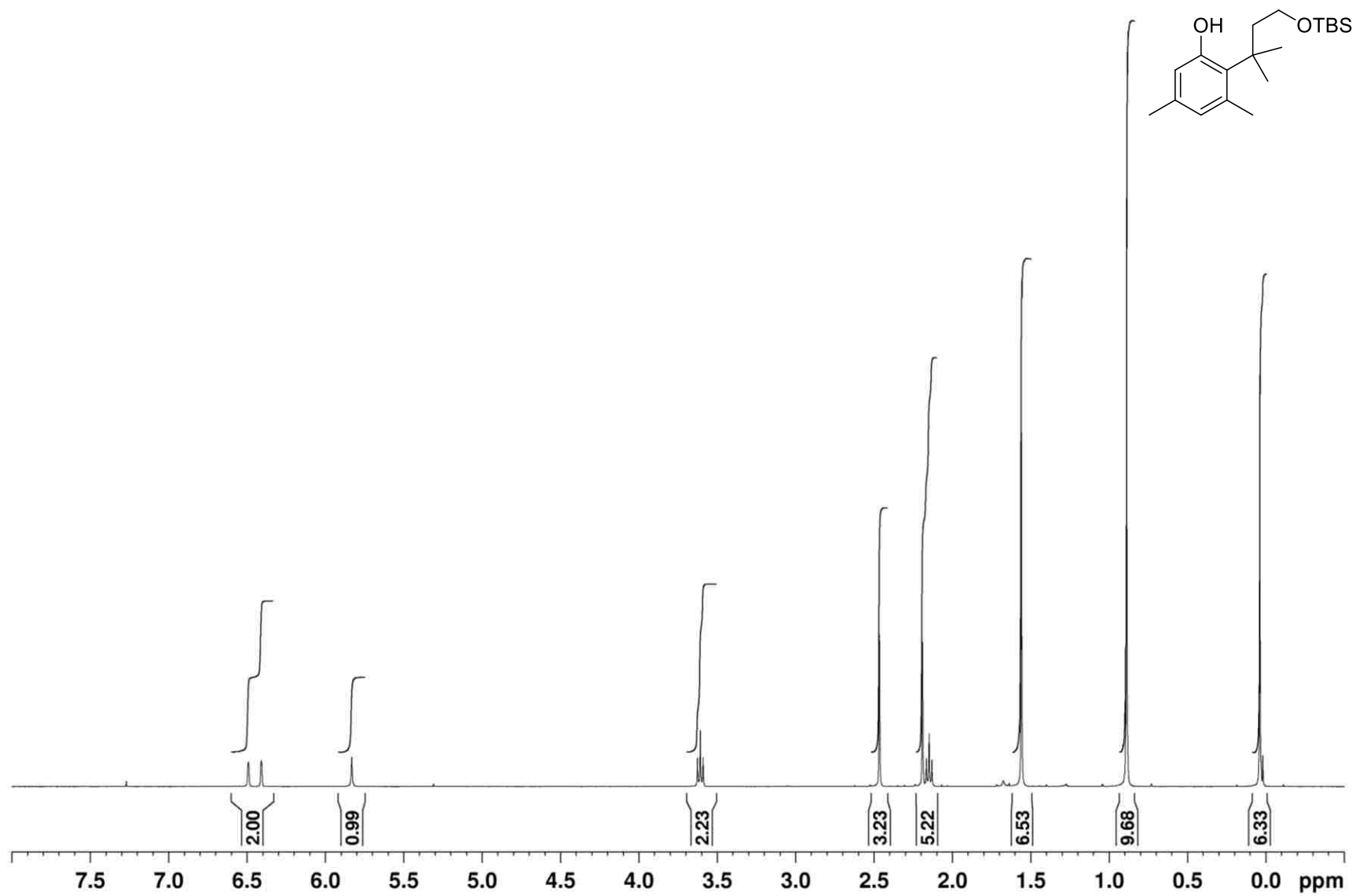
Compound **179** (Scheme 4.20) – ^{13}C NMR spectrum

3,5-dimethyldiol in CDCl_3 at 100 MHz



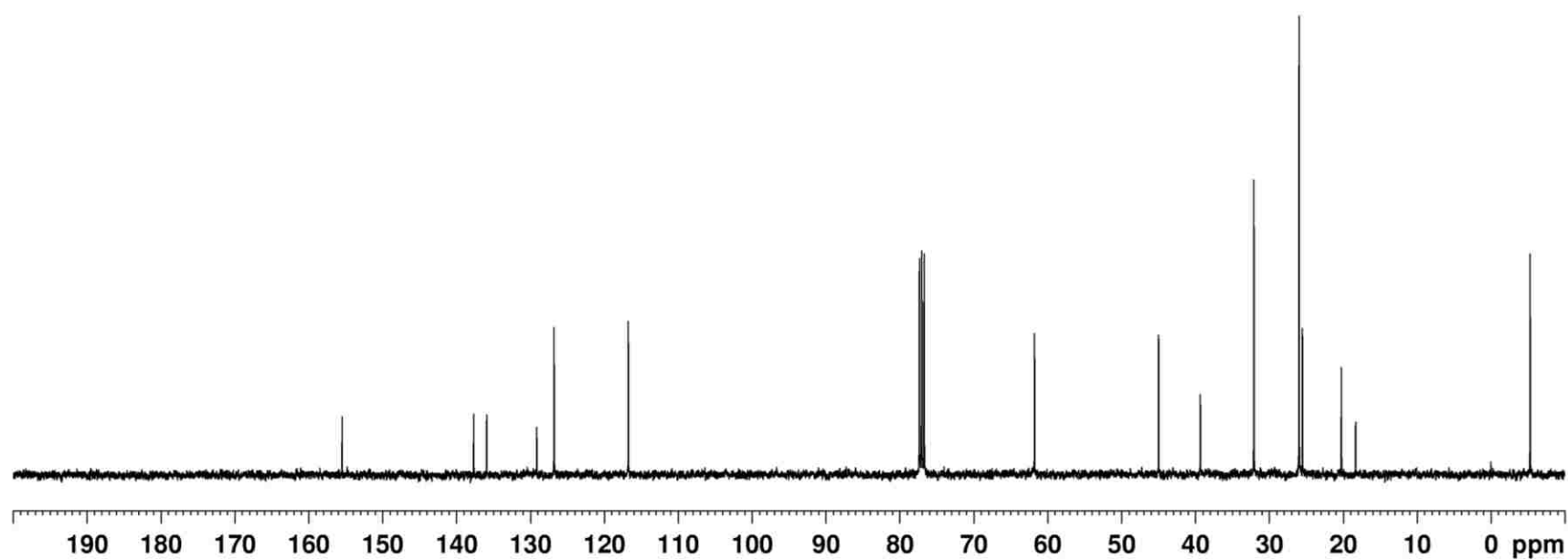
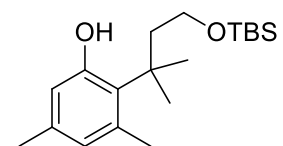
Compound **180** (Scheme 4.20) – ^1H NMR spectrum

3,5-dimethyl TBS ether in CDCl_3 at 400 MHz



Compound **180** (Scheme 4.20) – ^{13}C NMR spectrum

3,5-dimethyl TBS ether in CDCl_3 at 400 MHz



4.10 References

1. a) Claisen, L. "Über umlagerung von phenol-allyläthern in C-allyl-phenole" *Ber. Dtsch. Chem. Ges.* **1912**, *45*, 3157-3166. b) Claisen, L., Eisleb, O. "Über die umlagerung von phenolallyläthern in die isomeren allylphenole" *Liebigs Ann. Chem.* **1913**, *401*, 21-119.
2. Woodward, R. B., Hoffmann, R. "The conservation of orbital symmetry" *Angew. Chem., Int. Ed. Engl.* **1969**, *8*, 781-853.
3. *The Claisen Rearrangement*; Hiersemann, M., Nubbemeyer, U., Eds.; WILEY-VCH: Weinheim, 2007
4. Ganem, B. "The mechanism of the Claisen rearrangement: Déjà vu all over again" *Angew. Chem. Int. Ed. Engl.* **1996**, *35*, 936-945.
5. Castro, A. M. M. "Claisen rearrangement over the past nine decades" *Chem. Rev.* **2004**, *104*, 2939-3002.
6. White, W. N., Wolfarth, E. F. "The *o*-Claisen rearrangement. VIII. solvent effects" *J. Org. Chem.* **1970**, *35*, 2196-2199.
7. Gajewski, J. J. "The Claisen rearrangement. Response to solvents and substituents: The case for both hydrophobic and hydrogen bond acceleration in water and for a variable transition state" *Acc. Chem. Res.* **1997**, *30*, 219-225.
8. White, W. N., Wolfarth, E. F. "The *ortho* Claisen rearrangement. IX. The effect of solvent on the substituent effect" *J. Org. Chem.* **1970**, *35*, 3585-3585.
9. Goering, H. L., Jacobson, R. R. "A kinetic study of the *ortho*-Claisen rearrangement" *J. Am. Chem. Soc.* **1958**, *80*, 3277-3285.
10. Kosower, E. M. "The effect of solvent on spectra. I. A new empirical measure of solvent polarity: Z-values" *J. Am. Chem. Soc.* **1958**, *80*, 3253-3260.
11. Gajewski, J. J., Jurayj, J., Kimbrough, D. R., Gande, M. E., Ganem, B., Carpenter, B. K. "The mechanism of rearrangement of chorismic acid and related compounds" *J. Am. Chem. Soc.* **1987**, *109*, 1170-1186.
12. Gibson, F. "The elusive branch-point compound of aromatic amino acid biosynthesis" *Trends Biochem. Sci.* **1999**, *24*, 36-38.
13. Severance, D. L., Jorgensen, W. L. "Effects of hydration on the Claisen rearrangement of allyl vinyl ether from computer simulations" *J. Am. Chem. Soc.* **1992**, *114*, 10966-10968.
14. Lee, A. Y., Karplus, P. A., Ganem, B., Clardy, J. "Atomic structure of the buried catalytic pocket of *Escherichia coli* chorismate mutase" *J. Am. Chem. Soc.* **1995**, *117*, 3627-3628.

15. Chook, Y. M., Gray, J. V., Ke, H., Lipscomb, W. N. "The monofunctional chorismate mutase from *Bacillus subtilis*. Structure determination of chorismate mutase and its complexes with a transition state analog and prephenate, and implications for the mechanism of the enzymatic reaction" *J. Mol. Biol.* **1994**, *240*, 476-500.
16. Alaoui, A. E., Saha, N., Schmidt, F., Monneret, C., Florent, J.-C. "New Taxol (paclitaxel) prodrugs designed for ADEPT and PMT strategies in cancer chemotherapy" *Bioorg. Med. Chem.* **2006**, *14*, 5012-5019.
17. a) Mellado, W., Magri, N. F., Kingston, D. G., Garcia-Arenas, R., Orr, G. A., Horwitz, S. B. "Preparation and biological activity of taxol acetates" *Biochem. Biophys. Res. Commun.* **1984**, *124*, 329-336. b) Kingston, D. G. I. "Taxol: the chemistry and structure-activity relationships of a novel anticancer agent" *Trends Biotechnol.* **1994**, *12*, 222-227.
18. Song, C. E., Oh, C. R., Roh, E. J., Lee, S.-G., Choi, J. H. "One-step synthesis of paclitaxel side-chain precursor: benzamide-based asymmetric aminohydroxylation of isopropyl *trans*-cinnamate" *Tetrahedron: Asymmetry* **1999**, *10*, 671-674.
19. Choudary, B. M., Chowdari, N. S., Madhi, S., Kantam, M. L. "A trifunctional catalyst for one-pot synthesis of chiral diols via Heck coupling–N-oxidation–asymmetric dihydroxylation: Application for the synthesis of diltiazem and Taxol side chain" *J. Org. Chem.* **2003**, *68*, 1736-1746.
20. Hauser, C. R., Renfrow Jr., W. B. "The removal of HX from organic compounds by means of bases. 111. The rates of removal of hydrogen bromide from Substituted *N*-bromobenzamides and their relative ease of rearrangement in the presence of alkali. The Hoffman rearrangement" *J. Am. Chem. Soc.* **1937**, *59*, 121-125.
21. Nicolaou, M. G., Yuan, C.-S., Borchardt, R. T. "Phosphate prodrugs for amines utilizing a fast intramolecular hydroxy amide lactonization" *J. Org. Chem.* **1996**, *61*, 8636-8641.
22. Nemoto, H., Katagiri, A., Kamiya, M., Kawamura, T., Matsushita, T., Matsumura, K., Ito, T., Hattori, H., Tamaki, M., Ishizawa, K., Miyamoto, L., Abe, S., Tsuchiya, K. "Synthesis of paclitaxel-BGL conjugates" *Bioorg. Med. Chem.* **2012**, *20*, 5559-5567.
23. Narayan, S., Muldoon, J., Finn, M. G., Fokin, V. V., Kolb, H. C., Sharpless, K. B. "'On water': Unique reactivity of organic compounds in aqueous suspension" *Angew. Chem. Int. Ed.* **2005**, *44*, 3275–3279.
24. Ross, R., Glomset, J. A., Kariya, B., Harker, L. "A platelet-dependent serum factor that stimulates the proliferation of arterial smooth muscle cells *in vitro*" *Proc. Natl. Acad. Sci. USA* **1974**, *71*, 1207-1210.
25. Cebler, J. C., Woodside, A. B., Poulter, C. D. "Dimethylallyltryptophan synthase. An enzyme-catalyzed electrophilic aromatic substitution" *J. Am. Chem. Soc.* **1992**, *114*, 7354-7360.

26. McIntosh, J. A., Donia, M. S., Nair, S. K., Schmidt, E. W. "Enzymatic basis of ribosomal peptide prenylation in cyanobacteria" *J. Am. Chem. Soc.* **2011**, *133*, 13698–13705.
27. Osuna, S., Kim, S., Bollot, G., Houk, K. N. "Aromatic Claisen rearrangements of *o*-prenylated tyrosine and model prenyl aryl ethers: Computational study of the role of water on acceleration of Claisen rearrangements" *Eur. J. Org. Chem.* **2013**, 2823-2832.
28. Harfenist, M., Thom, E. "Influence of structure on the rate of thermal rearrangement of aryl propargyl ethers to the chromenes. Gem-dimethyl effect" *J. Org. Chem.* **1972**, *37*, 841-848.
29. White, W. N., Gwynn, D., Schlitt, R., Girard, C., Fife, W. "The ortho-Claisen rearrangement. I. The effect of substituents on the rearrangement of allyl *p*-X-phenyl ethers" *J. Am. Chem. Soc.* **1958**, *80*, 3271–3277.
30. Edagwa, B. J., Taylor, C. M. "Peptides containing γ,δ -dihydroxy-*L*-leucine" *J. Org. Chem.* **2009**, *74*, 4132-4136.
31. Choi, K-H., Hong, Y-D., Choi, O-J., Choi, S-J. "^{99m}Tc(CO)₃-Labeled histidine-arylpiperazines as potential radiotracers for a neuroreceptor targeting" *Bull. Korean Chem. Soc.* **2006**, *27*, 1189-1193.
32. Crich, D., Cai, F. "Stereocontrolled glycoside and glycosyl ester synthesis. Neighboring group participation and hydrogenolysis of 3-(2'-benzyloxyphenyl)-3,3-dimethylpropanoates" *Org. Lett.* **2007**, *9*, 1613-1615.
33. Chantarasriwong, O., Cho, W. C., Batova, A., Chavasiri, W., Moore, C., Rheingold, A. L., Theodorakis, E. A. "Evaluation of the pharmacophoric motif of the caged Garciniaxanthones" *Org. Biomol. Chem.* **2009**, *7*, 4886-4894.

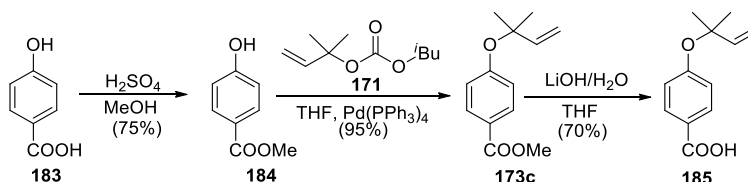
CHAPTER 5: INCORPORATION OF AN ANIONIC SUBSTRATE FOR A CLAISEN REARRANGEMENT INTO NANOGUMBOS

5.1 1,1-Dimethylallyl Aryl Ether Building Block: A Model System for Photothermal Rearrangement

To emulate TaxolTM release from the prodrug delivery system *in vivo*, the prodrug model system needs to be combined with a NIR-absorbing laser dye. Incorporation of the prodrug into an ionic liquid requires the introduction of an anionic functional group. As this will not be trivial, and the prodrug model system is valuable, a DMA aryl ether building block was synthesized for optimization of photothermal rearrangement studies.

5.2 Synthesis of an Anionic Substrate for a Claisen Rearrangement

Commercially available 4-hydroxybenzoic acid (**183**) was protected as the methyl ester to give phenol **184**. The DMA group was installed via isobutyl prenyl carbonate, and the methyl ester was removed to give 4-(1,1-dimethylallyloxy)benzoic acid (**185**) as a colorless solid in good yield.



Scheme 5.1: Synthesis of 4-(1,1-dimethylallyloxy)benzoic acid **185**

Previously prepared aryl prenyl ethers (Chapter 4), were volatile liquids where **185** is solid. Presumably, the carboxylic acid's ability to hydrogen bond leads to stronger intermolecular forces and a more ordered structure. Recrystallization of **185** from ethyl acetate and hexanes yielded thin, needle like crystals. Analysis by X-Ray crystallography revealed a monomer with a refractory index of 12% illustrated in Figure 5.1, A. The steric influence of the *gem*-dimethyl group on the conformation of the allyl moiety is apparent. When compared to

the unsubstituted counterpart, 4-(allyloxy)benzoic acid (**187**, Figure 5.1, B), the methyl groups in **185** orient the allyl group toward the aromatic ring. This facilitates the [3,3']-rearrangement, as evidenced in Chapter 4.

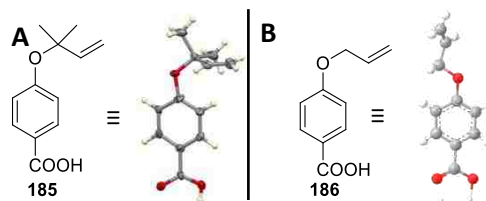


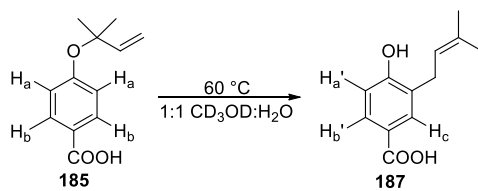
Figure 5.1: Crystal structures of 4-(1,1-dimethylallyloxy)benzoic acid (**185**) and 4-(allyloxy)benzoic acid (**186**) reported by Zugenmaier ¹

5.3 Kinetic Studies of Claisen Rearrangement of Aryl Prenyl Ethers

As discussed in Chapter 4, Harfenist and Thom reported that the thermal rearrangement of propargyl ethers to chromenes followed first-order kinetics.² They postulated that this acceleration was due to the *gem*-dimethyl effect, specifically the rotamer that orients the methyl groups away from the ring and the alkyne towards the ring lowering the barrier for activation. With experimental evidence for the alkene being oriented towards the aromatic ring, it seemed further investigation of the rate-accelerating effects of the *gem*-dimethyl on aryl Claisen rearrangements was of interest. One can assume that prenyl ethers would follow the same kinetic behavior as propargyl ethers. To our knowledge, rate constants for the rearrangement of aryl prenyl ethers in aqueous solutions have not been reported. Compounds **185**, **173c**, **173b**, **168** were chosen for the kinetic studies, as they presented an opportunity to explore substituent effects on the rate-acceleration.

To monitor the rate of disappearance of starting material, ¹H-NMR spectroscopy was used. A typical sample was prepared using a known quantity of prenyl ether, which was dissolved in a 1:1 solution (300 μ L total) of deuterated methanol and deionized water. The

solution, in an NMR tube, was then heated to 60 °C in the magnet of the spectrometer, with the sample spinning. Spectra were recorded at fifteen minute intervals. For each spectrum, the integrals of the *gem*-dimethyl protons of the reactant and aromatic protons of the product (Figure 5.2, H_a') can be measured, because the aromatic and *gem*-dimethyl signals are well resolved and do not overlap each other. In Figure 5.2 you can clearly see the H_c singlet forming as the prenyl group rearranges from the oxygen to the *ortho* position on the ring, reducing the intensity of H_a.



Scheme 5.2: Aryl Claisen rearrangement of prenyl ether **185**

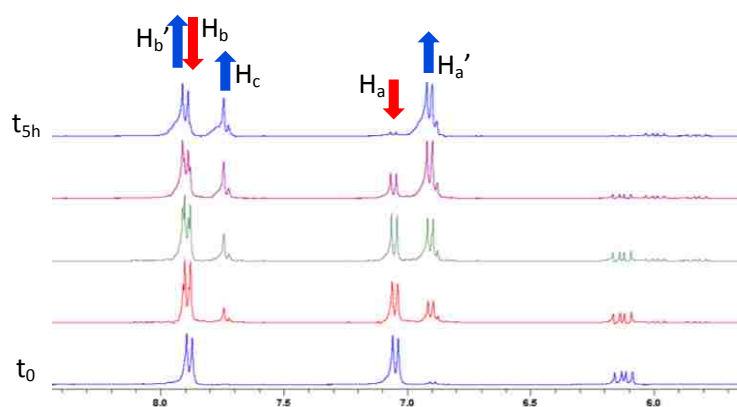


Figure 5.2: Time profile of ¹H-NMR spectra of reaction mixture

Integration of the area under the *gem*-dimethyl signal (δ 1.53, s, 6H, 100%) was compared with the area under the growing H_a' aromatic signal (δ 6.9, d) with the progress of the reaction expressed as a percentage conversion. These calculated percentages were plotted against reaction time (Figure 5.3). The resulting polynomial curves suggest that the thermal rearrangement of prenyl aryl ethers follow first-order rate kinetics. Therefore, the rate constant

can be obtained from Equation (1), dividing 0.693 by the half-time it takes for the reaction to reach 50% completion. Another advantage of first-order reactions is that they are independent of the concentration of the starting reactant, eliminating the need to control concentration of starting material for each substrate.

$$k = \frac{0.693}{t_{1/2}} \quad (1)$$

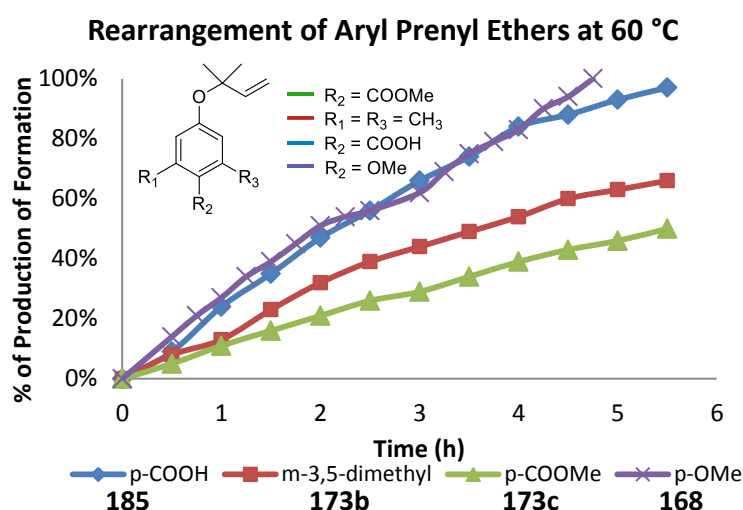


Figure 5.3: Plot of percentage of product formed versus reaction time of prenyl phenyl ethers.

Initial results closely mimic studies done by White *et al.* on the substituent effects of the *ortho*-Claisen rearrangement³ in that electron withdrawing groups at the *para* position slow down the reaction whereas electron donating groups speed up the reaction. A comparison of the rate constants follows a similar pattern, with derivative **185** being significantly faster than derivatives **173c**, and **173b** despite the electron withdrawing group at the *para* position (Table 5.1). This can be explained by the carboxylic acids ability to hydrogen bond. It has already been established that hydrogen bonding decreases the activation energy due to solvation.⁴ If you combine that with the increasing polarity of the solvent due to the increased concentration of

phenolic protons over time, you get an accelerated reaction rate. Compound **173c** does not have hydrogen-bonding capability, and therefore the methyl ester's electron withdrawing characteristics takes precedence, destabilizing the charged transition state which slows the reaction down considerably.

Table 5.1: Rate constants and relative rates for rearrangement of aryl prenyl ethers (**185**, **173c**, **173b**, **168**) at 60 °C in 1:1 CD₃OD:H₂O compared with the rate constant of 1-(allyloxy)-4-methoxybenzene in carbitol at 181 °C prepared by White *et al.*

Prenyl ether	R ₁	R ₂	R ₃	$k \times 10^5(\text{sec}^{-1})$	k_{rel}	Yield ^{a,b} (%)
185	H	H	COOH	8.6	2.5	97
173c	H	H	COOMe	3.5	1	50
173b	Me	Me	H	5.5	1.5	66
168	H	H	OMe	9.6	3.7	100
188^c	H	H	OMe	9.2 ^c	2.6	60 ^c

^a After 5.5 hours. ^b Percent conversion ^c See reference 3

Comparison of the rate constant of 1-(allyloxy)-4-methoxybenzene (**188**, Table 5.1), calculated by White *et al.*³ to the similar compound **168**, indicates a similar reaction rate. However, the rate constant of **188** was calculated for temperatures above 180 °C in carbitol. The presence of the prenyl group allows for comparable rates, at much lower temperatures.

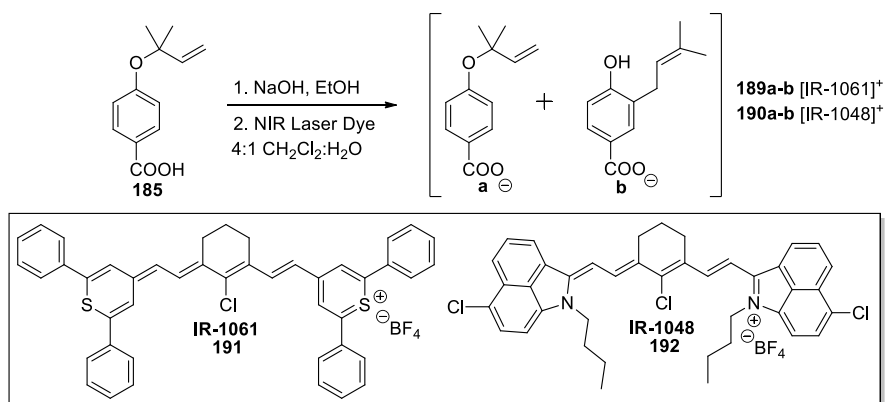
5.4 Assembly of NIR-GUMBOS Model System

With substantial experimental evidence of accelerated rearrangement via the prenyl group at reasonable temperatures, we now focused our efforts on ionic pairing of our aryl prenyl ether anion to a cationic NIR laser dye. Our heat source *in vivo* would come from laser irradiation of organic near-infrared absorbing dyes, specifically polymethine cyanine-based dyes, as they are highly touted for their molar absorptivity, photostability, and tunability.⁵ We expect that upon irradiation with the appropriate wavelength NIR laser, heat will be generated. This indirect heat is expected to induce rearrangement of the prodrug moiety, releasing the

Taxol™ side chain. These dyes have been reported to reach temperatures of over 400 °C, even when complexed with organic anions.⁵

Previous work by John Dumke (Warner Group, LSU) on NIR-absorbing nanoGUMBOS utilized heptamethine cyanine laser dyes 1061 and 1048 as the preferred counter-ion (Scheme 5.3). Naturally, these dyes were our starting point.

To prepare the NIR-GUMBOS we used the ion exchange method. Prenyl ether **185** was reacted with 1.05 equivalents of sodium hydroxide in ethanol for thirty minutes. The resulting salt was concentrated, and redissolved in a biphasic 4:1 dichloromethane-water solution. IR-1061 or IR-1048 laser dye was added as a tetrafluoroborate salt solution in dichloromethane, and the reaction stirred for two days (Scheme 5.3).



Scheme 5.3: Ion exchange of aryl prenyl ether **186** and IR-1061 and IR-1048 laser dye

Unfortunately, exposure to water, even at room temperature for an extended period of time led to partial rearrangement of compound **186**. This gave a mixture of products by TLC, seemingly the target compound **189a** if IR-1061 was used, along with the salt containing the rearranged carboxylate anion **189b**. This was observed with both dyes. The aqueous layer contained nominal amounts of the expected NaBF₄ salt. Tetrafluoroborate ions are used to render salts more soluble in organic solvents. It seems from the lack of sodium

tetrafluoroborate recovered from the aqueous layer, that there are significant sodium and tetrafluoroborate impurities present in the GUMBOS. It was apparent that traditional ion exchange procedures, as well as the BF_4^- ion, were not suitable for this water-sensitive substrate. Alternative procedures and dyes were sought.

5.4.1 IR-780: An Antitumorigenic Cationic Dye

We selected NIR-absorbing laser dyes IR-655 and IR-780 (Figure 5.4) based on their iodine cation which would give more water soluble salts, and their absorbance in the NIR therapeutic optical window. They also had reduced costs compared to IR-1048 and IR-1061. Significant work by the Shi group has revealed new insight into IR-780 as a potential theranostic agent.

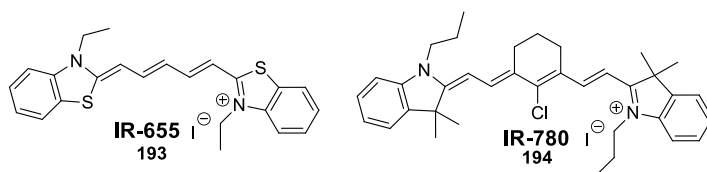


Figure 5.4: Phthalocyanine-based dyes that absorb at 655 and 780 nm

In 2010, Shi and coworkers reported the unexpected accumulation of IR-780 preferentially in tumor cells over normal cells.⁶ When cancer cells were exposed to sulfobromophthalein (BSP), an organic anion transporter peptide (OATP) inhibitor, reduced uptake of IR-780 suggested that cellular uptake was facilitated by OATPs.

Two follow-up studies were reported by Shi and coworkers in 2014. The first focused on the mechanism of IR-780's tumor selective activity and how the dye transcends the tumor cell mitochondria membrane.⁷ Through a series of cell motility inhibitor assays on cancer cell lines, it was determined that preferential accumulation in the mitochondria by IR-780 was dictated by energy metabolism, OATPs, and plasma membrane potential. Inhibition of common modes of

cellular transport like ATP binding-cassette (ABC) transporters and endocytosis did not affect the uptake of IR-780.

An energy dependent pathway was established, due to a cellular response of the dye uptake at low temperature (0 °C). Various cancer cell lines were treated with endocytosis inhibitors Cyto-D and PAO. These inhibitors did not affect the uptake of IR-780 (Scheme 5.5, A), ruling out endocytosis as the mechanism of internalization. However when they treated these same cell lines with different OATP inhibitors (Scheme 5.5, B) they saw suppression of cellular uptake, suggesting that OATPs play a large role in facilitating transport of IR-780 into cancer cells.

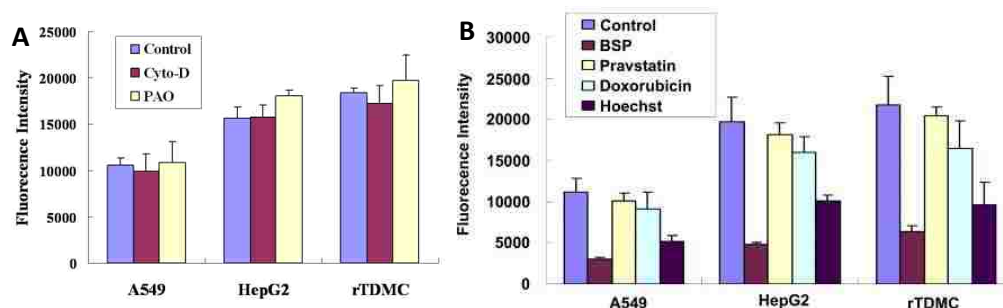


Figure 5.5: Cancer cell lines incubated with IR-780 A) Treated with endocytosis inhibitors: control (blue), with Cyto-D (maroon), PAO (yellow) B) Treated with OATP inhibitors: control (blue), Bromsulphthalein (BSP) (maroon), Pravastatin (yellow), Doxorubicin (light blue), Hoechst 33342 (purple). Reprinted with permission.⁷

The second paper heralded the emergence of IR-780 as anti-tumorigenic.⁸ The Shi group first tested IC_{50} values of IR-780 in different cancer cell lines, noting that longer incubation periods led to smaller IC_{50} values. Lung cancer cell line A549 was most affected by IR-780, so the remaining assays concentrated on this cell line. When drug-resistant A549 cells were treated with IR-780, they established that IR-780 preferentially accumulated in drug resistant (DR) cells (Figure 5.6, A). Once accumulated, the dye was able to prevent further cell proliferation of the

tumor cells, and even prevented tumor recurrence (Figure 5.6, B), with better results than existing anticancer drugs.

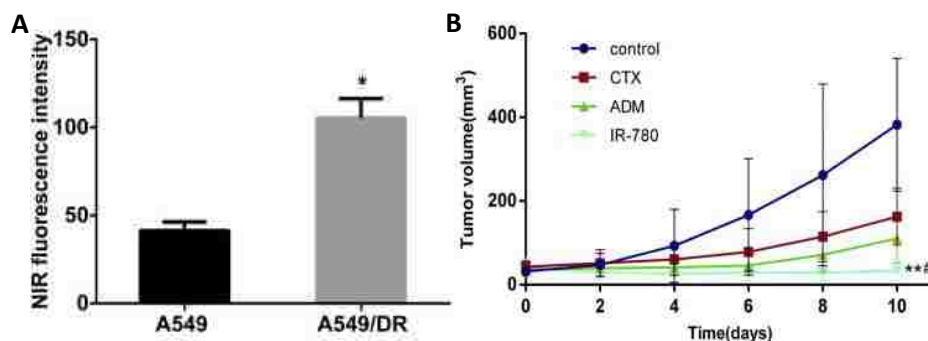
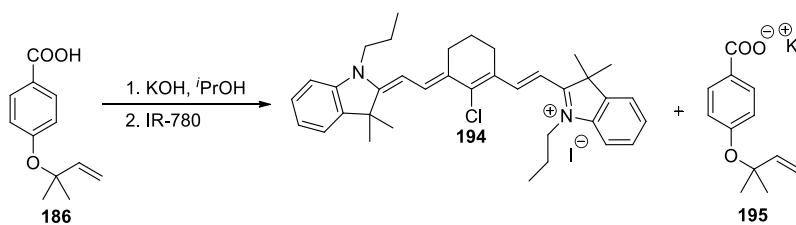


Figure 5.6: A) The uptake of IR-780 and the influence on the mitochondrial activities of A549/DR cells. A549/DR cells exhibit increased staining of IR-780 B) The tumor volume and weight of mice received cyclophosphamide (CTX), doxorubicin hydrochloride (ADM) and IR-780 treatment at dosage of 20, 2.0 and 5.0 mg/kg respectively. Reprinted with permission.⁸

Preliminary tests suggest that IR-780 is biocompatible with no acute toxicity at high dosage (10-fold), and can be safely eliminated from the body in a few days.⁹ With this new information establishing IR-780 as tumorigenic and tumor targeting, IR-780 was chosen as our NIR laser dye for model studies.

5.4.2 Single Solvent Ion Exchange

The ion exchange method was repeated with the new laser dye as described above, with a few changes (Scheme 5.4). Only one solvent was used, thus relying on potassium iodide's low solubility in isopropanol to precipitate out. The solution of potassium salt of the aryl prenyl ether **186** was not concentrated; instead the laser dye was added directly to the solution after thirty minutes.



Scheme 5.4: Single solvent ion exchange of aryl prenyl ether **186** and IR-780 laser dye

Some precipitate was observed after two days, however NMR analysis (Figure 5.7) of the product after aqueous work-up suggests that complete ion exchange did not take place. The ratio of aryl prenyl ether carboxylate **195** to NIR cation **194** was 5:1 (Figure 5.7, C). This incomplete ion exchange was attributed to relative solubility of starting materials. Once the aryl prenyl ether was converted to its potassium salt it became slightly insoluble in isopropanol. IR-780 was also slightly insoluble in isopropanol.

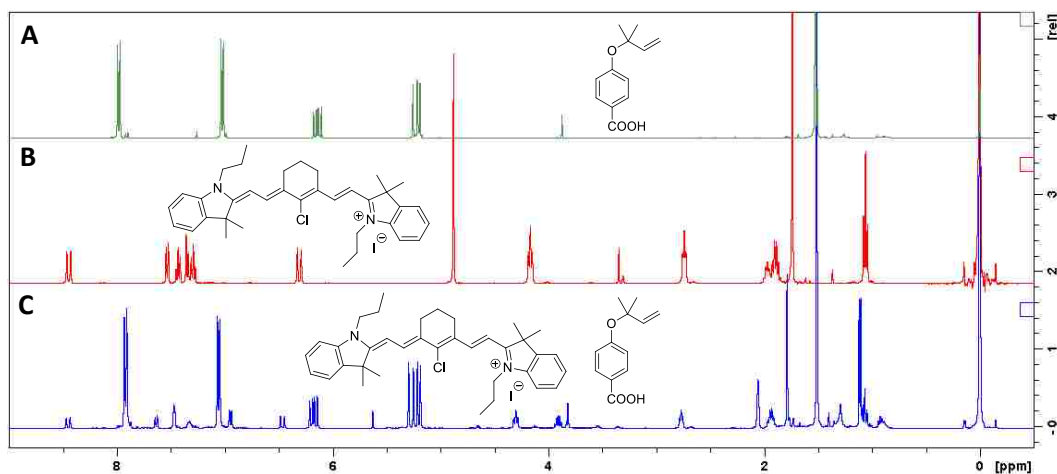


Figure 5.7: ^1H -NMR of aryl prenyl ether **186**, IR-780, and IR-780 based GUMBOS

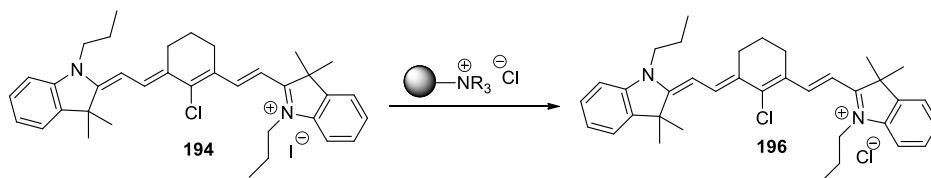
5.4.3 Ion Exchange Resin Chromatography

On the upside, the lack of rearrangement of the aryl prenyl ether under the conditions described in Scheme 5.4 encouraged optimization of single solvent ion exchange conditions for GUMBO formation. Partial insolubility of the starting material prompted a change to ethanol. Potassium iodide is fairly soluble in ethanol; potassium chloride is not. It was impractical to do a

halide ion exchange using the biphasic method as this would not guarantee complete exchange. Ion exchange resins presented a clear way to exchange the halide counter-ion of IR-780.

Ion exchange resins consist of polymeric beads or resin that are covalently bound to tethers, usually quaternary ammonium cations for anion exchange and sulfate anions for cation exchange. When salts are passed through the charged resin, the affinity for certain ions over others will induce an ion exchange. Amberlyst A-26 is a strongly basic, quaternary ammonium based resin designed for non-aqueous applications.

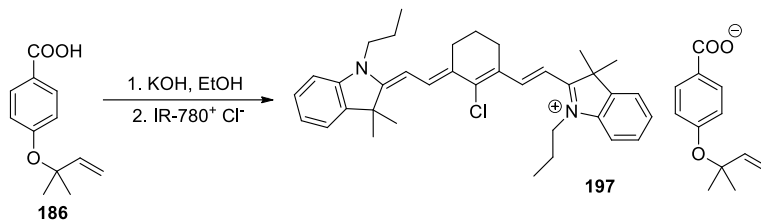
IR-780⁺Cl⁻ was prepared by passing a solution of IR-780⁺I⁻ in methanol through a column that contained A-26, which had been previously treated with an aqueous solution of HCl. The ammonium cation's higher affinity for chlorine ions combined with the hydroxyl anion's basicity ensured complete ion exchange for Cl⁻ ions (Scheme 5.5). Proton NMR of the resulting compound looked identical to the starting material. Mass spectrometry in negative-ion mode confirmed the disappearance of the iodine anion, which was presumably replaced by chlorine. Due to the low molecular weight of chlorine atoms, and lack of instrument sensitivity in that range, chlorine anions cannot be detected by mass spectrometry.



Scheme 5.5: Halide exchange of IR-780 from iodide to chloride anion via ion exchange resin

The single solvent ion exchange method was used with the IR-780⁺Cl⁻ **196**. After addition of chlorinated IR-780 **196**, immediate precipitation was observed. Because of this, the reaction time was reduced to four hours instead of the traditional two days. Proton NMR analysis

revealed a 1:1 ratio of the GUMBOS salt **197** (Scheme 5.6). The prenyl ether carboxylate anion was detected by HRMS.



Scheme 5.6: Single solvent ion exchange of chlorinated IR-780 and DMA aryl ether

Solubility of the IR-780 based GUMBOS in deuterated solvents was limited to methanol, precluding the ability to monitor the disappearance of the carboxylic acid proton as an indicator of deprotonation. Infrared spectroscopic analysis revealed absorption bands at 1602, 1593, 1397, and 1703 cm^{-1} which are consistent with the presence of a carboxylate anion (Figure 5.8, A).

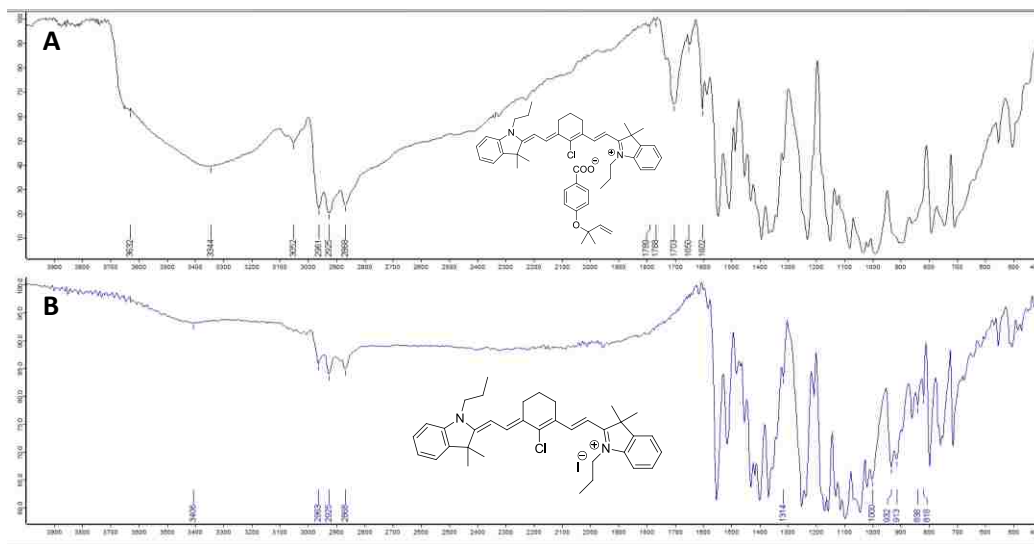


Figure 5.8: FT-IR spectrum of NIR GUMBOS **197** (A) and IR-780 iodide **196** (B)

5.5 Preparation of nanoGUMBOS

NanoGUMBOS can be prepared via the ion diffusion method (Figure 5.9). A solution of bulk GUMBOS is prepared in a volatile solvent that is miscible with water, usually acetone or ethanol. 100 microliters of that solution is injected into five milliliters of water (Figure 5.9, A). This is then sonicated (Figure 5.9, B) using either a sonicating bath or a sonicating probe for a predetermined length of time. The homogenous mixture is stored at room temperature for a minimum of one day to let the nanoparticles “grow” (Figure 5.9, C).

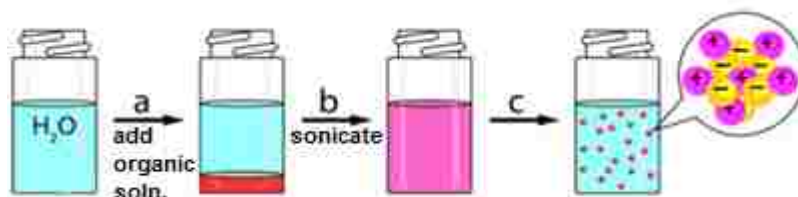


Figure 5.9: Ion diffusion method for making nanoparticles

Preparation of IR-780-based nanoGUMBOS through the reprecipitation method using the sonication probe produced nanoparticles that ranged from 30-50 nm in length (Figure 5.10). Using the sonication bath, 100 nm nanoparticles were formed (Figure 5.11).

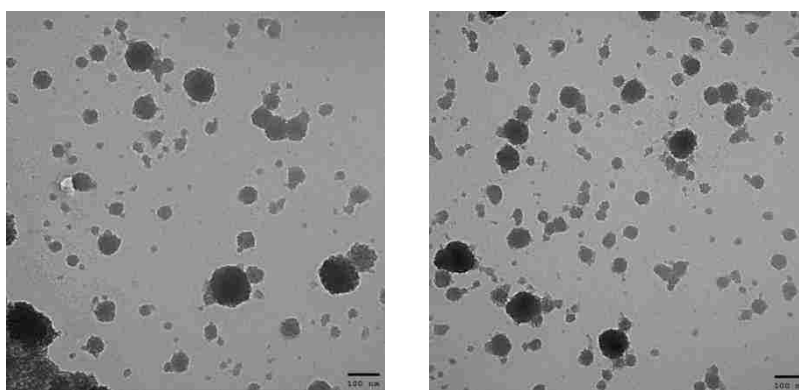


Figure 5.10: nanoGUMBOS prepared using sonication probe with 24 hour crystal growth
These nanoparticles were visualized using transmission electron microscopy (TEM). Aggregation of the nanoparticles became problematic after prolonged growth periods. This could result

from a number of factors including: interaction of the cationic dye with the TEM laser, partial rearrangement of the DMA aryl ether, particles not being redistributed before TEM analysis, and slow nanoparticle growth.

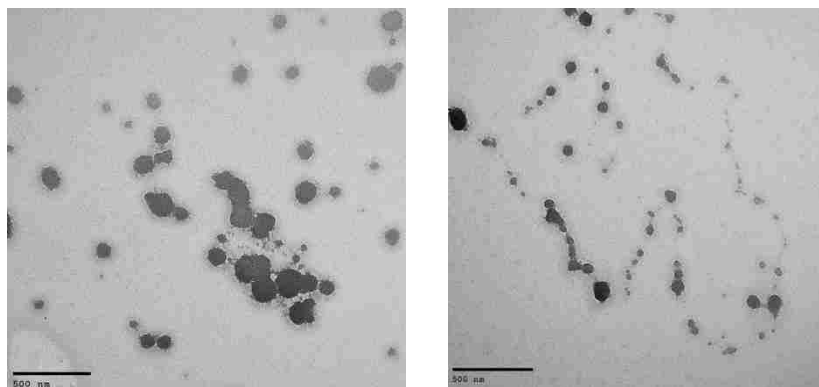
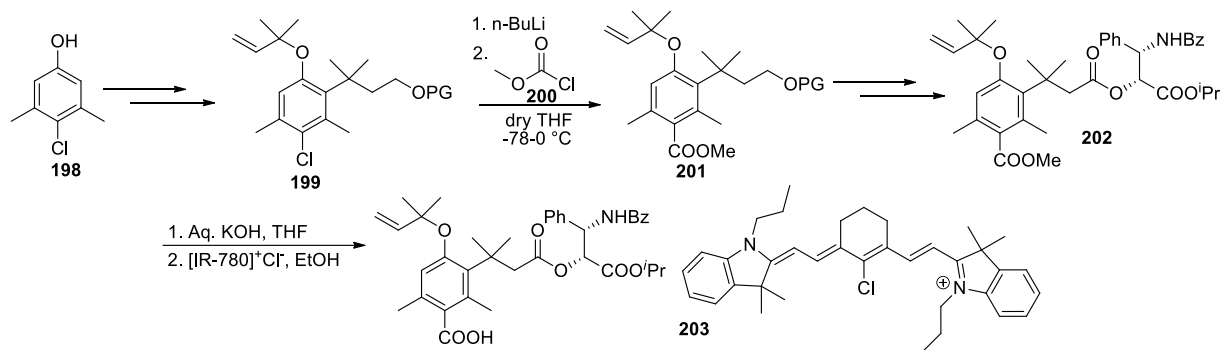


Figure 5.11: NanoGUMBOS prepared using sonication bath with 24 hour crystal growth

Optimization of these conditions, including nanoparticle growth at lower temperatures is currently in progress.

5.6 Future Work

A synthetic route for installing an anionic terminus on to the prodrug model system needs to be explored. Ideally, this would be in place at the outset and carried throughout the synthesis to avoid competing alkylation with the phenyl group in the TaxolTM sidechain. Scheme 5.7 outlines a proposed route to installing an anionic terminus, which would start with a halogen already installed in the *para*-position of 3,5-dimethylphenol (Scheme 5.7, **198**). Synthesis of compound **199** will then follow a series of steps analogous to the preparation of the protected diol **181** in Chapter 4 (Scheme 4.21). With the diol suitably protected, the halogen could then be displaced with methyl chloroformate¹⁰ to give the protected methyl ester **201**. The methyl ester is sturdy, and should be able to survive the remaining chemical transformations.



Scheme 5.7: Synthesis of the 2nd generation NIR GUMBO **203**

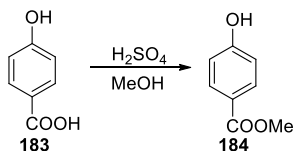
Deprotection of the ether protecting group on the gem-dimethyl substituent *ortho* to the prenyl ether and subsequent oxidation to the acid and coupling to the TaxolTM sidechain alcohol will give us compound **202**. This second generation model system would then be treated with an aqueous solution of potassium hydroxide to cleave the methyl ester. The resulting potassium salt will be converted to the ion pair with IR-780⁺I⁻ through ion exchange resin chromatography to give NIR GUMBO **203**.

In summary, we have described the synthesis of a trimethyl lock-based prodrug delivery model system that incorporated the TaxolTM amido alcohol sidechain as a model for the drug, and utilized an aryl Claisen rearrangement as the molecular trigger. We investigated the thermal rearrangement of the model system, and identified 1,1-dimethyl allyl ether as a rate-accelerating group for Claisen rearrangements. This group effectively lowers the temperature required for rearrangement to more biologically feasible temperatures. We have also demonstrated effective ionic pairing of prenyl aryl ethers to cationic NIR laser dye IR-780.

5.7 Experimental Section

General Methods: All reactions were performed under a dry nitrogen atmosphere unless otherwise noted. All chemicals and reagents were purchased from Sigma-Aldrich and Fisher and were used without further purification. Flash chromatography was performed using 230-400 mesh silica gel (40-63 μm) from Sigma-Aldrich. Reactions were followed by thin layer chromatography (TLC) on pre-coated aluminum-backed 60 F254 silica plates from EMD Chemicals, Inc. Compounds were visualized under UV fluorescence or by staining with KMnO_4 . ^1H and ^{13}C NMR spectra were recorded at room temperature on a Bruker AV-400 or Bruker Nanobay-400 and are reported in parts per million (ppm) on the δ scale relative to residual CHCl_3 or CH_3OH in deuterated solvents or tetramethylsilane as an internal standard. Coupling constants (J) are reported in Hertz (Hz). High resolution mass spectrometry (HRMS) was carried out using an Agilent 6210 electrospray ionization-time-of-flight (ESI-TOF) mass spectrometer.

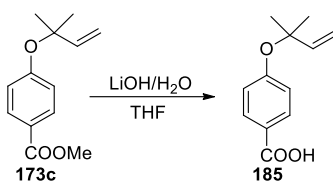
5.7.1 Procedures



Scheme 5.8: Synthesis of compound **184**

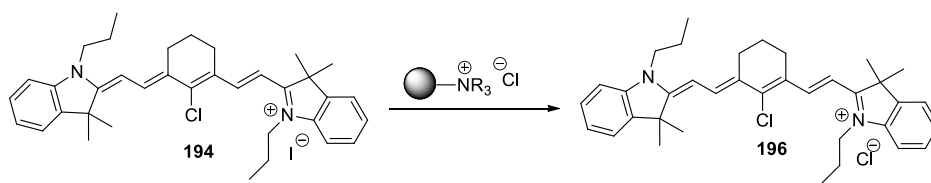
Methyl 4-hydroxybenzoate (**184**).¹¹ Concentrated H_2SO_4 (0.5 mL) was added to a suspension of 4-hydroxybenzoic acid (**183**) (500 mg, 3.62 mmol, 1.0 equiv.) in MeOH (3.3 mL), and the solution was heated at reflux for 1 h. After cooling to rt, aq. 1M NaOH (~2-3 mL) was added to neutralize the solution. The mixture was allowed to stand for 15 minutes to allow for maximum precipitation. The mixture was poured into a beaker, where cool water (0 $^\circ\text{C}$) for a total volume of 85 mL. The colorless precipitate was collected by filtration was filtered and dried to give

methyl 4-hydroxybenzoate (343 mg, 62%). Additional product was recovered by extracting the aqueous solution with EtOAc (3 x 20 mL). The organic extracts were combined, dried over MgSO₄, filtered, and concentrated to give a combined yield of 413 mg (75%). *R_f* 0.15 (3:1 Hexanes-EtOAc). ¹H-NMR (400 MHz, CD₃OD) δ 3.84 (s, 3H, OMe), 6.82 (d, *J* = 8.6 Hz, 2H, Ar-H), 7.87 (d, *J* = 8.6 Hz, 2H, Ar-H); ¹³C-NMR (100 MHz, CD₃OD) δ 50.8, 114.7, 120.8, 131.3, 162.1, 167.3.



Scheme 5.9: Synthesis of compound **186**

Aryl prenyl ether (**185**).¹² A solution of LiOH (0.44 mg, 1.85 mmol, 1.8 equiv.) in H₂O (1.23 mL, 1.5 M) was added to a solution of **173c** (222 mg, 1.01 mmol, 1.0 equiv.) in THF/H₂O (3:1, 18 mL) and was stirred at rt overnight. Water (4.5 mL) was added, and the solution concentrated to remove the THF. The solution was acidified to pH 6 by the dropwise addition of 1 M HCl (10 mL) and extracted with EtOAc (3 x 20 mL). The combined organic layers were washed with brine (20 mL), dried over MgSO₄, filtered and concentrated. The residue was purified on silica gel eluting with 5:1 hexanes:EtOAc → 1:1 Hexanes:EtOAc to give a colorless solid (104 mg, 50%). *R_f* 0.15 (3:1 Hexanes-EtOAc). ¹H-NMR (400 MHz, CDCl₃) δ 1.53 (s, 6H, CH₃x2), 5.20 (d, *J* = 10.8 Hz, 1H, HC=CH₂), 5.23 (d, *J* = 17.5 Hz, 1H, HC=CH₂), 6.14 (dd, *J* = 17.6, 10.9 Hz, 1H, CH=CH₂), 7.02 (d, *J* = 8.8 Hz, 2H, Ar-H), 7.98 (d, *J* = 8.8 Hz, 2H, Ar-H); ¹³C-NMR (100 MHz, CDCl₃) δ 27.2, 80.4, 114.1, 119.5, 122.0, 131.7, 143.8, 161.4, 172.2.



Scheme 5.10: Preparation of IR-780⁺Cl⁻ through ion exchange chromatography

IR-780⁺Cl⁻ (**196**).¹³ A glass column (1 cm diameter) was packed with 1.25 g of Amberlyst A-26. The resin was washed with water (12.5 mL). The solvent bed was then progressively equilibrated with H₂O-MeOH mixtures, starting with 75% H₂O-25% and increasing the MeOH content in 25% increments until reaching 100% MeOH. A 1% solution of HCl in MeOH was passed through the resin until the eluents had the same pH as the acid solution (1.3 pH). The resin was washed with MeOH until a constant pH was observed. A solution of IR-780⁺I⁻ (0.08 mmol) in 5 mL of MeOH was passed slowly through the resin with no external pressure. The resin was washed with MeOH until all dye had eluted off the resin. The eluent was collected and concentrated to give IR-780⁺I⁻ in 95% yield. ¹H-NMR (400 MHz, MeOD) δ 1.06 (t, 6H, Pr-CH₃), 1.73 (s, 12H, CMe₂), 1.89 (sext., *J* = 7.1 Hz, 4H, CH₂CH₃), 1.96 (t, *J* = 5.6 Hz, 2H, CH₂CH₂C=CCl), 2.73 (t, *J* = 6.0 Hz, 4H, CH₂C=CCl), 4.17 (t, *J* = 7.0 Hz, 4H, CH₂N), 6.31 (d, *J* = 14.1 Hz, 2H, =CH-C=N), 7.29 (t, *J* = 7.3 Hz, 2H, Ar-H), 7.35 (d, *J* = 7.8 Hz, 2H, Ar-H), 7.43 (t, *J* = 7.5 Hz, 2H, Ar-H), 7.53 (d, *J* = 7.3 Hz, 2H, Ar-H), 8.44 (d, *J* = 14.1 Hz, 2H, Ar-H); ¹³C-NMR (100 MHz, CDCl₃) δ 10.3, 20.5, 25.9, 27.0, 45.3, 49.3, 101.0, 111.0, 122.1, 125.2, 126.5, 128.5, 141.2, 142.3, 144.1, 149.7, 173.0.

Integration Data

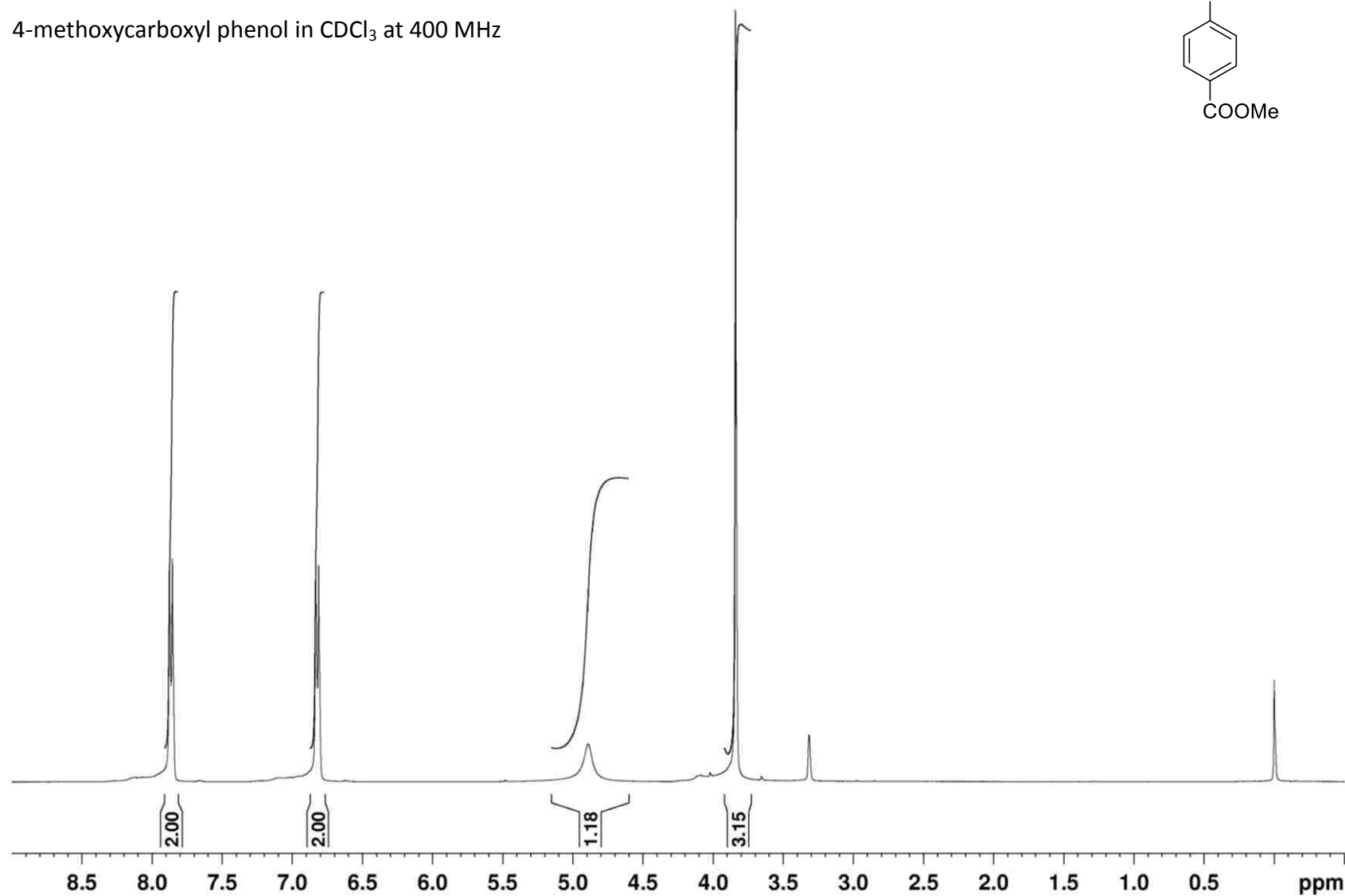
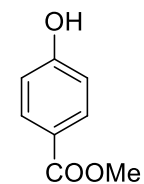
Time (in h)	<i>p</i> -COOH	m-3,5-dimethyl	<i>p</i> -COOMe	<i>p</i> -OMe
Ar-H _a '-Integration				
0	0	0	0	0
0.5	0.6154	0.0877	0.0559	0.1597
1.0	1.8544	0.151	0.1243	0.1243
1.5	3.2763	0.3011	0.1924	0.1924
2.0	5.217	0.4722	0.2654	0.2654
2.5	7.5215	0.6421	0.3455	0.3455
3.0	11.7917	0.8008	0.4126	0.4126
3.5	16.8133	0.973	0.5043	0.5043
4.0	31.8337	1.1925	0.65	0.65
4.5	42.1926	1.476	0.754	0.754
5.0	74.0698	1.7034	0.8542	0.8542
5.5		1.9284	0.9807	0.9807

Reference peak set at 6 for compound **185**, and 1 for compounds **173b**, **173c**, **168** and stayed constant

5.7.2 ^1H and ^{13}C - NMR Spectra

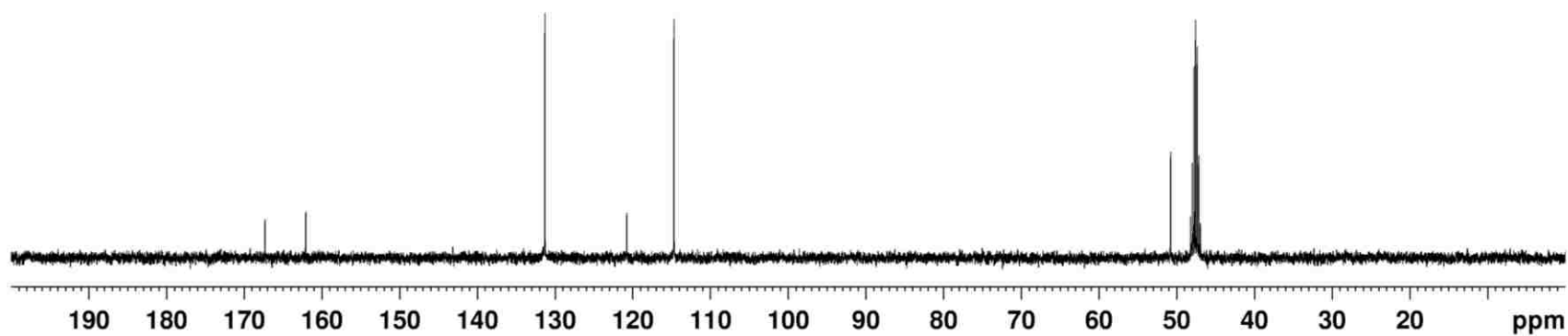
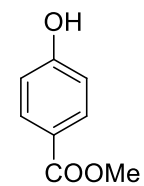
Compound **184** (Scheme 5.1) – ^1H -NMR spectrum

4-methoxycarboxyl phenol in CDCl_3 at 400 MHz



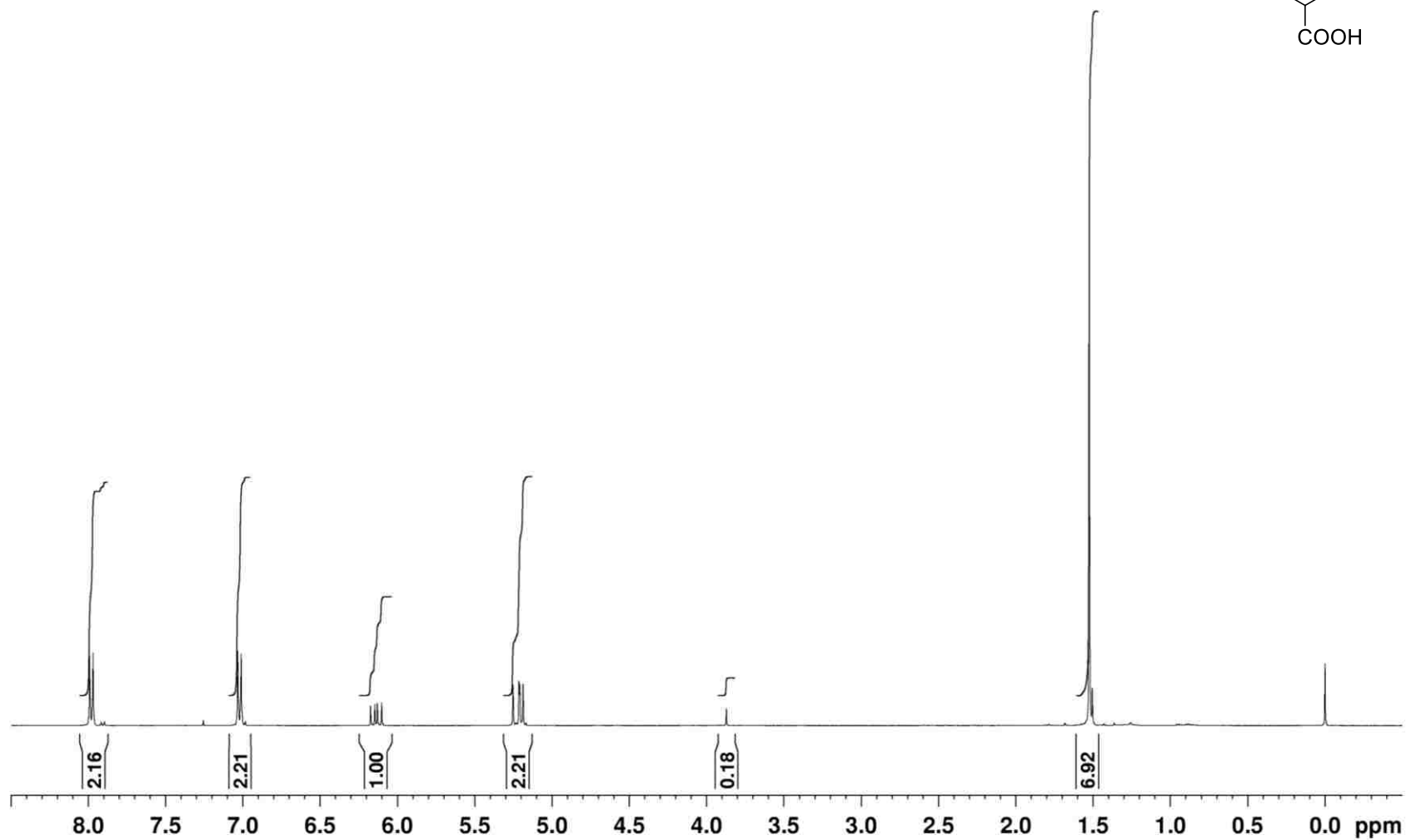
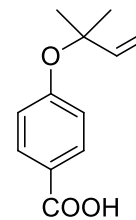
Compound **184** (Scheme 5.1) – ^{13}C -NMR spectrum

4-methoxycarboxyl phenol in CDCl_3 at 100 MHz



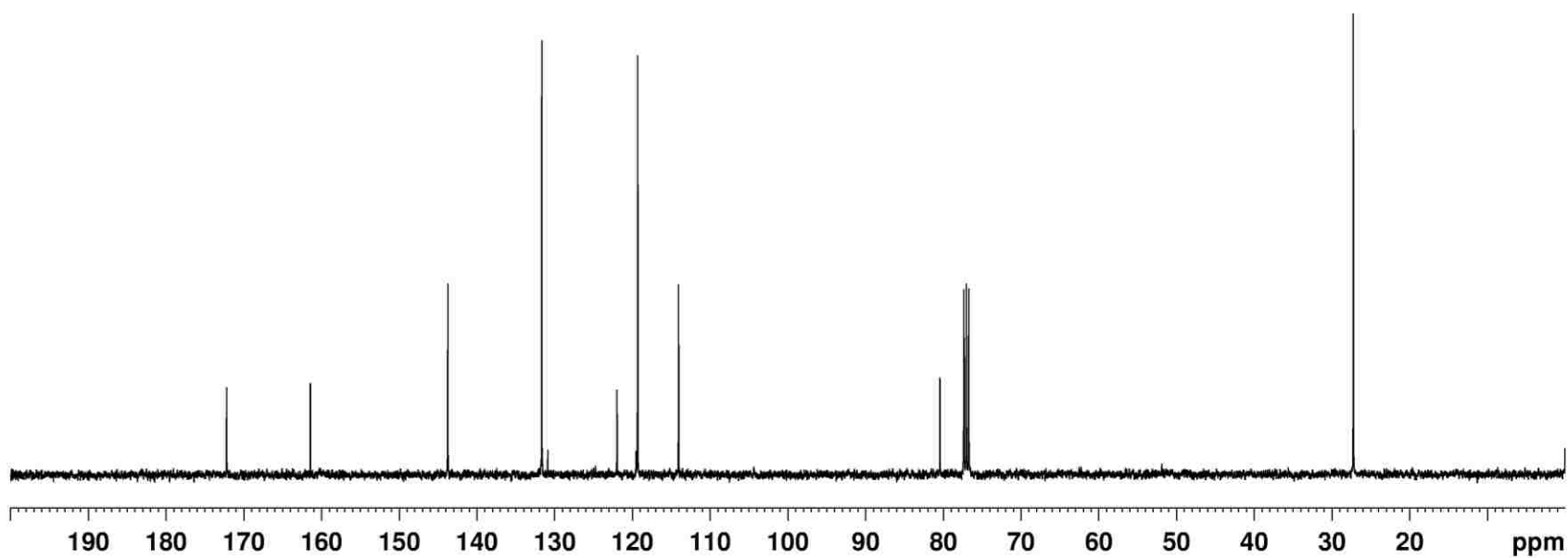
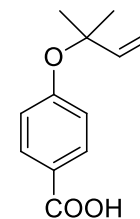
Compound **185** (Scheme 5.1) – ^1H -NMR spectrum

Prenyl *p*-COOH phenyl ether in CDCl_3 at 400 MHz



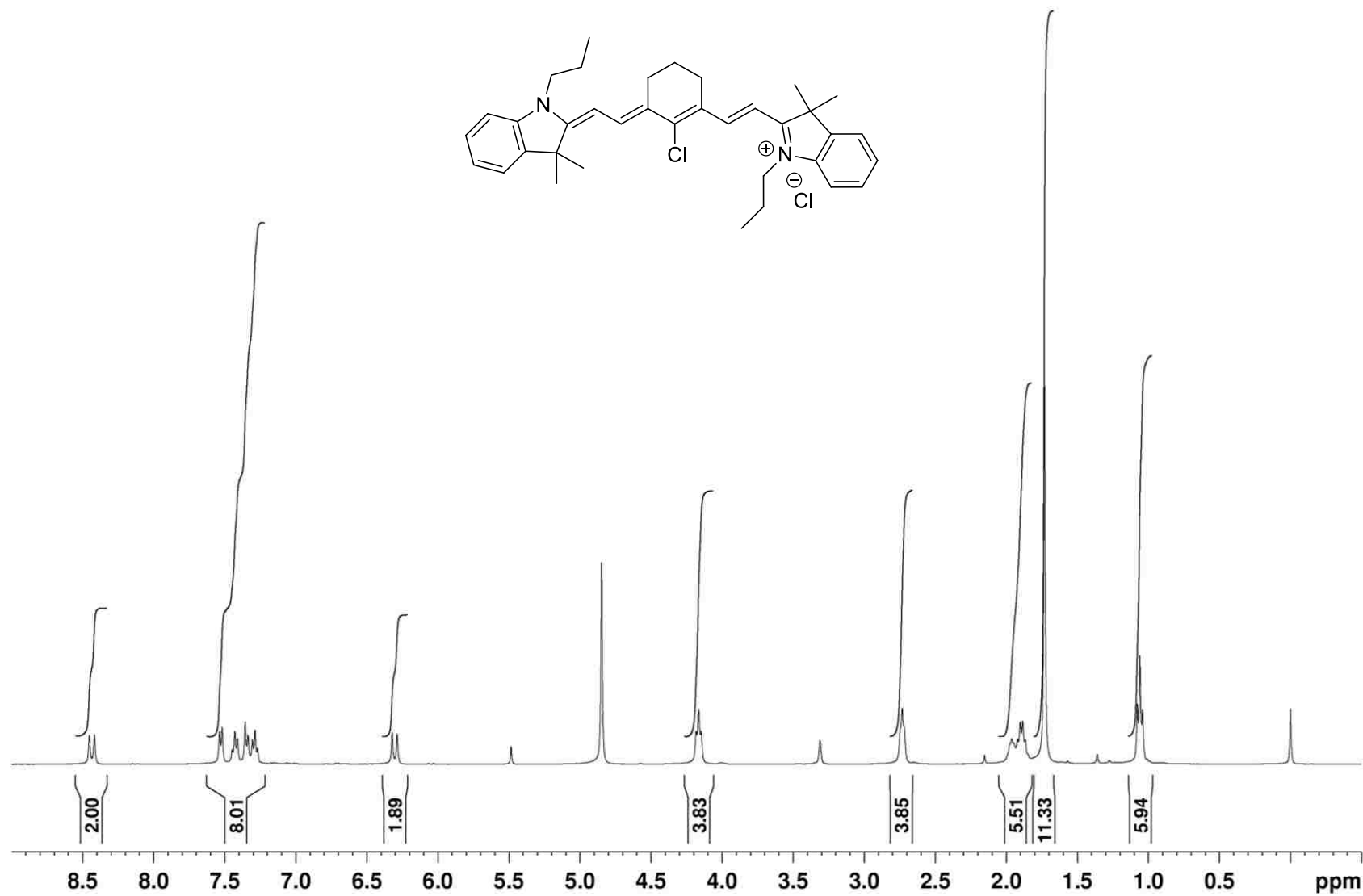
Compound **185** (Scheme 5.1) – ^{13}C -NMR spectrum

Prenyl *p*-COOH phenyl ether in CDCl_3 at 100 MHz



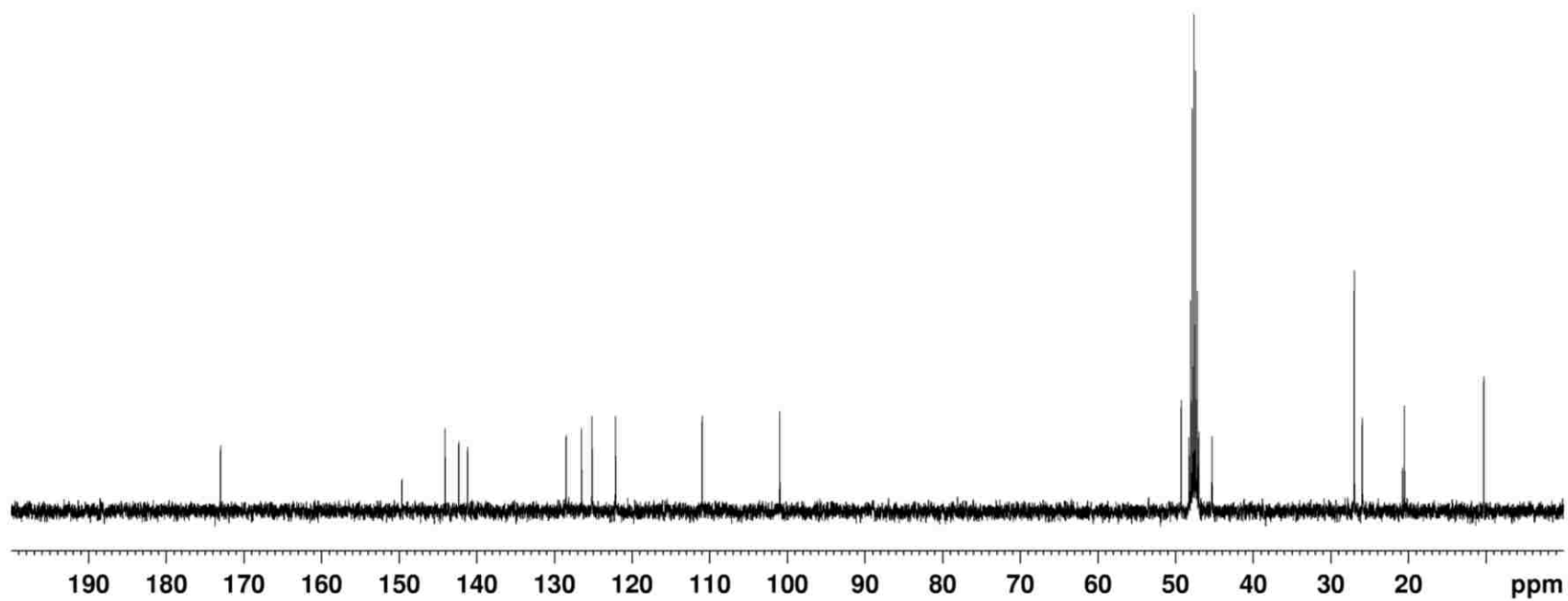
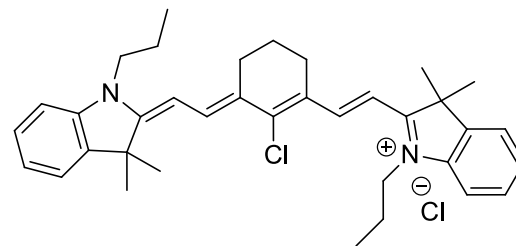
Compound **196** (Scheme 5.5) – $^1\text{H-NMR}$ spectrum

$[\text{IR-780}]^+\text{Cl}^-$ in MeOD at 400 MHz



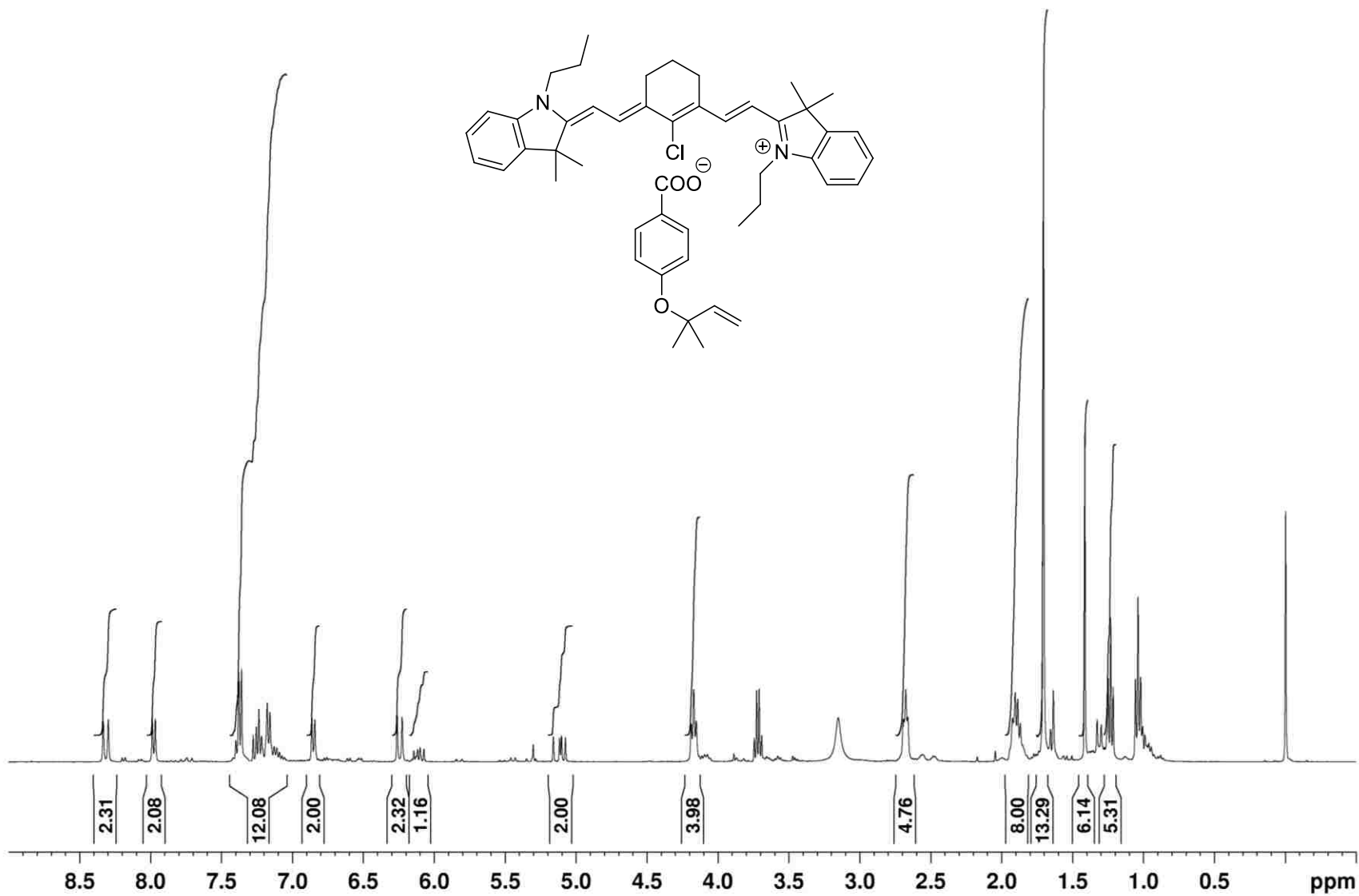
Compound **196** (Scheme 5.5) – ^{13}C -NMR spectrum

$[\text{IR-780}]^+\text{Cl}^-$ in MeOD at 100 MHz



Compound **197** (Scheme 5.6) – $^1\text{H-NMR}$ spectrum

$[\text{IR-780}]^+[\text{Prenyl } p\text{-COOH phenyl ether}]^-$ in CDCl_3 at 400 MHz



5.8 References

1. Zugenmaier, P. "Review of crystalline structures of some selected homologous series of rod-like molecules capable of forming liquid crystalline phases" *Int.J.Mol.Sci.* **2011**, *12*, 7360-7400.
2. Harfenist, M.; Thom, E. "Influence of structure on the rate of thermal rearrangement of aryl propargyl ethers to the chromenes. Gem-dimethyl effect" *J. Org. Chem.* **1972**, *37*, 841-848.
3. White, W. N., Gwynn, D., Schlitt, R., Girard, C., Fife, W. "The ortho-Claisen rearrangement. I. The effect of substituents on the rearrangement of allyl *p*-X-phenyl ethers" *J. Am. Chem. Soc.* **1958**, *80*, 3271-3277.
4. Osuna, S., Kim, S., Bollot, G., Houk, K. N. "Aromatic Claisen rearrangements of *o*-prenylated tyrosine and model prenyl aryl ethers: Computational study of the role of water on acceleration of Claisen rearrangements" *Eur. J. Org. Chem.* **2013**, 2823-2832.
5. Luo, S., Zhang, E., Su, Y., Cheng, T., Shi, C. "A review of NIR dyes in cancer targeting and imaging" *Biomaterials* **2011**, *32*, 7127-7138.
6. Zhang, C., Liu, T., Su, Y., Luo, S., Zhu, Y., Tan, X., Fan, S., Zhang, L., Zhou, Y., Cheng, T., Shi, C. "A near-infrared fluorescent heptamethine indocyanine dye with preferential tumor accumulation for in vivo imaging" *Biomaterials* **2010**, *31*, 6612-6617.
7. Zhang, E., Luo, S., Tan, X., Shi, C. "Mechanistic study of IR-780 dyes as a potential tumor targeting and drug delivery agent" *Biomaterials* **2014**, *35*, 771-778.
8. Wang, Y., Liu, T., Zhang, E., Luo, S., Tan, X., Shi, C. "Preferential accumulation of the near infrared heptamethine dye IR-780 in the mitochondria of drug-resistant lung cancer cells" *Biomaterials* **2014**, *35*, 4116-4124.
9. Zhang, C., Wang, S., Xiao, J., Tan, X., Zhu, Y., Su, Y., "Sentinel lymph node mapping by a near-infrared fluorescent heptamethine dye" *Biomaterials* **2010**, *31*, 1911-1917.
10. Jiang, C-S., Zhou, R., Gong, J-X., Chen, L-L., Kurtan, T., Shen, X., Guo, Y-W. "Synthesis, modification, and evaluation of (R)-de-O-methylsalsolidin and analogs as nonsteroidal antagonists of mineralocorticoid receptor" *Bioorg. Med. Chem. Lett.* **2011**, *21*, 1171-1175.
11. Ahmed, S., James, K., Owen, C. P. "Inhibition of estrone sulfatase (ES) by derivatives of 4-[(aminosulfonyl)oxy] benzoic acid" *Bioorg. Med. Chem. Lett.* **2012**, *12*, 2391-2394.
12. Wipf, P., Uto, Y. "Total synthesis and revision of stereochemistry of the marine metabolite Trunkamide A" *J. Org. Chem.* **2000**, *65*, 1037-1049.
13. Cai, D-N., Huang, K., Chen, Y-L., Hu, X-B., Wu, Y-T. "Systematic study on the general preparation of ionic liquids with high purity via hydroxide intermediates" *Ind. Eng. Chem. Res.* **2014**, *53*, 6871-6880.

APPENDIX

Letters of Permission

10/6/2014

Society for Applied Spectroscopy Mail - Re: Thesis Permission



Bonnie Saylor <exdir@s-a-s.org>

Re: Thesis Permission

1 message

C. Batton <chyree.batton@gmail.com>
To: Bonnie Saylor <exdir@s-a-s.org>

Mon, Oct 6, 2014 at 1:02 PM

Hi Bonnie,

Thank you for your help. The information you requested is provided below:

Title: Photothermal Response of Near-Infrared-Absorbing NanoGUMBOS
Applied Spectroscopy, Volume 68, Issue 3, Pages 340-352

I am requesting to use Figure 10a on pg 348, and Figure 11a on pg 348

If you need more information please let me know.

On Mon, Oct 6, 2014 at 9:48 AM, Bonnie Saylor <exdir@s-a-s.org> wrote:

Dear Ms. Batton,

Thank you for your request for permission from the Society for Applied Spectroscopy. In order to process your request I will need the figure numbers, page numbers, journal issue etc. I will then be able to approve your request.

Regards,

Bonnie Saylor
Executive Director
Society for Applied Spectroscopy

Bonnie Saylor
Executive Director
Society for Applied Spectroscopy
5320 Spectrum Drive
Suite C
Frederick, MD 21703
301-694-8122
www.s-a-s.org



Permission granted for the use requested.
Granted this 6th day of Oct. 2014.
Full citation required.

Bonnie Saylor
Bonnie Saylor, Executive Director, SAS

On Mon, Oct 6, 2014 at 10:45 AM, Stephanie Iocco <sasadmin@s-a-s.org> wrote:

----- Forwarded message -----

From: "C. Batton" <chyree.batton@gmail.com>
Date: Oct 5, 2014 4:09 PM
Subject: Thesis Permission
To: <sasadmin@s-a-s.org>
Cc:

Hello,

I am currently writing my dissertation and want to use two figures from a paper that was published in my co-advisor's group titled "Photothermal response of near-infrared-absorbing NanoGUMBOS". I was using the online tool to request permission, but the end price said \$108. I have requested permission from other journals and have not had to pay as long as I am requesting permission for reuse in a thesis/dissertation. Is

<https://mail.google.com/mail/u/0/?ui=2&ik=fe151736fd&view=pt&search=inbox&type=148dcb485a168f&th=148e669f6d46597a&siml=148e669f6d46...> 1/2

**JOHN WILEY AND SONS LICENSE
TERMS AND CONDITIONS**

Oct 03, 2014

This is a License Agreement between Chyree S Batton ("You") and John Wiley and Sons ("John Wiley and Sons") provided by Copyright Clearance Center ("CCC"). The license consists of your order details, the terms and conditions provided by John Wiley and Sons, and the payment terms and conditions.

All payments must be made in full to CCC. For payment instructions, please see information listed at the bottom of this form.

License Number	3481160139251
License date	Oct 03, 2014
Licensed content publisher	John Wiley and Sons
Licensed content publication	CA: Cancer Journal for Clinicians
Licensed content title	Cancer Statistics, 2005
Licensed copyright line	Copyright © 2005 American Cancer Society
Licensed content author	Ahmedin Jemal,Taylor Murray,Elizabeth Ward,Alicia Samuels,Ram C. Tiwari,Asma Ghafoor,Eric J. Feuer,Michael J. Thun
Licensed content date	Feb 24, 2009
Start page	10
End page	30
Type of use	Dissertation/Thesis
Requestor type	University/Academic
Format	Print and electronic
Portion	Figure/table
Number of figures/tables	1
Original Wiley figure/table number(s)	Figure 1
Will you be translating?	No
Order reference number	4
Title of your thesis / dissertation	Synthetic Routes to Therapeutic Agents via Masked Functionalities: From Orthogonal Peptide Crosslink to Photothermal Cancer Prodrug
Expected completion date	Dec 2014
Expected size (number of pages)	250
Total	0.00 USD
Terms and Conditions	

**ELSEVIER LICENSE
TERMS AND CONDITIONS**

Oct 03, 2014

This is a License Agreement between Chyree S Batton ("You") and Elsevier ("Elsevier") provided by Copyright Clearance Center ("CCC"). The license consists of your order details, the terms and conditions provided by Elsevier, and the payment terms and conditions.

All payments must be made in full to CCC. For payment instructions, please see information listed at the bottom of this form.

Supplier	Elsevier Limited The Boulevard, Langford Lane Kidlington, Oxford, OX5 1GB, UK
Registered Company Number	1982084
Customer name	Chyree S Batton
Customer address	464 E. Boyd Dr. BATON ROUGE, LA 70808
License number	3481150634033
License date	Oct 03, 2014
Licensed content publisher	Elsevier
Licensed content publication	Nanomedicine: Nanotechnology, Biology and Medicine
Licensed content title	Nanomaterials in combating cancer: Therapeutic applications and developments
Licensed content author	Samina Nazir, Tajammul Hussain, Attiya Ayub, Umer Rashid, Alexander John MacRobert
Licensed content date	January 2014
Licensed content volume number	10
Licensed content issue number	1
Number of pages	16
Start Page	19
End Page	34
Type of Use	reuse in a thesis/dissertation
Intended publisher of new work	other
Portion	figures/tables/illustrations
Number of figures/tables/illustrations	2

Format	both print and electronic
Are you the author of this Elsevier article?	No
Will you be translating?	No
Order reference number	3
Title of your thesis/dissertation	Synthetic Routes to Therapeutic Agents via Masked Functionalities: From Orthogonal Peptide Crosslink to Photothermal Cancer Prodrug
Expected completion date	Dec 2014
Estimated size (number of pages)	250
Elsevier VAT number	GB 494 6272 12
Permissions price	0.00 USD
VAT/Local Sales Tax	0.00 USD / 0.00 GBP
Total	0.00 USD
Terms and Conditions	

INTRODUCTION

1. The publisher for this copyrighted material is Elsevier. By clicking "accept" in connection with completing this licensing transaction, you agree that the following terms and conditions apply to this transaction (along with the Billing and Payment terms and conditions established by Copyright Clearance Center, Inc. ("CCC"), at the time that you opened your Rightslink account and that are available at any time at <http://myaccount.copyright.com>).

GENERAL TERMS

2. Elsevier hereby grants you permission to reproduce the aforementioned material subject to the terms and conditions indicated.

3. Acknowledgement: If any part of the material to be used (for example, figures) has appeared in our publication with credit or acknowledgement to another source, permission must also be sought from that source. If such permission is not obtained then that material may not be included in your publication/copies. Suitable acknowledgement to the source must be made, either as a footnote or in a reference list at the end of your publication, as follows:

“Reprinted from Publication title, Vol /edition number, Author(s), Title of article / title of chapter, Pages No., Copyright (Year), with permission from Elsevier [OR APPLICABLE SOCIETY COPYRIGHT OWNER].” Also Lancet special credit - “Reprinted from The Lancet, Vol. number, Author(s), Title of article, Pages No., Copyright (Year), with permission from Elsevier.”

4. Reproduction of this material is confined to the purpose and/or media for which permission is hereby given.

5. Altering/Modifying Material: Not Permitted. However figures and illustrations may be altered/adapted minimally to serve your work. Any other abbreviations, additions, deletions and/or any other alterations shall be made only with prior written authorization of Elsevier Ltd. (Please

**ELSEVIER LICENSE
TERMS AND CONDITIONS**

Oct 03, 2014

This is a License Agreement between Chyree S Batton ("You") and Elsevier ("Elsevier") provided by Copyright Clearance Center ("CCC"). The license consists of your order details, the terms and conditions provided by Elsevier, and the payment terms and conditions.

All payments must be made in full to CCC. For payment instructions, please see information listed at the bottom of this form.

Supplier	Elsevier Limited The Boulevard,Langford Lane Kidlington,Oxford,OX5 1GB,UK
Registered Company Number	1982084
Customer name	Chyree S Batton
Customer address	464 E. Boyd Dr. BATON ROUGE, LA 70808
License number	3481141442750
License date	Oct 03, 2014
Licensed content publisher	Elsevier
Licensed content publication	Biomaterials
Licensed content title	Mechanistic study of IR-780 dye as a potential tumor targeting and drug delivery agent
Licensed content author	Erlong Zhang,Shenglin Luo,Xu Tan,Chunmeng Shi
Licensed content date	January 2014
Licensed content volume number	35
Licensed content issue number	2
Number of pages	8
Start Page	771
End Page	778
Type of Use	reuse in a thesis/dissertation
Intended publisher of new work	other
Portion	figures/tables/illustrations
Number of figures/tables/illustrations	2
Format	both print and electronic

Are you the author of this Elsevier article?	No
Will you be translating?	No
Order reference number	2
Title of your thesis/dissertation	Synthetic Routes to Therapeutic Agents via Masked Functionalities: From Orthogonal Peptide Crosslink to Photothermal Cancer Prodrug
Expected completion date	Dec 2014
Estimated size (number of pages)	250
Elsevier VAT number	GB 494 6272 12
Permissions price	0.00 USD
VAT/Local Sales Tax	0.00 USD / 0.00 GBP
Total	0.00 USD
Terms and Conditions	

INTRODUCTION

1. The publisher for this copyrighted material is Elsevier. By clicking "accept" in connection with completing this licensing transaction, you agree that the following terms and conditions apply to this transaction (along with the Billing and Payment terms and conditions established by Copyright Clearance Center, Inc. ("CCC"), at the time that you opened your Rightslink account and that are available at any time at <http://myaccount.copyright.com>).

GENERAL TERMS

2. Elsevier hereby grants you permission to reproduce the aforementioned material subject to the terms and conditions indicated.

3. Acknowledgement: If any part of the material to be used (for example, figures) has appeared in our publication with credit or acknowledgement to another source, permission must also be sought from that source. If such permission is not obtained then that material may not be included in your publication/copies. Suitable acknowledgement to the source must be made, either as a footnote or in a reference list at the end of your publication, as follows:

“Reprinted from Publication title, Vol /edition number, Author(s), Title of article / title of chapter, Pages No., Copyright (Year), with permission from Elsevier [OR APPLICABLE SOCIETY COPYRIGHT OWNER].” Also Lancet special credit - “Reprinted from The Lancet, Vol. number, Author(s), Title of article, Pages No., Copyright (Year), with permission from Elsevier.”

4. Reproduction of this material is confined to the purpose and/or media for which permission is hereby given.

5. Altering/Modifying Material: Not Permitted. However figures and illustrations may be altered/adapted minimally to serve your work. Any other abbreviations, additions, deletions and/or any other alterations shall be made only with prior written authorization of Elsevier Ltd. (Please contact Elsevier at permissions@elsevier.com)

**ELSEVIER LICENSE
TERMS AND CONDITIONS**

Oct 03, 2014

This is a License Agreement between Chyree S Batton ("You") and Elsevier ("Elsevier") provided by Copyright Clearance Center ("CCC"). The license consists of your order details, the terms and conditions provided by Elsevier, and the payment terms and conditions.

All payments must be made in full to CCC. For payment instructions, please see information listed at the bottom of this form.

Supplier	Elsevier Limited The Boulevard, Langford Lane Kidlington, Oxford, OX5 1GB, UK
Registered Company Number	1982084
Customer name	Chyree S Batton
Customer address	464 E. Boyd Dr. BATON ROUGE, LA 70808
License number	3481141085691
License date	Oct 03, 2014
Licensed content publisher	Elsevier
Licensed content publication	Biomaterials
Licensed content title	Preferential accumulation of the near infrared heptamethine dye IR-780 in the mitochondria of drug-resistant lung cancer cells
Licensed content author	Yang Wang, Tao Liu, Erlong Zhang, Shenglin Luo, Xu Tan, Chunmeng Shi
Licensed content date	April 2014
Licensed content volume number	35
Licensed content issue number	13
Number of pages	9
Start Page	4116
End Page	4124
Type of Use	reuse in a thesis/dissertation
Portion	figures/tables/illustrations
Number of figures/tables/illustrations	2
Format	both print and electronic
Are you the author of this	No

Elsevier article?

Will you be translating? No

Order reference number 1

Title of your thesis/dissertation Synthetic Routes to Therapeutic Agents via Masked Functionalities: From Orthogonal Peptide Crosslink to Photothermal Cancer Prodrug

Expected completion date Dec 2014

Estimated size (number of pages) 250

Elsevier VAT number GB 494 6272 12

Permissions price 0.00 USD

VAT/Local Sales Tax 0.00 USD / 0.00 GBP

Total 0.00 USD

Terms and Conditions

INTRODUCTION

1. The publisher for this copyrighted material is Elsevier. By clicking "accept" in connection with completing this licensing transaction, you agree that the following terms and conditions apply to this transaction (along with the Billing and Payment terms and conditions established by Copyright Clearance Center, Inc. ("CCC"), at the time that you opened your Rightslink account and that are available at any time at <http://myaccount.copyright.com>).

GENERAL TERMS

2. Elsevier hereby grants you permission to reproduce the aforementioned material subject to the terms and conditions indicated.

3. Acknowledgement: If any part of the material to be used (for example, figures) has appeared in our publication with credit or acknowledgement to another source, permission must also be sought from that source. If such permission is not obtained then that material may not be included in your publication/copies. Suitable acknowledgement to the source must be made, either as a footnote or in a reference list at the end of your publication, as follows:

“Reprinted from Publication title, Vol /edition number, Author(s), Title of article / title of chapter, Pages No., Copyright (Year), with permission from Elsevier [OR APPLICABLE SOCIETY COPYRIGHT OWNER].” Also Lancet special credit - “Reprinted from The Lancet, Vol. number, Author(s), Title of article, Pages No., Copyright (Year), with permission from Elsevier.”

4. Reproduction of this material is confined to the purpose and/or media for which permission is hereby given.

5. Altering/Modifying Material: Not Permitted. However figures and illustrations may be altered/adapted minimally to serve your work. Any other abbreviations, additions, deletions and/or any other alterations shall be made only with prior written authorization of Elsevier Ltd. (Please contact Elsevier at permissions@elsevier.com)

VITA

Chyree S. Batton was born in the spring of 1987 in Fort Sill, Oklahoma. She lived in several places after that, including Germany, before settling down in Louisville, Kentucky, where she lived until she was 18. It was shortly after her aunt died, that she realized she had a passion for chemistry. This love wasn't fully realized until she left Kentucky to attend Spelman College in Atlanta, Georgia where she studied chemistry and received her Bachelor of Science in 2009. There she was under the mentorship of Dr. Leyte Winfield, where she studied and developed novel transition metal based anti-cancer compounds. She was the recipient of many scholarships, grants, and fellowships for her research during her tenure.

In the Fall of 2009, Chyree was accepted into the doctoral program in the department of chemistry at Louisiana State University where she is currently a doctoral candidate in organic chemistry working under the tutelage of Dr. Carol M. Taylor. Her graduate dissertation work was composed of two projects. The first was the synthesis of an orthogonally protected τ -histidinoalanine building block. The second, which is in collaboration with Dr. Isiah Warner, involved the preparation of an ionic liquid-based prodrug-delivery system that utilizes a photothermal trigger.

Chyree has a younger brother and two younger sisters. Chyree is a member of the National Society for Black Chemists and Chemical Engineers and the American Chemical Society.